

The Effect of Physical Variations on the Products of Miller-Urey Experiment.

Dissertation

zur Erlangung des Grades
des Doktors der Naturwissenschaften
der Naturwissenschaftlich-Technischen Fakultät
der Universität des Saarlandes

von
Sina Ravanbodshirazi

Saarbrücken
2024

Tag des Kolloquiums: 23.10.2024

Dekan: Prof. Dr.-Ing. Dirk Bähre

Berichterstatter: Prof. Dr. Albrecht Ott

Prof. Dr. Claus Jacob

Akad. Mitglied: Dr. Yazdan Rashidi

Vorsitz: Prof. Dr. Gregor Jung

Abstract

Investigating the origins of life without direct historical data presents a significant challenge due to the lack of the ability to observe the conditions on early Earth firsthand.

This thesis extends beyond the traditional focus on specific outcomes to explore the broader potential chemical space through a series of experiments inspired by the classical Miller-Urey setup.

We analyzed the Miller experiment, the gas phase, the broth, and the solid phase composition using GC-MS, HPLC-Mass spectroscopy, FTIR, SEM, EDX, XRD, UV-Vis absorption, UV-Vis excitation, and Fluorescence. The research incorporates variations of the Miller-Urey experimental settings, including temperature, initial pressure, ammonia concentration, and the spark generator. Additionally, this work presents the real-time experiments to track changes over time.

The study systematically maps the products. This metabolomics-inspired workflow allows for confident identification of features, each representing a distinct product within the complex mixture.

By integrating these diverse approaches, we offer new insights into the possibilities of prebiotic chemistry and its implications for the search for origin of life.

The experimental results demonstrate that specific environmental conditions significantly enhance the molecular diversity, leading to the formation of precursors essential to life.

Keywords: Miller-Urey Experiment, Complex Chemical Networks, Environmental Conditions, Origins of Life, analytical techniques.

Zusammenfassung

Die Erforschung der Ursprünge des Lebens ohne direkte historische Daten stellt eine erhebliche Herausforderung dar, da die Bedingungen auf der frühen Erde nicht aus erster Hand beobachtet werden können. Diese Arbeit geht über den traditionellen Fokus auf spezifische Ergebnisse hinaus, um den breiteren potenziellen chemischen Raum durch eine Reihe von Experimenten zu erkunden, die vom klassischen Miller-Urey-Setup inspiriert sind.

Wir analysierten das Miller-Experiment hinsichtlich der Gasphase, der "Ursuppe" und der Festphasen-Zusammensetzung unter Verwendung von GC-MS, HPLC-Massenspektrometrie, FTIR, SEM, EDX, XRD, UV-Vis-Absorption, UV-Vis-Anregung und Fluoreszenz.

Unsere Arbeit umfasst Variationen der Miller-Urey-Experimenteinstellungen, einschließlich der Auswirkungen von Temperatur, Anfangsdruck, Ammoniakkonzentration und dem Funkeninduktor. Darüber hinaus werden Echtzeitexperimente vorgestellt, um Veränderungen Zeitabhängig zu verfolgen.

Unsere Studie kartiert systematisch die Produkte. Dieser von der Metabolomik inspirierte Workflow ermöglicht eine sichere Identifizierung von Merkmalen, die jeweils ein spezifisches Produkt innerhalb des komplexen Gemisches darstellen.

Durch die Integration dieser unterschiedlichen Ansätze bieten wir neue Einblicke in die Möglichkeiten der präbiotischen Chemie und deren Implikationen für die Suche nach dem Ursprung des Lebens. Die experimentellen Ergebnisse zeigen, dass spezifische Umweltbedingungen die molekulare Vielfalt erheblich erhöhen und zur Bildung wesentlicher Molecularer Vorstufen des Lebens führen.

Schlüsselwörter: Miller-Urey-Experiment, komplexe chemische Netzwerke, Umweltbedingungen, Ursprünge des Lebens, analytische Techniken.

Acknowledgements

I want to start by thanking my advisors, Prof. Dr. **Albrecht Ott**, and Prof. Dr. **Gregor Jung** for their constant support, guidance, and invaluable insights throughout this research. Their encouragement and expertise have been crucial in shaping this thesis.

I'm also deeply grateful to my **committee members** for their helpful feedback and constructive criticism, which have greatly improved the quality of this work.

Special thanks to my **colleagues** and **friends** in the Prof. Dr. Albrecht Ott's Group for their friendship and for creating a stimulating environment. Your support and discussions have been a source of motivation and inspiration.

I am also thankful to my **family** for their constant support and understanding. Their belief in me has been a cornerstone of my perseverance.

This has been a guiding principle throughout my research, reminding me of the importance of curiosity and the relentless pursuit of knowledge.

Thank you all for your contributions and encouragement. This thesis would not have been possible without your support.

Finally, I want to share a note from Horace Walpole, an English writer who first used "serendipity" in a letter he wrote to his friend Horace Mann on 28 January 1754. The name "Serendip" comes from an old Persian name for Sri Lanka (Ceylon). The word has been exported into many other languages with the general meaning of "unexpected discovery" or "fortunate chance". Walpole explained an unexpected discovery he had made about a lost painting of Bianca Cappello by Giorgio Vasari by reference to a classical Persian story (The Three Princes of Serendip). In this story, The princes told his correspondent:

"Always making discoveries, by accidents and sagacity, of things which they were not in quest of."

Sina Ravanbodshirazi

Saarbrücken, November 13, 2024

Contents

1	Introduction	1
2	Philosophy and Definitions of Life	4
2.1	Challenges in Defining Life: A Philosophical Perspective	4
2.2	The Interdisciplinary Nature of Life's Definition	4
2.3	Autotrophic and Heterotrophic	5
2.4	The Origin of the Life Building Blocks	6
2.5	Defining Life's Boundaries	7
2.6	The multidisciplinary nature and characteristics of life	9
3	Earth's Primordial Conditions	11
3.1	Formation and Evolution of Early Earth	11
3.2	Atmospheric Development on Early Earth	11
3.3	Water Accumulation and Ocean Formation	12
3.4	Energy Harvesting in Prebiotic Environment	13
4	Prebiotic Theories	14
4.1	Origins of Amino Acids	14
4.2	Origins of Nucleobases	15
4.3	Origins of Carbohydrates	15
4.4	Hydrogen Cyanide	16
4.5	The Lipid world	17
4.6	The Journey from Myth to Science	19
4.7	Prebiotic Chemistry and Evolution	20
4.8	Theories of Chemical Evolution	21
4.9	The Warm-Little Pond Hypothesis	22
4.10	The Importance of Cycles	25
4.11	Hydrothermal Vents	29
4.12	Water-Soil Interface	32
4.13	Impact Theory	33

4.14	Evolution Theories	34
4.15	Quantum-level simulations and Emergent Molecules	36
5	The Miller-Urey Experiment	38
6	The Complexity of Prebiotic Soup Characterization	42
6.1	Introduction to Analytical Challenges	42
6.2	Key Analytical Techniques in Prebiotic Systems Chemistry	42
6.3	Instrumental Analysis and Its Contributions	43
6.4	Systems Chemistry and Retro Synthetic Approach	44
6.4.1	Gas Chromatography-Mass Spectrometry (GC-MS)	46
6.4.2	Mass Spectrometry	49
6.4.3	High-performance Liquid Chromatography (HPLC)	53
6.4.4	UV-Visible Absorption spectroscopy	55
6.4.5	Fluorescent Analysis	57
6.4.6	UV-Visible Emission Spectroscopy	58
6.4.7	Infrared Spectroscopy (IR)	59
6.4.8	(SEM/EDX)	60
6.5	Combining Techniques for Multi-modal Analysis	61
7	Materials and methods	62
7.1	Miller-Urey Experiment Setup	62
7.2	Temperature Characterization	64
7.3	Pressure Characterization	68
7.4	PH	72
7.5	Liquid Phase Extraction	73
7.6	Spark Generators	74
7.7	GC-MS	75
7.7.1	Liquid Phase	76
7.7.2	Gas Phase	77
7.8	FTMS	78
7.9	HPLC-FTMS	80

7.10	HPLC-UV-Vis	82
7.11	Real-time UV-Vis Absorption	82
7.12	FTIR	82
7.13	UV-Vis Excitation	84
7.14	XRD	85
7.15	SEM/EDX	85
8	Results and discussion	87
8.1	GC-MS	87
8.1.1	Liquid Phase	87
8.1.2	Gas phase	95
8.2	FTMS	98
8.2.1	Kendrick Mass Defect	100
8.3	HPLC-FTMS	103
8.4	Real-time UV-Vis absorption	104
8.5	Fluorescence	112
8.6	HPLC-UV-Vis	114
8.7	Gas Phase IR absorption	116
8.8	UV-Vis Gas phase Excitation	120
8.9	SEM/EDX microscopy	125
8.10	XRD	130
9	Conclusions	131
10	Suggested Future Works	132

List of Tables

1	Words used in life defenitions	9
2	Experimental conditions	63
3	Temperature-Dependent pressure changes with ammonia concentration	70
4	Spark generator electrical characteristics	75
5	FTMS Instrument adjusted parameters.	79
6	HPLC Gradient method	80
7	HPLC-FTMS Instrument adjusted parameters.	81
8	UV-Vis Spectrophotometer adjusted parameters	83
9	FT-IR Instrument adjusted parameters.	84
10	Examples of Detected Compounds in the Liquid Phase Across Samples S₁ - S₈	89
11	Representative Compounds Identified in the Liquid Phase via GC-MS Analysis	91
12	Number of chemical formula assigned by GC/MS	92
13	The 20 most abundance fragments as observed by GC/MS	94
14	Examples of detected compounds in the gas phase	97
15	Compound Detection Results in Samples S ₁ to S ₈ (Appendix)	160

List of Figures

1	Schematic representation of enzymatic reactions in vesicles	19
2	Chemical evolution theory	21
3	Progress in origin of life	22
4	Hydration-Dehydration cycles	24
5	Major cycles and fluxes on early Earth	27
6	Diagram of a protometabolic reaction cycle	28
7	Hydrothermal vent chimneys	29
8	The timeline of evolution	36
9	Miller experiment	41
10	Bottom-up molecular evolution and analytical advancement	44
11	Gas Chromatography-Mass Spectrometry (GC-MS) system	47
12	Binding energy of nuclei as a function of mass number	52
13	KMD simulation	53
14	High-Performance Liquid Chromatography (HPLC) system	54
15	Energy level transition	55
16	Electronic energy levels and transitions	56
17	Electron transitions and their typical compounds.	56
18	One-pot reactor design	63
19	Local temperatures within the Miller-Urey experiment flask under different conditions	67
20	Temperatures and ammonia concentration effect on the pressure	69

21	Pressure propagation as a function of time $P(t)$	71
22	Temperature-Humidity relationship	72
23	pH shift in water	73
24	Voltage-time characterization of spark generators	74
25	NIST database	76
26	Schematic Picture of the IR Gas Cell	83
27	GC-MS of Liquid phase	89
28	Example of GC-MS chromatogram in the gas phase	96
29	FTMS spectrum of the miller soup	98
30	FTMS spectrum view of the miller soup for samples 1-8	99
31	Kendrick Mass Defect analysis of miller experiment using CH_2 mass base	102
32	HPLC-FTMS chromatogram of the miller soup	104
33	Real-time UV-Vis absorption spectra trends	105
34	Real-time UV-Vis absorption for miller-urey experiments at 80 °C, 100 °C, and 120 °C	106
35	Real-time UV-Vis absorption of miller-urey experiments at different am- monia concentrations	109
36	Real-time UV-Vis absorption of miller-urey experiments at different am- monia concentrations in 120 hours	111
37	Excitation-Emission fluorescence spectrum	113
38	HPLC-UV-Vis chromatogram of miller sample	115
39	Infrared spectrum of a gas Phase sample after a sparking run-time of 7 days	116
40	Gas phase FTIR spectrums	119

41	Emission wavelengths in the miller experiment with dual spark generators	121
42	UV-Vis emission spectras of gases under varied spark discharge conditions	124
43	Pictures of electrodes	126
44	SEM pictures of black material in earth pole	127
45	SEM pictures of black material in positive pole	128
46	EDX analysis of the black material	129
47	XRD of black material	130

List of publications

- I. Sina Ravanbodshirazi et al. “The Nature of the Spark Is a Pivotal Element in the Design of a Miller–Urey Experiment”. In: *Life* 13.11 (2023), p. 2201
- II. Marc Finkler et al. “Full incorporation of the noncanonical amino acid hydroxyllysine as a surrogate for lysine in green fluorescent protein”. In: *Bioorganic & Medicinal Chemistry* 41 (2021), p. 116207

1 Introduction

The origin of life on Earth remains a profound mystery that continues to engage scientists across multiple disciplines. This thesis aims to bridge the gaps in our understanding by studying complex prebiotic broths, mixtures that simulate the chemical environment of early Earth. These broths, created under controlled laboratory conditions, enabled us to explore how simple organic molecules could have evolved into the complex structures necessary for life.

To analyze these prebiotic mixtures, this research employs a variety of advanced analytical techniques, including GC-MS, HPLC-Mass spectroscopy, FTIR, SEM, EDX, XRD, UV-Vis absorption, UV-Vis excitation, and Fluorescence. These methods provide detailed insights into the molecular interactions and transformations within the broths, helping to identify potential pathways through which life's building blocks could have formed. Our experiments focus on how variables such as temperature, pressure, ammonia concentration, and spark generators influence these chemical processes. By altering these conditions, we can observe changes in the synthesis and stability of key organic molecules.

Biological organisms are highly organized chemical systems. They can reproduce themselves and are much more complex than systems that can be made synthetically. We do not know the exact processes that led to the formation of the first organisms. The first forms of life appeared on Earth about 4 billion years ago, within approximately 100 million years. According to current knowledge, early Earth had a complex mix of organic and inorganic substances in all states of matter, and it was supplied with various forms of energy (such as electrical discharges from lightning, light and heat from the sun, and hydrothermal vents, also known as black smokers). Scientists have gained many insights into the conditions on prebiotic Earth and proposed numerous reaction pathways to explain the formation of important biomolecules.

In the 1950s, Stanley Miller and Harold Urey showed that biomolecules could form under prebiotic conditions. In their experiment, they boiled water in a possible prebiotic atmosphere with electrical discharges. After a few days, a complex mixture of organic substances had formed, including amino acids. Amino acids are the building blocks of proteins and are essential in all living organisms. In the following decades, experiments showed that sugars, nucleobases (building blocks of genetic material, RNA, and DNA),

lipids (building blocks of cell membranes) and other important biomolecules could also be synthesized under prebiotic conditions. It is now accepted that the molecules making up today's living organisms could have formed on early Earth. However, it is still not clear how these molecular building blocks organized themselves in the "primordial soup" to form units that could maintain and reproduce themselves, leading to what we call life.

The origin of life on Earth remains one of the most important open questions in science. Around 4.5 billion years ago [3], from the gas and dust left over by a newly formed sun, our planet, Earth, came into existence. During the following hundred million years, the young Earth was bombarded by meteorites and comets and had hot nascent oceans and many violent volcanic eruptions [4]. However, within about a billion years, life had arisen. The current timeline for when life arose is part of an ongoing debate, but it is estimated to be 2.5 to 3.7 billion years ago. Similarly, where life arose is also still an open question. The specifics of the environment that cradled the first forms of life (e.g., atmospheric/oceanic composition, range of temperatures, etc.) remain unknown and are highly debated among the scientific community, depending on who you ask [5, 6].

Many different theories have been developed as to where life could have started, considering a plethora of scenarios and their plausibility for supporting life. For example, in the theory of drying ponds or wet/drying cycles, abiotically synthesized simple organic compounds concentrate as a pool evaporates and the total volume is reduced. This can promote condensation and polymerization, with the loss of water molecules. The discovery of hydrothermal vents awoke significant interest in more extreme environments, where the redox potential of a hot and mineral-enriched environment could serve as an energy source to overcome the thermodynamic barriers of making life's building blocks [7, 8]. Even really cold environments [9] or atmospheric aerosols [10] have been considered. Furthermore, there is always the possibility that life's building blocks already existed in outer space and reached Earth during the Late Heavy Bombardment (LHB) period through meteorites [11].

The complexity of even the simplest life forms is astonishing, and consequently, the transition of non-living, simple chemical compounds into the molecules of life remains one of the biggest mysteries in science. The uncertainty revolving around almost every aspect of life's origin leaves the door open for a myriad of possibilities. However, we can try to narrow it down. There are three things that we know about life, which will

guide us in the quest to understand life's origins:

1. All of life's building blocks (e.g., proteins, carbohydrates, nucleic acids, and lipids) are primarily composed of carbon, hydrogen, nitrogen, oxygen, phosphorus, and sulfur, also known as 'CHNOPS' [12].

2. The ability to undergo evolution, to change and adapt is one of the most important features of life as we know it. Darwin's work *On the Origin of Species* initiated a discussion on evolution that continues to this day, now attempting to fill the gap between inanimate matter and life. The chemical 'evolution' of simple organic molecules into a higher level of organization and complexity is triggered by the relationship with the environment. Much like the theory of evolution, the molecules that are more suited to the environment are more likely to survive, continue to change, evolve, and adapt as necessary for their survival due to the dynamic environment. A deeper discussion on the relationship between the environment and evolution is discussed in Henderson's book 'The fitness of the environment,' or as some call it, 'Darwin's fitness' [13]. Currently, the general working definition of life by NASA is 'a self-sustained chemical system capable of undergoing Darwinian evolution' [14].

3. The synthesis of biomolecules was not accomplished by nature in pristine laboratory conditions. All possible pathways for the one-pot synthesis of life's building blocks result in a very messy and complex mixture of products. The transition from a combinatorial explosion of products into constrained reaction networks is necessary for the construction of biomolecules at sufficient yields. The energy required to overcome the thermodynamic barriers of this construction can be obtained from the environment, in a process that Schrödinger describes as 'feeding from negentropy' [15]. This reflects the need for temporal organization, self-replication, and autocatalysis in complex systems [16]. However, exactly how this happened remains unknown, and we set out to explore this with the help of modern analytical techniques.

2 Philosophy and Definitions of Life

2.1 Challenges in Defining Life: A Philosophical Perspective

How did life begin on the earth? How can we find life elsewhere in the universe? What exactly do we call alive? Or if we discover something new, could we attribute it to the living world? Therefore, the answer of the question "**What is life?**" is bonded to our decision. The fundamental concept of life also addresses the fundamental questions such as How does life originate? Are we alone in the universe? What is the future of humans in space? Even though we really need a clear definition of life, there isn't yet one that works well for all purposes.

2.2 The Interdisciplinary Nature of Life's Definition

When we try to define the "**minimal life**" concept as simplest form of life, it's a bit like picking what goes into a recipe based on personal choice; there's no strict rule. People might agree on some of the main ingredients that are needed for life, but not everyone will pick the same ones. It's like drawing a line for the bare minimum of what life is, and everyone draws it differently. In short, what we consider the simplest life is just a bunch of chemical reactions that have some key parts which most people agree are important [14, 17]. These properties include:

- A. Self-sustaining homeostasis: A minimal living system must have the ability to uphold a steady internal environment and control its internal processes.
- B. Utilization of external energy: It ought to be able to obtain and use energy from its surroundings.
- C. Defined by a semipermeable compartment: A minimal living system needs to possess a boundary or compartment that isolates it from its surroundings while permitting the exchange of specific substances.
- D. Internal process of component production: It should have the capacity to internally generate its own components or molecules essential for its operation.

of defining terms. The two most frequent groups were self-reproduction and evolution, which were identified as the minimal set of defining terms for a concise and inclusive definition of life [18]. This definition encompasses the idea that life involves the ability to reproduce and undergo variations or changes.

2.3 Autotrophic and Heterotrophic

Theories on the origin of life categories are divided into two main categories: autotrophic and heterotrophic origins. These categories are based on their different approaches to carbon metabolism in the earliest cells. Autotrophs are able to make their own food from inorganic materials, turning carbon dioxide into organic matter. They managed to live and grow in tough places like hydrothermal vents and sulfurous springs. This ability laid the groundwork for life on Earth, opening doors to more complex life forms. Heterotrophs, in contrast, relied on the organic compounds produced by autotrophs to fuel their energy and growth. This distinction between autotrophs and heterotrophs contributed to the development of a diverse range of life, leading to the formation of intricate food chains and enhancing life's diversity. The dynamic interplay between autotrophs and heterotrophs was pivotal in evolving life from its simple origins to the elaborate, interconnected ecosystems observed today. [19, 20, 21, 22].

Autotrophy: Theories about the origins of life, particularly those focusing on autotrophic beginnings, propose that the earliest cells made use of simple, readily available inorganic materials abundant in the oxygen-free environment of the planet. These materials included hydrogen (H_2), carbon dioxide (CO_2), nitrogen (N_2), and hydrogen sulfide (H_2S), along with transition metals, especially iron sulfide (FeS) and nickel-iron sulfide ($FeNiS$) as catalysts. There are several reasons why these components are significant: [19]:

First, FeS and $FeNiS$ centers serve as essential catalysts in the carbon and energy metabolism of modern anaerobic autotrophs. This connection forms a direct link from the origin of life to the cellular functions observed today. [23].

Second, FeS and $FeNiS$ compounds are prevalent in environments lacking oxygen, both in the contemporary world and on the ancient Earth, highlighting their importance

through time. [24].

Third, the catalytic properties of FeS and FeNiS arise from their unfilled d and f electron orbitals, which readily form unstable bonds with carbon and nitrogen. This characteristic supports the hypothesis that the first cells relied on CO₂ for their carbon needs, showcasing a fundamental aspect of early life's adaptation to its environment. [20].

Heterotrophy: Theories suggesting heterotrophic beginnings are commonly supported by chemists [25, 26, 27]. From the perspective of biology, the hypothesis of heterotrophic origins presents three principal problems:

First, they fail to align with the chemistry observed in current cells. They beginning with the use of cyanide [28], formamide [29], and synthesis using UV light [28].

Second, considering the conditions of the early Earth and the challenges faced by prebiotic chemistry experiments in accurately replicating these conditions, geochemists often note that the scenarios proposed by heterotrophic origin theories are improbable for the early Earth[30].

Third, space-borne organic compounds are proposed as carbon sources for the earliest cells. However, these compounds are unfermentable in heterotrophic theory to have realistically served as the carbon foundation for the first cells [20].

2.4 The Origin of the Life Building Blocks

Various theories propose mechanisms for the formation of complex organic molecules on early Earth, with a common emphasis on reducing conditions for substance formation [27]. According to the Impact Hypothesis, organic substances may have been delivered to Earth through meteorite impacts, supported by evidence of organic material in interstellar space and on meteorites [31, 32, 33, 34].

Alternatively, it is hypothesized that the initial organic molecules originated in deep-sea volcanoes, where hydrogen sulfide (H₂S) emerges. Minerals at these locations could catalytically facilitate reactions, such as the exergonic reaction of iron(II) sulfide and hydrogen sulfide, providing the chemical energy necessary to reduce carbon monoxide or dioxide, thus generating more complex organic molecules [35].

Another perspective suggests that the first organic molecules resulted from reactions in an aqueous medium or with atmospheric gases (e.g., carbon monoxide CO, carbon dioxide CO₂, methane CH₄, nitrogen N₂, ammonia NH₃). Potential energy sources for these reactions include sunlight, energy from meteorite impacts, radioactive decay, electrical discharge, chemical energy from reactions, and surface heat on Earth [36, 37].

A. I. Oparin (1924) and J. B. S. Haldane (1929) developed the idea that chemical evolution preceded biological evolution, giving rise to the first organic molecules. Then, these molecules were subject to natural selection at the molecular level. Subsequent experiments, such as the Miller-Urey experiment, recreated conditions on the primordial Earth to comprehend the processes of chemical evolution.

2.5 Defining Life's Boundaries

The lack of a universally accepted definition of life, hinders progress in understanding the transitional pathway from inanimate chemical systems to the first forms of life, which further complicates the understanding of this transitional pathway. Emphasizing that the choice of properties and their hierarchy is still unclear, and there is no consensus among scientists [17, 38]. Regarding the challenges in defining life and the limitations of current definitions, is argued that definitions often use undefined terms and confuses description with definition, or arbitrarily define life in terms of minimal living systems. There is no natural, objective, or intrinsic indicator in the series of transitional systems that allows us to determine which system with specific properties is considered minimal life definition. The properties and subsystems necessary for a system to be considered living are arbitrary and depend on individual judgment [17]. Various theories and viewpoints on life exist, each shaped by individual perspectives and interests. In scientific discussions, numerous definitions abound, yet a unanimous agreement remains elusive. The limitations of current definitions of life, can be categorized into three groups [39, 40]:

1. Definitions that use undefined terms: Some definitions of life rely on terms that themselves lack clear and precise definitions. This creates a circular and unsatisfactory approach to defining life, as the definition relies on terms that are not adequately defined themselves.

2. Definitions that combine descriptions of life: Another limitation is the tendency to combine various descriptions of life to form a definition. This approach fails to provide a concise and distinct definition and instead presents a collection of characteristics or properties associated with life without a clear delineation.
3. Definitions that arbitrarily define minimal life: Some definitions arbitrarily define a specific step in the gradual transition from complex chemical systems to primitive living systems as minimal life. This approach lacks a solid scientific basis and is subjective in determining which properties or characteristics are essential for a system to be considered living.

These limitations highlight the challenges in formulating a comprehensive and universally accepted definition of life. These limitations hinder the progress towards a complete definition and demonstrate the difficulties in defining life in a precise and unambiguous manner. Different disciplines approach and understand the concept of life based on their specific scientific interests, premises, and contexts. The interdisciplinary nature of defining life is recognized, and the search for a universally accepted definition continues. Each theory, hypothesis, or point of view adopts its own definitions of life based on scientific interests and premises. This lack of consensus has led to the existence of hundreds of working definitions of life within scientific discourse. a productive approach to defining life would involve constructing a general and universal series of systems in which living systems are presented as a particular case within a broader interdisciplinary context. This context would include chemical, supramolecular, abiotic, prebiotic, paraliving, and metaliving systems, among others [17]. Based on the vocabulary analysis, the definition of life is suggested to be **”Life is self-reproduction with variations”**. This definition is derived from the analysis of 123 definitions of life 1.

Table 1: **Words used in life defenitions.** List of most frequent words used in the definitions of life, table from: "Vocabulary of Definitions of Life Suggests a Definition" by Edward N. Trifonov, published in the Journal of Biomolecular Structure & Dynamics, © Adenine Press (2011), reprinted by permission of Informa UK Limited, trading as Taylor & Francis Group [18].

Words Used in Life Defenitions							
Life	123	Organic	11	Internal	7	Capacity	5
Living	47	Alive	10	Replication	7	Different	5
System	43	Evolution	10	Being	6	Force	5
Matter	25	Materials	10	Change	6	Form	5
Systems	22	Reproduction	10	Characteristics	6	Functional	5
Environment	20	Existence	9	Entity	6	Highly	5
Energy	18	Defined	8	External	6	More	5
Chemical	17	Growth	8	Means	6	Mutation	5
Process	15	Information	8	Molecules	6	Necessary	5
Metabolism	14	Open	8	One	6	Network	5
Organism	14	Processes	8	Order	6	Objects	5
Organization	14	Properties	8	Organisms	6	Only	5
Complexity	13	Property	8	State	6	Organized	5
Ability	12	Reproduce	8	Things	6	Reactions	5
Itself	12	Through	8	Time	6	Three	5
Able	11	Complex	7	Way	6	Some	5
Capable	11	Evolve	7	Based	5	Biological	5
Definition	11	Genetic	7	Self-	5		
				reproduction			

2.6 The multidisciplinary nature and characteristics of life

The nature of the transitional pathway from inanimate chemical systems to the first forms of life on the Earth is a central question in astrobiology and transitional biology. It involves understanding how life originated through a process of prebiotic chemical evolution. This transitional pathway explores the possible states and processes that occurred as inanimate chemical systems and gradually transformed into the first living

organisms. It is a multidisciplinary field that investigates the properties and characteristics of these transitional states, aiming to uncover the fundamental principles and mechanisms that led to the emergence of life.

3 Earth's Primordial Conditions

3.1 Formation and Evolution of Early Earth

The Earth, formed approximately 4.5 billion years ago, has undergone significant changes that have shaped the conditions for the emergence of life. Understanding these early conditions is crucial for unraveling the mystery of life's origin. This section is about the atmospheric evolution, and the various geological and chemical processes that set the stage for the appearance of life [41, 27, 42]. The Earth, formed approximately 4.5 billion years ago through the accretion of solids in the solar nebula [41, 27], witnessed the traces of the first life forms around 3.8 - 4 billion years ago [41, 42]. The period during which life existed in a liquid phase spans about 100 million years ago, following the Earth's formation and the emergence of liquid water [43]. Multicellular life evidence dates back 3.5 billion years [44], with eukaryotes appearing approximately 2 billion years ago [41]. Dinosaurs roamed the Earth between 228 and 65 million years ago [45], and the earliest human fossils are around 200,000 years old [46].

During the early stages of Earth's formation, temperatures were exceptionally high $+70 \pm 15^\circ\text{C}$ [47] due to processes like meteorite impacts, accretion, and radioactivity. As the Earth cooled, a solid surface formed, initially consisting of molten rock and later marked by intense volcanic activity. The continuous change in the composition of the Earth's surface resulted from denser matter being drawn into the Earth's interior by gravity, while less dense matter remained on the surface. Initially, the surface likely comprised primarily of iron compounds and silicates, with the iron content decreasing over time.

3.2 Atmospheric Development on Early Earth

The Earth's atmosphere underwent significant changes during its creation, influenced by factors such as high temperatures, solar winds, and insufficient gravity. Noble gases and hydrogen (H_2) escaped the atmosphere due to these conditions [26, 43, 48].

The accretion phase involved constant meteorite impacts that brought gaseous substances, primarily carbon dioxide (CO_2) and nitrogen monoxide (NO), to Earth. Other components of the early atmosphere originated from volcanic eruptions, gas emissions

from the Earth's mantle, and various chemical processes, including weather reactions with the mantle's rocks, photochemical reactions from UV radiation, and reactions with iron components from meteorites or impact-induced shock heating [41, 42, 43].

Although the exact composition of the Earth's early atmosphere remains unclear and controversial, sedimentary rock analyses suggest an atmosphere primarily composed of carbon dioxide (CO_2), nitrogen (N_2), and traces of carbon monoxide (CO), hydrogen (H_2), and sulfur gases. The atmosphere was weakly reducing, lacking free oxygen [41, 42, 43].

One criticism of this thesis revolves around the weakly reducing atmosphere's inability to explain the diversity of organic substances crucial for life's formation. For instance, hydrogen cyanide (HCN), considered significant in the formation of amino acids, may have been formed to a limited extent. The metabolism of the first life forms seems to have been based on hydrogen chemistry, suggesting a potential claim that the presence of hydrogen in the primordial atmosphere was higher than the CO_2 and N_2 [42]. Or there were locally reducing environments?

3.3 Water Accumulation and Ocean Formation

Earth gained water from water-containing outgassing and icy meteorites. About 3.8 billion years ago, this water fell as rain and formed oceans. It's not clear how long these early oceans lasted. Also, there's a mystery about how the Earth was warm enough for liquid water since the young Sun didn't shine as brightly then [41, 42, 43].

Various parameters, such as the pH value of a primordial ocean and its physical state, remain uncertain and interconnected with other parameters of the primordial Earth system. Different conditions likely existed at different times in various locations on the prehistoric Earth. These uncertainties highlight the complexity of the processes leading to the origin of life, with theories evolving over decades, now suggesting a generally weaker reducing atmosphere than in the 1950s when Stanley Miller conducted his famous experiment[49].

3.4 Energy Harvesting in Prebiotic Environment

Primitive cells may have harvested energy from their environment through three potential sources [50]: chemical energy in the form of chemical bonds or oxidation-reduction reactions [51], light energy, and energy arising from chemical disequilibria in submarine or subterranean sites [52]. The availability of these energy sources is highly plausible in the prebiotic environment. Chemical energy, for example, could have been derived from the chemical bonds present in the organic compounds available on the early Earth, such as carbonaceous meteorites. These compounds were synthesized abiotically in the early solar system and could have provided a rich mixture of organic compounds for energy harvesting. Additionally, light energy became the predominant energy source, just as it is today. However, the question arises: How could primitive cellular life have harnessed this energy? To capture light energy, a pigment system must initially absorb photons and then convert them into usable forms of chemical energy. It's reasonable to consider that photosynthetic structures similar to those in present-day life were not present. Instead, pigment systems such as polycyclic aromatic hydrocarbons (PAHs), organic iron complexes, porphyrins, and proteinoids might have been integrated into bilayer membranes [53, 50]. The prevalence of PAH as a significant organic component in carbonaceous meteorites has been confirmed [54], and it's likely that PAHs and their derivatives were among the most common organic compounds in the early Earth environment. If life began on the Earth's surface, could have been utilized by primitive cells. Furthermore, energy arising from chemical disequilibria in submarine or subterranean sites could have been another potential source of energy for primitive cells. These energy sources would have been crucial for the establishment of a recognizable metabolism within cellular boundaries and for the development of the complex network of catalytic reactions associated with metabolism.

4 Prebiotic Theories

4.1 Origins of Amino Acids

Amino acids are the building blocks of proteins, playing a crucial role in all living cells. Various experiments simulating prebiotic Earth conditions have yielded amino acids [41, 55]. These experiments differ in the composition of reactants, energy sources, and the yields of different amino acids.

In an experiment by Kobayashi et al., a flask containing water and an atmosphere of carbon monoxide (CO), carbon dioxide (CO₂), and nitrogen (N₂) was irradiated with particles (protons, helium nuclei, and electrons) with energies ranging from 2.5 MeV to 1 GeV. The yellowish solution contained various amino acids, mainly glycine, aspartic acid, serine, and alanine [56].

Amino acid photosynthesis was demonstrated in an aqueous solution of 3% paraformaldehyde, illuminated with light (500 W, tungsten lamp) in the presence of inorganic catalysts [57]. Amino acids were also formed in the gas mixture of the Miller experiment by UV irradiation when methane was replaced by ethane [58].

Shockwaves, generated by meteorite impacts and lightning on early Earth, provided another energy source. Experiments involving rapid compression and heating of gas mixtures containing hydrocarbon gases (e.g., methane, ethane), ammonia, and water in a shock tube revealed the formation of amino acids, along with aldehydes and cyanohydrins [59].

Amino acids were also identified as a result of chemical energy from the reaction of simple substances. Mixtures of cyanohydrin and ammonia at 90°C [60], as well as paraformaldehyde and hydroxylamine hydrochloride (H₄NOCl) at 80-100°C [55], produced numerous amino acids (including aspartic acid, threonine, glycine, alanine). Additionally, organic acids such as formic acid, lactic acid, glycolic acid [55], and uric acid [60] were formed.

The formation of amino acids through thermal energy has also been reported [61].

4.2 Origins of Nucleobases

The nucleobases adenine, thymine, guanine, cytosine, and uracil, fundamental components of DNA and RNA, are of particular interest [62]. Adenine was synthesized by heating a solution of ammonium hydroxide and cyanogen at 90°C [63]. Further investigations yielded additional purine synthesis [64]. Pyrimidines were produced through reactions of cyanoacetylene (C_3HN) with cyanate ($CHON$) [65]. Cyanoacetylene can be a product of sparks in a prebiotic atmosphere [66], and the formation of cyanates under prebiotic conditions has been demonstrated [65]. Nucleobases have also been found on meteorites [41].

4.3 Origins of Carbohydrates

There are more than 200 distinct monosaccharides identified, classified according to their carbon atom count and whether they function as polyhydroxy aldehydes ($-CH = O-$) or polyhydroxy ketones ($-C = O-$). Further classification of aldoses and ketoses is based on the number of carbon atoms in their primary chain [67].

The Formose reaction [68, 69], discovered in the late 19th century, generates up to 40 sugars from simple building blocks [41]. In an alkaline solution of formaldehyde (CH_2O) with the presence of metal hydroxides, numerous parallel and subsequent reactions occur. However, the exact processes and products are not fully identified [70].

Calcium forms complexes with organic substances in the Formose mixture and acts catalytically. Initially, two reaction pathways compete: the Cannizzaro reaction, where two aldehydes ($R-COH$) react to form an acid ($R-COOH$) and an alcohol ($R-CHOH$), and an autocatalytic process (Formose primary reaction) that produces glycolaldehyde ($C_2H_4O_2$) from two formaldehyde molecules. Subsequent secondary reactions form carbohydrates like hexoses and heptoses, catalyzing further reactions [71, 68, 69]. The dominance of either pathway depends on the concentrations of formose and calcium. If the Formose reaction prevails, the Cannizzaro reaction proceeds relatively slowly but can convert additional formaldehyde and later-formed aldehydes. The mixture becomes progressively acidic over time. In a later phase, sugar formation occurs not through additional formaldehyde additions but through self- and mixed additions of lower sugars [71, 68, 69].

In addition to the Formose reaction, carbohydrates have been found in experiments exploring prebiotic synthesis pathways. Experiments involving spark discharges in an atmosphere of water, methane, and ammonia identified monosaccharides as well as polysaccharide-like molecules [72].

Of particular interest are sugars present in RNA and DNA. The synthesis of ribose is significant for the emergence of the RNA world. Although ribose is produced in the Formose reaction, it is unstable [73]. Therefore, in prebiotic synthesis, it either had to react immediately to form a nucleotide or was stabilized. Ribose produced in a mixture of formaldehyde and glycolaldehyde (as in the Formose reaction) results in a brownish polymeric mixture that is challenging to characterize. The addition of borates (salts of boric acid) prevents these reactions, thus stabilizing ribose [73].

Sugar alcohols and sugar acids have also been detected on meteorites [41].

4.4 Hydrogen Cyanide

Hydrogen cyanide (HCN) is attributed significant importance in chemical evolution, likely being one of the first molecules to form under prebiotic conditions. It has been detected in experiments related to chemical evolution (such as the Miller experiment), in interstellar space, and predicted in simulations of the chemistry of the early atmosphere [41, 74, 75, 76]. Hydrogen cyanide is believed to be a crucial building block for the formation of biomolecules like adenine [77], other purines [41], and amino acids [78]. Additionally, hydrogen cyanide is known for self-condensation, yielding various polymers, with synthesis pathways clarified only for the initial stages [79, 60]. Adenine is a pentamer of hydrogen cyanide, and longer polymers, including heteropolypeptides and polymerized dimers $C_2H_2N_2$, are formed [80, 81]. Glycolonitrile, a product of formaldehyde CH_2O with hydrogen cyanide, promotes polymerization [82]. Evidence suggests the formation of cyclic polymers [83]. Under simple conditions, an aqueous solution of ammonium cyanide gives rise to amino acids, fatty acids, and purines [60]. This mixture has been extensively studied and comprises over 1600 substances [79, 83].

4.5 The Lipid world

Investigating the origins of cellular life unveils the crucial role of membrane self-assembly. The early evolution of cellular life was significantly influenced by membrane-bound compartments. Components of these early membranes, likely amphiphiles such as short-chain fatty acids, were abundantly available on the early Earth. Their ability to self-assemble into stable vesicles encapsulating hydrophilic solutes with catalytic activity laid the foundational mechanisms for cellular life [84]

The process of encapsulating catalytic species within membranous compartments, especially vesicles, was pivotal. It created a protected microenvironment conducive to the survival of spontaneous molecular systems, facilitating the emergence and sustenance of primitive cellular systems. This encapsulation allowed for the accumulation of polymeric products, contributing to the development of a recognizable metabolism within cellular boundaries [52].

Studies on carbonaceous meteoritic material and laboratory models of plausible Fischer-Tropsch-type reactions suggest that vesicle-forming amphiphiles were present on the early Earth, participating in the formation of boundary membranes crucial for early cellular life. These amphiphiles formed vesicles with properties akin to liposomes, which are primary components of contemporary cellular membranes. They tend to be less stable and more permeable to ionic solutions, but a higher permeability could be an advantage in the absence of specialized transport proteins. As life evolved, stable bilayer membranes emerged, fostering the coevolution of catalysts, metabolism, and membrane-forming compounds. These membranes evolved to support an extensive metabolism dependent on external nutrient solutes [52].

Recent investigations have highlighted that encapsulation procedures such as dehydration/rehydration and pH vesiculation allow the trapping of all components of complex catalytic systems within vesicles. These systems remained active within the vesicular compartment, protected from degradation agents by the membrane boundaries. Such membrane-protected environments were likely crucial for the survival of molecular systems on the path to the first forms of cellular life [52].

The varied origins of energy available to primitive cells were fundamental in establishing metabolic processes and catalytic reactions. Primitive cells likely harvested energy from their environment through chemical bonds, light energy, and energy from chem-

ical disequilibria in submarine or subterranean sites. The availability of these energy sources was crucial for establishing a metabolism and developing complex catalytic reaction networks within cellular boundaries [50, 51, 85, 52].

Furthermore, encapsulation of single molecules within vesicles was common on early Earth, suggesting that early cellular metabolism might have been inherently simple until the evolution of protein-mediated transport systems. These encapsulation processes, showcased in studies by Oberholzer et al., provided insights into gene amplification, catalyst coevolution, and the development of membrane-forming compounds in the evolutionary process [86, 87, 52].

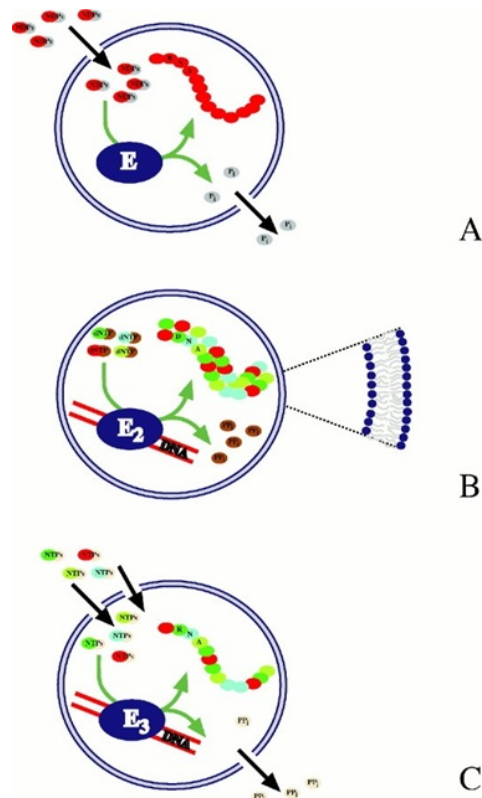


Figure 1: **Schematic representation of enzymatic reactions in vesicles** [52].
(Picture reused with permission from John Wiley and Sons)

A: The PNPase enzyme (E) is encapsulated within liposomes. ADP is added to the external medium and must passively diffuse across the amphiphile bilayers to be processed by the enzyme.

B: The DNA polymerase enzyme (E2), along with its template (primers omitted), and substrates are encapsulated simultaneously.

C: The T7 RNA polymerase (E3) and its template are encapsulated inside the vesicles. NTPs are added externally as an energy source and substrates for the enzyme.

4.6 The Journey from Myth to Science

For thousands of years, creation myths like Genesis attributed the ability to create living beings from inanimate matter to a transcendent figure [88]. The notion that the spontaneous emergence of life was a result of chance also existed in early history, for instance, the belief that frogs emerged from humus after the Nile was flooded [88].

The ancient Greek concept of ether germs, akin to atoms of inanimate matter, existing universally and fostering life in fertile areas (panspermia), persisted until Louis Pasteur refuted it in the mid-19th century [89].

A. I. Oparin (1924) and J. Haldane (1929) developed the idea that chemical evolution preceded biological evolution, giving rise to the first organic molecules. These molecules were then subject to natural selection on a molecular level. Subsequent experiments, such as the Miller-Urey experiment, recreated conditions on the primordial Earth to comprehend the processes of chemical evolution.

4.7 Prebiotic Chemistry and Evolution

Ernst Haeckel proposed a theory of the origin of life in the 1870s that integrated progressive chemical steps of growing complexity. He asserted that living matter could have been formed by combinations between carbon and specific atoms, which would produce aggregates becoming increasingly complex and eventually developing into the simplest organisms [90].

Oparin criticizes Haeckel's theory in 1938, stating that the theory proposed by Ernst Haeckel involves a fundamental error, specifically the implication that the simplest organisms can arise all at once from inorganic matter. Haeckel's theory suggests that there is no difference between the formation of a crystal and that of a living cell. Oparin challenges the idea of life arising spontaneously or existing eternally and presents theories about the origin of life based on space, time, and physical conditions. Oparin argues the physical state of stars and planets, could synthesis the carbon and nitrogen compounds in them. Oparin suggests that the cooling earth produced hydrocarbons derived from primordial carbides and ammonia, both in a reduced state. He proposes that primary carbohydrates and proteins may have been formed in primitive waters as the materials were drying up. Oparin also mentions that the chemists had succeeded in synthesizing practically all known organic substances in vitro under artificial conditions, which supports the idea of a chemical basis for the origin of organic protoplasm [91], according to protoplasmic view of life, the protoplasmic substance combines all vital properties [92].

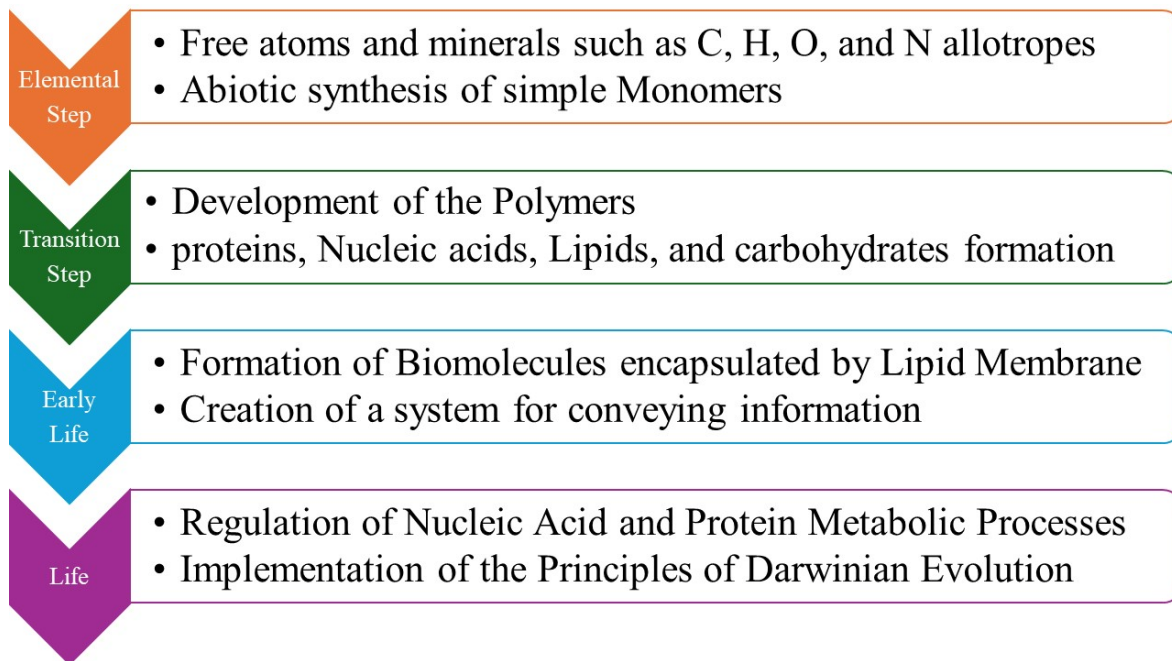


Figure 2: **Chemical evolution theory.** Tracing the transition from non-living molecules to life through molecular self-organization, selective polymerization according to Darwinian evolution [93].

4.8 Theories of Chemical Evolution

Following Darwin's evolution principle, scientists believed that living organisms evolved from non-living matter. Numerous theories emerged, but none endured. In the 1920s, Alexander Oparin and John B. Haldane revisited the concept, outlining a chemical evolution pathway [94]. Their study outlined a series of chemical stages that would amplify the complexity and utility of organics produced abiotically in a reducing atmosphere. The step-by-step buildup and linking of these compounds could result in the formation of aggregates, leading to the emergence of coacervates or protocells, the ancestors of the first heterotrophic microbes [95]. In the theory known as 'Primordial Soup,' it is suggested that as Earth became suitable for life, non-living monomers transformed into polymers. This progression resulted in the emergence of the first protocell, [96].

Carl Woese's introduction of Archaea (formerly Archaeobacteria) in the late seventies sparked the idea that investigating this third form of life could aid in reconstructing the Last Universal Common Ancestor (LUCA) for all living organisms [97]. It is hy-

pothesized that progression from simple chemical reactions to essential elements of life required a selective process of some kind [98]. This could be achieved through an exchange of energy with the environment because the required level of order exceeds what one-pot batch reactions of these molecules can achieve. This assumption suggests the existence of an unknown pathway, akin to natural selection, guiding "messy" reactions toward a higher organizational order, leading to a more complex system [99].

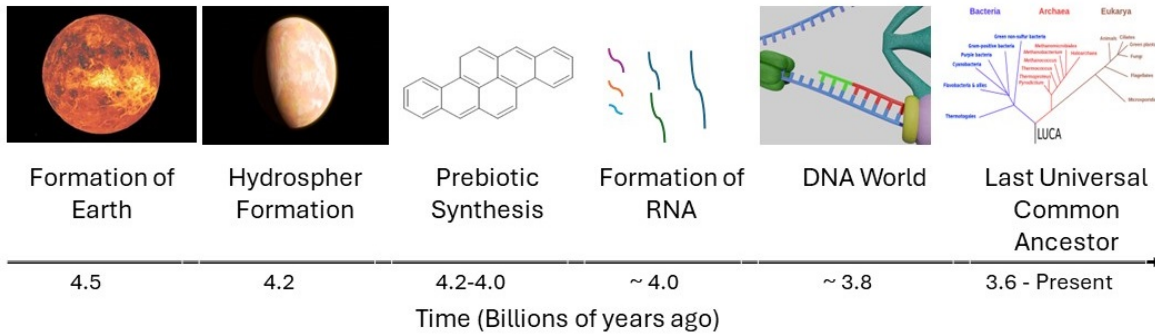


Figure 3: **Progress in the origin of life.** The transition steps to the Last Universal Common Ancestor (LUCA)

4.9 The Warm-Little Pond Hypothesis

In a paragraph from a letter on February 1st, 1871, Charles Darwin wrote to his close friend Joseph Dalton Hooker, he said: «it is often said that all the conditions for the first production of a living being are now present, which could ever have been present. But if (and oh what a big if) we could conceive in some **warm little pond** with all sort of ammonia and phosphoric salts, light, heat, electricity present, that a protein compound was chemically formed, ready to undergo still more complex changes, at the present such matter would be instantly devoured, or absorbed, which would not have been the case before living creatures were formed»[100]. It's unclear if he was aware of significant chemical discoveries like the synthesis of alanine by Adolf Strecker [101] in 1850.

It is necessary to mention that the transition from simple building blocks to biopolymers is not thermodynamically favorable in the biological solvent (water). It requires an additional energy input to facilitate this transition [102].

Some authors have proposed the idea that external energy plays a crucial role in the synthesis of living matter from minerals [102]. They have explored various potential sources of this external energy, including atmospheric electrical discharges and thermal springs.

Others assert that no external energy is necessary to synthesis biologically important substances from simple mineral compounds [103, 104, 105, 106]. Among the theories, Life Origination Hydrate Theory (LOH-Theory) asserts that natural processes stem from chemical transformations driven by universal laws and thermodynamics. Randomness implies insufficient information with the potential to align with natural regularities. Researchers trace nature's path using thermodynamics as a guide, seeking environmental cues to decode the underlying logic [102, 107].

In hydrothermal pools, there can be a combination of organic substances, including potential monomers and compounds that can create membrane-like vesicles. As the water evaporates during the dehydration phase, lipid membranes accumulate in layers on the surfaces of minerals located at the pool's edge due to fluctuations in the water level. It could provide the thermodynamically favorable conditions demanded for reactions [108, 109, 110]. As in the dry phase, bond formation is favorable, but diffusion is restricted, and this bonding restriction could be solved by the re-hydration cycles [111].

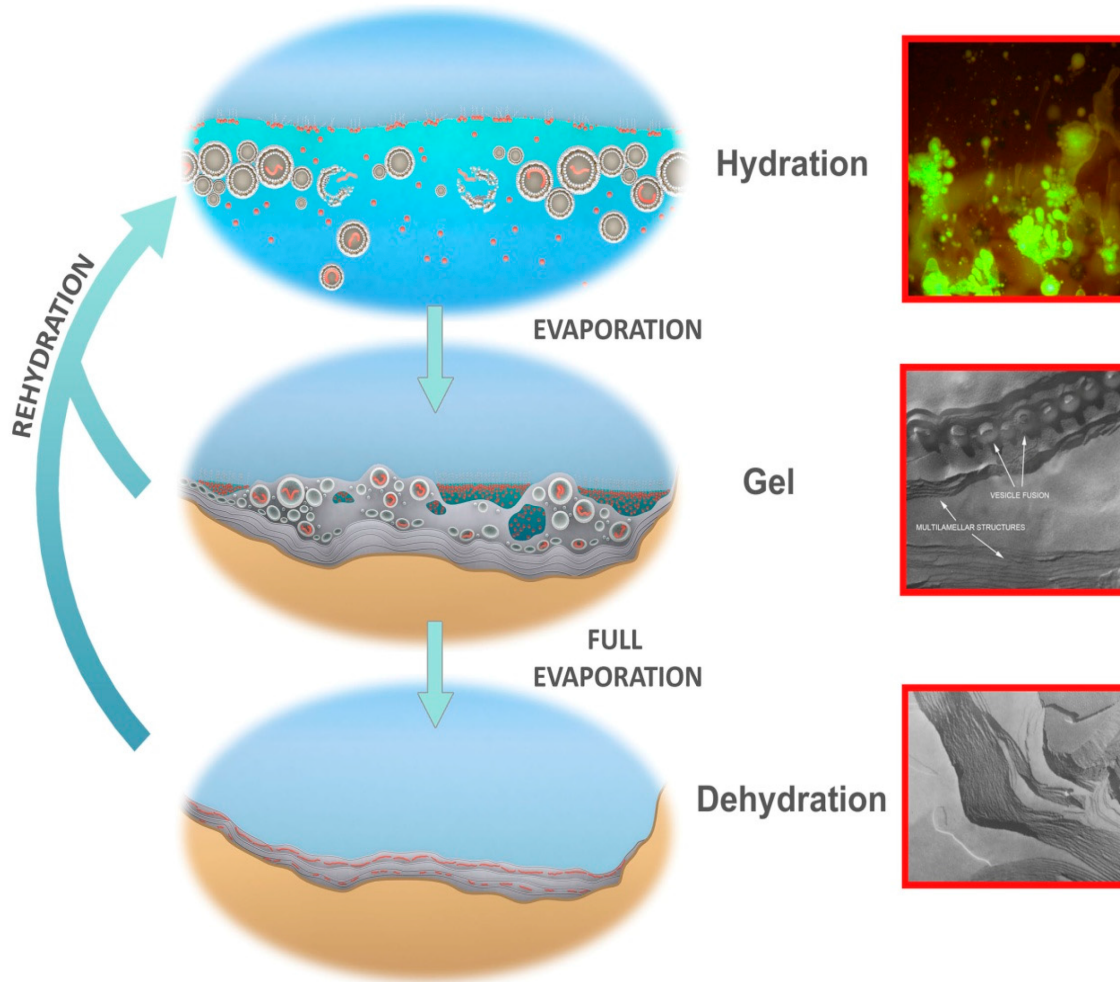


Figure 4: **Hydration-Dehydration cycles.** Visual representation of a hypothetical prebiotic environment on early Earth, often described as a 'warm little pond,' where abiotic substances gradually condensed into complex polymers, laying the groundwork for the emergence of proto-cell. Reproduced from MDPI journal Life, 2016, no permissions needed after citation [112].

Ecosystems are complex adaptive systems. They are full of surprises. Over time, small changes at the bottom create big patterns at the top. It's like mixing different chemicals and seeing what happens. But it's not just about chemicals. The environment and how things organize themselves also matter. Plus, evolution adds its touch to make each ecosystem unique. The big question is: how do these ecosystems stay strong and keep working when things around them change? It's like trying to understand a puzzle

from the past. [113].

4.10 The Importance of Cycles

Imagine nature as a skilled chef who keeps reusing the same key ingredient to whip up a variety of dishes. This is similar to what happens in recursive biochemical pathways. In each cycle, a special part of a molecule is cleverly reused, like the chef's favorite spice, allowing for a new reaction to take place. This process is vital in making important substances like fats and oils in nature, showing the smart way nature prepares essential ingredients for life [114].

From reusing molecular building blocks to creating essential life molecules during the primordial freeze-thaw cycles, there is a remarkable connection in how life may have started.

life's essential molecules, like RNA, could have formed on early Earth through natural freeze-thaw cycles. Laboratory experiments simulating these ancient conditions show that simple RNA segments can link up into more complex structures during such cycles. This concept is further supported by the natural occurrence of these cycles in Earth's early climate and the stability of RNA under these conditions [115, 116, 117, 118, 119].

Furthermore, The non-linearity of the equations that rule the evolution of biological systems allows for the co-existence of various self-organizing systems, in addition the life definition should also involve into the account. [120, 121, 122].

In prebiotic broth studies, the role of reaction cycles in creating complex systems is unexplored [93]. This idea to bring selectivity to these mixtures has not yet deeply investigated. There is potential for these reactions to create self-sustaining, evolving chemical systems in labs [123, 124, 125]. The right conditions could bring about such life-like systems, paving the way for new experiments. These studies are valuable because they can reveal key elements needed for life-like chemistry, even if they don't succeed right away.

When free energy is applied to organic matter without Darwinian evolution, the matter devolves into a wide range of compounds. Mixtures are rearranged, leading to an ever-increasing number of molecular species generated in experiments, which also presents a challenge for analysis. This leads to unfavorable beginnings for biology, a scenario

known as the "asphalt problem", which is not preferable for biological processes [126, 127, 128]. Organic compounds including alkanes C_{12} - C_{44} , fatty acids, alcohols, amines, aromatics, and heterocycles. The detected compounds have a wide range of degrees of aromaticity and chemical variability [1].

A continuous, recursive process might have driven the complexity of non-living materials towards a higher level of order, eventually leading to the emergence of a living entity in the origin of life.

Finding the correct chemical starting points and the conditions for these processes to occur but also creating the right analytical tools for precise and scientifically accurate study of the complex behaviors of these systems. It's crucial to design experiments that thoroughly investigate chemistries that are not in equilibrium, in both water-based and more varied environments like soft, interface-rich ones. These experiments should include detailed, time-sensitive analysis of specific aspects, such as the chirality of the species involved or their catalytic effects [129].

An autocatalytic cycle is essentially a loop of reactions in which, when operated on the right mixture of substances, the quantity of at least one component in the cycle increases over time. The presence of these cycles is key to the potential self-organization of sugar chemistry. Recent findings suggest that the inherent complexity of this chemistry can be managed by repeatedly interacting with mineral environments [130].

Furthermore, the development of both self-driven and mutually-driven catalytic loops, along with the formation of stable, non-equilibrium structures, could pave the way for the evolution of protocellular structures. See Figure 6. These structures would have greater stability and adaptability, suggesting a continuous, recursive process that could lead to the complexification of non-living material into a more ordered form, eventually giving rise to living entities in the origin of life [129].

There has been an important discussion about how the length of chemical cycles on early Earth could be compared with laboratory experiments. This debate also considers other environmental factors such as temperature, energy sources, initial compounds and etc. It is important to take into account the duration of experimental conditions to create a realistic setting for synthesizing organic materials. This approach helps to ensure our experiments closely mimic the actual conditions of early Earth, providing us with more accurate and meaningful results [131, 132, 1, 133].

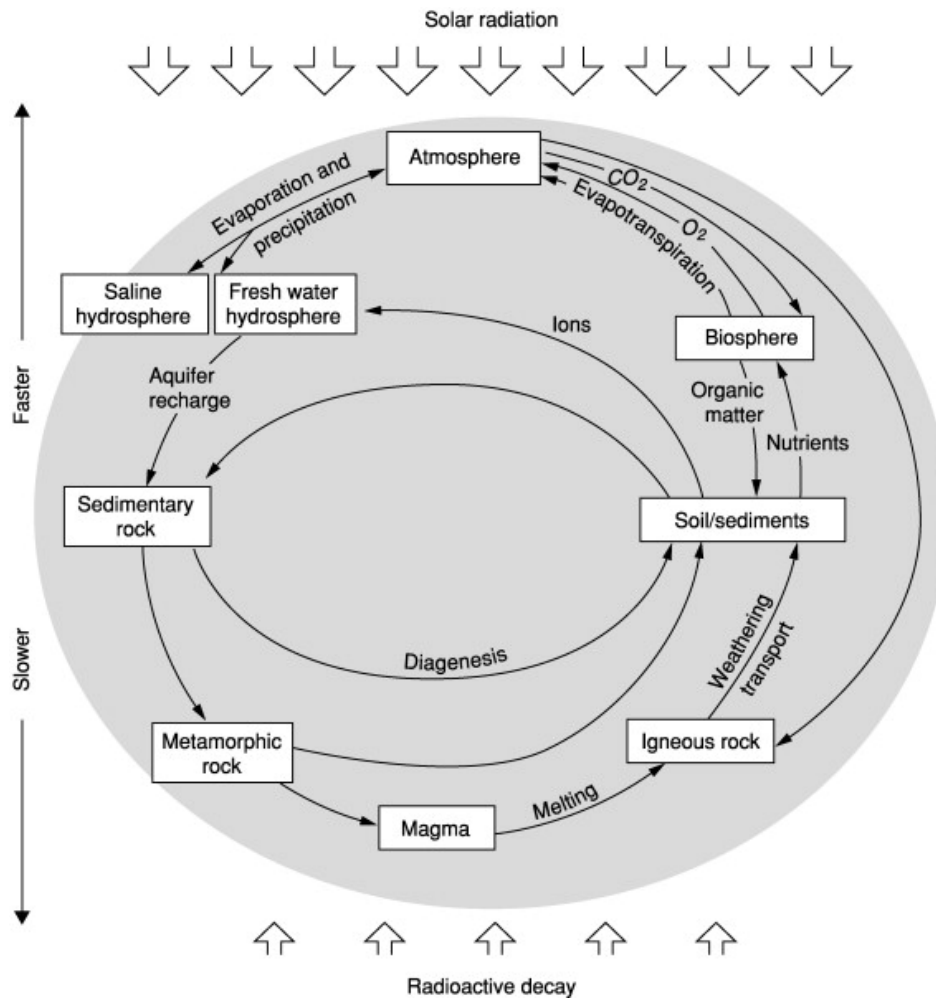


Figure 5: **Visual Representation of Major Cycles and Fluxes on Early Earth.** Emphasizing the length and dynamics of natural cycles during Earth's early stages.[134].

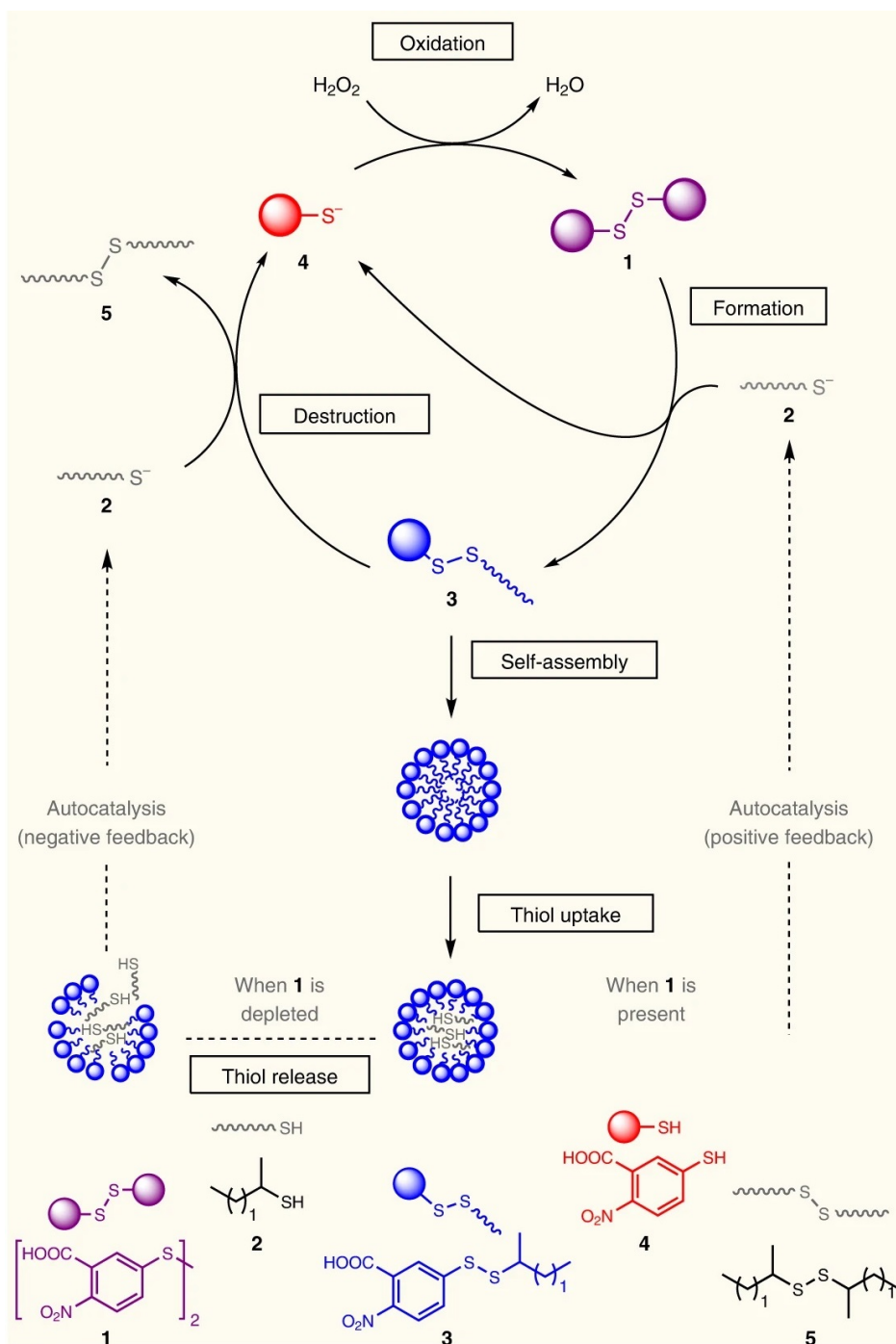


Figure 6: **Diagram of a protometabolic reaction cycle.** Showcasing the stages of formation, self-assembly, thiol interaction, and oxidation. This cycle illustrates the key steps in developing stable, non-equilibrium structures, crucial for evolving protocellular forms that could transform abiotic material into organized, life-like entities, reused photo with permission from Nature Chemistry [135].

4.11 Hydrothermal Vents

Hydrothermal vents present a fascinating environment in the study of life's origins. Their unique chemical and thermal dynamics make these environments highly suitable for the processes of chemical evolution. The continuous flow of thermal energy in these vents is thought to have played a crucial role in the evolution of the planet, including the early stages of prebiotic chemistry [136].

It is also proposed that the synthesis of amino acids, fundamental building blocks of life, could have occurred deep within the Earth's crust. These amino acids might then have been carried upward with hydrothermal fluids to cooler waters [137]. In these less extreme environments, with lower temperatures and the presence of clay minerals, there was an ideal setting for the formation of peptides and protocells [138]. This theory has suggested a plausible pathway for the emergence and development of life's precursors in the depths of early Earth's oceans since its first report on 1949 in the central portion of the Red Sea [139].

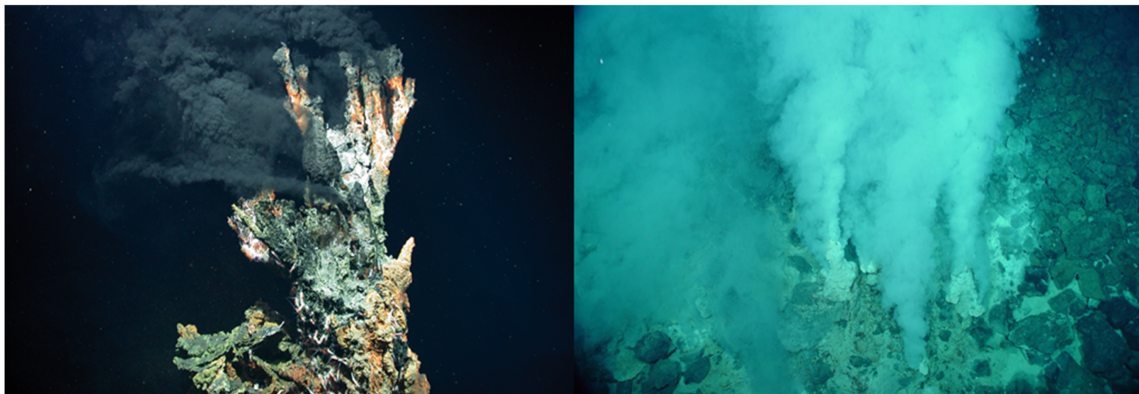


Figure 7: **Hydrothermal vent chimneys.** The candelabra black smoker hydrothermal vent chimney. Photo credit: Center for Marine Environmental Sciences, University of Bremen (left). The Champaign vent, a white smoker hydrothermal vent, re-used photo from the public domain image provided by the National Oceanic and Atmospheric Administration of the United States (right).

Russell et al., in their works from 1989 and 1993, highlighted the critical role of protons in energy and metabolic processes during the early stages of life on Earth. Their hypothesis emphasized the importance of the protonmotive force, driven by pH gradients,

coupled with the redox potential of iron monosulphide membranes. This synergy was crucial in meeting the energy requirements of nascent life, significantly influenced by the low pH and high CO₂ concentration of the Hadean ocean, helping the regeneration of vital pyrophosphates for life formation. These conditions led to the synthesis of organic anions and highlighted the role of elements such as iron, sulfur, and phosphate in early metabolism [140, 141, 142, 143].

Expanding upon this, William Martin and Michael J. Russell estimated that life originated around 4.2 billion years ago at the convergence of hot, alkaline submarine waters and the acidic, iron-rich Hadean ocean. The ensuing creation of an iron monosulphide membrane, serving as a semi-permeable barrier energized by redox potential and protonmotive force, was instrumental in fostering the synthesis and development of early metabolizing systems. This phenomenon likely led to the emergence of the earliest systems for replication and organic polymer production [140].

The two fundamental mechanisms identified by Russell et al. for facilitating the synthesis and evolution of early life through hydrothermal vents are: [140, 141, 142, 143]

1. The protonmotive force driven by pH gradients.
2. Ion movement across iron monosulphide membranes.

Further explorations suggested the possibility of life originating from medium-temperature alkaline hydrothermal springs flowing into an acidic, iron-rich ocean. This theory, supported by thermodynamic calculations and computer modeling, proposed that an alkaline solution, feeding early proto-cellular forms and interacting with seawater, could form a critical chemical barrier. Such an environment might encourage the formation of hydrophobic colloidal iron sulfide membranes, interacting with hydrothermal organosulfur molecules and possibly evolving from reliance on hydrothermal conditions to more autonomous processes, thereby offering a compelling perspective on the potential origins of life on Earth [143, 142].

Cleaves et al. presented a framework for submarine hydrothermal systems (SHSs), which could facilitate the formation of oligopeptides as a central subject to understand the origin of life on Earth. Their study specifically explored the synthesis of these complex organic molecules under conditions that would mimic natural SHS environments. Their findings called into question the likelihood of SHSs being conducive to

oligopeptide formation, given the stark differences between the experimental conditions necessary for their synthesis and the actual conditions found in SHSs.

They highlighted key factors such as the concentration of amino acids, temperature, and reaction times, and how these differ significantly from the conditions that would have been present in early Earth's SHSs. Cleaves et al.'s conclusions suggest that while laboratory conditions can be manipulated to favor oligopeptide synthesis, these conditions are not realistically reflective of natural SHS environments. This gap between experimental settings and natural conditions challenges the idea of SHSs as primary sources for the complex molecules required for the development of life, directing the scientific inquiry towards other potential environments that might have been more suitable for the emergence of life [144].

Laboratory experiments aiming to recreate hydrothermal conditions for studying the origins of life typically involve heating aqueous solutions containing prebiotic building blocks at high temperatures and high pressures, using specialized reactors [145, 144, 146].

Minerals, particularly pyrite (FeS_2), played a pivotal role in facilitating the synthesis of complex molecules. Pyrite, a naturally occurring iron disulfide mineral with its positively charged surface due to polyvalent metal ions like Fe^{2+} , acted as a catalyst in the surface reaction systems crucial for the origin of life. These minerals provided the necessary surface for strong ionic bonding, essential for the formation of large polyanionic biomolecules found in ancient biochemical pathways. The catalytic properties of pyrite and similar minerals made the synthesis of complex organic molecules more feasible by enabling these molecules to bond strongly yet flexibly. This flexibility allowed for lateral migration and interaction on mineral surfaces, leading to more dynamic and diverse biochemical reactions [35]. These minerals significantly ease the creation of complex molecular structures in tandem associated with the protonmotive force hypothesis by Russell.

However, from the perspective of physical organic chemistry, this approach presents challenges. The formation of a peptide bond in water requires a significant amount of energy, estimated to be around 2.5–3.6 kcal/mole [147, 148]. This energy requirement suggests that a high-temperature environment, such as that simulated in these experiments, might be necessary to facilitate this key biochemical process.

The process of directly condensing amino acids into peptides is not thermodynamically

favorable [149]. Consequently, many researchers have chosen to use high initial concentrations of amino acids, ranging from 1 to 10^{-2} M [150, 151, 152, 153]. Others, have worked with activated amino acids [154, 155] or explored prebiotic condensing agents [156, 157] to facilitate easier peptide synthesis. Specifically, Imai et al. successfully produced oligomers up to hexamers by exposing concentrated glycine solutions (10^{-1} M) to high temperatures (200–250 °C) and pressures (240 bar) for brief periods (34 or 78 seconds) [151].

The high temperatures involved also pose a risk of decomposition of organic compounds [158, 159], which could compete with the polymerization process. Consequently, this might shift the balance between monomers and polymers towards net depolymerization, or in other words, towards the breakdown of the polymers.

Despite these challenges, numerous experiments have successfully demonstrated the condensation of amino acids into short peptides under hydrothermal conditions, especially when certain catalysts are present. The catalysts such as copper (Cu^{2+}) ions [160], alumina (found in clays) [161], and fatty acids [162].

4.12 Water-Soil Interface

Graham Cairns-Smith, an organic chemist and molecular biologist from the University of Glasgow, developed an alternative theory based on the interaction of clay minerals with prebiotic soup. He proposed that defects on mineral surfaces could act as selective and information-bearing agents in chemical evolution, suggesting that molecules with stronger interactions with the silicon surface could survive environmental fluctuations, leading to the emergence of perfect microenvironments for early life [163]. Clay minerals have been shown to selectively catalyze the synthesis and adsorption of certain compounds under prebiotic conditions [164, 165], such as formamide condensation in clay minerals resulting in the synthesis of nucleobases and amino sugars [166], and the silicate-mediated formose reaction selectively stabilizing pentoses and hexoses relevant in modern biology [167].

The role of minerals in prebiotic experiments aligns with the theory of mineral evolution developed by Bob Hazen, suggesting that the diversity of minerals on Earth today arose after the great oxygenation event [168], indicating that only a subset of minerals was available on early Earth. Origins of Life scientists, including pioneers such as

Bernal and later Orgel, have acknowledged the catalytic capacity of mineral surfaces, hypothesizing their non-trivial role in chemical evolution [154]. This hypothesis is supported by recent studies focusing on interactions of life's building blocks with minerals, demonstrating that the adsorption of compounds such as nucleotides and amino acids on mineral surfaces could favor polymerization [169]. However, various parameters (solubility, molecule size, mineral charge, pH and temperature) determine the adsorption rate of biological building blocks on mineral surfaces, resulting in a complex array of conditions [170]. Lambert's review concludes that while amino acids polymerization can be favored in the adsorbed state, it results in a slower overall process. Surman et al.'s work systematically explored the polymerization of amino acids in different environments, including mineral surfaces, revealing distinct product ensembles as a result of environmental variations[169].

Clay minerals, particularly montmorillonite, have shown improved yields and longer peptides than in other experiments, suggesting their potential roles in polymerization, protection against hydrolysis, and improved directionality through surface adsorption [161, 171].

The roles of mineral surfaces in the abiotic synthesis of RNA monomers have also been explored, with borate minerals aiding the stabilization of ribose and phosphate minerals providing a pathway for prebiotic phosphorylation of nucleosides into nucleotides [172].

The potential role of mineral surfaces in protecting, selecting, and catalyzing reactions of prebiotic organic molecules, hypothesized as an important stepping-stone in the transition from simple chemicals to complex organic molecules. Mica and other clays, along with various transition metals such as Fe, Ni, Co and Cu, and sulfide and borate minerals, are proposed to have played key catalytic roles in the synthesis of prebiotic organics [173, 174, 175].

4.13 Impact Theory

Some question if prebiotic molecules came from space, like carbonaceous chondrites in meteorites particularly carbonaceous chondrites found in meteorites. These meteorites contain organic carbon, standard amino acids and nucleic acid bases. This raises the question: Did the prebiotic ingredients arrive on Earth through meteorites and comets?

Supporters of the impact theory argue that meteorites and comets that reached the early Earth's surface contained sufficient organic carbon to create an abundant prebiotic soup [176, 177].

Abiogenesis suggests a series of evolutionary steps leading from a prebiotic mixture to the formation of a proto-organism. Aaron S. Burton et al. explore the implications of nonterrestrial amino acids and nucleobases in meteorites, suggesting that meteoritic bombardment and differences in parent-body chemistry lead to diverse amino acid structural types. The study emphasizes the revolutionary impact on Astrobiology, suggesting that extraterrestrial-synthesized molecules may have played a role in life's origins. The research highlights the diverse environments within the parent bodies of meteorites, which offers a unique range of prebiotic chemistry on Earth [178].

Organic molecules on early Earth had different sources: delivery by extraterrestrial objects, synthesis due to impact shocks, and synthesis by other energy sources like ultraviolet light or electrical discharges. The dominance of each source depended on the composition of the early terrestrial atmosphere [179].

Supporters of the impact theory claim that meteorites and comets brought sufficient organic carbon to Earth's surface to create a rich soup. However, questions arise about whether this material could survive intense heating during entry into the Earth atmosphere and subsequent collisions [179].

Exogenous sources continue to bring organic molecules to Earth. This includes interplanetary dust particles gently decelerated by the atmosphere and meteorites that are large enough to survive but not completely ablated during their fall [180, 181, 182].

Studies in Stevns Klint, Denmark, have suggested that a considerable portion of cometary organics might survive giant impacts [183]. However, measurements and simulations argue otherwise [180, 184]. Zahnle and Grinspoon propose the potential role of orbital evolution and circularization of orbits through mutual collisions in enhancing Earth's collection efficiency and increasing dust accretion [185].

4.14 Evolution Theories

Over time, the earth has seen mammoths and dinosaurs, ice ages, continents coming together or drifting apart, and dramatic comet and asteroid impacts. It has also witnessed

the birth of curious humans eager to understand it all. In the "Earth's Deep History" book presented by Martin J. S. Rudwick, the discussion explores the seventeenth century alongside Archbishop James Ussher, who claimed the cosmos was created in 4004 BC. The narrative then shifts to the late 1700s and early 1800s, marking an intellectual triumph. During this time, curious thinkers, now identified as "geologists," successfully realized that rocks, fossils, mountains, and volcanoes serve as Earth's natural historical archives [186]. In 1907, based on Darwin's idea of evolution [187], Arthur Holmes utilized radioactive decay of uranium to determine the age of ancient terrains in Sri Lanka, estimating it to be around 1640 million years [188]. To establish a timeline of evolution, we need both paleobiological and biogeochemical evidence. This timeline not only helps us understand the sequence of evolutionary events, but also provides insights into how evolutionary rates varied over time [189].

Life seems to have been present when the oldest well-preserved sedimentary rocks were formed [190]. The exact timing of life's evolution before this period is uncertain. In ancient metaturbidites from southwestern Greenland, there is reduced carbon (graphite) with a C-isotopic composition consistent with autotrophy [191]. In addition, structures interpreted as microbialites have been reported, although subject to controversy. These rocks were dated about 3710 million years ago [192]. Another indication of early biological carbon fixation comes from a ^{13}C -depleted organic inclusion in a zircon dated at 4100 ± 10 million years ago [193]. However, there is some uncertainty due to the possibility of abiological fractionation in this small sample from Earth's early interior.

The second significant milestone in the history of life was the initial increase in oxygen in the atmosphere and surface oceans, known as the Great Oxygenation Event (GOE). This environmental transition is crucial biologically and is recorded geologically and geochemically. The end of large mass-independent sulfur isotope fractionation in sedimentary sulfides and the last appearance of redox-sensitive minerals such as detrital grains in sedimentary rocks are key indicators of the GOE [194].

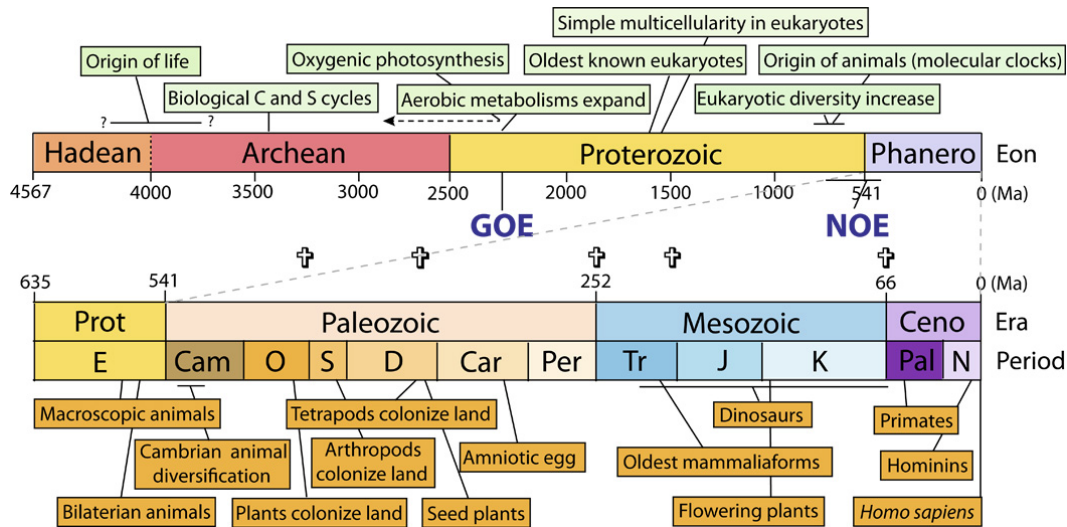


Figure 8: **The timeline of evolution through fossils, environmental clues, and precise geochronology**[195]. Phanero, Phanerozoic; Prot, Proterozoic; Ceno, Cenozoic; E, Ediacaran; Cam, Cambrian; O, Ordovician; S, Silurian; D, Devonian; Car, Carboniferous; Per, Permian; Tr, Triassic; J, Jurassic; K, Cretaceous; Pal, Paleogene; Neo, Neogene. The crosses indicate the times of major mass extinctions.

4.15 Quantum-level simulations and Emergent Molecules

In the broader context of Artificial Life research, simulations play a pivotal role in elucidating the principles of complexity and contributing to a more generalized understanding of living systems. The discourse surrounding the interpretation of results in Artificial Life research is underscored by controversy, questioning whether simulations can be considered as authentic manifestations of life [196, 197].

The strong version of the Artificial Life perspective posits that emergent computational patterns in simulations not only simulate life but actually realize the phenomenon of life. This point of view suggests that with robust computational support and appropriate criteria, genuine examples of life could be synthesized. However, the strength of this Artificial Life thesis is contingent on specific definitions and paradigms, leading to ongoing debates about its validity and limitations [197, 198]. This raises fundamental questions about the intricate relationship between explaining life through computational models and defining the emergent patterns in these models as true instances of life.

The development of a general reactive machine learning (ANI-1xnr) using an active learning approach combined with a nanoreactor molecular dynamics sampler has been completed and trained. This model is capable of simulating the behavior of C, H, N, and O elements in a wide range of real-world reactive systems. It closely matches experimental structures in carbon solid-phase nucleation and graphene ring formation studies and produces reliable predictions in cases where experimental data is not available [199].

Additionally, an ab initio nanoreactor simulation to discover new molecules and mechanisms in chemical reactions showed new pathways for glycine synthesis from primitive compounds that were proposed to exist on the early Earth. The nanoreactor allows reactions to occur freely and explores a wide range of possibilities. But the nanoreactor is not designed to replicate the physicochemical conditions of any specific environment [200].

In a quantum-level theoretical study employing ab initio molecular dynamics, a departure from the activation energy of electric discharge, it was observed that a strong electric field favors the formation of small intermediate molecules, such as formic acid and formamide, in Miller-like experiments [201].

Simulations in Artificial Life research can contribute to a more general understanding of living systems. The role of simulations in the context of Artificial Life research, mentions that there is controversy regarding how to interpret the results of Artificial Life research and whether simulations can be considered as realizations of life [196, 197]. The strong version of Artificial Life claims that emergent computational patterns in simulations may not simply simulate life but actually realize the phenomenon of life. This perspective suggests that by having strong enough computational support and appropriate criteria, it is possible to synthesize genuine examples of life. However, the strong thesis of Artificial Life depends on specific definitions and paradigms used, and there are debates about the validity and limitations of this claim [197, 198]. It raises questions about the relationship between explaining life through computational models and defining the emergent patterns in these models as true instances of life.

5 The Miller-Urey Experiment

Stanley Miller arrived at the University of Chicago in 1951 to pursue a Ph.D. He attended a lecture by Harold Urey, a Nobel Prize-winning professor of chemistry who had isolated deuterium in 1934, on his 1952 paper [25]. Miller approached Urey about conducting a prebiotic synthesis experiment. Initially discouraged, Urey eventually agreed to let Miller proceed for a year [25].

In 1953, Stanley Miller and Harold Urey conducted the most renowned experiment simulating early Earth conditions [49]. They hypothesized a hot, water-covered Earth with a reducing atmosphere. In a sealed glass apparatus, they created an atmosphere containing ammonia (NH_3), methane (CH_4), and hydrogen (H_2). Water (H_2O) was boiled, and the gas and vapor mixture circulated past electrodes producing sparks (see Figure 9). After a week, amino acids such as glycine and alanine were confirmed via thin-layer chromatography [49].

Miller used water (H_2O), methane (CH_4), ammonia (NH_3), hydrogen (H_2), and an electric arc to simulate the primitive ocean, atmosphere, and lightning. Paper chromatography showed that amino acids were produced in Miller's experiment, suggesting the formation of organic compounds under primitive Earth conditions [49]. Miller and his colleagues further studied electric-discharge synthesis of amino acids [176, 202].

Subsequent experiments with different setups and gas compositions detected additional amino acids and organic acids [76]. Experiments with hydrogen sulfide (H_2S) produced sulfur-containing amino acids [203]. Oxygen inhibited amino acid production, while replacing the condenser and spark discharge resulted in fewer amino acids and more hydrocarbons [76]. Adjusting hydrogen content ensured reducing conditions even at higher carbon oxidation states [41].

The spark discharge primarily produced aldehydes ($-\text{CHO}$) and hydrogen cyanide (HCN), along with amines ($-\text{NH}_2$), nitriles/cyanides ($-\text{CN}$), and isonitriles ($-\text{NC}$) [204, 76]. The gases produced included carbon monoxide (CO) and hydrogen (H_2). The Strecker synthesis was proposed for amino acid formation, as similar results were obtained with hydrogen, hydrogen cyanide, and aldehydes [78]. Hydrocarbons in the spark likely formed through formaldehyde condensation [76].

Various organic acids resulted from nitrile hydrolysis, including pathways for alanine

synthesis [76, 78]. Adding ammonium iron(II) sulfate $(\text{NH}_4)_2\text{Fe}(\text{SO}_4)_2$ to explore iron catalysis showed inconclusive results [78].

In weekly sample extractions, amino acids formed continuously until saturation, ammonia decreased, and hydrogen cyanide and formaldehyde appeared initially and then degraded. Increased gas circulation and discharges over boiling water yielded similar quantities of amino acids and hydroxylated substances [205]. Silent discharge experiments detected fewer amino acids and aldehydes, with little hydrogen cyanide [206, 78].

This mixture, known as prebiotic broth, contained various small organic compounds. Subsequent research identified the Strecker reaction as a major synthetic route to amino acids. For example, glycine was detected among the products of the electric-discharge reaction from aldehydes, hydrogen cyanide, and ammonia [207]. Oro and Kimball synthesized adenine from hydrogen cyanide and ammonia [55, 63]. Sanchez, Ferris, and Orgel showed that cyanoacetylene, a product of electric discharge on methane and nitrogen, is a plausible source of pyrimidine bases such as uracil and cytosine [65, 208]. Sugars were also readily formed from formaldehyde [68, 209].

This discovery renewed interest in creating prebiotic broths similar to those produced in the Miller-Urey experiment.

Using different gas mixtures increases the variety of chemical compounds observed in these experiments [210, 76, 211, 212, 213]. The gas mixture can also be changed to more oxidizing mixtures, which might be closer to early Earth's atmosphere. However, previous experiments concluded that a highly reductive atmosphere was needed to produce a complex broth [212].

Bada et al. showed that adding oxidation inhibitors like ferrous iron before hydrolysis greatly increased the yield of amino acids, even in a more oxidizing gas mixture [210]. This finding challenged the belief that Earth's atmosphere was too oxidizing for a prebiotic broth to form naturally.

The production of organic compounds using electric discharges in neutral gas mixtures was found to be less efficient than the reducing gas mixture of the original setup. However, significant amounts of amino acids were still produced from neutral gas mixtures [210].

Using borosilicate glass as a catalyst in the reaction vessel significantly increased the

diversity and yield of organic molecules [214].

The catalytic role of transition metals such as nickel / iron (Ni / Fe) and iron sulfide (FeS) can help reduce nitrogen gas (N_2) to ammonium (NH_4^+) in a water-based solution [215, 216].

In our group's previous work, we mentioned that the production of molecular species, such as polyethyleneglycol, which are typically not favored under reactor conditions, suggests the presence of unidentified organocatalysts [217].

Instead of using a spark, other energy sources like UV light [218, 219], X-ray [220, 221], laser photolysis [222], and high-energy proton irradiation can replace the spark [223].

Experiments suggested that complex molecules that include amino acid precursors were formed from simple molecules like HCN in the gas phase [223].

A recent study by Mohammadi et al. proposed that formic acid, an intermediate in Fischer–Tropsch synthesis, could have accumulated on early Earth through various pathways [224, 225]. They also suggested that ammonium salts of formic acid might have been precursors to formamide. Ferus et al. revisited the Miller–Urey experiments using electric discharge and laser-driven plasma simulations in a reducing atmosphere to study nucleobase formation from formamide.

In previous findings performed in our group, reactor design is highlighted as an important factor affecting the complex mixture of a Miller-Urey-type experiment [226].

In our recent work, we demonstrated that the type of spark generator employed significantly influenced the range of synthesized compounds [1].

Inspired by Francis Crick's development of a molecular model for DNA [227] and Miller and Urey's "Prebiotic Soup" hypothesis [49, 76, 78], Leslie Orgel began exploring the relationship between proteins (polymerized amino acids) and DNA/RNA (polymerized nucleic acids). He hypothesized that these biopolymers had an early connection during chemical evolution and envisioned peptide-nucleic acid polymers as potential predecessors [39].

However, Orgel's theory remains unproven due to challenges in polymerizing abiotically generated monomers in a prebiotic broth. This lack of polymerization ability is a significant obstacle when working with the Primordial Soup. Interest has grown in understanding how environmental conditions could have facilitated self-organization and

the transition into information [16]. Orgel proposed that once reproducible polymers are achieved from any natural abiotic material, Darwinian evolution principles would promote selection and evolution [16].

Despite Orgel's hypothesis, the chemical evolution of abiotic material remains debated. The significance of DNA/RNA versus proteins/peptides in prebiotic chemistry is a central point of interest. Recent evidence includes the simultaneous synthesis of amino acids and nucleobases in a Miller-Urey-type experiment [228].

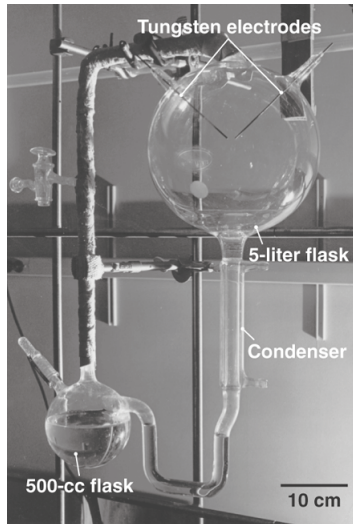


Figure 9: Setup used in the original Miller experiment [206].

6 The Complexity of Prebiotic Soup Characterization

Exploring the origins of life, we confront a complex puzzle: deciphering the array of compounds produced during the abiotic synthesis within prebiotic soups. This diversity requires an exact examination of the molecules' physical and chemical attributes, laying the groundwork for our understanding of these intricate chemical mixtures and how we can extract meaningful information from them.

Our work is to shed light on the mixture and apply various analytical techniques to unravel the intricacies of prebiotic chemistry. We examine mass spectrometry closely, chromatography, and spectroscopy, aiming to enhance our comprehension of this complex chemical domain.

6.1 Introduction to Analytical Challenges

The evolution of life is explained by the creation of its essential elements. Despite the exploration of numerous scenarios, we are faced with a significant challenge: the vast diversity of chemical compounds generated in laboratory simulations of prebiotic environments. This complexity challenges us to consider how to enhance our analytical techniques to isolate and identify the essential components for life among this chemical diversity. We are approaching the discovery of cutting-edge analytical technologies that could further reveal the secrets of life's beginnings.

6.2 Key Analytical Techniques in Prebiotic Systems Chemistry

In recent decades, chemical analytical methods have seen rapid advances, providing detailed molecular insights into individual samples. Techniques such as mass spectrometry, chromatography, UV-vis, and IR spectroscopy have been pivotal in enhancing the separation and detection of samples. These tools have enabled the analysis of thousands of chemicals, offering a comprehensive view of the complex mixtures that we study.

6.3 Instrumental Analysis and Its Contributions

Mass Spectrometry (MS) GC-MS and FTMS: These methods allow for the detailed analysis of both volatile and nonvolatile components, providing a spectrum of the mass-to-charge ratio (m/z) of the molecules. By analyzing the mass-to-charge ratio (m/z) and volatile profiles, we uncover the molecular elemental formula (and structure) that may hint at prebiotic pathways.

Chromatography and Spectroscopy HPLC-UV: This technique provides electromagnetic spectra of nonvolatile synthesised compounds, offering clues into their structure. FTIR Spectroscopy: This technique is based on the vibrational levels of the chemical functional groups. Infrared absorption technique is used to provide information regarding the non-volatile synthesized chemicals in the liquid phase and volatile molecules in the gas phase. It provides us the molecular architecture of the synthesized prebiotic samples.

Imaging and Structural Analysis SEM and XRD: Through scanning electron microscopy and X-ray diffraction, we visualized the morphology and crystalline structure and the elemental composition of solid prebiotic artifacts.

Combining the techniques described above helps us to understand the complex mixture of chemicals that could have led to the start of life on Earth. This mixture of analytical techniques allows us to dive deep into prebiotic chemistry, identifying not just the molecules we know are important, but also discovering physical and chemical characterizations of the soup mixture that could be part of the early days of Earth [93].

By applying a non-targeted approach, we gather as much information as possible from the Miller experiment. With this approach, we're not just looking for specific molecules; we're exploring the entire chemical landscape that could have existed before life began. This broad strategy helps us uncover the variety of substances, from simple to complex, that might have played a role in the origins of life. As technology improves, our ability to detect and understand these substances improves, which helps us to have a big picture of this highly prebiotic mixture chemistry.

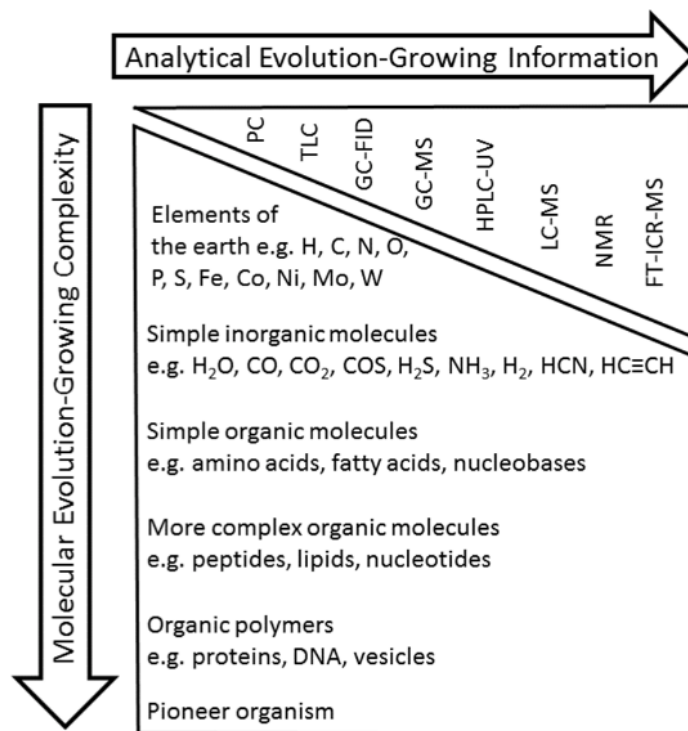


Figure 10: **Bottom-up molecular evolution and analytical advancement.** The Molecular Evolution and Advancements in Analytical Techniques in the Study of Life's Origin. Reproduced without permission from MDPI [229].

6.4 Systems Chemistry and Retro Synthetic Approach

The reaction processes in complex mixtures often cannot be analyzed using simple methods because many interactions can influence each other. These challenges are known from the analysis of stoichiometry and gene expression. One way of investigating the properties of a complex chemical system is by interpreting it as a network [230].

The field of systems chemistry explores the dynamic and complex interactions within a network of chemical reactions. This approach is crucial to understanding the emergent properties and collective behaviors of molecular systems, which are often more than the sum of their parts. By analyzing these networks, scientists can gain insight into the rules and principles that govern the behavior of complex chemical mixtures [231].

The retrosynthetic method is a strategic approach used in organic chemistry to plan the synthesis of complex molecules by working backward from the target molecule to

simpler precursor molecules. This method involves breaking down the target molecule into smaller, more readily available starting materials, which can then be synthesized using known chemical reactions. The retrosynthetic method allows chemists to design efficient and practical routes for the synthesis of complex organic compounds by identifying key disconnections and retrosynthetic steps. This approach is widely used in the field of organic synthesis to streamline the process of creating complex molecules [232, 233].

The retrospective synthesis method, or retrosynthetic analysis, serves as a bridge between systems chemistry and traditional organic chemistry. This method, which is adept at reverse engineering of chemical systems, can be instrumental in establishing connections within chemical networks. It mirrors the process of planning and constructing sequences of chemical bonds in the synthesis of complex organic molecules. While a comprehensive methodology for integrating systems chemistry is still emerging, researchers are making significant strides. By applying retrosynthetic principles, they are deciphering the fundamental rules that govern interactions among members of molecular networks. This fusion of retrosynthetic strategies with systems chemistry is opening new frontiers in understanding and manipulating complex chemical systems [234, 235, 232, 233].

In the field of prebiotic chemistry, systems chemistry aims to enhance the understanding of various environmental conditions and initial substances to synthesize non-biological originated materials in an organized approach.

The exploration of networks aimed to find conditions favorable for self-reproduction in a complex mixture. In this complex web of chemical reactions, order could emerge autonomously, potentially undergoing a selection process that simplified the network into present-day biological metabolisms. For an evolutionary process to occur, the network needs to be energetically driven and reach a state close to chaos. Only then can the system maintain enough developmental capability and exhibit complex dynamics. This suggests that the order in contemporary organisms is a result of a natural order rooted in organic chemistry rather than a selection process. Self-reproduction would occur if a substantial number of catalytic polymers formed within a network of organic molecules [236].

These studies consistently aimed to confirm or adhere to specific hypotheses or theories, restricting the options for creating precursor chemicals and linking them together.

Systems Chemistry, as a scientific discipline, focuses on examining networks of interacting molecules, aiming to generate new functions from a collection of molecular components at various class system levels, resulting in emergent properties [234].

In the context of prebiotic chemistry, system chemistry aims to systematically broaden investigations into various environmental conditions for the synthesis of abiotic material in a systematic way [231].

The most complex synthetic chemical systems known today are less intricate than the simplest biological systems. This prompts the question of which chemical systems on the prebiotic Earth could have acquired enough 'complexity' to give rise to life [234, 237].

Retro synthetic' method, capable of reverse-engineering chemical systems, might be the most effective approach. This method could assist in creating connections between members of chemical networks, much like planning and constructing sequences of chemical bonds in the synthesis of complex organic molecules. Although a comprehensive methodology for systems chemistry is still in its infancy, researchers are laying the groundwork by deciphering the fundamental rules that govern interactions among members of molecular networks [234, 235].

What does 'complexity' mean in systems chemistry? In this field, we borrow a definition from information science, and it fits well: complex systems need more information for their description compared to simple systems. Specifically, complex chemical systems have richer connections among their members than simpler ones. While a single molecule's complexity is limited by the bonds its atoms can form, the overall complexity of a group of interacting molecules can be more than the sum of individual complexities. These interactions might involve supramolecular fits, subcomponent exchanges, or catalytic processes. As the connections between the members of the networks become denser, it becomes easier for complex behavior to emerge, allowing the networks to respond to stimuli in more intricate ways [234, 238].

6.4.1 Gas Chromatography-Mass Spectrometry (GC-MS)

GC-MS typically involves the use of a gas chromatograph with a single capillary column. The column is linked to a detector like the flame ionization detector (FID) or thermal conductivity detector (TCD) through an interface to generate chromatographic peaks.

However, for more complex samples, mass spectrometry (MS) provides mass spectra unique to each compound, aiding in identification. In this work, we employed the mass spectrometry in the gas chromatogram detector. In GC-coupled mass spectrometers, electron ionization (EI) is commonly used as the ionization source. In EI, high-energy electrons interact with gas-phase atoms or molecules to form ions before being analyzed in the detector.

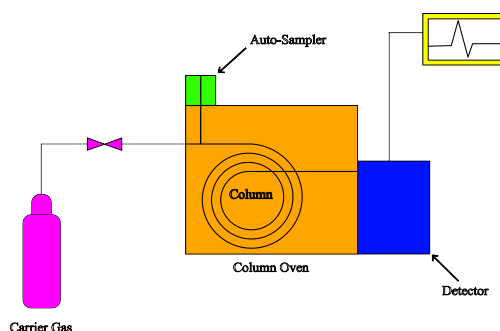


Figure 11: **Schematic representation of a Gas Chromatography-Mass Spectrometry (GC-MS) system.** The system is composed of a gas supply, an injection port, a chromatographic column, a mass spectrometer, and a data analysis unit. The sample is vaporized in the injection port, separated by the column, ionized and analyzed based on mass-to-charge ratio in the mass spectrometer, and the resulting data are processed and displayed in the analysis unit.

In gas chromatography, separation occurs mainly by dividing the analytes between the gaseous mobile phase and a stationary phase while passing them through a capillary column. The column is coated with a thin liquid layer of stationary phase, which holds onto the gaseous analytes carried by the mobile phase. Helium or hydrogen are commonly used as carrier gases. Stationary phases vary in polarity. Analytes are partitioned differently based on properties such as polarity and boiling points [239]. Those with a stronger attraction to the stationary phase take longer to pass through the column, while those with a weaker attraction pass through more quickly [240]. A typical GC setup includes a carrier gas source, sample injector, capillary column, oven, and detector. We'll briefly discuss the operation of these key components below.

A mass analyser measures the mass-to-charge ratio (m/z) of ions produced from the analytes. MS detection involves three main steps: ionization, separation, and detection.

Let us briefly discuss each step.

Firstly, the analyte enters the mass spectrometer through the ionization source. Two common ionization sources are used: electron impact (EI) and chemical ionization (CI), with EI being more prevalent. In EI, molecules are bombarded with high-energy electrons (typically 70 eV), ionizing them by removing an electron. However, these molecular ions are unstable, this leads to fragmentation. These fragments can be identified based on characteristic patterns [240].

Secondly, ions are separated based on their mass-to-charge ratio (m/z) within the mass analyzer, which operates in a vacuum. Two common types of mass analyzer are typically used, namely, quadrupole (q) and time-of-flight (TOF). In this study we used the quadrupole (q) system. In quadrupole MS (qMS), separation is achieved by adjusting the radio frequency (rf) and direct current (dc) voltages applied to the four rods of the quadrupole. This manipulation allows only ions with specific m/z ratios to reach the detector at a given rf/dc ratio.

Quadrupole mass analyzers consist of four parallel rods, with rf applied to two opposite rods and dc voltage applied to the remaining two. This setup creates a changing magnetic field through which ions travel. By adjusting the rf and dc voltages, only one ion becomes resonant and reaches the detector, while others collide with the rods [240].

The final step of MS involves detection of ions. This is typically performed in qMS detectors using an electron multiplier.

Quadrupole MS instruments can operate in two modes: full-scan mode, which is used for identifying unknown compounds, and selected-ion monitoring (SIM), which is more sensitive and used for analyzing target compounds.

SPME Solid phase micro-extraction (SPME), developed in the early 1990s by Pawliszyn et al. [241], involves using a fiber coated with a stationary phase to extract compounds from gas or liquid phases. It is known as a sorptive technique because analytes partition into the stationary phase [242]. SPME offers three sampling modes [243]: headspace extraction (HS), direct immersion, and membrane-protected SPME. Commercially available SPME coatings include polydimethylsiloxane (PDMS), carbowax (CAR), polyacrylate (PA), polyethylene glycol (PEG), and adsorbents like

divinylbenzene (DVB), or mixtures thereof. SPME is known for its excellent sensitivity, especially for volatile compound extraction. It is capable of extracting a wide range of volatile compounds, making it potentially suitable for gas phase analysis. This method reduces interference from nonvolatiles, leading to simpler chromatograms for easier compound identification and quantification.

6.4.2 Mass Spectrometry

Mass spectrometry serves as a versatile analytical technique for the qualitative and quantitative detection of various substances. The essential requirement for this process is the ability to ionize the substances [244, 245, 246]. Once ionized, different substances can be separated based on their unique mass-to-charge ratio (m/z) [247].

Complex mixtures of substances may require the preliminary separation of individual components before mass spectrometry analysis can be performed [248]. This separation can be achieved through suitable chemical purification methods or chromatographic techniques, such as coupling the mass spectrometer with a chromatograph [247]. This setup includes a stationary phase that facilitates the separation of substances based on various parameters, such as size, charge, and polarity, resulting in different retention times for different substances [247]. Depending on the mobile phase used in the chromatography process followed by mass spectrometry, the technique is called LC-MS for liquids or GC-MS for volatile liquids or gases [249, 250].

The substance under investigation, known as the analyte, must first be ionized in the ion source. For this purpose [246, 248], various ionization methods are employed, which can be classified into soft and hard ionization techniques [251, 252]. Soft ionization methods, such as Electrospray Ionization (ESI), generally do not cause the molecules to fragment and preserve their original structure. While, hard ionization methods, like Electron Impact Ionization (EI), lead to the fragmentation of molecules [247]. This fragmentation results in a specific ion fragment pattern for each substance, acting as a unique "fingerprint" that can be matched with suitable databases (e.g. NIST) [247].

In a mass analyzer, the generated ions in an ion source are separated by an analyzer based on their mass-to-charge ratio (m/z) [246, 247, 253]. Various techniques are used for this purpose [246, 247, 253]. Examples include Quadrupole, Time-of-Flight, and magnetic or electrostatic sector field, as well as ion trap analyzers [246, 247, 253, 254].

These can be used individually or in combination (as in tandem mass spectrometers) to achieve the desired analysis [246, 247, 253, 254].

Following ions generation, ions accelerate to reach a specific speed dependent on their mass-to-charge ratio (m/z) through an acceleration voltage U [247, 253].

In Equation 1, $v\left(\frac{m}{z}\right)$ represents the velocity of an ion, which depends on its mass-to-charge ratio $\frac{m}{z}$. The velocity is calculated by taking the square root of the product of two times the elementary charge e , the acceleration voltage U , and the inverse of the mass of the ion m , taking into account its charge z . v signifies the speed at which the ion travels as a result of being propelled by the applied voltage U in a mass spectrometer [247, 253].

$$v\left(\frac{m}{z}\right) = \sqrt{\frac{2zeU}{m}} = \sqrt{(2eU) \cdot \left(\frac{m}{z}\right)^{-1}} \quad (1)$$

The accelerated ions then pass through the ion analyzer and interact with magnetic or electric fields depending on their (m/z) ratio [246]. These interacting fields may include an electric quadrupole (quadrupole analyzer) or magnetic and electric fields (in magnetic and electrostatic sector field analyzers). This interaction separates ions with different (m/z) ratios on distinct paths [246, 248, 255].

Another method for separating ions is ion trap analyzers, such as the Fourier Transform Ion Cyclotron Resonance (FT-ICR) analyzer. Ions are initially stored by interaction with an electric quadrupole or a static magnetic or electric field [256, 248, 255, 257, 258]. Changes to these interacting fields or the addition of other fields allow the ions to escape from the trap. Depending on the (m/z) ratios, only ions with a specific (m/z) ratio are released, enabling separation. This process will be explained using an FT-ICR analyzer as an example [257, 258, 259, 260, 261, 262, 263].

In an FT-ICR analyzer, ions are stored by being forced into circular paths with small cyclotron radii within a magnetic field, where the cyclotron frequency f_{Cyc} is their orbital frequency, as shown in Equation 2 where f_{Zyk} denotes the cyclotron frequency, m is the ion mass, z is the charge state of the ion, e is the elementary charge, and B is the magnetic field strength [257]. By briefly applying a broadband electric alternating field (chirp), resonance phenomena occur among the stored ions, since this excitation signal encompasses the cyclotron frequencies of the ions. This causes the excited ions to move synchronously in a circle with a larger cyclotron radius. When the excitation signal is

turned off, the ions continue to move in phase on this path, with their orbital frequency determined by their cyclotron frequency. Since the cyclotron frequency depends on m/z , this leads to the separation of ions with different m/z ratios [257, 258, 259, 260, 261, 263].

$$f_{\text{Zyk}}\left(\frac{m}{z}\right) = \frac{zeB}{2\pi m} = \frac{eB}{2\pi} \cdot \left(\frac{m}{z}\right)^{-1} \quad (2)$$

After separation in the analyzer, the ions need to be detected, which is accomplished with a detector [246, 264]. Various types of detectors are used, such as Faraday cups or secondary electron multipliers (SEMs), which are used in photomultipliers and microchannel plates (MCPs) [247, 253]. When ions hit these detectors, secondary electrons are emitted [256, 265, 266]. These can directly generate more secondary electrons, amplifying the original signal (in MCP detectors), or hit a scintillator to produce photons, which trigger an enhanced signal in a photomultiplier (Daly detector) [267, 255, 265, 266].

In mass spectrometers that feature an FT-ICR analyzer, electrodes serve as detectors [257, 261]. As the ions are excited to a larger cyclotron radius, they approach the radially arranged detector plates, generating a signal with each orbit. Due to the varying cyclotron frequencies of the ions, a cumulative measurement signal emerges, which can be viewed as the superposition of individual ion movements. Through the Fourier transformation, the different m/z ratios of the ions can be derived from this cumulative signal [257, 258, 259, 260, 261, 263].

Mass Defect According to nuclear particle experiments, the total mass of a nucleus m_{nuc} is less than the sum of the masses of its constituent nucleons (protons and neutrons). The mass difference, or mass defect, is given by

$$\Delta m = Zm_p + (A - Z)m_n - m_{\text{nuc}} \quad (3)$$

where Zm_p is the total mass of the protons, $(A - Z)m_n$ is the total mass of the neutrons, and m_{nuc} is the mass of the nucleus. According to Einstein's special theory of relativity, mass is a measure of the total energy of a system $E = mc^2$. Thus, the total energy of a nucleus is less than the sum of the energies of its constituent nucleons. The formation

of a nucleus from a system of isolated protons and neutrons is therefore an exothermic reaction—meaning that it releases energy. The energy emitted, or radiated, in this process is $(\Delta m)c^2$.

The binding energy is equal to the amount of energy released in forming the nucleus and is therefore given by Eq. 4 for the binding energy.

$$E_b = (\Delta m)c^2 \quad (4)$$

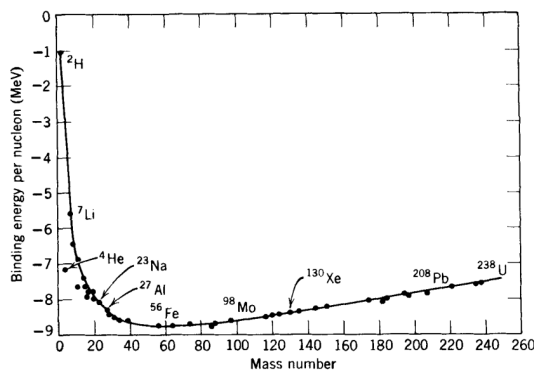


Figure 12: **Binding energy of nuclei as a function of mass number.** Reproduced by Permission from: John Wiley & Sons 1992 [268].

Kendrick Mass Defect The Kendrick mass scale condenses the data in such a way that homologs can be distinguished by their consistent Kendrick mass defect (KMD) [247]. As modern mass spectrometry instruments continuously advance in resolution and mass precision, the Kendrick mass scale helps us to analyse complex mixtures. The scale is based on the precise mass of CH_2 group that has a 14.015650 u mass scale of the IUPAC. The Kendrick mass scale convert the IUPAC mass scale m_{IUPAC} , to the Kendrick mass scale m_{Kendrick} , being determined by the ratio $\frac{14.000000}{14.015650} = 0.9988834$:

$$m_{\text{Kendrick}} = 0.9988834 \times m_{\text{IUPAC}} \quad (5)$$

The Kendrick mass defect is thus represented by:

$$m_{\text{defect Kendrick}} = m_{\text{nominal Kendrick}} - m_{\text{Kendrick}} \quad (6)$$

In this context, $m_{\text{nominal Kendrick}}$ is the nominal Kendrick mass, which is the integer value closest to the calculated Kendrick mass.

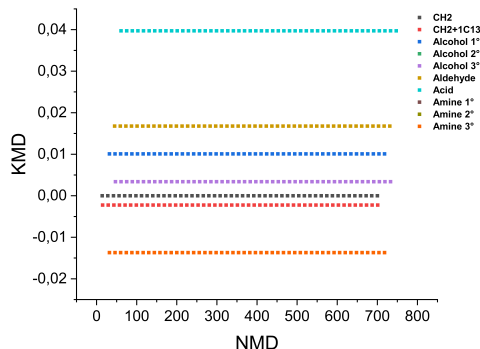


Figure 13: **Simulated KMD vs. Nominal Kendrick mass for some compound classes of CH_2 .**

6.4.3 High-performance Liquid Chromatography (HPLC)

High-Performance Liquid Chromatography (HPLC) represents a critical advance in the field of analytical chemistry, enabling the precise separation, identification, and quantification of the components within complex mixtures. This technique has become indispensable in a wide range of scientific disciplines, including pharmaceuticals, environmental science, and biochemical research [269, 270].

HPLC operates on the principle of liquid chromatography, where the mixture to be analyzed is passed along with a liquid solvent (mobile phase) through a column packed with a solid adsorbent material (stationary phase). The components of the mixture interact differently with the stationary phase, leading to their separation as they move at different speeds. The efficiency of HPLC, attributed to the high pressures used to push the mobile phase through the column, allows the separation of components that would otherwise co-elute under normal gravitational forces [271].

The combination of HPLC with various detectors, such as UV/VIS spectroscopy, refractive index detectors, photodiode array (PDA), and mass spectrometry (MS), has further expanded its analytical capabilities. For instance, HPLC-MS has become a powerful tool in proteomics and metabolomics, offering sensitive and selective analysis of complex samples [272].

At its core, HPLC leverages the differential affinities of compounds in a mixture to create a stationary phase and a mobile phase. The stationary phase, typically a column containing silica-based particles, provides resistance against the flow of the mobile phase, which can be a variety of solvents. When a mixture is introduced into the column, its constituents interact with the stationary phase to differing degrees on the basis of their polarity, size, and other chemical properties. As the mobile phase passes through the column under high pressure, compounds are retained for different durations before being eluted and detected, effectively separating them.

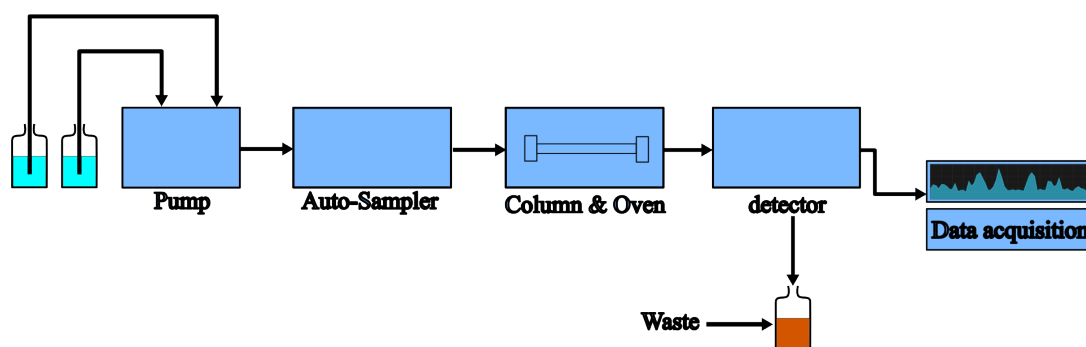


Figure 14: **Schematic illustration of a High-Performance Liquid Chromatography (HPLC) system.** The essential components include a solvent reservoir, pump, injector, analytical column, detector, and data processing system. The solvent from the reservoir is pumped through the column where the separation of the sample occurs. The detector measures the analytes and the results are processed for analysis.

The power of HPLC lies in its versatility. By modifying the composition of the stationary and mobile phases, as well as other operational parameters such as temperature and flow rate, the HPLC can be adapted to analyze a vast range of compounds. For instance, reverse-phase HPLC that was employed in this work used a nonpolar stationary phase and a polar mobile phase. This method is commonly used for the separation of small molecules.

Detection in HPLC systems is often performed using UV-VIS absorbance, which is suitable for compounds that absorb light within the ultraviolet or visible spectrum. Other detectors, like fluorescence and diode array detectors, are used for specific applications requiring heightened sensitivity or simultaneous detection of multiple wavelengths, respectively [273].

The coupling of HPLC with MS has expanded the technique's applicability even further, allowing for the characterization of molecular structures through mass analysis. This tandem approach, known as LC-MS, can provide both the high resolution necessary to separate complex mixtures and the ability to identify and quantify substances by their mass-to-charge ratios [274].

6.4.4 UV-Visible Absorption spectroscopy

UV-Vis spectroscopy operates on the principle that when continuous radiation passes through a transparent medium, selective absorption of radiation occurs, leading to the formation of an absorption spectrum characterized by distinct gaps. This phenomenon is a result of energy uptake by atoms or molecules, facilitating a transition from a lower-energy ground state to a higher-energy excited state. As shown in Figure 15, a process depicted by quantized excitation models.

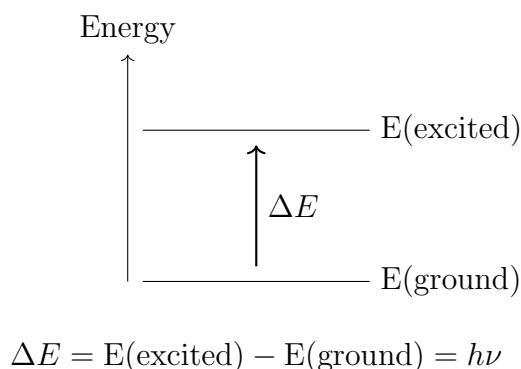


Figure 15: **Energy level transition from ground state to excited state.**

The specificity of UV-Vis spectroscopy lies in its ability to probe transitions between electronic energy levels, within the ultraviolet and visible regions of the electromagnetic spectrum. This absorption of energy prompts an electron to ascend from an occupied molecular orbital, typically the highest occupied molecular orbital (HOMO), to an unoccupied orbital with greater potential energy, known as the lowest unoccupied molecular orbital (LUMO). The energy disparity between these electronic states in molecules typically spans from 125 to 650 kJ/mole, indicating the quantized nature of electronic transitions [275].

The electron distribution within molecular orbitals—ranging from sigma (σ) orbitals

associated with single bonds, pi (π) orbitals from double bonds, nonbonding (n) orbitals, to the highest energy antibonding (σ^* and π^*) orbitals—illustrates the potential transitions. However, not all conceivable transitions are manifest. This is the imposition of selection rules that restrict transitions based on changes in spin quantum number and other molecular symmetries [275]. (See Figures 16 and 15).

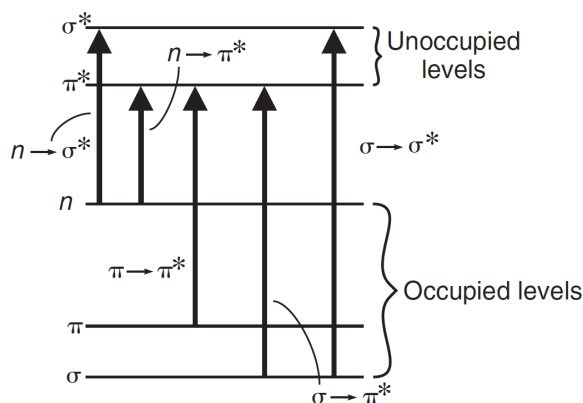


Figure 16: **Electronic energy levels and transitions.**

Despite the theoretical prohibition of some transitions, exceptions are observed, albeit with reduced intensity. Such forbidden transitions typically exhibit lower molar absorptivity compared to allowed transitions.

There are a range of potential electron transitions, each characterized by distinct energy levels. Some of these transitions are particularly mentioned in Figure 17 (Alkanes are exception here).

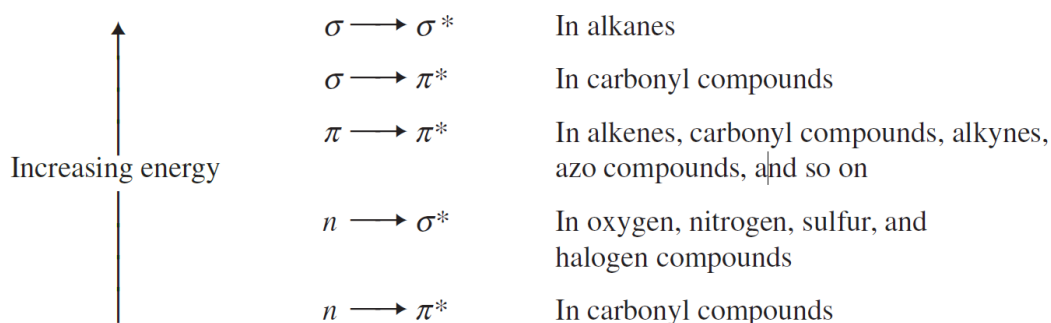


Figure 17: **Electron transitions and their typical compounds [275].**

The Beer-Lambert law quantifies the relationship between light absorption and the concentration of absorbing species within a sample, as shown in Equation 7. Where A represents absorbance, I_0 and I the incident and transmitted light intensities respectively, c the molar concentration, l the path length of the sample cell, and ε the molar absorptivity. This law is the basis for the use of UV-vis spectroscopy to analyze and measure solute concentrations by looking at absorbance at specific wavelengths. [275].

$$A = \log \left(\frac{I_0}{I} \right) = \varepsilon cl \quad (7)$$

The Beer-Lambert law allows UV-vis spectroscopy to serve as a robust analytical tool in the characterization of organic samples, offering insights into molecular structures, electronic configurations, and the concentration of components within a mixture. Its application extends across various domains.

6.4.5 Fluorescent Analysis

Light emission from an atom or molecule not in thermal equilibrium with its surroundings, like black body radiation, referred as luminescence. Luminescence occurs when the atom or molecule relaxes from a higher energy state (A^*) to a lower one (A). This can be categorized on the basis of how the initial excited state (A^*) is achieved; for example, chemiluminescence results from chemical reactions, while photoluminescence occurs through photon absorption. Photoluminescence is divided further into fluorescence and phosphorescence, differing in how the excited molecule's electron spin state changes as it returns to its ground state [276, 277].

Historically, before the discovery of quantum mechanics, this distinction was made by observing that fluorescent materials stop emitting light immediately after the light source is removed, while phosphorescent materials continue to glow in the dark even after the excitation source is gone. A typical fluorescence lifetime is in the range of 1–10 ns, while phosphorescence lifetime usually lies in the range of ms–s and even longer.

Fluorophores are essential in fluorescence spectroscopy. They are the parts of molecules responsible for making them glow. Typically, fluorophores are molecules containing π electrons or aromatic rings, such as tyrosine, tryptophan, and fluorescein [278] so that UV/vis radiation can be absorbed.

Radiative relaxation leads to emission at a specific wavelength λ_{em} , which is typically red-shifted (lower energy) from the λ_{ex} due to some energy loss in the excited state.

6.4.6 UV-Visible Emission Spectroscopy

Exploring the physics of emission spectra in atmospheric pressure plasma experiments, particularly with gases such as CH_4 , NH_3 , and H_2O , involves quantum mechanics and electrodynamics principles. The emission of light in plasma is governed by the quantum transitions of electrons between different energy levels, with the energy difference directly relating to the emitted light's wavelength (λ) or frequency (ν), as described by Planck's equation [279]:

$$E = h\nu = \frac{hc}{\lambda} \quad (8)$$

Here, E denotes the photon energy emitted during the transition, h is Planck's constant (6.626×10^{-34} Js), c represents the speed of light in a vacuum (3.00×10^8 m/s), and λ and ν are the wavelength and frequency of the emitted photon, respectively.

The process of electron impact excitation, crucial in atmospheric plasma interactions with gases, leads to emission. The excitation's cross-section, σ_{exc} , is influenced by the electron's energy (E_e) and the threshold energy (E_{th}) required for excitation [279]:

$$\sigma_{exc}(E_e) \propto \frac{1}{E_e} \ln \left(\frac{E_e}{E_{th}} \right) \quad (9)$$

Upon excitation, the electron's return to a lower-energy state results in photon emission, the energy of which aligns with the difference between the initial and final-state energies (E_i and E_f).

The electron temperature (T_e) in plasma physics impacts the distribution of electron energies. This distribution is often represented by the Boltzmann distribution:

$$f(E_e) \propto E_e^{1/2} \exp \left(-\frac{E_e}{k_B T_e} \right) \quad (10)$$

where $f(E_e)$ signifies the probability density function for electrons of energy E_e (in joules, J), E_e is the electron energy (in joules, J), k_B is the Boltzmann constant (1.381×10^{-23} J/K), and T_e is the electron temperature (in kelvins, K).

These processes and their quantitative frameworks are crucial for understanding the chemistry facilitated by plasma environments, such as those in Miller-Urey type experiments.

6.4.7 Infrared Spectroscopy (IR)

Infrared spectroscopy determines how covalent bonds in molecules absorb specific frequencies of IR radiation, which falls between visible light and microwaves, in the 2.5 to 25 micrometers range. This section of the spectrum is replete with molecular vibrational activities that provide insights into the chemical structure of molecules.

The wavelength (λ) and frequency (ν) of electromagnetic radiation are interlinked by equation $\nu = c/\lambda$, with c denoting the speed of light. Planck's equation, $E = h\nu$, ties energy (E) to frequency, where h is Planck's constant[279]. This relationship underscores the different impacts of radiation across the spectrum, from the high-energy potential of X-rays to disrupt molecular bonds to the gentler nudges by radio frequencies causing nuclear or electronic spin transitions, useful in NMR or ESR techniques.

The strength of a bond and the mass of bonded atoms define the frequency at which molecules absorb IR radiation. Represented as two masses on a spring, the molecule's vibrational energy fluctuates between kinetic and potential forms and is proportional to the vibration frequency:

$$E_{\text{osc}} \propto h\nu_{\text{osc}} \quad (11)$$

The natural frequency of a harmonic oscillator is determined by:

$$\tilde{\nu} = \frac{1}{2\pi c} \sqrt{\frac{K}{\mu}} \quad (12)$$

Hooke's Law provides the basis for this expression, where μ is the reduced mass of the system:

$$\mu = \frac{m_1 m_2}{m_1 + m_2} \quad (13)$$

The force constant K varies between bonds, influencing the vibration frequency. Stronger bonds and lighter atoms result in higher vibrational frequencies.

Triple bonds vibrate at higher frequencies than single or double bonds due to greater bond strength. Conversely, as bonded atomic mass increases, vibrational frequency decreases:

$$\text{C-H} > \text{C-C} > \text{C-O} > \text{C-Cl} > \text{C-Br} > \text{C-I} \quad (14)$$

The vibrational IR spectrum is usually expressed in wavenumbers ($\tilde{\nu}$, cm^{-1}), with a range that typically spans from 4000 to 400 cm^{-1} , encompassing the frequencies for most molecular bonds.

Selective absorption in IR spectroscopy leads to quantized energy state transitions. Each type of chemical bond resonates within distinct portions of the IR spectrum, enabling structural analysis of molecules. For instance, C-H bonds absorb around $3000 \pm 150 \text{ cm}^{-1}$, and C=O bonds near $1715 \pm 100 \text{ cm}^{-1}$, preferring bonds with time-varying dipole moments. Symmetric bonds like in H_2 and Cl_2 are IR inactive due to their constant dipole moments.

6.4.8 (SEM/EDX)

Scanning electron microscopy (SEM) is a cornerstone analytical technique, offering insights into the microstructural characteristics of materials. Originating from the pioneering work of Zworykin et al. in 1942 [280], SEM technology has evolved significantly, driven by advances in electron optics, source technology, and signal processing capabilities.

The operational principle of SEM centers around the interaction between a focused beam of high-energy electrons and the target specimen. This interaction yields a plethora of signals, each encoding different aspects of the specimen's surface and compositional properties. Among these signals, secondary electrons (SE) and backscattered electrons (BSE) are predominant, providing detailed topographical and compositional

information, respectively. The intensity of the BSE signal, for instance, is closely tied to the atomic number (Z) of the specimen, a relationship that can be quantitatively described by the equation:

$$I_{\text{BSE}} \propto Z^{\frac{1}{m}} \quad (15)$$

where I_{BSE} denotes the intensity of the backscattered electron signal, and m is a material-dependent parameter.

Modern SEMs are characterized by their exceptional lateral resolution, reaching down to the nanometer scale, and a depth of field that provides a three-dimensional perspective of the specimen surface. These capabilities are attained by sophisticated lens systems and the utilization of high-brightness electron sources, such as field emission guns (FEG), which enhance both the resolution and signal-to-noise ratio of the acquired images.

The adaptability of SEM is further exemplified by its extensive range of applications, from biological imaging to the investigation of semiconductor devices. The technique's versatility is augmented by various detectors and accessories, enabling specialized analyses such as energy-dispersive X-ray spectroscopy (EDX) for elemental composition analysis [281].

6.5 Combining Techniques for Multi-modal Analysis

One innovative approach for exploring the chemical complexity of prebiotic soups is through multi-modal analysis, which involves merging the capabilities of different analytical instruments. This strategy enhances the chemical information obtained from a single sample, although it demands great attention to the compatibility of sample preparation and analysis protocols across different techniques.

7 Materials and methods

7.1 Miller-Urey Experiment Setup

Experiments were performed in a 5L flask as a reactor equipped with an overpressure valve responding to a pressure of 1.3 bar (NORMAG-Germany) as shown in Figure 18 and Figure 21. First, 300 mL HPLC-grade water (Fisher Chemical) was added to the reactor. The 5L flask was evacuated 3 times using a vacuum pump and subsequently filled with methane (N25 Air Liquide-Germany) to effectively remove any residual air from the flask and degas the water. Subsequently, the desired amount of ammonium hydroxide 35% w/w solution (see Table 2)(Fisher Chemical) was injected into the flask through a silicon septum (DWK Life Sciences-Germany) using a glass syringe (Fortuna Optima Luer Lock-Germany) with a needle. Then the 5-L flask was partly immersed in a bath of heated silicon oil, equipped with a magnetic stirrer. The reactor was allowed to equilibrate overnight prior to sparking. The electric discharge occurred in the gaseous phase between two semi-sharp electrodes. We employed a tungsten electrode with 6 mm in diameter, 15 mm cone length, and a tip with 0.5 mm radius. Driven by flyback-based (FB-1), (FB-2) or a capacitor-based (C-1) high-voltage spark generators were used (see Figure 24 and Table 4).

All experiments were carried out for 5 days. We conducted four sets of experiments, focusing on temperature (samples 1, 2, and 3), pressure (samples 2 and 6), ammonia concentration (samples 4, 2, and 5) and the spark generator (samples 2, 7, and 8)(see Table 2). The electric discharge occurred in the gaseous phase between two semi-sharp electrodes. We utilized tungsten electrodes in our experiment. They were 30 cm in length, 6 mm in diameter, exhibited a length of their cone of 15 mm and a tip with 0.5 mm radius. At the opposite end of the electrodes, there was a 20 mm deep pit with a 2.5 mm internal diameter for the connection of high-voltage and earth cables through a ferrule embedded within the hole. The analysis using Energy Dispersive X-ray Spectroscopy (EDX) revealed the composition of tungsten to be highly pure, with only trace amounts of impurities, notably Iron, Cobalt, Nickel, and Copper. Two flyback-based (FB-1 and FB-2) and a capacitor-based (C-1) high-voltage spark generators were used as shown in Figure 24 and Table 4.

Table 2: Experimental conditions.

Experiment # ¹	Temperature ²	NH ₃ ³	Initial Pressure ⁴	Spark Generator	Product Weight ⁵
Sample 1	+80	5.83	1.0	FB-1	3.0
Sample 2	+100	5.83	1.0	FB-1	15.6
Sample 3	+120	5.83	1.0	FB-1	10.0
Sample 4	+100	0.11	1.0	FB-1	1.6
Sample 5	+100	11.66	1.0	FB-1	5.2
Sample 6	+100	5.83	0.7	FB-1	4.0
Sample 7	+100	5.83	1.0	FB-2	5.1
Sample 8	+100	5.83	1.0	CA-1	9.3

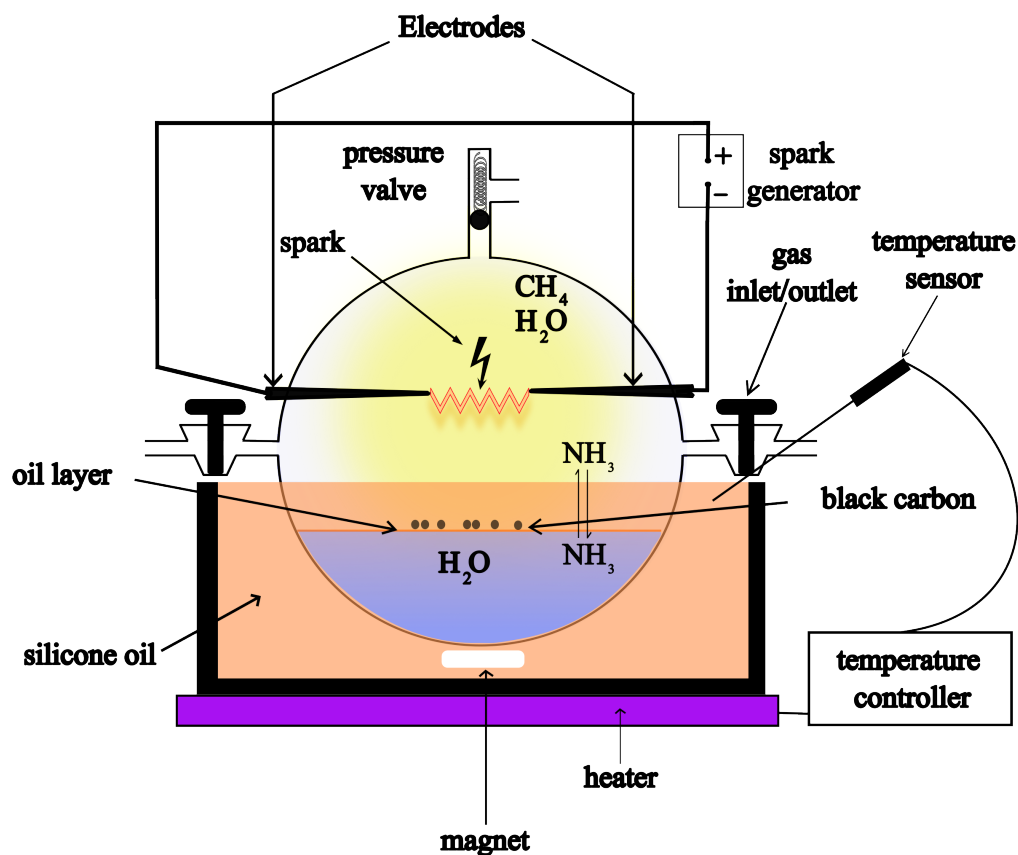
¹ Indicates the number of the experiment (for reference).

² Temperature refers to the silicon oil bath (°C).

³ The ammonia concentration refers to the initial amount of dissolved ammonia in the liquid phase (gr/L).

⁴ The initial pressures are measured at room temperature (bar).

⁵ product yield (mg).



63

Figure 18: **One-pot reactor design.** Traditional circulating reactor design simplified to a one-pot system for enhanced experimental control and thorough parameter analysis. Reactor setup: 5 L flask equipped with an overpressure valve, calibrated to respond at 1.3 bar.

Due to the inherent complexity involved in analyzing prebiotic mixtures, it has become almost necessary to adopt a selective approach when characterizing these materials. Typically, before conducting any analysis, the products generated must be divided into fractions based on their properties. For example, volatile and non-volatile substances require distinct instrumentation or the application of derivatization reagents, such as GC-MS for volatiles and semi-volatiles, or LC-MS for non-volatile components. Furthermore, there is an insoluble fraction, primarily composed of polymerized material, and fully characterizing it remains a significant analytical challenge.

7.2 Temperature Characterization

We calibrate the temperature and humidity in a chamber without mass circulation to check how much they differ in different parts of the chamber [282]. We also look at other factors, such as different spots, stability, and more, to understand how the chamber works and how it might affect the materials we synthesize in it. These parameters are very important for our research and help us to figure out how accurate our measurements are when we study the chemical composition of our experimental soup. The main goals of calibrating the chamber are:

- To adjust the temperature and humidity readings in the chamber based on standard reference tools and note any needed corrections.
- To figure out how uncertain the temperature and humidity measurements might be during experiment, and also how uncertain they might be when we're using the chamber under specific experimental conditions.

This guide details how to set up and calibrate a chamber with its own heating and cooling system, which is crucial to accurately estimating temperature.

The chamber can handle temperatures from -90°C to 350°C . However, it's important to wait until the temperature has been stable for at least 60 minutes before taking measurements, ensuring no significant changes occur. For calibration, we conducted under the specifications of the environmental testing standard DIN EN 60068-3-5 (DIN EN 60068-3-5, 2002) [283].

When testing how well the chamber maintains the temperature (its homogeneity), we conducted tests under a typically experimentally loaded chamber condition, as shown in Figure 19.

The actual temperature in the chamber differs from the oil bath. We can provide specific temperatures for certain area, if we measured and estimate the impact of heating source and the temperature gradient as best as we can (see Figure 19).

The relationship between pressure and temperature in our experimental chamber is vital for controlling experimental conditions. Monitoring these parameters helps us understand how changes in temperature affect pressure stability, as shown in Figure 20. This understanding is crucial for fine-tuning our setup to ensure that chemical reactions proceed under optimal conditions, in accordance with DIN EN 60068-3-5 standards [283].

The output of the K-type thermocouple was connected to a data logger (Testo 176 T4), which in turn was linked to Testo Comfort Software Basic 5.0 on a computer. The hot junctions of the thermocouple wire were inserted into the reactor, and the sensors were placed in the designated measurement areas. Once the temperature stabilized under the desired conditions, the setup to begin recording was completed. The data logger recorded the temperature in real time at a data acquisition rate of one temperature value per second, with a resolution of $0.1\text{ }^{\circ}\text{C}$ and a scan rate of once every second. The recorded value represents the actual temperature measured each second, not an average value.

In Figure 19, we can see the local temperatures under different conditions. These figures illustrate the temperatures within the chamber, providing information on how the system maintains thermal homogeneity. Each subplot in Figure 19 corresponds to a specific experimental setup, demonstrating the temperature variations for the Miller soup, gas phase, and the surrounding oil bath.

As shown in Figures 19a, 19b, and 19c, the liquid phase represents the temperature of the Miller soup measured at two different points to evaluate the uniformity of the temperature. The region above the liquid phase represents the temperature at the top of the Miller soup and in the gas phase, while the gas phase represents the temperature at the center of the Miller flask. Figures 1-a, b, and c depict the Miller experiments conducted at 80, 100, and 120 $^{\circ}\text{C}$, respectively, as adjusted in the oil bath.

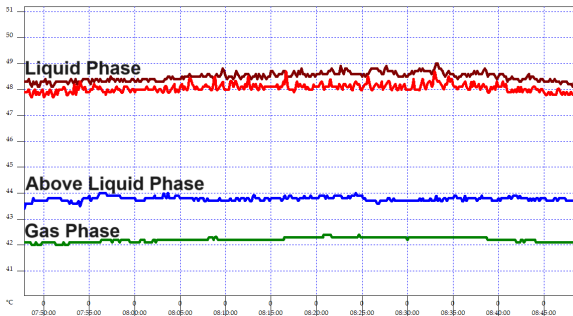
In Figure 19d, the temperatures of the oil bath outside the flask (adjusted to 100 °C), Miller soup, gas phase at the center of the flask, and ambient temperature are plotted. The temperature in two conditions was evaluated: initially with a silicone heating band around the neck of the flask turned off, then turned on to prevent water condensation around the neck where high-voltage electrodes are introduced to avoid short circuits and sparking at the electrode tips.

In Figure 19e, the temperatures of the oil bath outside the flask (adjusted to 80 °C), Miller soup, gas phase at the center of the flask and the ambient temperature are plotted. The temperature was evaluated in two conditions: first, with the lab chemical hood turned off and then with the ventilation turned on, introducing an airflow of roughly 0.5 m/s to the hood.

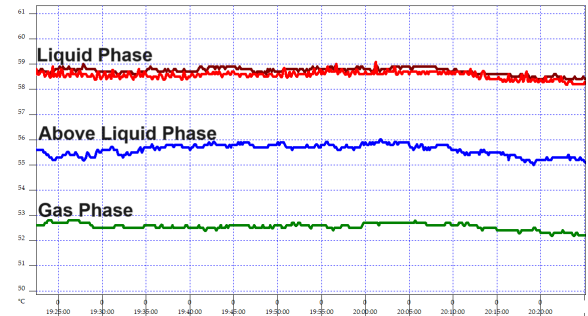
In Figure 19f, the temperatures of the oil bath outside the flask (adjusted to 100 °C), Miller soup, gas phase at the center of the flask and the ambient temperature are plotted. The temperature was evaluated in two conditions: first, with the chemical hood turned off and then with the ventilation turned on, introducing an airflow of roughly 0.5 m/s to the hood.

In Figure 19g, the temperatures of the oil bath outside the flask (adjusted to 100 °C), Miller soup, gas phase at the center of the flask, and ambient temperature are plotted. Initially, the peristaltic pump used to circulate the Miller soup for real-time analysis was turned off, and then the effect of turning on the peristaltic pump is plotted.

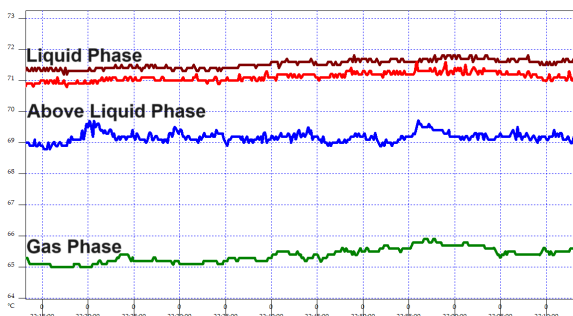
In Figure 19h, the temperatures of the oil bath outside the flask (adjusted to 100 °C), Miller soup, gas phase at the center of the flask, and ambient temperature are plotted. Initially, the sparking used as the driving force of the Miller experiment was turned off, and then the effect of turning on the spark on the temperature is presented.



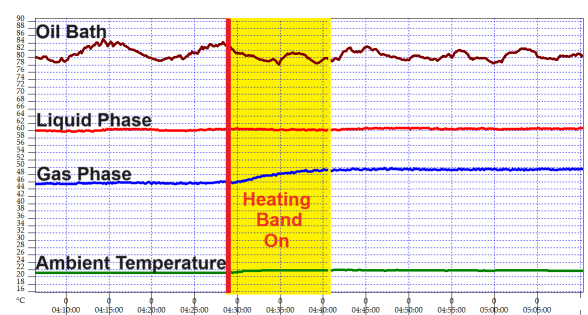
(a) Temperatures in 80 °C Oil Bath



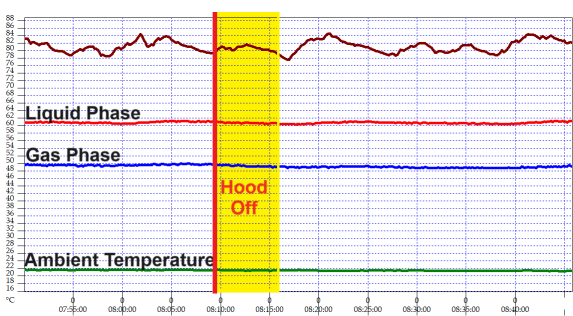
(b) Temperatures in 100 °C Oil Bath



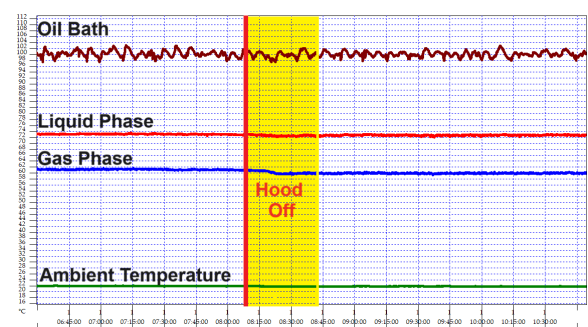
(c) Temperatures in 120 °C Oil Bath



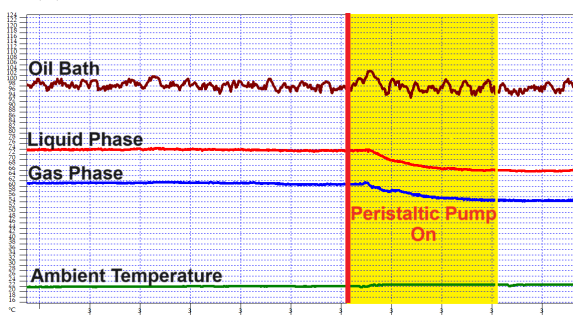
(d) Temperatures Effect of Heating Band



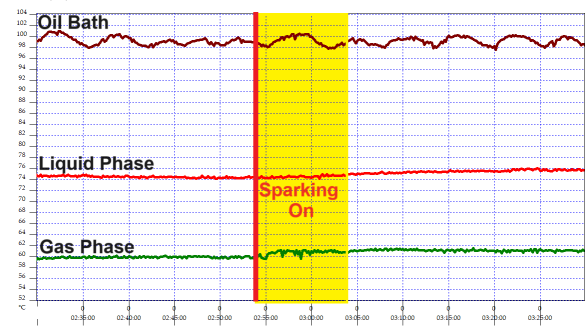
(e) Temperatures effect of Hood Air flow



(f) Temperatures effect of Hood Air flow



(g) Temperatures effect of Pump flow



(h) Temperatures effect of Sparking

Figure 19: Local temperatures within the Miller-Urey experiment flask under different conditions.

7.3 Pressure Characterization

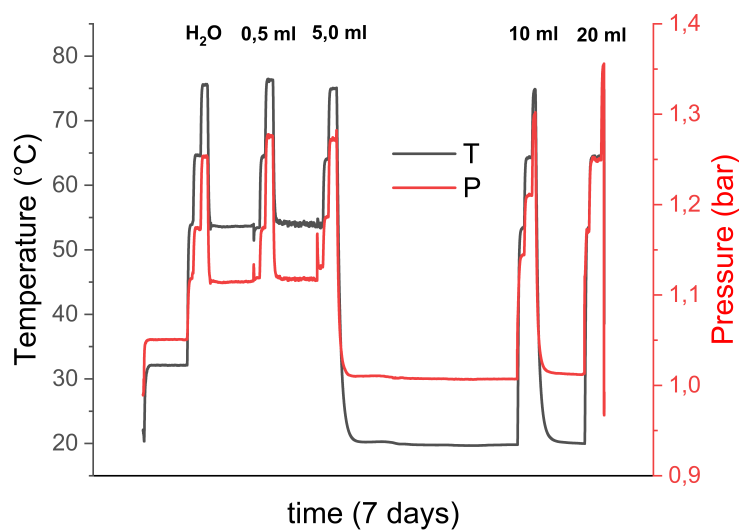
The evaluation of pressure within an experimental chamber is crucial for understanding the physical and chemical behaviors under controlled conditions. Precise pressure evaluation, is essential for experiments sensitive to pressure changes, such as synthesis or chemical reactions. Calibration ensures stabilization of the chamber at a target pressure for at least 30 minutes to ensure that there are no significant fluctuations.

We also assess the pressure of the chamber during the sparking condition by using the pressure logger in typically loaded conditions as shown in Figure 21. This helps determine how well the chamber maintains consistent pressure across different areas, which is vital to the accuracy of experimental outcomes. By understanding and controlling these pressure variations, we can optimize a specific conditions and cosequently the experimental results, enhancing the reliability and reproducibility of our research.

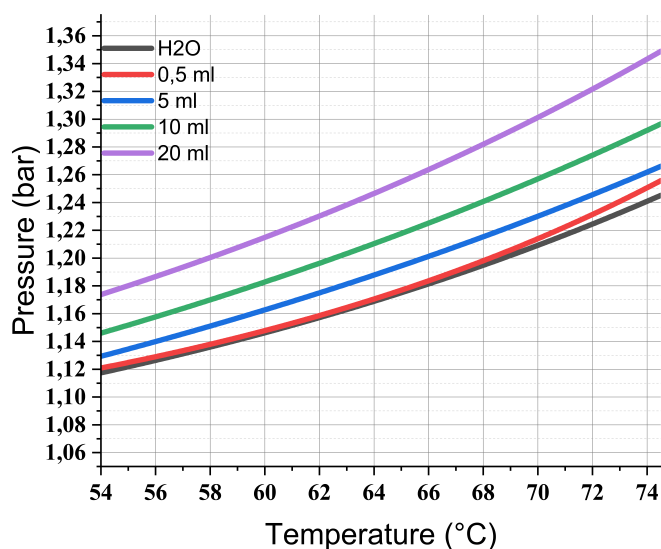
The absolute pressure in the reactor of the Miller experiment was measured using a high-temperature pressure logger (PR 140, manufactured by Madge Tech, Inc., Warner, NH, USA) positioned at the bottom of the inner side of the liquid phase. The temperatures of both the liquid and the vapor phases were recorded using a temperature logger at 10-second intervals.

In Figure 20a, the effect of temperature and ammonia on pressure is evaluated. As shown, there are five cycles. Initially, in the first cycle (from left), pure water is applied at three different temperatures of 80, 100, and 120 °C is applied, and the pressure is measured. In the second cycle, the temperature of the water is reduced to 80 °C, and then 0.5 ml of ammonia is injected into the sealed flask. The same temperature program of 80, 100, and 120 °C is applied again to compare the pressure with the added ammonia. In the third to fifth cycles, the same temperature program is applied with different concentrations of 5.0, 10, and 20 ml of 35% W/W ammonia injected into the flask. The measured pressure is presented in Table 3.

Figures 20b is plotted using data presented in Table 3, showing the relationship between temperature and pressure in water and four different ammonia concentrations of 0.5 ml, 5.0 ml, 10.0 ml, and 20.0 ml ammonia.



(a) Ammonia's Effect on Pressure



(b) Ammonia Pressure Change Diagram

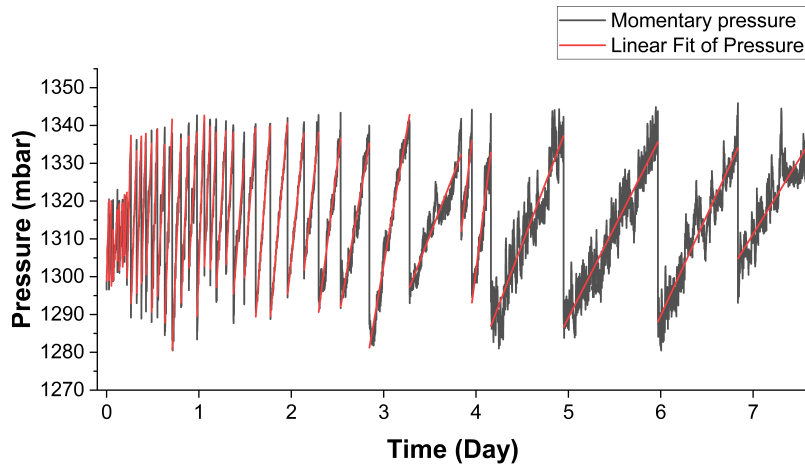
Figure 20: **Temperatures and ammonia concentration effect on the pressure.**

Figure 21a shows the measured absolute pressure in the ongoing Miller experiment over 7 days. The pressure oscillates, reaching a cut-off point of 1.3 bar, controlled by a gas release valve to prevent over-pressure in the flask during the experiment. The

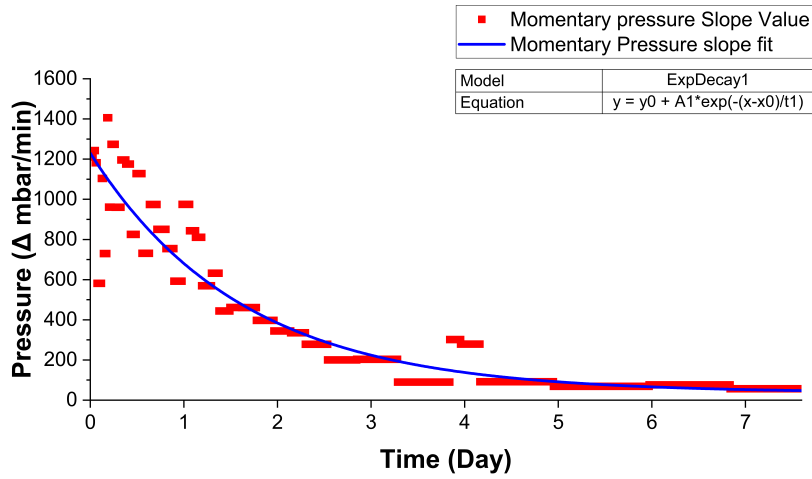
Table 3: **Temperature-Dependent pressure changes with ammonia concentration.**

	80 °C	100 °C	120 °C
Water	1.1144 bar	1.1748 bar	1.2533 bar
0.5 ml Ammonia	1.1182 bar	1.1744 bar	1.2759 bar
5.0 ml Ammonia	1.1293 bar	1.1865 bar	1.2705 bar
10.0 ml Ammonia	1.1446 bar	1.2105 bar	1.3002 bar
20.0 ml Ammonia	1.1700 bar	1.2502 bar	1.3543 bar

increasing pressure oscillation has been fitted with a linear regression line for each cycle, and the slope has been calculated. This slope, depicting a decreasing pattern over time, is plotted in Figure 21b to illustrate the real-time gas production propagation .



(a) $P(t)$ diagram as a function of time.



(b) Slope of the $P(t)$ diagram as a function of time.

Figure 21: **Pressure propagation as a function of time $P(t)$.**

Figure 22 represents the temperature and absolute humidity measured in the atmospheric pressure: in the Miller soup (red line) and in the air (black line).

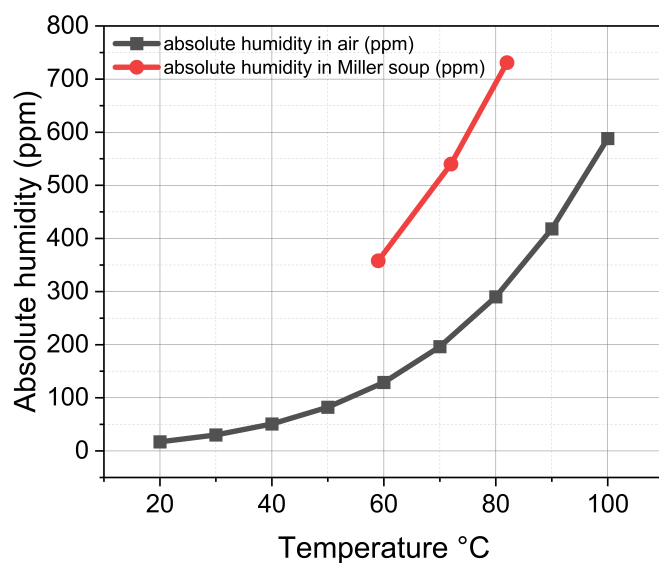


Figure 22: **Temperature-Humidity relationship.**

7.4 PH

Evaluating the pH in an experimental setup where ammonia is added to water is critical for understanding the chemical dynamics influenced by changes in acidity or alkalinity. Which includes allowing us to evaluate the solution PH when the experiment starts as depicted in Figure 23.

The pH values of the ammonium hydroxide solution were measured using a multi-function pH meter (model PCE-PHD 1, PCE Instruments France EURL, Strasbourg, France). The pH was measured via a glass electrode at ambient temperature while the solution was being stirred by a magnet.

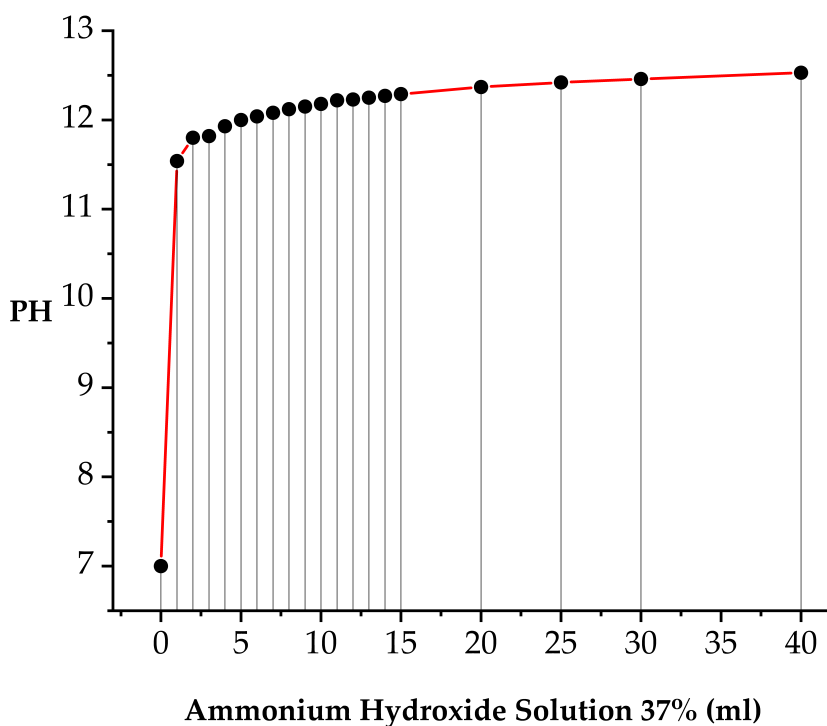


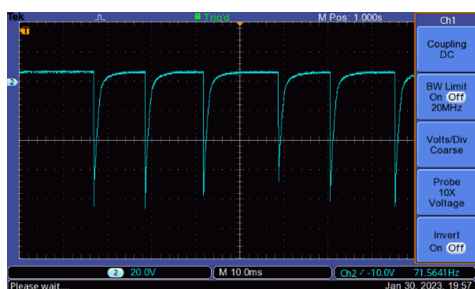
Figure 23: **pH shift in water.** pH change in water with ammonia additions from 0 to 40 ml.

7.5 Liquid Phase Extraction

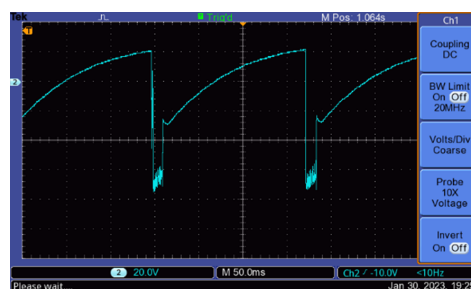
We employed the 3-phase extraction method based on the Dyer technique for our experiments. Following the methodology outlined by Bligh and Dyer [284], we initiated the extraction process by combining methanol and chloroform with the broth, achieving a final volume ratio of 2:2:1 for chloroform/methanol/prebiotic broth. The mixture was vigorously shaken on a shaker within a separatory funnel at 150 rpm for 5 minutes, facilitating the separation of layers until the upper layer became clear. Subsequently, the organic phase (lower layer) was extracted through a stopcock integrated into the separatory funnel. The organic phase underwent drying at room temperature under a nitrogen purge. The samples were preserved under a nitrogen atmosphere at -80°C until further analysis.

7.6 Spark Generators

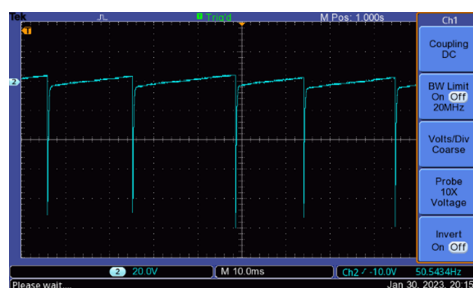
In our experimental setup, we employed three distinct types of spark generators to initiate and study reactions involving organic compounds. Two of these generators are based on fly-back technology, while the third utilizes a capacitor-based system with a DC positive single pole to charge the circuit. This setup is designed to generate a voltage breakdown and subsequent spark, which is critical for producing plasma under controlled conditions. Each generator has been carefully characterized to understand its specific voltage and current profiles, which are crucial as these parameters directly influence the nature of the plasma generated. The variances in plasma characteristics are expected to offer diverse pathways for chemical reactions, potentially leading to different outcomes in the synthesis or transformation of organic compounds. This detailed characterization is depicted in Figure 24 and Table 4, illustrating the unique electrical signatures associated with each generator type [1].



(a) Voltage-time characterization of FB-1 spark generator.



(b) Voltage-time characterization of FB-2 spark generator.



(c) Voltage-time characterization of CA-1 spark generator.

Figure 24: **Voltage-time characterization of spark generators [1].** In the oscilloscope, we used a probe to scale down 1000 volts to 1 volt for display.

Table 4: **Spark generator electrical characteristics.**

Spark generators	FB-1	FB-2	CA-1
V input	19.00 V	15.00 V	11.50 kV
I input	0.100 A	0.500 A	0.107 mA
V Output (max)	9 kV	10 kV	11 kV
Sparking frequency	71 Hz	10 Hz	50 Hz

7.7 GC-MS

We used Agilent 8890 GC System equipped an HP-5MS capillary column (composed of 95% dimethylpolysiloxane and 5% diphenyl; dimensions: 30m x 0.25m x 0.25 mm) from Agilent technologies coupled to a 5977B GC/MSD mass detector utilized for GC-MS analysis. Each sample injected in splitless-mode, with 1.0 μL per injection. The injector temperature was maintained at 280 $^{\circ}\text{C}$, the MS transfer line at 280 $^{\circ}\text{C}$, and the detector at 230 $^{\circ}\text{C}$. Helium served as the carrier gas, with a constant flow rate of 1.0 mL min^{-1} . The temperature gradient was initiated at 70 $^{\circ}\text{C}$, held for 8 minutes and followed by an incremental increase at a rate of 3.5 $^{\circ}\text{C}$ per minute to 280 $^{\circ}\text{C}$. With a final hold time of 9 minutes In all MS scans, a positive ion polarity with 70 eV EI power was employed. Mass spectra were scanned from 50-550 m/z at a scan rate of 0.9 scans/s. The compounds were identified by matching their MS fragmentation patterns. These patterns were compared to known compounds in the AMDIS software (Version 2.72) and NIST (Version 2.3, USA) database as shown in Figure 25. This database includes all known organic compounds found in the Miller-Urey product mixtures. The NIST 14 database search used compounds modified with a silylation reaction to make mass-spectral matching easier. Commercial mass spectral libraries can be searched with a probability-based matching algorithm (PBM). This algorithm verifies peaks in the reference spectrum against the unknown spectrum, ignoring extra peaks in the unknown. This approach allows for quick analysis, even when dealing with mixed compound spectra due to poor separation. However, this method may yield low-quality matches or unreasonable matches, resulting in uncertainty in the results. The PBM algorithm considers both mass and abundance values to identify significant peaks in the reference spectrum.

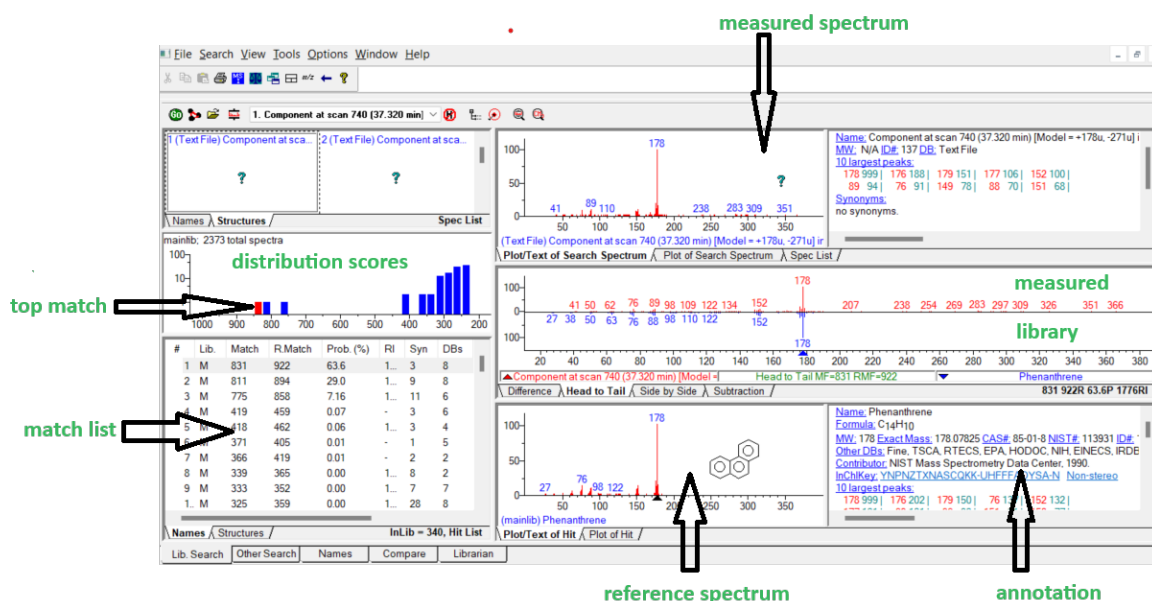


Figure 25: **NIST database.** The NIST software performs an integrated database search of electron impact (EI) mass-spectral patterns by comparing the measured spectrum of an experimental sample with a reference library. In this case, it indicates a 63% quality match for the compound phenanthrene.

To exploit the relative quantification of primary formed fragments, we used the Bruker DataAnalysis software (Version 5.0). This software lists the intensities of all detected m/z during the time course of measurement.

7.7.1 Liquid Phase

We used the extracted samples prepared via the Bligh and Dyer method as described in Section 7.5 to extract and dry the organic phase of the prepared Miller-Urey soup. 1 mg of the sample was derivatized by adding 200 μ L of the derivatizer (BSTFA + TMCS, 99:1, Sylon BFT) obtained from Supelco (Bellefonte, PA, USA), followed by incubation at 70 $^{\circ}$ C for 2 hours. During derivatization, the labile hydrogen atoms are replaced by trimethylsilyl groups, reducing the molecular polarity to facilitate chromatographic separation.

7.7.2 Gas Phase

HS-SPME exposes the fiber coating above a solvent-free liquid medium or exposed in the gas phase to extract volatile compounds, and it's the most commonly used method. Direct immersion involves placing the fiber directly into the liquid sample, where the analytes are distributed between the fiber and the sample matrix [285].

The membrane-protected mode is mainly used for highly polluted samples to protect the fiber. After extracting volatile compounds, the analytes are desorbed from the fiber at high temperatures in a split/splitless GC injector for analysis[286]. Various sample preparation techniques are available, chosen based on the characteristics of the sample. Liquid-liquid extraction (LLE), solid phase extraction (SPE), and solid phase microextraction (SPME) are commonly used with complex semi-volatile and volatile samples.

The PDMS Arrow (1.1 mm: Carbon WR/PDMS 0.95 μm , Agilent Technologies, Switzerland) was preconditioned according to the manufacturer's instructions, then inserted into the reactor for 60 minutes to adsorb the organic compounds in the gas phase. After sampling, the SPME fiber was withdrawn from the needle, removed from the reactor and inserted into the injector port (250 $^{\circ}\text{C}$) of the GC-MS system for 6 min, where the analytes were thermally desorbed and transferred directly to the analytical column.

Agilent 8890 GC system equipped an HP-5MS capillary column (composed of 95% dimethylpolysiloxane and 5% diphenyl; dimensions: 30m x 0.25m x 0.25 mm) from Agilent technologies coupled to a 5977B GC/MSD mass detector utilized for GC-MS analysis. The MS transfer line at 280 $^{\circ}\text{C}$, and the detector at 230 $^{\circ}\text{C}$. Helium served as the carrier gas, with a constant flow rate of 1.0 mL min⁻¹. The temperature gradient was initiated at 40 $^{\circ}\text{C}$, held for 8 minutes and followed by an incremental increase at a rate of 20 $^{\circ}\text{C}$ per minute to 280 $^{\circ}\text{C}$. With a final hold time of 2 minutes In all MS scans, a positive ion polarity with 70 eV EI power was employed. Mass spectra were scanned from 50-450 m/z at a scan rate of 0.9 scans/s. The compounds were identified by matching their MS fragmentation patterns. These patterns were compared to known compounds in the AMDIS software (Version 2.72) and the NIST database (Version 2.3, USA) database as shown in Figure 25. This database includes all known organic compounds found in the Miller-Urey volatile mixtures in the gas phase. The NIST 14 database search.

7.8 FTMS

The samples, prepared according to the method described in Section 7.5, were dissolved in 1 ml of a 50:50% acetonitrile:water solution + 0.1% V/V formic acid. 20 μ l of the prepared sample was directly injected into the mass spectrometer (SolariX FTICR-ESI, Bruker) following the adjusted parameters listed in Table 5. The obtained raw mass spectra were analyzed using Compass DataAnalysis software (Bruker Compass DataAnalysis Version 5.0, Bruker), and Origin (Origin 2020b, OriginLab) for data evaluation.

Table 5: FTMS Instrument adjusted parameters.

Category	Parameter	Value/Setting
General Settings	Size	1M
	Low m/z	100.35
	High m/z	1000.00
	Avg Scans	40
	Accum (s)	0.25
	Polarity	Positive
	API High Voltage	Enabled
	Source Quench	Enabled
	Serial mode	Disabled
API Source Settings	Capillary Voltage	4500 V
	End Plate Offset	-500 V
Source Gas Tune	Nebulizer Pressure	2.5 bar
	Dry Gas Flow	6.0 L/min
	Dry Temperature	240 °C
Ion Transfer - Source Optics	Capillary Exit	220.0 V
	Deflector Plate	200.0 V
	Funnel 1 Voltage	150.0 V
	Skimmer 1 Voltage	15.0 V
	Funnel RF Amplitude	150.0 Vpp
Ion Transfer - Octopole and Quadrupole	Frequency	5 MHz
	RF Amplitude	350.0 Vpp
	Q1 Mass	50.00 m/z
Collision Cell and Transfer Optics	Collision Voltage	-1.5 V
	DC Extract Bias	0.5 V
	RF Frequency	2 MHz
	Collision RF Amplitude	1600.0 Vpp
	Time of Flight	0.700 ms
Gas Control and Analyzer Settings	Flow	32%
	Gas Control	Enabled
	Transfer Exit Lens	-14.0 V
	Analyzer Entrance	-7.0 V

7.9 HPLC-FTMS

Samples that were prepared according to the method described in Section 7.5 were dissolved in 1 ml solution of 50:50 % of acetonitril: Water. 50 μ l of the prepared sample was analysed using an HPLC system consisting of an “UFLCXR -LC-20AD XR SHIMADZU” HPLC pump equipped with a “SIL-20AC XR“ autosampler intelligent “CBM-20A“ communication processing unit, a “CTO-20AC“ column oven. In order to separate the sample we used a reversed-phase and polar column (Luna Omega 3 μ m Polar C18 100 ÅLC Column 250 * 4.6 mm Tosoh, TSK-GEL ODS 80TS, 250 \times 4.6 mm i.d., stainless steel) from Phenomenex (Torrance, CA, USA). Samples were separated using a linear gradient programm obtained from ultrapure water (A) and acetonitrile (B) without further buffer or PH adjustments as shown in Table 6. Mass spectrometer (SolariX FTICR-ESI, Bruker) used as the detector for HPLV-FTMS analysis and the adjusted parameters for the detector is listed in Table 7. The obtained raw mass spectra were analyzed using Compass DataAnalysis software (Bruker Compass DataAnalysis Version 5.0, Bruker) for data evaluation.

Table 6: **HPLC Gradient method.**

Step	time ¹	Oven Temperature ²	Flow ³	%A ⁴	%B ⁵
1	00.00	+50	0.5	90	10
2	10.00	+50	0.5	90	10
3	10.10	+50	0.5	90	10
4	170.00	+50	0.5	0	100
5	195.00	+50	0.5	0	100
6	210.00	+50	0.5	90	10
7	210.10	+50	0.5	90	10
8	256.00	+50	0.5	90	10

¹ Indicates the time for starting step (min).

² Temperature refers to the Oven Temperature ($^{\circ}$ C).

³ Flow refers to the flow of liquid phase in through the column (ml/min).

⁴ %A refers the percentage of pure water in the mobile phase.

⁵ %B refers the percentage of Acetonitrile in the mobile phase.

Table 7: HPLC-FTMS Instrument adjusted parameters.

Category	Parameter	Value/Setting
General Settings	Size	1M
	Low m/z	100.35
	High m/z	1000.00
	Avg Scans	1
	Accum (s)	0.25
	Polarity	Positive
	API High Voltage	Enabled
	Source Quench	Enabled
Serial Mode	Enabled	
API Source Settings	Capillary Voltage	4500 V
	End Plate Offset	-500 V
Source Gas Tune	Nebulizer Pressure	2.5 bar
	Dry Gas Flow	6.0 L/min
	Dry Temperature	240 °C
Ion Transfer - Source Optics	Capillary Exit	220.0 V
	Deflector Plate	200.0 V
	Funnel 1 Voltage	150.0 V
	Skimmer 1 Voltage	15.0 V
	Funnel RF Amplitude	70.0 Vpp
Ion Transfer - Octopole and Quadrupole	Frequency	5 MHz
	RF Amplitude	350.0 Vpp
	Q1 Mass	50.00 m/z
Collision Cell and Transfer Optics	Collision Voltage	-1.5 V
	DC Extract Bias	0.5 V
	RF Frequency	2 MHz
	Collision RF Amplitude	1600.0 Vpp
	Time of Flight	0.700 ms
Gas Control and Analyzer Settings	Flow	40%
	Gas Control	Enabled
	Transfer Exit Lens	-14.0 V
	Analyzer Entrance	-7.0 V

7.10 HPLC-UV-Vis

Samples that were prepared according to the method described in Section 7.5 were dissolved in 1 ml solution of 50:50 % of acetonitril: Water. 50 μ l of the prepared sample was analysed using an HPLC system consisting of an “Jasco-ChromPass Chromatography” HPLC-PDA system equipped with a “Jasco AS-2059.SF plus“ autosampler intelligent “Jasco MD-2010 plus detector“, using a reversed-phase column (Luna Omega 3 μ m Polar C18 100 ÅLC Column 250 * 4.6 mm Tosoh, TSK-GEL ODS 80TS, 250 \times 4.6 mm i.d., stainless steel) from Phenomenex (Torrance, CA, USA). Samples were separated using a linear gradient obtained from ultrapure water (A) and acetonitrile (B) without further buffer or PH adjustments as shown in Table 6

7.11 Real-time UV-Vis Absorption

The experimental setup for real-time UV-Vis absorption is designed to pass the liquid phase of the Miller-Urey experiment, referred to as “Miller soup,” through a solvent filter, and to pump the liquid using a peristaltic pump with a flow rate of 1.5 mL/min. The pump circulates the liquid phase through a PTFE tube with a 2 mm inner diameter and a 3 mm outer diameter (Carl Roth, Germany), which then passes through a sample flow cell (Starna Scientific, 71F-Q-10; with a 10 mm optical path length, Atascadero-USA) to maintain a circulation of freshly synthesized soup. Absorption spectra were measured with a double-beam spectrophotometer (Varian-CARY 50 Probe, Australia). The absorbance of all samples was measured after the lamp and the liquid had sufficiently equilibrated and stabilized before data recording. All measurements were carried out at room temperature. The parameters of the spectrophotometer is presented in Table 8:

7.12 FTIR

FTIR analysis of the gas phase performed according to the following procedure: The Miller experiment was stopped by disconnecting the spark power. Then, using a Hamilton S-1000 syringe (Hamilton Company, Nevada, USA) 200 mL of the gas phase was sampled at room temperature at predetermined times during the experiment. The sampling was conducted under a pressure of approximately 1.3 bar using a needle through

Table 8: UV-Vis Spectrophotometer adjusted parameters.

Category	Parameter	Value/Setting
Instrument Control	Start	700.0 nm
	Stop	220.0 nm
Cycle	Cycle mode	Enabled
	Cycle count	120
	Cycle time	60.00 min
Scan Controls	Ave time(s)	0.0125
	Data interval (nm)	1.00
	Scan rate (nm/min)	4800.00
Y Mode	Mode	Abs
Beam Mode	Beam mode	Dual Beam

a silicon septum embedded in the reactor window to seal the reactor. to prevent air from entering to the syringe and mixing with the sample, The gas sample was immediately injected into a home-designed gas phase cell.

The gas cell as schematic picture is shown in Figure 26, consisted of a glass tube with 14 cm in length and 2.5 cm in internal diameter, equipped with two embedded holes of 2 mm diameter located at the body of tube as in/outlet for sample and helium purging. Both ends of the glass tube were sealed with two 5 cm KBr IR-transparent windows, which are sandwiched between two silicon sealant. Each silicon sealing septa had a central hole of 1 cm diameter to allow the passage of an IR laser. The windows were held in place by three long screws (2 mm diameter and 17 cm length) and six butterfly screws, which were indirectly pressed against a metal O-ring (7.5 cm external diameter and 22 mm internal hole diameter). This IR gas cell ensured a tight seal by pressing the silicon sealants against the gas cell.

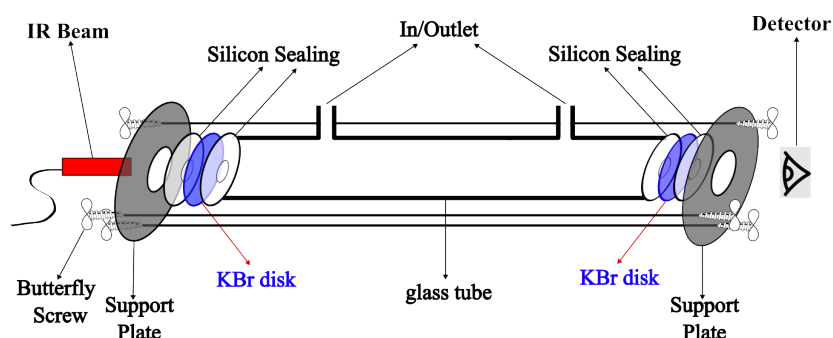


Figure 26: Schematic Picture of the IR Gas Cell.

Prior to analysis, the gas cell was purged with helium to remove any residual air. When the gas cell embedded in the FTIR spectrophotometer (SHIMADZU IRTracer-100, Japan) and zeroing the cell transmittance, the gas phase from the Miller experiment was injected directly without further preparation. Absorption was measured in mid-IR over a range of 400-4000 cm^{-1} . Detailed adjustments of the method of the FTIR spectrometers are presented in Table 9.

Table 9: FT-IR Instrument adjusted parameters.

Category	Parameter	Value/Setting
Data Evaluation	Data Evaluation	Enabled
	IFG Noise	110
	IFG similarity	54
	Aperture delay	0 s
IR Range	IR Range	MID
Light Source	Light source	Infrared
	Standby Mode	[Checked]
	Zero filling	None
Measurement Mode	Measurement Mode	%Transmittance
	Apodization	Happ-Genzel
	No. of Scans	20
	Resolution	4 cm^{-1}
	Range	500 to 4000 cm^{-1}

7.13 UV-Vis Excitation

The UV-Vis excitation setup involved preparing a 5 L flask, which was initially evacuated three times using a vacuum pump and filled with methane (N25, Air Liquide, Düsseldorf-Germany) to purge residual air and degas the water. Ammonium hydroxide (35% w/w solution, Fisher Chemical, Loughborough-UK) was then injected through a silicon septum (DWK Life Sciences, Holzminden-Germany) using a glass syringe (Fortuna Optima Luer Lock, Fisher Scientific, Schwerte-Germany). The flask was partially immersed in a heated silicon oil bath with a magnetic stirrer and allowed to equilibrate overnight before sparking. Spark discharge was executed in the gaseous phase between two tungsten electrodes. The typical interelectrode gap is 7 mm. Electrodes have 30 cm in length, and 6 mm in diameter with a 15 mm cone length and a 0.5 mm tip radius. Connections for high-voltage and earth cables were made through a 20 mm deep pit at the electrode ends with a 2.5 mm internal diameter, secured by a ferrule. Purity analysis via Energy Dispersive X-ray Spectroscopy (EDX) indicated minimal

impurities, with trace amounts of Iron, Cobalt, Nickel, and Copper. Spark generation was facilitated using two flyback-based (FB-1 and FB-2) and one capacitor-based (C-1) high-voltage generators (detailed in Supplementary Materials[1]).

The apparatus configuration is shown in Figure 18, features a rod-to-rod electrode in a glass reactor with a gas in/outlet valve utilized for both gas injection and release, maintaining atmospheric pressure conditions. Spectral data was captured via a lens mounted outside the reactor, directing light to a spectrophotometer through a short optical fiber (SMA and FC/PC Patch Cable, Lasertack GMBH, Germany) spanning 250-1200 nm, with a core diameter of 600 μm and length of 1.5 m. Spectral acquisition was performed using a spectrometer (Toshiba TCD1304AP, Japan) within a 200-1100 nm detection range, integrating each spectrum for 100 ms and averaging over 100 acquisitions to reduce noise effects.

7.14 XRD

The black material that formed around the electrodes was collected after the experiment, which involved shaking and vibrating the tungsten electrode. The powder samples were then deposited on a silicon sample plate and subjected to X-ray diffraction (XRD) analysis. This analysis was performed using a Bruker AXS D8 Advance diffractometer, equipped with a nickel-filtered copper X-ray source ($\text{CuK}\alpha$), operating at 40 kV and 40 mA, and a VANTEC-500 2D detector.

7.15 SEM/EDX

The black material formed around the electrodes was collected after the experiment, which was performed by shaking and vibration of the tungsten electrode. The samples were dispersed in an acetone solution and briefly sonicated. The dispersed samples were then dried on a silicon sample plate, and the sample was subjected to Scanning electron microscopy (SEM) analysis.

Scanning electron microscopy (SEM) images were recorded using a JEOL JSM-7500F field-emission scanning electron microscope. Energy-dispersive X-ray spectroscopy (EDX) was performed at 12 kV with an X-Max Silicon Detector from Oxford Instruments, utilizing AZtec software. The samples were dispersed in acetone solution and

tip-sonicated briefly directly before being drop-cast onto a TEM copper grid coated with a lacy carbon film.

8 Results and discussion

8.1 GC-MS

We conducted GC-MS analysis across two distinct phases (liquid phase and gas phase) to ensure comprehensive coverage of both the liquid and gas phases of our samples. Initially, the liquid phase was extracted, dried and subsequently derivatized following the protocols described in Section 7.5 of our study. This preparation was crucial to enhance the detection and quantification of volatile and semi-volatile organic compounds. In parallel, the gas phase analysis was performed independently, employing an advanced SPME (Solid Phase Microextraction) technique. This method, detailed in Section 7.7.2, involved the use of a specialized SPME needle designed to absorb and analytes from the gas phase, significantly improving the detection of the molecules present in the gas phase. These dual analytical approaches allowed to investigate the chemical properties and interactions present in both phases.

8.1.1 Liquid Phase

The GC-MS analysis revealed a large variety of organic compounds including alkanes ($C_{12} - C_{44}$), fatty acids, alcohols, amines, aromatics, and heterocycles among others (Table 11 and Table S4 in the Supplementary Materials [1]).

The detected compounds have a wide range of degrees of aromaticity and chemical variability as shown in Table 11 and Table S4 in the Supplementary Materials [1]. We identified several compounds that were common in all samples, regardless of the applied conditions (see Table 2), e.g., alkanes, fatty acids, and carbamates. However, the samples showed major differences in composition with respect to the experimental conditions. Table 10 shows that Guanine and ethanimidic acid consistently formed in the prebiotic broths except in sample 1 (80 °C). Cyanophenol was not detected in samples 1 (80 °C), 2 (100 °C), and 8 (CA-1 spark generator). Oxalic acid was only observed in samples prepared at 120°C (sample 3), or at high-ammonia concentrations (sample 5) or with spark generator FB-2 (sample 7). We also detected components such as symmetrical arrangements of ketone groups, di-ketones, and bisphenols, which can be considered radical traps for oxidation. 1,4-benzoquinone was identified in all samples, except for sample 4 (lower concentration of ammonia).

The presence of alkanes, ethers, and hydroxyls showed consistent levels in the samples analysed in the previous work [226]. Notably, esters were absent in some conditions, but appeared in significant quantities [226]. Alkynes and amines were not initially detected in the aqueous phase. However, Nitriles were predominantly found in specific condition [226].

Homologous series suggested to originate from straight-chain alkanes ($C_{16} - C_{28}$). Numerous branched and unbranched alkanes, alkenes, fatty alcohols, phenols, vinyl ethers, and combinations of esters with acid groups is also reported [226].

A scarcity of nitrogen-containing compounds has detected in the organic phase in previous study possibly due to the higher solubility of amines, amides, and other nitrogen compounds in the hydrophilic phase during the liquid-liquid extraction in n-hexane/water [226].

These results show reproducibility between our work and previous studies, with a few specific differences noted, particularly in the detection of amines. These differences could be attributed to variations in gas composition used for soup preparation, experiment runtime, sample preparation methods, and the molecular assignment techniques applied.

Differences in alkane chain lengths between this work and previous study [226] could also be attributed to library and instrumental limitations. The library in this study suggested longer straight-chain alkanes compared to previous research. This difference may originated from the strong fragmentation of analytes caused by electron impact ionization and the NIST databases that provides alkanes structures with the highest matching factor.

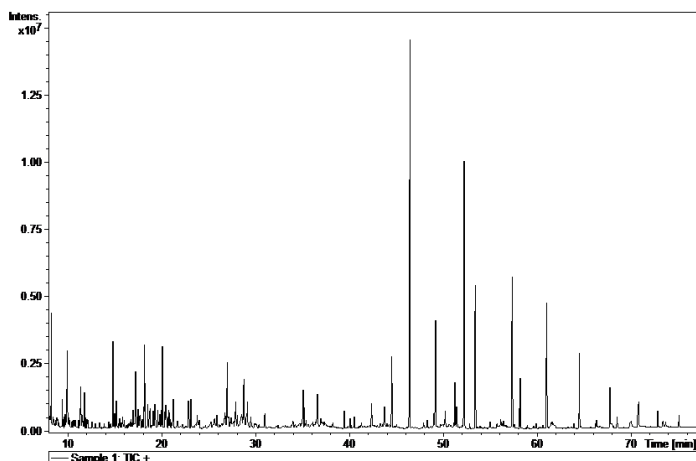


Figure 27: GC-MS of Liquid phase.

Table 10: Examples of Detected Compounds in the Liquid Phase Across Samples S₁-S₈.

Compound name	S ₁	S ₂	S ₃	S ₄	S ₅	S ₆	S ₇	S ₈
Alkanes C ₁₂ - C ₄₄	+	+	+	+	+	+	+	+
Aromatics	+	+	+	+	+	+	+	+
PAHs				+		+	+	
Carbamat	+	+	+	+	+	+	+	+
Ethanimidic acid		+	+	+	+	+	+	
Guanine		+	+	+	+	+	+	
Aliphatic Amines	+	+	+	+	+	+	+	+
Pyridinol	+	+	+	+	+	+		
Fatty acids	+	+	+	+	+	+	+	+
m-Phenylenediamine		+	+	+	+		+	
Cyanophenol		+	+	+	+	+		
Benzamide		+	+	+		+		
Dimethylphenol		+	+	+	+			
Phenol	+		+	+	+	+		
Urea					+	+	+	+
Oxalic acid		+		+		+		
Methoxyphenol			+	+		+		
Pyrazine-2-carboxamide				+	+			+
14-Benzoquinone	+	+	+			+	+	+
4-Pyrimidinecarboxaldehyde						+	+	+
Benzyl alcohol			+	+	+			
Fatty alcohols	+	+	+	+	+			+
Butadyne	+	+	+					
Methylbenzamide				+			+	+
Ethyl-acridone				+			+	+
Glycolic acid	+		+	+				
Biphenyldiol				+	+	+		
Biphenylene derivative				+				+
ethylene glycol	+	+	+		+	+		
PEG strands	+		+					+
Amino-O-cresol				+			+	

Short polyethylene glycol (PEG) strands were detected in samples 1, 3, and 8, while the possible corresponding monomer, ethylene glycol, was detected in samples 1, 2, 3, 5, 6, and 7. A distinct set of polycyclic aromatic hydrocarbons (PAHs) was observed in samples 5, 7, and 8 (Table 10).

Table 11: Representative Compounds Identified in the Liquid Phase via GC-MS Analysis.

ID	Image	ID	Image
1	<p>Mass spectrum for 2-Propanone, N-butyl-. The x-axis is m/z from 40 to 300, and the y-axis is relative intensity from 0 to 100. Major peaks are at m/z 44, 58, 72, 87, and 99. The chemical structure shows a butyl group attached to the nitrogen of a 2-propanone molecule.</p>	2	<p>Mass spectrum for Diethyl ether. The x-axis is m/z from 40 to 360, and the y-axis is relative intensity from 0 to 100. Major peaks are at m/z 44, 72, 86, 100, 114, 128, 142, and 156. The chemical structure shows two ethyl groups attached to an oxygen atom.</p>
3	<p>Mass spectrum for N-Butylhexanone, bis(tert-butyl) ether. The x-axis is m/z from 40 to 240, and the y-axis is relative intensity from 0 to 100. Major peaks are at m/z 41, 55, 73, 87, 101, 115, 130, 144, 158, 172, 186, 200, 214, 228, and 244. The chemical structure shows a hexanone chain with two tert-butyl groups attached to the oxygen atom.</p>	4	<p>Mass spectrum for Dihexyl ether. The x-axis is m/z from 40 to 300, and the y-axis is relative intensity from 0 to 100. Major peaks are at m/z 44, 73, and 146. The chemical structure shows two hexyl groups attached to an oxygen atom.</p>
5	<p>Mass spectrum for Hexanoic acid, TMS derivative. The x-axis is m/z from 40 to 180, and the y-axis is relative intensity from 0 to 100. Major peaks are at m/z 45, 59, 73, 87, 101, 115, 130, 144, 158, 172, and 186. The chemical structure shows a hexanoic acid chain with a TMS group attached to the oxygen atom.</p>	6	<p>Mass spectrum for 1-Heptanol, TMS derivative. The x-axis is m/z from 40 to 180, and the y-axis is relative intensity from 0 to 100. Major peaks are at m/z 41, 55, 73, 87, 101, 115, 130, 144, 158, 172, and 186. The chemical structure shows a heptanol chain with a TMS group attached to the oxygen atom.</p>
7	<p>Mass spectrum for Phenol, TMS derivative. The x-axis is m/z from 40 to 180, and the y-axis is relative intensity from 0 to 100. Major peaks are at m/z 45, 59, 73, 87, 101, 115, 130, 144, 158, 172, and 186. The chemical structure shows a phenol ring with a TMS group attached to the oxygen atom.</p>	8	<p>Mass spectrum for Phenyl (2-bromohalobutanoate) (2-bromohalobutanoate). The x-axis is m/z from 40 to 300, and the y-axis is relative intensity from 0 to 100. Major peaks are at m/z 45, 59, 73, 87, 101, 115, 130, 144, 158, 172, and 186. The chemical structure shows a phenyl ring attached to a 2-bromohalobutanoate chain.</p>
9	<p>Mass spectrum for Pyridine, 2,4-dimethyl-. The x-axis is m/z from 40 to 260, and the y-axis is relative intensity from 0 to 100. Major peaks are at m/z 42, 56, 70, 84, 98, 112, 126, 140, 154, 168, 182, 196, 210, 224, 238, 252, and 266. The chemical structure shows a pyridine ring with two methyl groups at the 2 and 4 positions.</p>	10	<p>Mass spectrum for Pyrene. The x-axis is m/z from 40 to 320, and the y-axis is relative intensity from 0 to 100. Major peaks are at m/z 50, 64, 78, 92, 106, 120, 134, 148, 162, 176, 190, 204, 218, 232, 246, 260, 274, 288, 302, 316, and 330. The chemical structure shows a polycyclic aromatic hydrocarbon with four fused benzene rings.</p>

Based on the Table 12 assigned compounds from GC-MS analysis, it is evident that experimental conditions (Table 2) significantly affect the chemical diversity detected. For instance, sample 3, which experienced the highest temperature of 120°C, demonstrated the most substantial variety with 351 assigned compounds, suggesting that higher temperatures facilitate the formation or detection of more chemical species.

Sample 6, which was subjected to a reduced pressure of 0.7 bars, showed a notably lower count of 124 compounds.

The effect of ammonia concentration is highlighted by the variation between samples 4 and 5; with an ammonia concentration of 0.11 gr/L, sample 4 presented 261 compounds, whereas sample 5 with a higher concentration of 11.66 gr/L showed an increase to 330 compounds, underscoring ammonia’s role in enhancing chemical diversity in such experimental setups.

The choice of spark generator also impacts the compound diversity, as seen in samples 7 and 8, where different generators (FB-2 and CA-1) contributed to a significant difference in detected compounds, 305 versus 160, respectively. These observations reinforce the critical influence of experimental parameters on the outcome of chemical analyses in prebiotic simulation experiments.

Table 12: **Number of chemical formula assigned by GC/MS.**

Experiment #	Number of assigned compounds
Sample 1	140
Sample 2	154
Sample 3	351
Sample 4	261
Sample 5	330
Sample 6	124
Sample 7	305
Sample 8	160

The 20 major fragments of each sample are shown in Table 13. We present the chemical structure as identified via the NIST database and in the literature [1]. Detected fragments consist of saturated hydrocarbons, fatty acids, esters, fatty alcohols, ketones,

ethers, aldehydes, sterols, ethylene glycol, and phenols, among others. The fragments 43, 57, 71, and 85 m/z were attributed to hydrocarbons. The fragments 341, 313, 147, 145, 132, 129, 117, and 45 m/z were attributed to fatty acids and fatty alcohols; 180, 166, and 165 m/z were attributed to phenol components. Some components were not among common molecule fragmentation products found in the literature, and we assigned these molecular fragments according to the GC-MS database, e.g., 330, 263, 222, and 221 m/z. Moreover, due to the derivatization, we found some ions that originated from the BSTFA removal of the labile hydrogens (see Section 7.7.1). Quantitatively, fatty acid fragments were the most abundant ones, except for sample 6, where the phenol motif dominated. In Table 13, we identified a strong similarity between samples 2 and 3, differing in temperature only (100 °C and 120 °C). The fragmentation pattern of sample 1 (produced at 80 °C) was similar but did not exactly follow the same path.

Fragments 117, 75, and 73 m/z (fatty acids, fatty alcohols, ethers, and aldehydes) were present in samples 2, 4, and 5. In low- and mid-ammonia concentrations, three more fragments were common (132, 57, and 43 m/z). These fragments were not among the top ten of the high-ammonia sample (sample 5). Reducing the pressure to 0.7 bars is achieved by decreasing the level of methane. Comparing sample 2 (at atmospheric pressure) and sample 6 (at 0.7 bars), we found that they exhibited the same three common fragments, 117, 73, and 75 m/z, which correspond to fatty acids, fatty alcohols, ethers, and aldehydes. Notably, fragment 73 m/z, representing ethers and aldehydes, held the second-highest rank. In the low-pressure condition (sample 6), the chromatogram was dominated by fragment 165 m/z, associated with phenols (Table 13).

Three distinct spark generators, FB-1, FB-2, and CA-1, were employed for the synthesis of samples 2, 7, and 8 (see Figure 24 and Table 4). For both flyback-based spark generators (FB-1 and FB-2), ions with m/z values of 145, 132, 129, 117, 75, 73, 57, and 43 (fatty acids, fatty alcohols, ethers, aldehydes, and hydrocarbons) ranked among the top ten most abundant ions. Conversely, sample 8, produced using spark generator CA-1, displayed the top five most abundant ions 165, 147, 180, 45, and 166 m/z (phenols, fatty acids, fatty alcohols, PEG, ethers, dicarboxylic acids, bisphenols, and ketones). However, ions with 165, 147, 180, and 166 m/z appeared in samples 5 and 6 among the top 10, suggesting that the CA-1 spark generator would (at least partly) compensate for lower ammonia/methane ratios (Table 13) [1].

Table 13: The 20 most abundance fragments as observed by GC/MS.

Experiment #	Fragments abundance decrease (m/z) →																	
Sample 1	73	117	75	132	313	129	57	221	43	145	147	71	341	355	85	55	281	
Sample 2	117	73	75	132	313	129	57	43	145	71	341	55	85	41	131	69	185	
Sample 3	117	73	75	132	313	129	57	43	145	71	341	85	55	41	131	69	314	
Sample 4	73	221	75	117	222	263	57	43	147	132	71	129	313	223	74	133	85	
Sample 5	73	165	75	147	180	117	221	330	175	45	129	43	74	114	128	166	257	
Sample 6	165	73	180	75	166	149	175	117	147	43	57	45	221	74	71	132	98	
Sample 7	117	73	341	75	132	129	145	57	43	55	342	131	71	226	69	133	41	
Sample 8	73	165	147	75	117	180	43	45	149	166	131	74	129	59	330	221	116	

Limitations of Our Analytical Method One significant limitation pertains to the vaporization of the analyte, which we improved through derivatization techniques. Another challenge concerns the effective separation of compounds within the GC-MS system. We used a HP-5MS UI fused silica capillary column (Agilent Technologies). It is nonpolar and will not provide optimal separation for polar compounds. However, development of a nontargeted comprehensive method for all compounds is impossible. Moreover, we expect several factors to contribute to a weak detection of certain compounds in our study, such as, for example, formic acid or amino acids (see Table 10 and Table S4 in the Supplementary Materials [1]), which were detected elsewhere by others [203, 287, 288].

- a. **Method and Run Time:** The five-day duration of our experiment may have impacted the composition by altering the ratios of components. Different run times can lead to variations in product yields and product composition.
- b. **Extraction Procedure:** The use of chloroform, a non-polar solvent as described in Section 7.5, for extraction may exclude or reduce the recovery of highly polar compounds.
- c. **Chemical Reactions:** During the drying or extraction process, unintended reactions could have occurred, potentially altering the composition in both the water-methanol and chloroform phases [284, 289].
- d. **GC-MS Method:** The wide range of compounds generated in our experiment posed a challenge for analysis. To ensure clarity and achieve robust results, we

focused on non-polar compounds with m/z values between 50 and 550. This allowed us to report compounds with acceptable signal-to-noise ratios while ignoring peaks that did not meet our predefined standards. This occurred in situations where substances could not be separated by the column because their migration properties were too similar.

8.1.2 Gas phase

The GC-MS analysis of the gas phase revealed a large variety of organic compounds as shown in Table 14 including: Benzene and toluene could form the backbone of more complex organic molecules, phenol and acetylacetone could partake in essential prebiotic reactions, potentially leading to larger biomolecules. The potential for polymerization is highlighted by styrene and butadiene, which is essential for forming larger molecular structures.

Additionally, pyridine and naphthalene, with nitrogenous bases and stable ring systems, could be the precursors to nucleotide synthesis. The varied hydrophobicity of alkylbenzenes might enrole the assembly of lipid bilayers or vesicles, facilitating the formation of primitive cell-like structures [290].

Consistent with previous findings, our study observed molecules in the gaseous phase with distinctive properties or reactive functional groups, including those featuring two symmetrical ketone groups and long carbon chains [226]. Additionally, both the gaseous and liquid phases revealed molecules combining benzene rings with ester bonds, alongside highly reactive groups such as oxiranes, isocyanates, peroxides, nitro compounds, and nitriles [226].

In this study, the quantities of compounds present in Miller gas compositions, such as benzene rings, appear to exhibit relative stability. Previous research has similarly indicated that benzene rings, esters, and alkynes maintain stable quantities in Miller gas compositions [226].

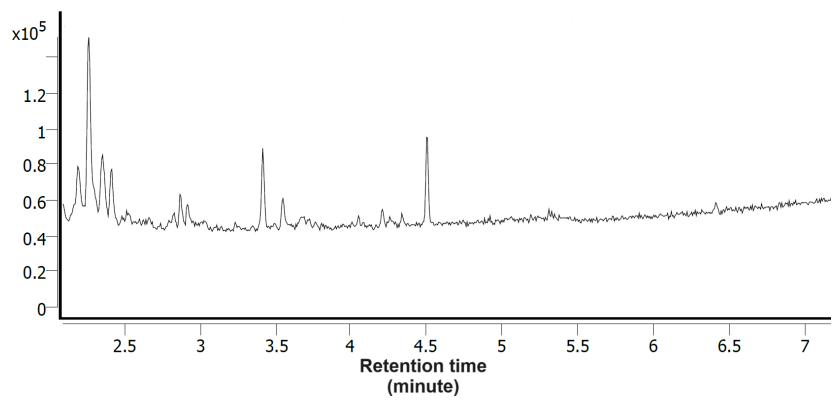
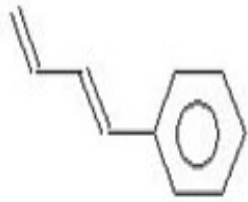
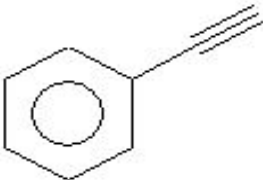
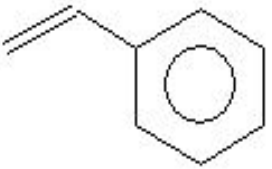
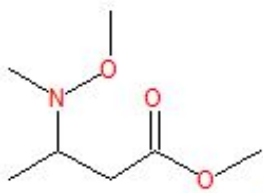
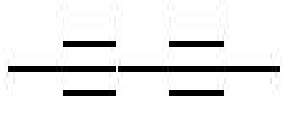
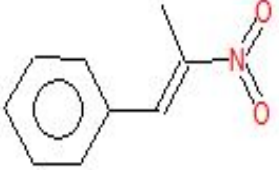

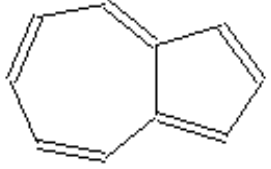
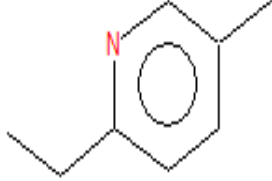
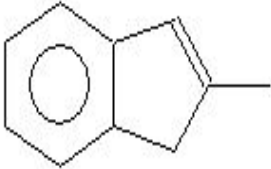


Figure 28: Example of GC-MS chromatogram in the gas phase.

Table 14: Examples of detected compounds in the gas phase.

ID	Image	ID	Image
1		2	
3		4	
5		6	
7		8	
9		10	

8.2 FTMS

In Figure 29, a spectrum of the m/z values between 100-1000 m/z is shown. The analysis was performed in positive mode and injected via shotgun injection method. Multiple peaks are visible in the spectrum. The method details for FTMS analysis of the Miller soup are described in Table 5. In Figures 30, FTMS spectrums of samples 1 to 8 synthesized under the conditions specified in Table 2 is presented.

In a current study performed in our group, the negative ion mode revealed tungsten species, prominently WO_3OH^- (m/z 248.93896), while the positive ion mode identified $\text{C}_8\text{H}_{13}\text{O}_4^+$ (m/z 173.08084), likely protonated carboxylic acids and esters [$\text{C}_8\text{H}_{12}\text{O}_4 + \text{H}^+$]. Chemical indices double bonds, and aromatic ring molecular classes [217] that has already also confirmed in our previous work [1]. Analysis of degree of saturation revealed a mean of 7.2 rings and double bonds, with an AI of 0.98, indicating substantial aromaticity [217].

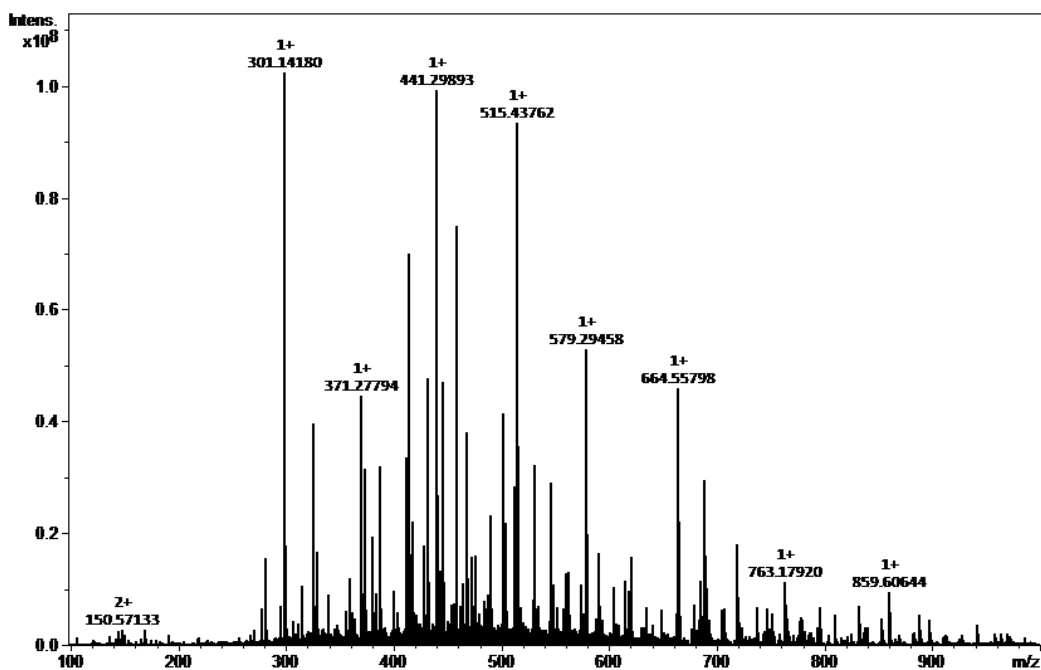
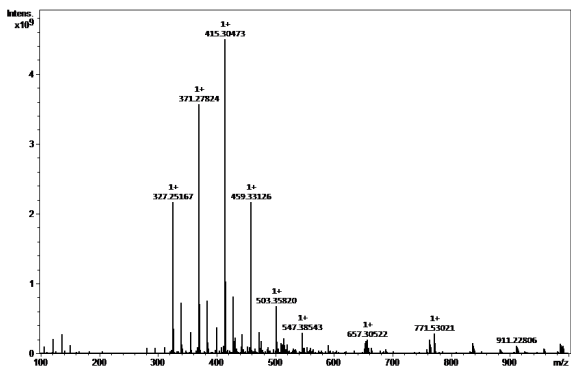
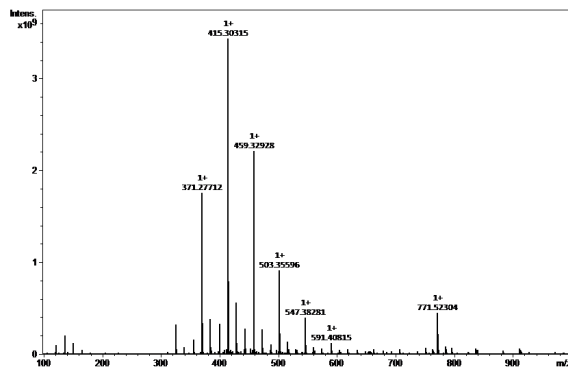


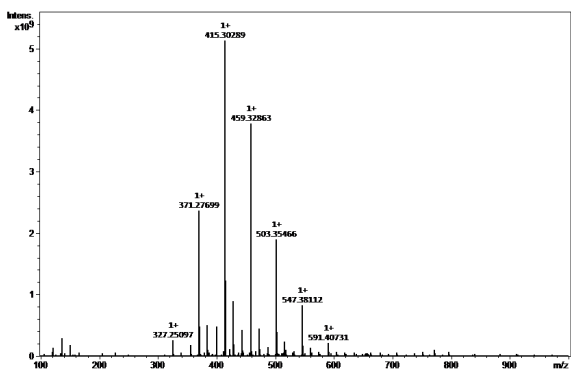
Figure 29: FTMS spectrum of the miller soup.



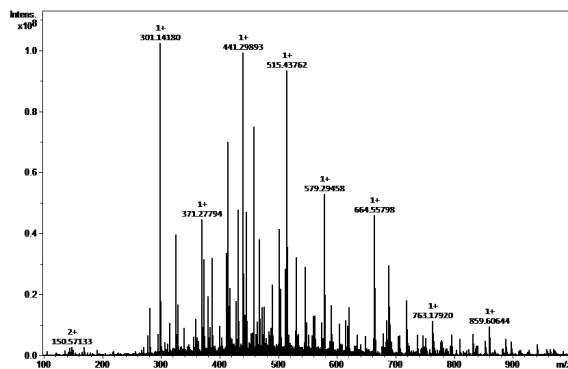
(a) FTMS-Sample 1



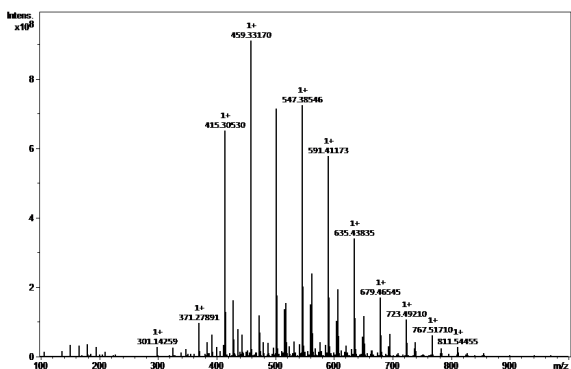
(b) FTMS-Sample 2



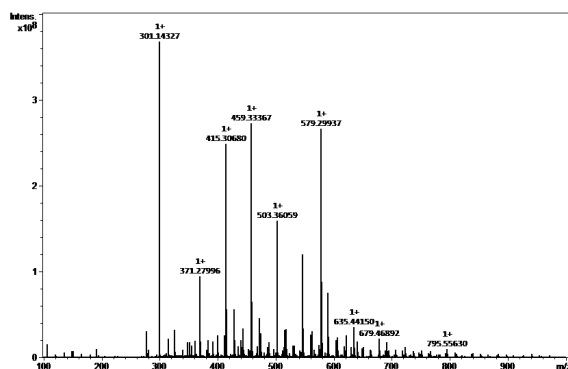
(c) FTMS-Sample 3



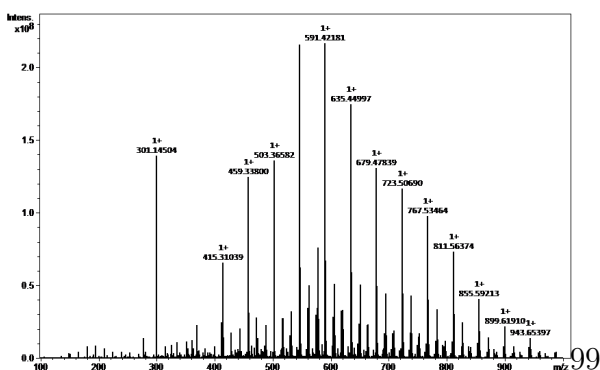
(d) FTMS-Sample 4



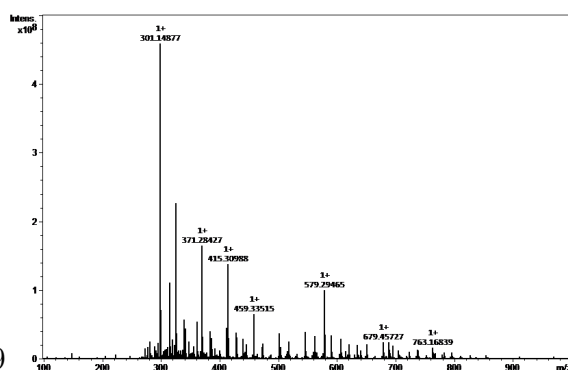
(e) FTMS-Sample 5



(f) FTMS-Sample 6



(g) FTMS-Sample 7



(h) FTMS-Sample 8

Figure 30: FTMS spectrum view of the miller soup for samples 1-8.

8.2.1 Kendrick Mass Defect

General Observations and discussion Across the samples 1-8, clustering around certain KMD values for CH_2 indicates the consistent formation of hydrocarbon and other polymer chains or related derivatives. These patterns illustrate how experimental variables influence chemical pathways and the stability of formed compounds (see Figure 31 and Chapter 6.4.2).

In a current study performed in our group using ESI FTICR with a gas ratio of 2:2:1 for $\text{CH}_4:\text{NH}_3:\text{H}_2$, mass spectra identified 668 substances in ESI^+ mode, and 487 substances in ESI^- mode 166 substances common to both modes (ESI^+ and ESI^-). Series analysis using Kendrick maps highlighted polyethylene glycol (PEG) species and other homologous series. Fragmentation analysis via ESI FTICR MS/MS confirmed PEG species and identified oligomers, suggesting PEG's presence not as a contaminant but with a hydrophobic alkane tail [217]. These results also confirmed in our spectrum results as shown in Figure 31.

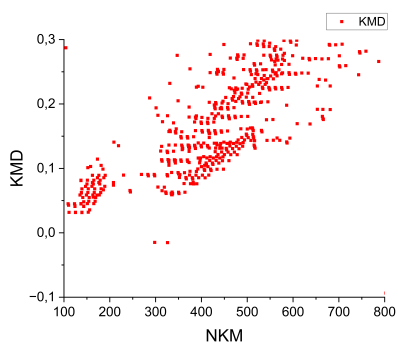
Individual Observations Temperature Variations: Increasing temperature from 80 °C (Sample 1) to 120 °C (Sample 3) shows a notable decrease in the density and spread of data points at higher nominal Kendrick mass (NKM) values. This suggests that higher temperatures may lead to the degradation or transformation of more complex molecules into simpler ones, or possibly affect the stability of certain compounds(see Figure 31 and Table 2).

Ammonia Concentration: Varying ammonia concentrations shows distinct trends. At a low concentration of 0.11 gr/L (Sample 4), the spread of KMD values is narrow, indicating fewer types or possibly less complex formations of molecules. Conversely, a higher concentration of 11.66 gr/L (Sample 5) shows increased complexity and a broader distribution of compounds, which suggests enhanced synthesis capabilities under ammonia-rich conditions(see Figure 31 and Table 2).

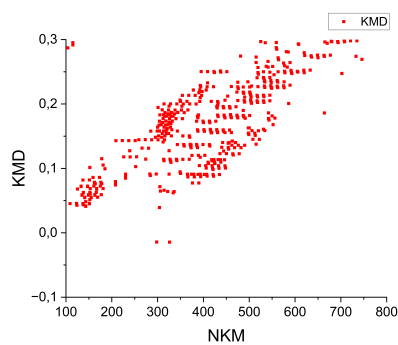
Initial Pressure: Changes in pressure, from 1.0 bar in most samples to 0.7 bar in Sample 6, show subtle shifts in distribution patterns. Lower pressure slightly reduces the spread of the data points, potentially indicating less diversity in molecular formation or changes in reaction kinetics (see Figure 31 and Table 2).

Spark Generator Type: The alteration in spark generator from FB-1 (Sample 2) to

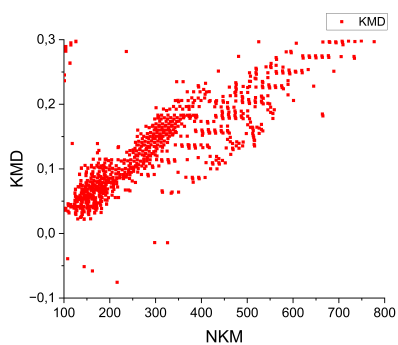
FB-2 (Sample 7) and CA-1 (Sample 8) shows only minor variations in the Kendrick Mass Defect (KMD) plots, suggesting that the type of spark generator has a less significant impact compared to variables like temperature or ammonia concentration. The FB-1 generator used in Sample 2 typically shows a balanced distribution of data points. Conversely, the FB-2 generator in Sample 7 and the CA-1 generator in Sample 8 introduce slight variations in the density and spread of KMD data points. These variations hint at the role of spark generators in shaping the chemical pathways and the types of compounds formed during the experiments (see Figure 31 and Table 2).



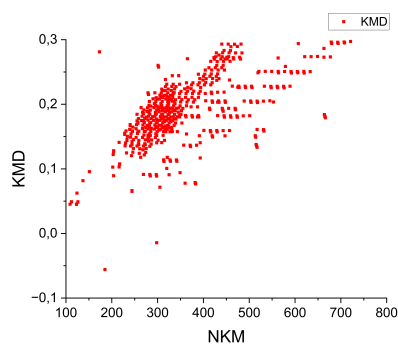
(a) KMD Sample 1



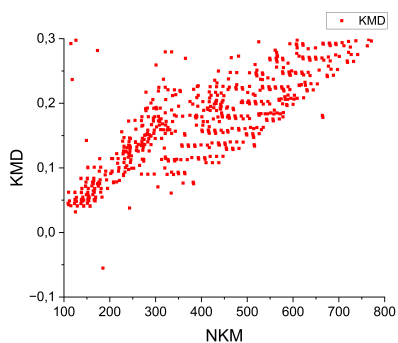
(b) KMD Sample 2



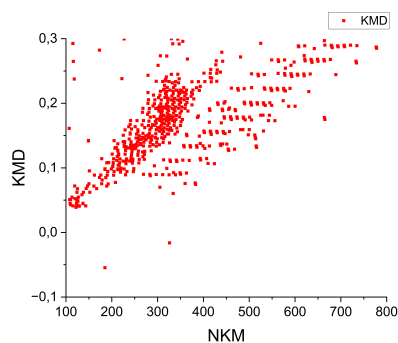
(c) KMD Sample 3



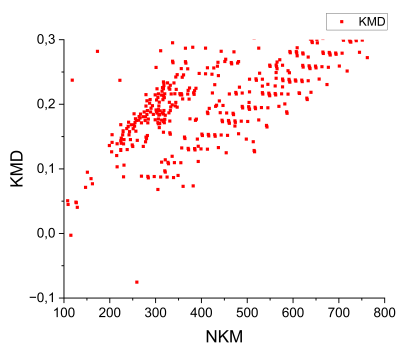
(d) KMD Sample 4



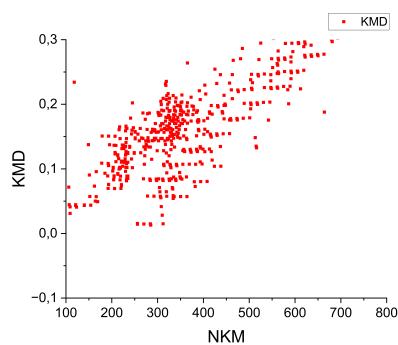
(e) KMD Sample 5



(f) KMD Sample 6



(g) KMD Sample 7



(h) KMD Sample 8

Figure 31: Distribution of compounds¹⁰² in kendrick mass defect analysis using CH_2 mass base.

8.3 HPLC-FTMS

The HPLC-MS chromatogram displayed in Figure 32 showcases a complex mixture of components, clearly resolved over the time course as specified in the procedural details in Table 6. The upper panel of the plot displays the mass-to-charge ratio (m/z) from 150 to 1000 over a time course, with varying intensities indicated by different colors. It appears that the sample contains a wide range of molecular species with different mass distributions, which are possibly indicative of polymers or polymer-like substances.

The retention time pattern and intensity variation suggest the presence of compounds with different polarities. Initially, the gradient started with 90 % water and 10 % acetonitrile, typically favoring the elution of more polar compounds. As the gradient shifts towards 100 % acetonitrile at 170 minutes, it facilitates the separation and detection of more non-polar, hydrophobic molecules. This is evidenced by the gradual shift in the plot from lower to higher retention times and from lower to higher m/z values. The higher m/z values towards the latter part of the chromatogram suggest the elution of larger or more complex molecules, possibly higher molecular weight polymers or non-polar compounds.

The change in solvent composition throughout the gradient (detailed in the Table 6) likely influences the detachment and elution patterns of different chemical entities within the mixture. Notably, Hydrocarbons, polyethylene glycol, a common polymer, is detected along with potential nitrogen-based polymers as shown in the upper picture of Figure 32 with a mass distance of 14 and 44 m/z respectively. These substances typically exhibit a broad range of m/z values due to varying chain lengths and degrees of polymerization. Some lines show a positive slope while others show a negative slope in the time course of the HPLC-MS analysis, indicating the diverse potential for hydrophilicity and hydrophobicity of the moieties attached to the polymer chains. This also reflects a diverse range of polymerization molecular weights in the Miller-Urey experiment mixture (see Figure 32).

The lower panel of the plot, showing total ion intensity against time, supports the findings from the upper panel by highlighting the overall ion abundance peaks at specific times. This panel confirms that the most ionizable and, therefore, detectable compounds elute primarily towards the latter half of the run, Corresponding with the switch to a non-polar mobile phase.

The method's use of a non-polar chromatography column and a solvent gradient enhanced its efficacy in separating a complex mixture based on polarity and molecular size. This experiment is particularly developed for samples where the target analytes range widely in both chemical nature and size, making it suitable for analyzing intricate mixtures like those often found in polymer research and complex organic matrices. The observed patterns in the chromatogram (both the positive and negative slopes) reflect the varying interaction strengths of the molecules with the column's stationary phase, influenced by their structural characteristics and the changing solvent environment.

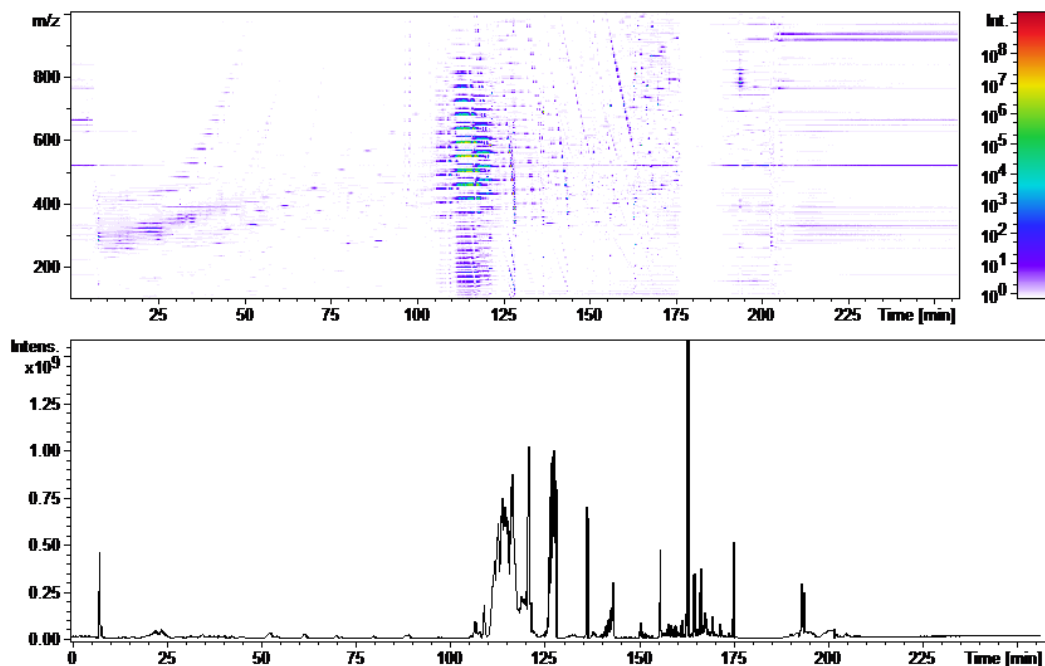


Figure 32: HPLC-FTMS chromatogram of the miller soup.

8.4 Real-time UV-Vis absorption

To create a comprehensive picture of how the absorbance of a sample changes over time using UV-Vis spectrometry, data integration is performed by plotting the measurements taken at hourly intervals in a single contour plot. In this visualization, the x-axis represents the time dimension, marked by each hour when a scan was performed. The y-axis corresponds to the wavelength of the light in nm. The color at any given point on the plot represents the absorbance at that particular time and wavelength. By mapping the data in this way, a contour plot is generated, which shows the evo-

lution of the sample's absorbance across the entire spectrum over the course of the experiment. This method effectively captures dynamic changes and makes it easier to observe trends such as the emergence of new absorbance peaks, providing insights into the reaction kinetics and the formation or decomposition of compounds over time.

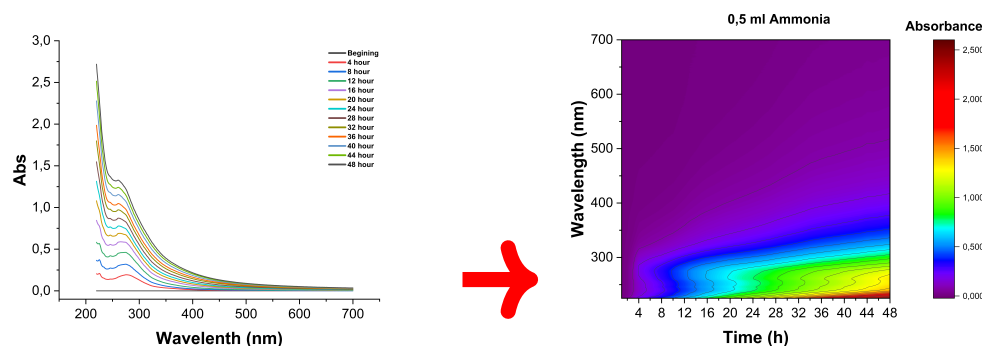


Figure 33: **Real-time UV-Vis absorption spectra trends.** UV-Vis absorption spectra displayed in contour plot to illustrate absorbance trends across wavelengths

The contour plots provided in Figure 34 illustrate the evolution of UV-Vis absorbance for a Miller-Urey-type reaction at different temperatures. The spectral data obtained at 80°C, 100°C, and 120°C reflect the thermodynamic and kinetic effects of temperature on the synthesis of organic compounds.

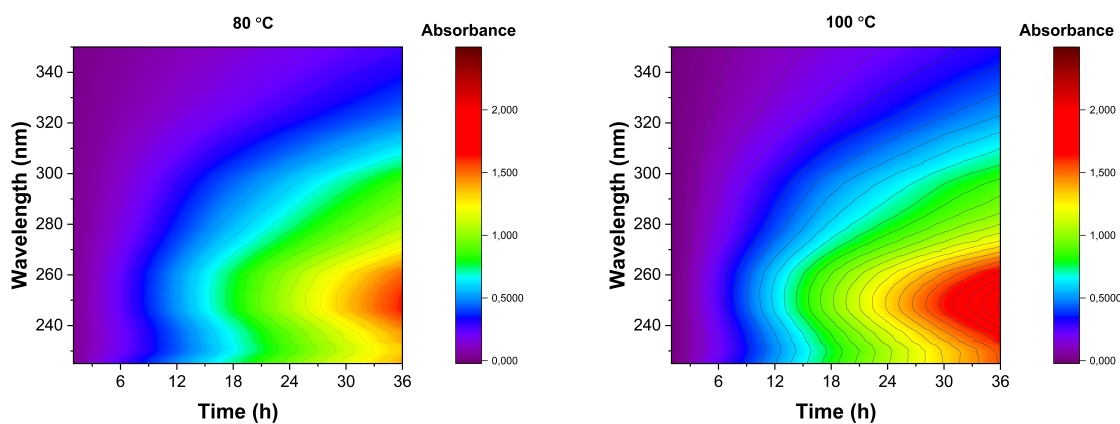
At the reactor temperature of 80°C, we observe a gradual increase in absorbance over time as shown in Figure 34a. This suggests the formation of chromophores capable of absorbing UV light under these relatively mild conditions.

Increasing the temperature to 100°C as shown in Figure 34b leads to an enhancement in absorbance, particularly within the mid-UV range. This trend shows a higher rate of complexation and formation of more organic structures with extended conjugation, which results in a broader and more intense UV absorbance.

At the elevated temperature of 120°C, as shown in Figure 34c resulted in a remarkable decrease in absorbance across a wide spectrum of UV wavelengths. It may be the potential for thermal degradation of these molecules also increases at such high temperatures.

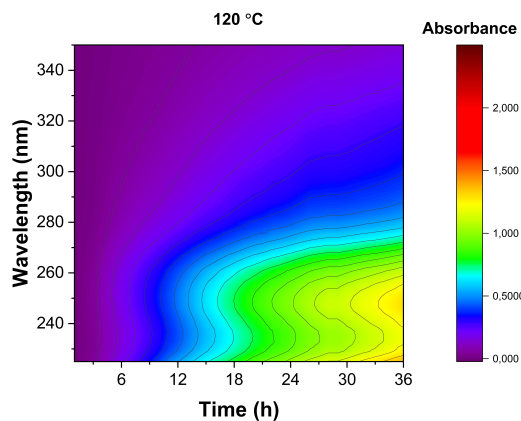
An optimal temperature appears to be one that balances the thermal energy available for reaction progression against the stability of the formed chromophoric compounds. While lower temperatures may not provide enough energy for complex reactions, higher temperatures could lead to significant degradation of the products. The results suggest

that a reactor temperature of approximately 100°C will provide an environment for the formation of stable, UV-absorbing species, optimizing the concentration of such compounds in the reaction mixture.



(a) UV-Vis absorption at 80 °C.

(b) UV-Vis absorption at 100 °C.



(c) UV-Vis absorption at 120 °C.

Figure 34: Real-time UV-Vis absorption for miller-urey experiments at 80 °C, 100 °C, and 120 °C.

Plots provided from UV-Vis spectrophotometry experiments reveal how the UV-Vis absorbance of Miller-Urey type reaction changes over time with different concentrations of ammonia.

In the first plot (Figure 35a) with 0.5 mL of ammonia, there's a gradual increase in absorbance with time, most notably at lower wavelengths. This suggests the formation of compounds with chromophores that absorb in the UV region, potentially simple

aromatic rings or unsaturated compounds. The presence of these in low concentration could be attributed to limited availability of nitrogen from ammonia for reactions to form more complex structures.

The second plot with 5 mL of ammonia shown in Figure 35b shows a change in absorbance across the spectrum. The absorption peaks shift more noticeably over time, indicating the formation of a broader range of organic compounds. The introduction of more ammonia has possibly facilitated the formation of compounds with multiple bonds and ring structures, which absorb at varying wavelengths due to different chromophores, resulting in the development of a richer array of products as indicated in the GC-MS results [1].

In the third plot with 10 mL of ammonia, the absorbance at all wavelengths increases significantly over time (Figure 35c), with the most intense absorption in the mid-UV range. This could be interpreted as a high concentration of ammonia driving the formation of more complex, condensed structures, such as polycyclic aromatic hydrocarbons (PAHs) and heterocycles. These compounds have extended conjugated systems which can result in stronger and broader UV-Vis absorption due to $\pi \rightarrow \pi^*$ transitions as their presence is proved in the GC-MS results [1].

With the addition of ammonia, not only the amount of nitrogen available for reactions increase, but the pH of the reaction mixture can also increase, potentially affecting the speciation of organic compounds and influencing their absorbance characteristics. The presence of saturated compounds, aliphatics with double bonds, benzene, polycyclic aromatics, and heterocycles containing oxygen and nitrogen points to a highly varied synthetic pathway that could involve radical reactions, condensation, and addition reactions, among others, facilitated by the high-energy spark discharge.

Increasing the concentration of ammonia in the reaction mixture correlates with an increase in both the diversity and the complexity of the organic compounds formed. This supports the idea that in prebiotic chemistry, the concentration of simple molecules like ammonia could have had a significant influence on the complexity of the resulting organic compounds.

In the experiment with high ammonia concentration, the UV-Vis spectral data shows unstable oscillations in absorbance over time. This phenomenon could be indicative of dynamic chemical equilibria in the reaction mixture where intermediate compounds are continuously formed and decomposed.

One possible mechanism for this oscillation is the presence of competing reaction pathways. With higher concentrations of ammonia, the formation of more complex molecules with multiple chromophores is facilitated. These compounds may absorb UV light more efficiently due to the presence of multiple π -bond systems and heteroatoms that create a delocalized electron network, allowing for transitions such as $\pi \rightarrow \pi^*$ and $n \rightarrow \pi^*$. However, as these complex molecules are formed, they may also be prone to further reaction, either with each other, with the excess ammonia, or with radicals generated by the spark discharge. Such secondary reactions could break down these compounds, resulting in a temporary decrease in absorbance.

Furthermore, the high-energy conditions provided by the spark generator could lead to the formation and depletion of highly reactive intermediates in a non-linear fashion, contributing to the oscillatory patterns observed. These intermediates may have significant absorbance in the UV range due to their electronic structures, and their transient nature would result in fluctuating absorbance values.

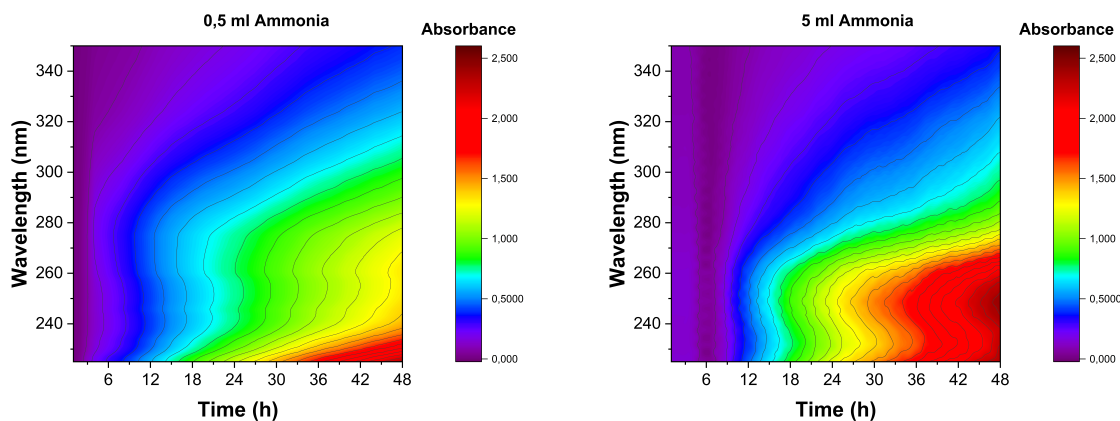
Another factor to consider is the potential for light scattering effects caused by the formation of larger particles or aggregates in the high ammonia concentration experiment. These could intermittently influence the measured absorbance by scattering the incident light, resulting in apparent oscillations in the absorbance data.

Ammonia with its lone pair of electrons can engage in a variety of chemical reactions, including nucleophilic addition or acting as a base. In an environment where UV light is abundant, ammonia can contribute to the formation of a range of nitrogen-containing organic compounds, including those with conjugated double bonds and aromatic rings. These structures are known as chromophores—molecular fragments that absorb visible or UV light.

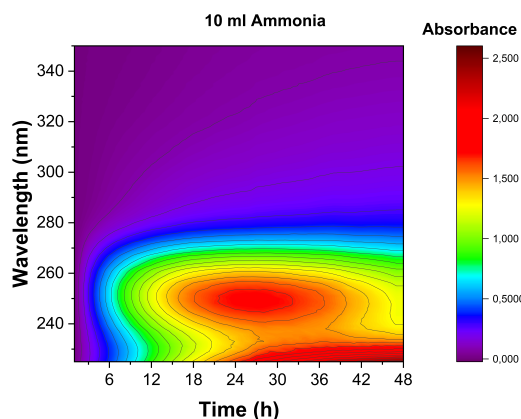
The chromophores within these newly synthesized organic molecules can efficiently absorb the energy from the UV light [291]. This absorption promotes electrons from their ground state (π -bond) to an excited state (π^* antibond), which is a higher energy orbital. Such $\pi \rightarrow \pi^*$ transitions are common in molecules with conjugated systems and can absorb a wide range of UV light wavelengths. This absorption is crucial as it allows the molecules to capture the energy needed to drive subsequent chemical reactions, including radical reactions which have high-energy chemistry environments.

The radical reactions are particularly significant. The energy absorbed from UV light can split chemical bonds, creating radicals [292]. These highly reactive species can

then initiate a chain of reactions, potentially leading to the formation of increasingly complex organic molecules. However, the same UV light and radicals that drive the formation of complex molecules can also lead to their degradation over time [293]. The energy absorbed by the chromophores can cause the molecules to become unstable and break apart, leading to a decrease in the observed UV absorbance as the pigments decompose [294].



(a) Real-time UV-Vis absorption for 0.5 ml NH₃, 48 hours (b) Real-time UV-Vis absorption for 5.0 ml NH₃, 48 hours



(c) Real-time UV-Vis absorption for 10 ml NH₃, 48 hours

Figure 35: **Real-time UV-Vis absorption of miller-urey experiments at different ammonia concentrations.**

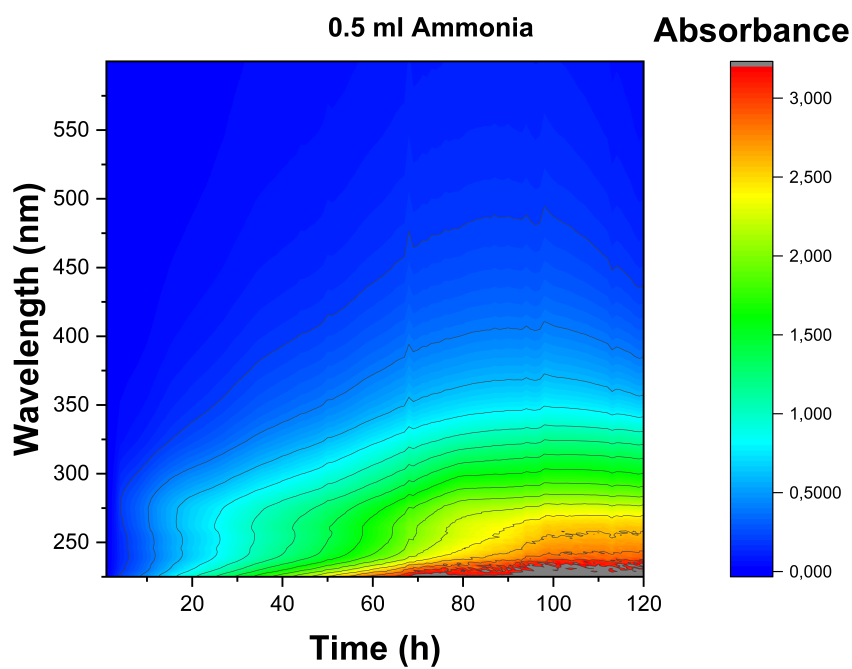
In the Figures 36 (a)&(b), the UV-Vis absorbance patterns of the experiment during a

120 hours performed with two different ammonia concentrations 0.5 and 5 ml (Figure 36a and Figure 36b respectively).

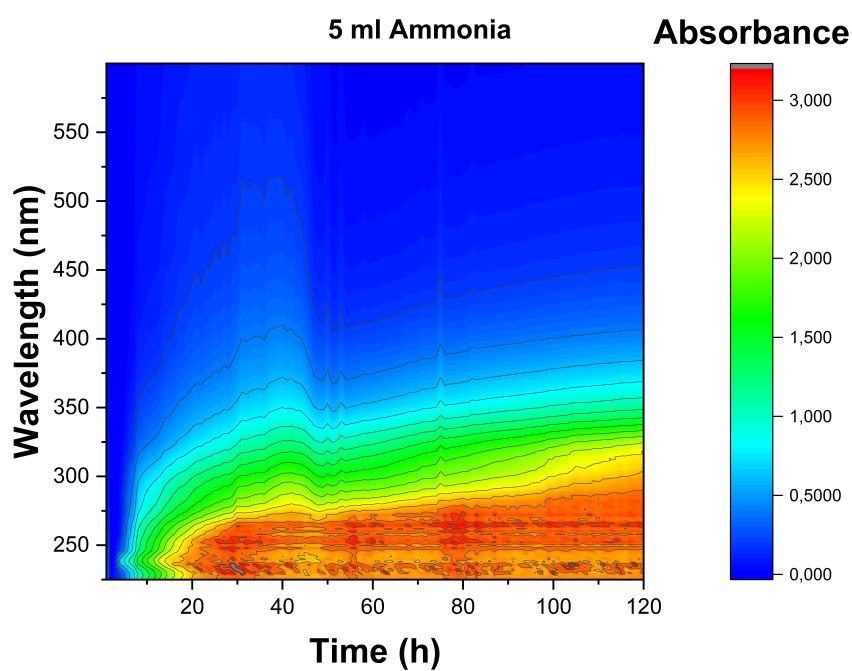
At a lower concentration of ammonia (Figure 36a), the UV-Vis absorbance data show a gradual increase over the extended period of 120 hours. This steady increase in absorbance suggests a consistent rate of formation synthesis of simple (comparing the polycyclic) organic molecules that absorb UV light. This could be attributed to the limited availability of nitrogen (either Ammonia) in the sample.

In contrast, the reaction with a concentration of 5 ml of ammonia (Figure 36b) presents a significantly different UV-Vis absorbance pattern. A dynamic increase, especially in the 250-350 nm range, points to the formation of more complex organic structures. The higher concentration of ammonia facilitates a broader array of chemical reactions.

1. **Complexation and Polymerization:** Longer reaction times could lead to the formation of larger macromolecules, presenting extensive conjugated systems which result in stronger UV-Vis absorbance.
2. **Chemical Equilibrium:** The system may be approaching a chemical equilibrium, balancing the rates of synthesis and degradation of compounds.
3. **Degradation of Compounds:** Potential instability of certain compounds could result in their degradation over time, altering the UV-Vis absorbance profile.
4. **Saturation Effects:** There may be saturation effects at play, especially at higher concentrations, which could limit the linear relationship between concentration and absorbance in the spectrophotometer.



(a) UV-Vis 0.5 ml NH₃, 120 hours



(b) UV-Vis 5.0 ml NH₃, 120 hours

Figure 36: Real-time UV-Vis absorption of 0.5 & 5.0 ml NH₃ in 120 hours.

8.5 Fluorescence

The excitation-emission fluorescence spectrum as shown in Figure 37 provides a view of the complex mixture of organic compounds within the miller soup. The dominant peak observed in the spectrum likely corresponds to aromatic compounds (as revealed in the GC-MS [1]) or conjugated systems present within the mixture, which are known to exhibit strong fluorescence when excited at specific wavelengths.

The $\pi - \pi^*$ transitions in aromatic systems and conjugated double bonds are primarily responsible for the absorption of photons leading to excitation. The spectral region with the highest intensity, showing a maximum at both excitation (around 350 nm) and emission (around 450 nm) wavelengths, could indicate the presence of aromatic heterocycle groups within the sample. These compounds typically exhibit such fluorescence characteristics due to their structured electronic configurations, which allow for energy absorption and subsequent emission within this range.

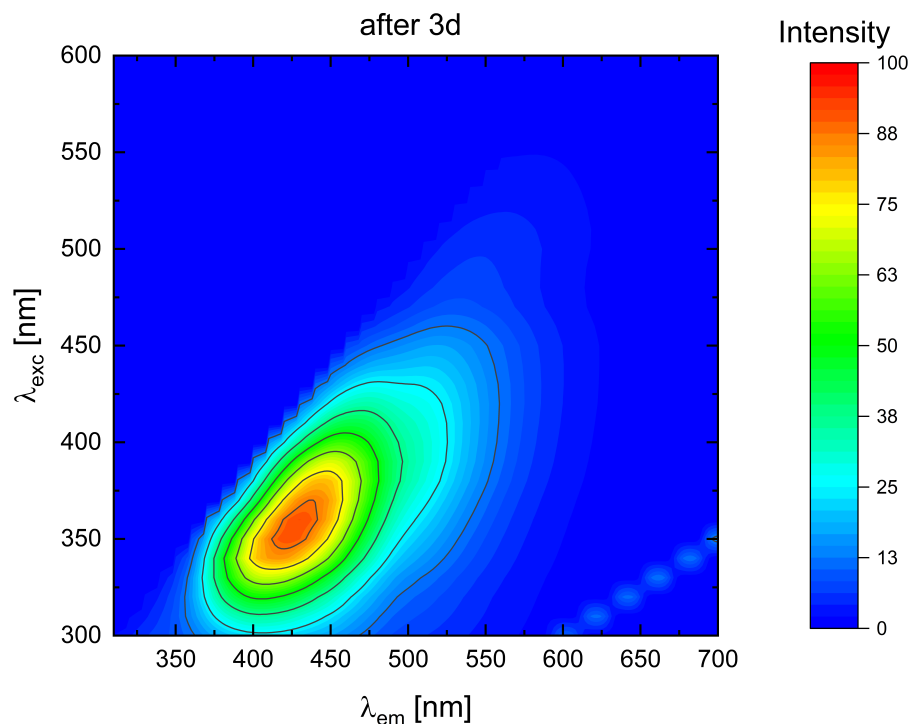


Figure 37: **Excitation-emission matrix (EEM) fluorescence spectrum.** The excitation wavelength λ_{exc} is plotted on the y-axis, and the emission wavelength λ_{em} on the x-axis, with the fluorescence intensity indicated by the color scale. The spectrum reveals a pronounced peak with maximum excitation around 350 nm and emission around 450 nm.

Furthermore, the broad emission profile suggests a diversity in the chemical environment of fluorescing species, hinting at the presence of various functional groups such as alcohols, amines, and carbamates, as seen in the GC-MS results [1].

The weak fluorescence emission above 500 nm may imply a lower concentration or absence of highly conjugated or larger polycyclic aromatic compounds, which would typically emit at longer wavelengths. The mixture's fluorescence indicates moderate aromaticity and suggests a wide variety of molecular structures, reflecting the chemical variability of the sample.

8.6 HPLC-UV-Vis

The HPLC-PDA chromatograms of the Miller soup samples, as shown in Figure 38, exhibit compounds with a broad range of polarity and absorbance wavelengths. Figure 38 also displays an intense light absorption between 30 and 45 minutes of retention time with an absorption between 240 and 275 nm mostly between 20 and 60 minutes in the retention time. Despite the use of an extended time, low flow rate, low slope rate of the mobile phase gradient, and a long reverse-phase column (see Section 7.9), the peak separation remains suboptimal. Furthermore, the UV-Vis detector only reveals the wavelength and intensity of absorption of samples and does not provide the exact structure of the compounds. It would be advantageous to combine the data from HPLC-PDA with other chromatographic methods, such as exact mass spectroscopy, to enhance the accuracy of detection.

In this part, we aimed to illustrate how the HPLC-UV-Vis "fingerprints" of the sample mixtures look. Based on our method, we start the separation procedure with a polar solvent (100 % water) and end with 100 % acetonitrile to wash out the compounds that were injected into our non-polar column. Given that, polar compounds wash out and are detected earlier than non-polar compounds. In other words, polar compounds have lower retention times compared to non-polar compounds, which have higher retention times to be washed out of our HPLC column.

Figure 38, representing the sample with the highest ammonia concentration. It displays a few distinct peaks with very high absorptions. We can observe high UV-Vis absorption wavelengths (up to 340 nm), indicative of highly conjugated systems or the presence of stable paired electrons of heteroatoms such as N and O in organic compounds. These transitions in electronic spectra ($n \rightarrow \pi^*$ [275]) suggest the presence of specific molecular structures within the samples.

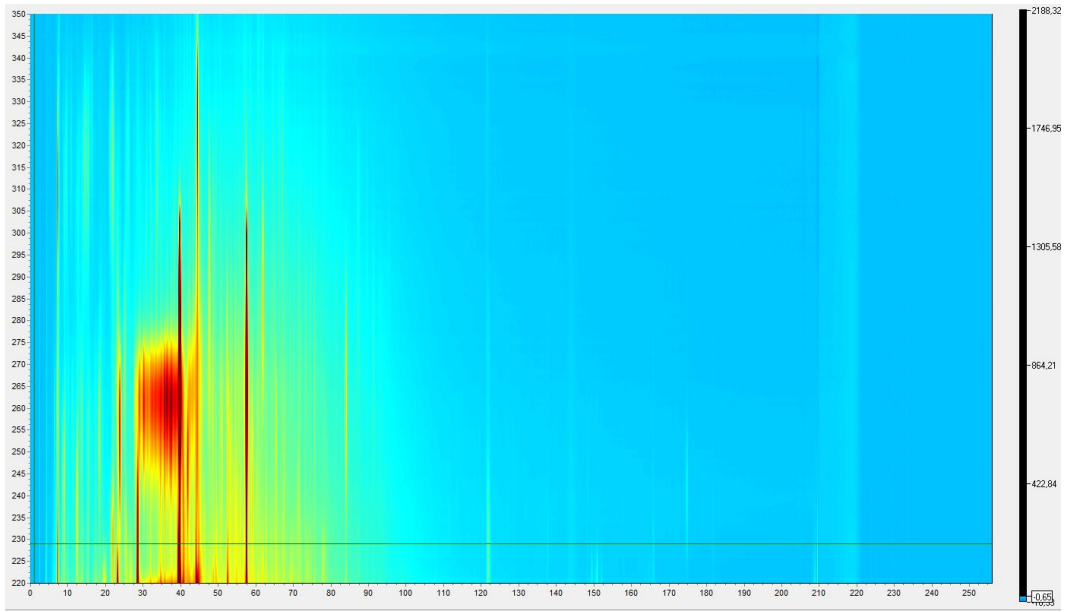


Figure 38: HPLC-UV-Vis chromatogram of Miller Sample.

8.7 Gas Phase IR absorption

Infrared spectroscopy analysis in the gas phase revealed several absorption bands in the infrared spectroscopy that help identify the molecular constituents of the complex mixture [295]. As an example we analysed one gas sample with a spark running time of 7 days with FTIR and the analysed spectrum presented in Figure 39. As shown in Figure 39, The broad absorptions spanning approximately 3200 to 3600 cm^{-1} , indicates O-H stretching vibrations. These are typically associated with alcohols, phenols, or carboxylic acids, suggesting the presence of hydroxyl-containing compounds. Additionally, Peaks measured from 2470 to 3200 cm^{-1} point to C-H stretching in methane and also alkanes, signaling the presence of hydrocarbon chains. The peak at 3016 cm^{-1} is attributed to =C-H stretching commonly observed in alkenes. N-H stretching vibrations were confirmed with peaks at 3263 and 3309 cm^{-1} , supporting the existence of amines or amides in the sample [275].

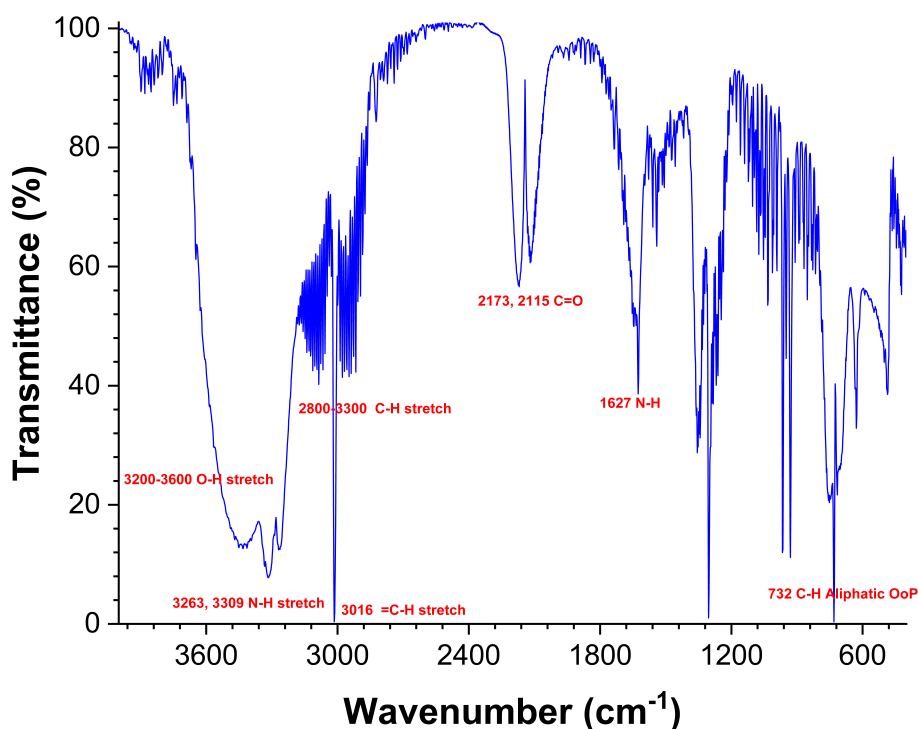


Figure 39: Infrared spectrum of a gas phase sample after a sparking run-time of 7 days.

The absorption observed in the range of 2240 cm^{-1} indicates the carbon-nitrogen triple

bonds, characteristic of nitriles ($C \equiv N$). This absorption is due to the stretching vibrations of the ($C \equiv N$) bond. Infrared absorption around 2123 cm^{-1} typically suggests the presence of a carbon-carbon triple bond ($C \equiv C$) or carbon-nitrogen triple bonds ($C \equiv N$) in nitriles or isocyanides. The specific peak can vary slightly based on the molecular environment and other attached groups, but generally, this absorption is characteristic of these types of triple bond stretching vibrations. The peak around 1625 cm^{-1} suggests $C = O$ stretching vibrations, common to ketones, aldehydes, esters, or amides. It also indicates the presence of $C = C$ stretching vibrations, commonly found in aromatic compounds or conjugated alkenes. This wavenumber can also signify the presence of N-H bending vibrations, particularly in amides, indicating the presence of unsaturated bonds or secondary amines [294, 275].

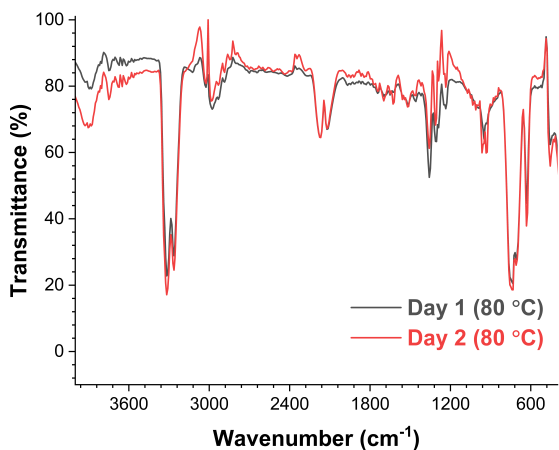
An absorption peak at 1303 cm^{-1} is generally indicative of C-N stretching vibrations, which are often found in aromatic amines. This type of vibration can be characteristic of the single bond interactions between carbon and nitrogen atoms within an aromatic framework. Additionally, this peak may also suggest the presence of O-H bending in alcohols and phenols, or C-H bending in functional groups such as methyl and methylene.

Additionally, peaks at Around 925 cm^{-1} could attributed to $=C-H$ out-of-plane bending in trans-alkenes. Peaks Around 964 cm^{-1} could indicate $=C-H$ out-of-plane bending in cis-alkenes. These vibrations are useful for identifying unsaturation in molecular structures and for distinguishing isomeric forms in a sample [275, 294, 296].

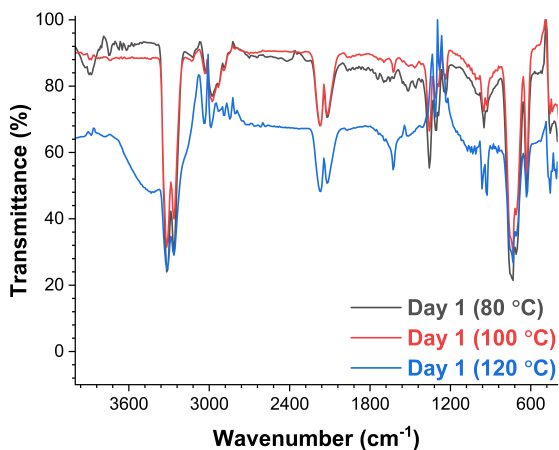
An infrared absorption peak at 731 cm^{-1} typically indicates the presence of C-H out-of-plane bending vibrations in aromatic compounds. This particular absorption is characteristic of mono-substituted benzene rings. Such out-of-plane bending motions occur when the hydrogen atoms of the aromatic ring move perpendicular to the plane of the ring, which can be indicative of the substitution pattern within the aromatic system. This is especially useful in distinguishing mono-substituted benzene derivatives from other types of substitution such as di-substituted or tri-substituted structures, where the patterns and frequencies of bending vibrations differ [275, 294, 296].

We also performed experiments and compared the IR spectra of the gas phase samples under varying parameters to observe changes in IR spectrums, as shown in Figure 40. This set of figures allows us to deduce the composition of the gas phase under different experimental settings and over time scans (temperature, time, and ammonia

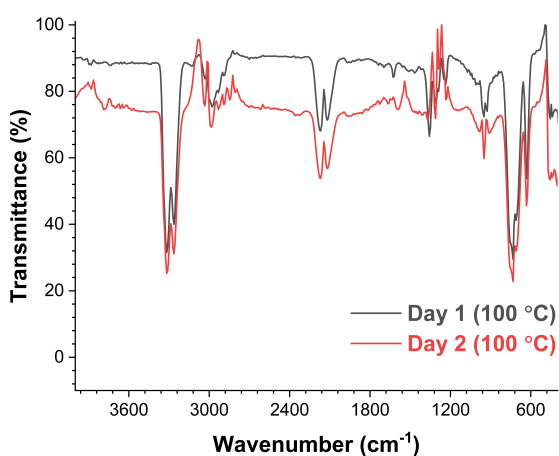
concentration). For instance, Figures 40a, 40c, and 40e represent the IR absorption of samples prepared with oil bath temperatures of 80, 100, and 120 °C (see Table 2) on the first day, along with a second day of running spark discharge. To facilitate a better comparison of the IR spectra, Figures 40b and 40d show the synthesized gas phase on the first and second days respectively at temperatures of 80, 100, and 120 °C. In Figure 40f, we present the IR spectra of gas phase samples synthesized on the second day of spark discharge using initial ammonia amounts of 5.0 mL and 10 mL to synthesize the mixture (see Table 2).



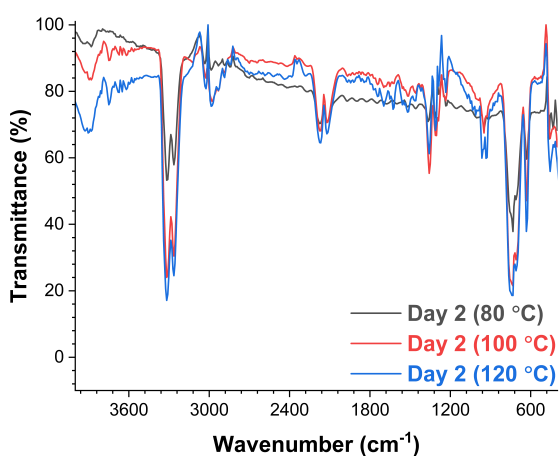
(a) 80 °C Days 1 & 2.



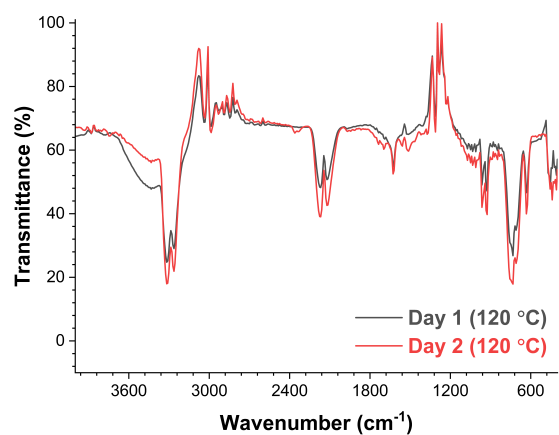
(b) 80 °C, 100 °C, and 120 °C Day 1.



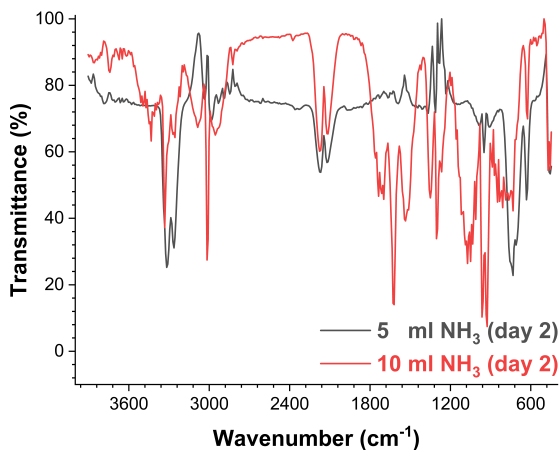
(c) 100 °C Days 1 & 2.



(d) 80 °C, 100 °C, and 120 °C Day 2.



(e) 120 °C Days 1 & 2.



(f) 100 °C Day 2-5, 10 ml NH₃.

Figure 40: Gas phase FTIR spectrums.

The IR spectras in the gas phase presented in Figure 40 show that a longer reaction time in the Miller experiment leads to more intense peaks without the appearance of new peaks. Additionally, higher temperatures result in new peaks and greater intensity compared to samples synthesized at lower temperatures. Ammonia also significantly affects peak intensity, with higher ammonia concentrations resulting in more detectable peaks in the IR spectrum.

8.8 UV-Vis Gas phase Excitation

Spark-induced breakdown spectroscopy (SIBS) is an experimental method to spectrally examine the emitted light of a spark.

The spark discharge can be divided into three main phases: breakdown, arc, and glow [297]. Each phase can be characterized by the secondary current and voltage trace. When the secondary voltage level exceeds the isolation resistance of the air gap, breakdown occurs. In this very short first phase, the spark current rises to a maximum before both the voltage and the current decrease rapidly to low levels. The moment when the voltage decrease (approximately 10% of initial level) is indicated as the transition to the arc-phase, lasting for some microseconds. In this phase, the voltage level remains constant before it switches to the glow phase. During this phase, the voltage remains constant while the current gradually decreases until the energy stored in the coil is depleted, indicating the end of the glow phase [298] (see section 7.6).

Breakdowns in gases have been extensively studied by Parigger [299], providing methods and simulation tools to characterize the plasma via atomic (H_α , H_β , H_γ) and diatomic spectra (OH, CN, C_2).

From the spectral response, the local fuel-air equivalence ratio of different fuels such as methane [300, 301], hydrogen [302], propane [303], and isooctane [303, 304] is reported.

The capability to obtain quantitative fuel-air equivalence ratios was demonstrated for methane-air [305, 306] and propane-air mixtures [305].

Emission lines of OH, NH, CN, and N_2 are not equally distributed across the electrode gap [298]. OH emissions are most prominent between the electrodes, while CN and N_2 emissions are enhanced at the center electrode and to a lesser extent on the ground

electrode. Besides the radicals of interest, many more atomic emission lines present [298].

In Figure 41, we present the emission spectra generated using two distinguished spark generators, CA-1 and FB-2. From this spectrum, we observe that the spark generator FB-2 produces more emission in the UV area compared to spark generator CA-1. Conversely, spark generator CA-1 provides sharper excitation lines compared to FB-2 in the visible area.

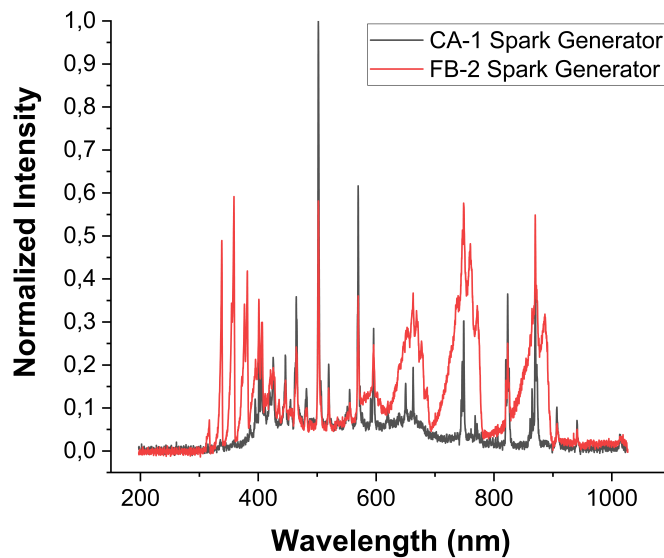


Figure 41: **Emission wavelengths in the miller experiment with dual spark generators.** Graph showing the emission wavelengths generated during the Miller experiment, utilizing two spark generators in the beginning of the experiment.

In Figure 42, we present the gas phase excitation emission spectra in the UV-Vis light range. The experiments performed under different conditions to compare. Figure A shows the Miller experiment gas at different scan times using CA-1 spark generators. Figures B, G, and L display the emitted UV-Vis spectra of the air when two different electrode distances at the tip of the electrodes provided for the spark-discharge using CA-1 spark generator. Figures C, H, and M show the emitted spectra of the air when different currents applied to the spark generator FB-2. Increasing the current leads to greater PAC dimensions, larger crater diameters, and enhanced erosion of the tool electrode [307]. Figure D presents the air emission spectra when exposed

to the FB-1 spark generator under three different currents of 0.6, 0.8, and 1.0 input current values. Figure I presents the emission spectra of the air exposed to the spark generator FB-2 with cables shielded to the earth as a usual compare emissions Spectra deposits temperatures the discharge procedure for high voltage cables and two very sharp electrodes. Figure N shows the emitted spectra of nitrogen gas when exposed to the spark discharge of a CA-1 spark generator with earth-shielded high-voltage wires and disconnected earth shielding for comparison. Figure E shows the air-emitted spectra when exposed to the spark discharge of two different spark generators (CA-1 and FB-2) with shielded high-voltage cables. Figure J displays the emitted spectra of the air when exposed to the spark discharge of Earth-shielded and disconnected cable shielding of the spark generator CA-1. In Figure O, we represented the emitted spectra of air with the CA-1 spark generator when two flat-tipped (larger flat and smaller flat) electrodes are used to apply the spark discharge with two different polarities. Figures F and K show the ammonia and methane excitation emission respectively when three different different spark generators (FB-1, FB-2, and CA-1) were used.

In the excitation spectra shown in Figure 42, we observe that longer sparking durations result in new peaks and increased intensity of the existing peaks. Greater electrode distance causes lower peak intensity regardless of the applied current. Different spark generators emit different wavelengths, and the intensity of these wavelengths varies among the generators. Higher applied currents produce more intense excited wavelengths without new detectable lines. The results also indicate that shielding the high voltage cables significantly affects the excitation spectrum, leading to more peaks in both intensity and new lines across all spark generators. Using flyback spark generators results in more UV light compared to capacitor spark generators, which produce more intense and sharper light in the visible spectrum. Shielded cables release more UV light excitation compared to non-shielded cables. Very sharp electrodes produce sharper excitation wavelengths compared to semi-sharp electrodes but do not result in new peaks. A sharp electrode tip promotes spark initiation and encourages axial radial growth of the plasma arc column (PAC) [307]. Additionally, flat electrodes demonstrate that electrode polarity plays an important role when the electrode sizes have different areas.

Energy dispersive X-ray spectroscopy (EDX) was used to characterize the composition of the electrodes at the electrode tip. It was confirmed that Iron, Cobalt, Nickel, and Copper lines match most of these atomic emission lines by comparing the measured

spectra with values from the database, even though their share was only a few percent in the alloy [1] (results discussed in Section 8.10).

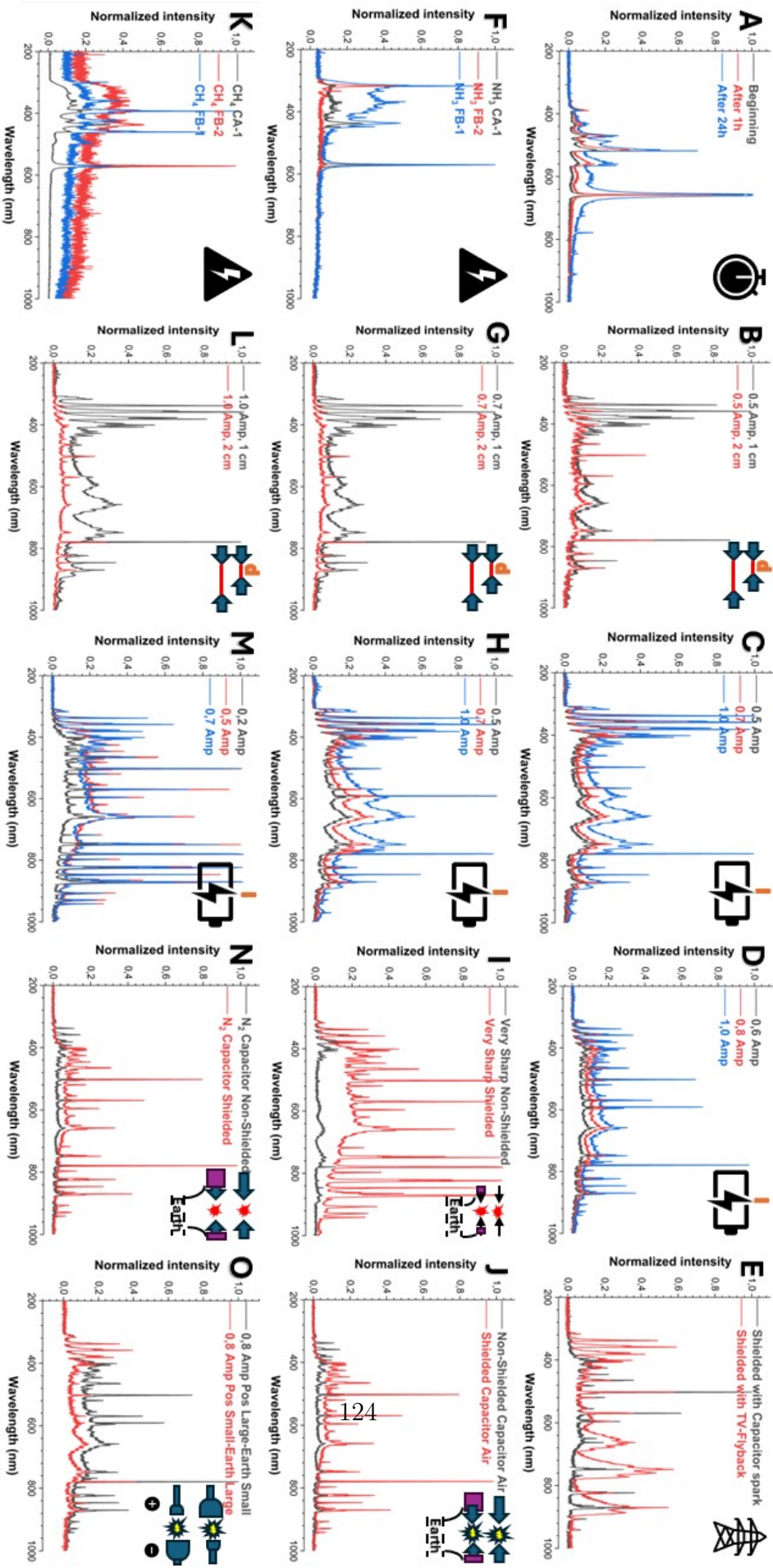


Figure 42: UV-Vis emission spectras of gases under varied spark discharge conditions.

8.9 SEM/EDX microscopy

Pristavita et al. dissociated methane by means of thermal plasma and produced hydrogen and carbon black [308]. Hydrogen and carbon black production from methane via stable DC spark discharge without using any catalyst is reported [309].

Shortly after the start of the electric discharge, an oil layer formed on top of the aqueous phase, while a thin deposit of black material started to form around the tip of the electrode (see Figure 43). This deposit exhibited a porous structural configuration and continuously underwent detachment from the electrodes, descending onto the oil layer.

In our group's previous work, the presence of this layer was reported during the experiments. The SEM images and EDS analysis of solid particles in the sample confirmed the presence of different solid structures in the mixture. The filamentous structures were mostly organic, while the porous grains were identified as tungsten compounds. [217].

The thickness was highly dependent on the temperature and spark generator. We observed a significant rise in the production of black material deposit at low temperature (sample 1); conversely, at high temperatures (sample 3), a negligible amount of black material formed. The utilization of the FB-2 spark generator (sample 7) resulted in a significant increase in black matter (compared to FB-1 and CA-1), whereas sample 8, delivered via the capacitor-based spark generator (CA-1), produced a minimal amount of black dust. All other samples exhibited an almost comparable amount of black matter regardless of the altered parameters [1] and (see Table 2).

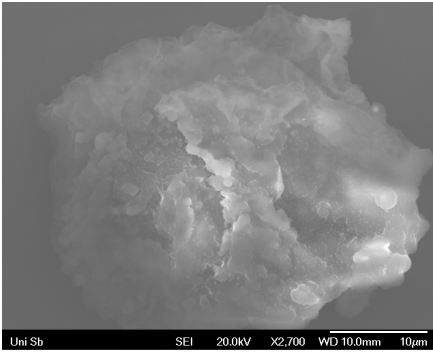


(a) Earth Pole

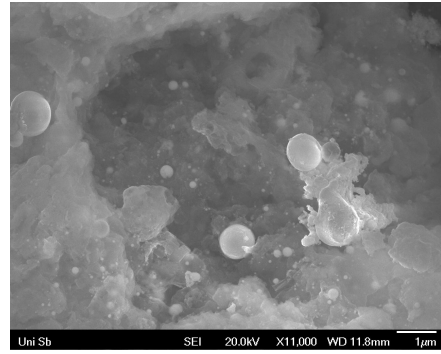
(b) Positive Pole

Figure 43: **Pictures of electrodes.**

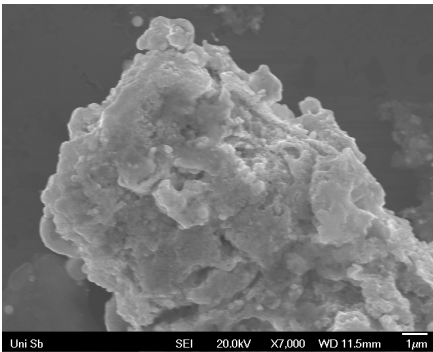
The SEM images depicted in Figures 44 and 45 show the morphology of the black material in earth and positive Poles samples. A diverse set of features is observed for the residue collected from the electrodes, including round spheres, sheet-like structures, and agglomerates. The diversity in morphologies suggests the presence of multiple phases, while the variations in contrast among these features may indicate multiple chemical compositions. This variety in phases and compositions is supported by the XRD results discussed in Section 8.10.



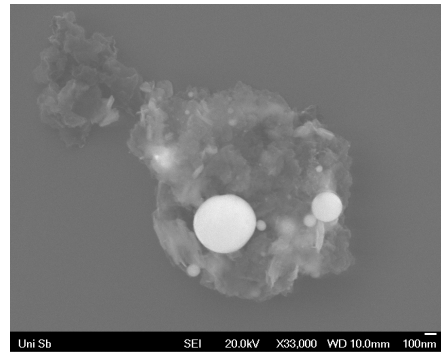
(a) SEM-Sample1 Negative Pole



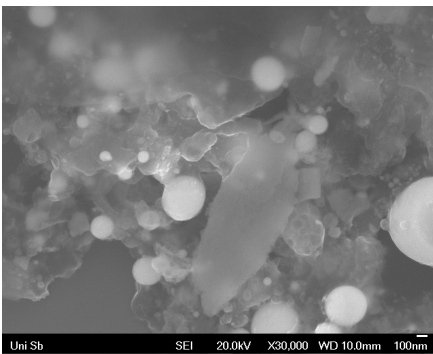
(b) SEM-Sample2 Negative Pole



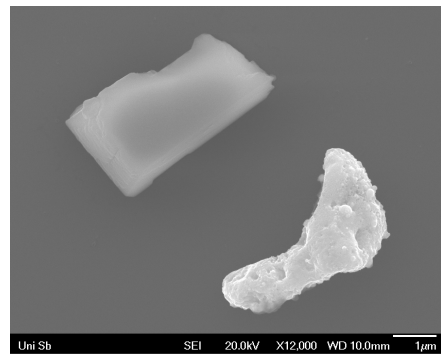
(c) SEM-Sample3 Negative Pole



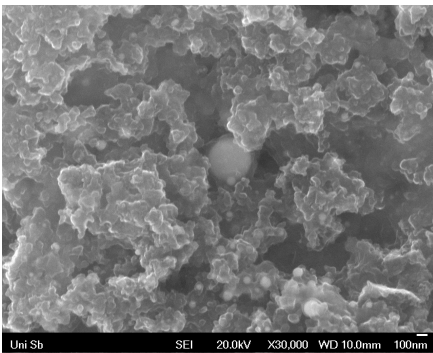
(d) SEM-Sample4 Negative Pole



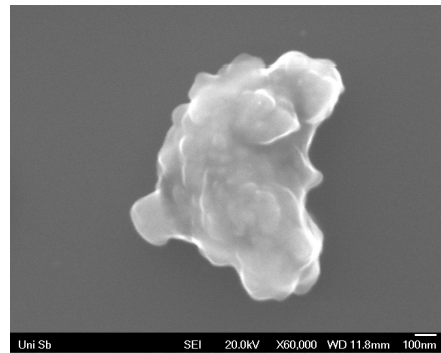
(e) SEM-Sample5 Negative Pole



(f) SEM-Sample6 Negative Pole

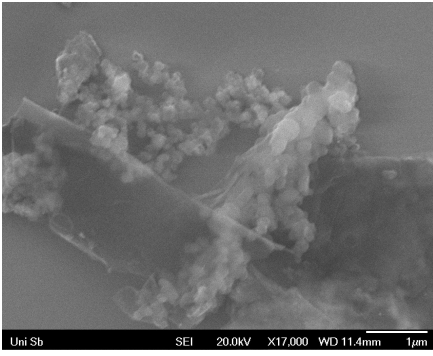


(g) SEM-Sample7 Negative Pole

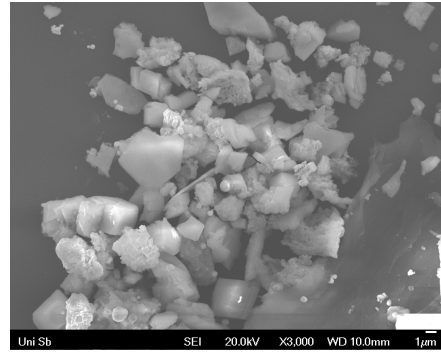


(h) SEM-Sample6 Negative Pole

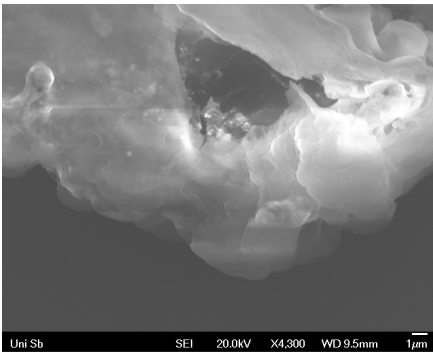
Figure 44: SEM pictures of black material in earth pole.



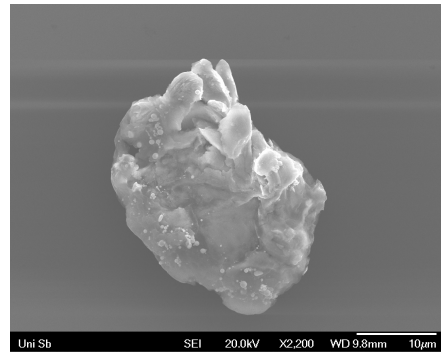
(a) SEM-Sample1 positive pole



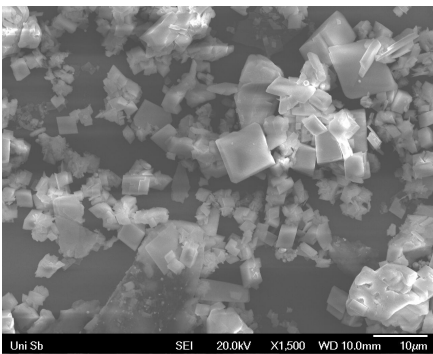
(b) SEM-Sample2 positive pole



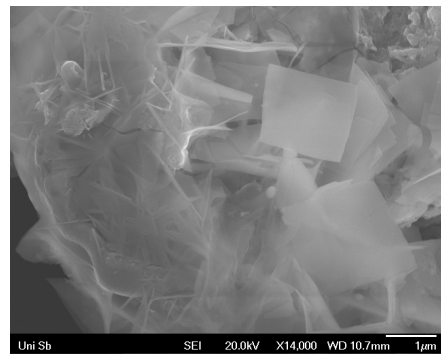
(c) SEM-Sample3 positive pole



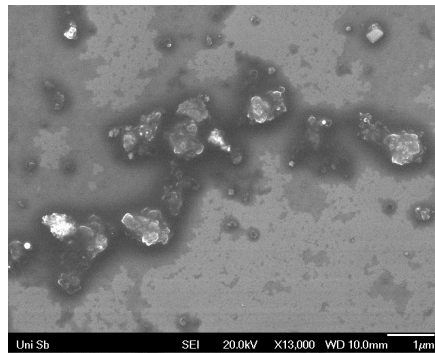
(d) SEM-Sample4 positive pole



(e) SEM-Sample5 positive pole

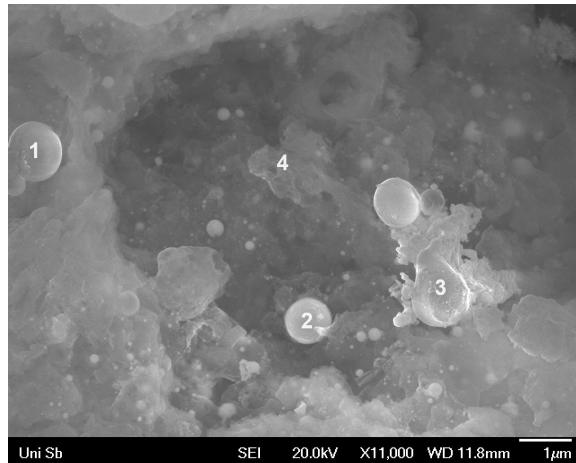


(f) SEM-Sample6 positive pole

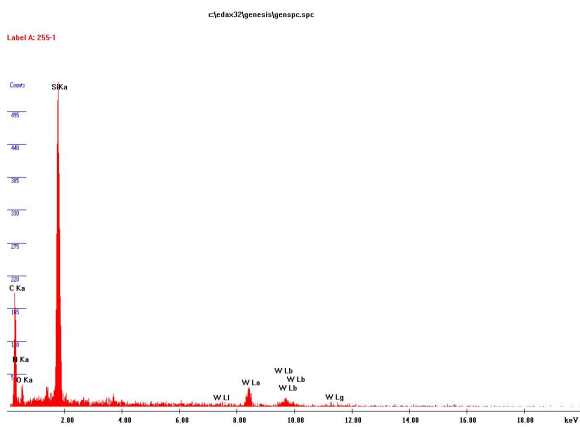


(g) SEM-Sample7 positive pole

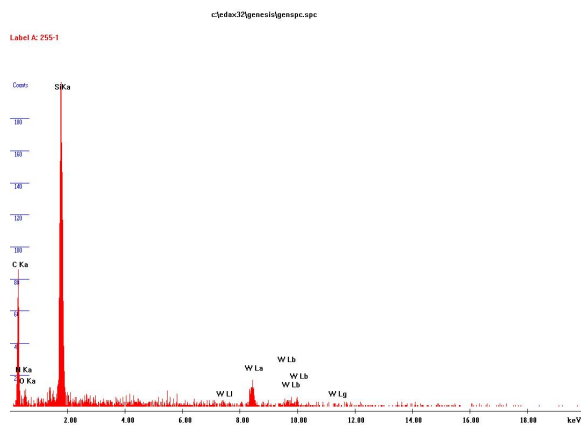
Figure 45: SEM pictures of black material in positive pole.



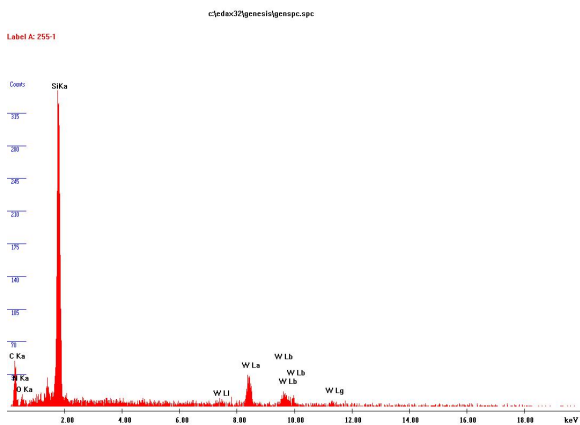
(a) SEM picture of black material



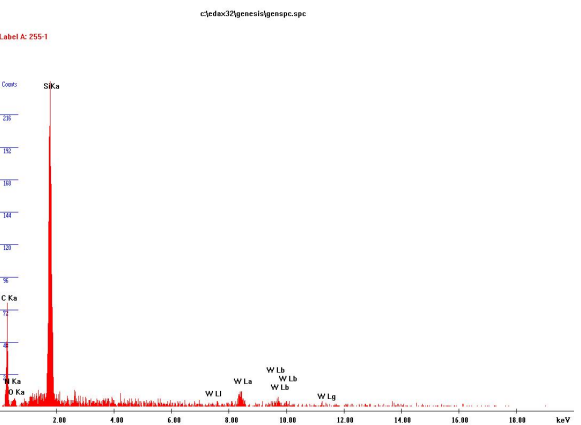
(b) Elemental analysis of position 1 in Figure 46a



(c) Elemental analysis of position 2 in Figure 46a



(d) Elemental analysis of position 3 in Figure 46a



(e) Elemental analysis of position 4 in Figure 46a

8.10 XRD

As shown in Figure 47, the XRD pattern of the residue material around the positive pole indicates the presence of tungsten (W) and tungsten oxide (WO_2), along with potentially other tungsten oxide derivatives and species such as ammonium tungsten oxide $(\text{NH}_4)_{10}\text{W}_{12}\text{O}_{41}$. The formation of ammonium tungsten oxide is likely due to the presence of ammonia and water vapor around the tungsten electrode during high-voltage sparking. The tungsten and tungsten oxide species formed as byproducts in this process could potentially serve as catalysts in various reactions, such as hydrogen production [310, 311].

The XRD pattern of the Earth electrode sample exhibits relatively fewer crystalline features compared to the positive electrode sample, along with broad, featureless peaks in the 10° to 35° 2θ range. The distinct reflections observed in this sample may suggest the presence of carbide species of tungsten such as W_2C , WC_{1-x} , and $\text{W}_2(\text{CO})$. These tungsten carbide species could potentially be used as electrocatalysts for methanol electro-oxidation and other reforming reactions applications [312, 313, 314].

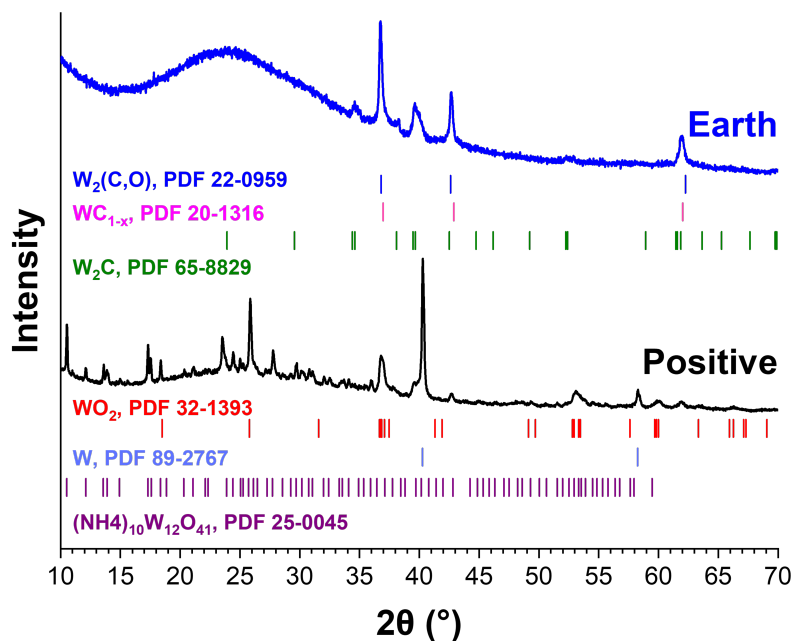


Figure 47: XRD of black material.

9 Conclusions

This work explored the production of prebiotic chemistry by simulating prebiotic conditions using a modified variation of the Miller-Urey experiment. Advanced analytical techniques such as GC-MS, HPLC-Mass Spectroscopy, FTIR, SEM, EDX, XRD, UV-Vis absorption, UV-Vis excitation, and fluorescence highlighted the significant role of physical parameters such as temperature, spark discharge, and the composition of the gaseous mixture. These parameters drastically influenced Miller-Urey's prebiotic synthetic routes, resulting in important differences in yields of different molecular categories (Tables 2, and 12).

Detailed chemical analysis identified new reactor outputs that come with variations in the Miller-Urey experimental setting, demonstrating the huge potential for the spontaneous generation of life's building blocks. These include amino acids, saturated and non-saturated hydrocarbons, carboxylic acids, nitrogen- and oxygen-containing compounds, and Polycyclic Aromatic Hydrocarbons (PAHs) (Subsections 8.1, and 8.7).

The choice of spark generator had the greatest impact on the range and diversity of synthesized compounds (Subsection 8.1). Ammonia significantly influenced the synthesis of aromatic and non-nitrogen-containing compounds (Subsection 8.1). Temperature also exhibited a notable influence on reactor output (Subsections 8.1, 8.2, 8.3, and 8.4).

This work primarily focused on analyzing complex systems related to the Miller-Urey experiment. Various analytical techniques, each with its strengths and weaknesses, have been explored with the choice of the best technique closely tied to the specific aims of the projects. The findings contribute to our understanding of prebiotic chemistry, demonstrating that small changes in physical conditions can profoundly affect the experimental output.

We conclude on a highly non-linear mechanism for synthesis. Possibly as a result of cooperative molecular interaction favoured by mutual catalysis or/and a complex underlying reaction network.

10 Suggested Future Works

In the ongoing exploration of prebiotic chemistry and the Miller-Urey experiment, future research directions that could significantly advance our understanding:

1. Investigating how varying physical parameters such as temperature, pressure, and other parameters influence the chemical diversity in the Miller soup using High-resolution mass spectroscope i.e. Kendrick mass defect plot and Van krevelen diagram.
2. Exploring the impact of different types of power supplies on the chemical composition of Miller soup will help in understanding how energy sources affect prebiotic syntheses.
3. A real time analysis of the mass distribution of molecules formed in the Miller experiment using mass spectroscopy.
4. The chromophoric properties of compounds within the Miller soup could be evaluated for their effectiveness as dyes in solar cells, potentially leading to novel, bio-inspired photovoltaic materials.
5. A detailed analysis of gases produced using varied power supplies and analytical techniques like SPME-GC-MASS and FTIR, enrich our understanding of the gaseous outputs.
6. Studying the presence and catalytic effects of carbon black and other solid particles in the Miller soup provides significant insights into their role in catalyzing prebiotic reactions.
7. Quantitative and qualitative real-time analysis of gas composition during the experiments using SPME-GC-MASS would provide a dynamic view of the chemical evolution.
8. Investigating micellar formation under prebiotic conditions have been crucial in the development of early cellular structures.
9. An in-depth study on the UV-Vis and fluorescence properties of the Miller soup could inform us about the stability and electronic properties of the compounds formed.

10. Utilizing AI to analyze massive datasets from I-V measurements over time could uncover patterns and predict behaviors in the electrical properties of the Miller soup, aiding in the identification of promising compounds for further study.
11. Exploring the use of chromophores derived from the Miller experiment in photocatalytic reactions could open new pathways in the development of sustainable and efficient photocatalytic agents.
12. How fuel starvation affects the reactor dynamics, determining whether they tend toward equilibrium or maintain dynamic non-equilibrium states.

References

- [1] Sina Ravanbodshirazi et al. “The Nature of the Spark Is a Pivotal Element in the Design of a Miller–Urey Experiment”. In: *Life* 13.11 (2023), p. 2201.
- [2] Marc Finkler et al. “Full incorporation of the noncanonical amino acid hydroxyllysine as a surrogate for lysine in green fluorescent protein”. In: *Bioorganic & Medicinal Chemistry* 41 (2021), p. 116207.
- [3] Simon J Knell and Cherry LE Lewis. “Celebrating the age of the Earth”. In: *Geological Society, London, Special Publications* 190.1 (2001), pp. 1–14.
- [4] Norman H Sleep et al. “Annihilation of ecosystems by large asteroid impacts on the early Earth”. In: *Nature* 342.6246 (1989), pp. 139–142.
- [5] Martin J Van Kranendonk. “Volcanic degassing, hydrothermal circulation and the flourishing of early life on Earth: A review of the evidence from c. 3490–3240 Ma rocks of the Pilbara Supergroup, Pilbara Craton, Western Australia”. In: *Earth-Science Reviews* 74.3–4 (2006), pp. 197–240.
- [6] J William Schopf. “Microfossils of the Early Archean Apex chert: new evidence of the antiquity of life”. In: *Science* 260.5108 (1993), pp. 640–646.
- [7] Lee D Hansen, Richard S Criddle, and Edwin H Battle. “Biological calorimetry and the thermodynamics of the origination and evolution of life”. In: *Pure and Applied Chemistry* 81.10 (2009), pp. 1843–1855.
- [8] David Deamer and Arthur L Weber. “Bioenergetics and life’s origins”. In: *Cold Spring Harbor Perspectives in Biology* 2.2 (2010), a004929.
- [9] Pierre de Marcellus et al. “Aldehydes and sugars from evolved precometary ice analogs: Importance of ices in astrochemical and prebiotic evolution”. In: *Proceedings of the National Academy of Sciences* 112.4 (2015), pp. 965–970.
- [10] Melissa G Trainer et al. “Haze aerosols in the atmosphere of early Earth: manna from heaven”. In: *Astrobiology* 4.4 (2004), pp. 409–419.
- [11] André Brack. “From interstellar amino acids to prebiotic catalytic peptides: a review”. In: *Chemistry & biodiversity* 4.4 (2007), pp. 665–679.
- [12] Alan W Schwartz. “Phosphorus in prebiotic chemistry”. In: *Philosophical Transactions of the Royal Society B: Biological Sciences* 361.1474 (2006), pp. 1743–1749.

- [13] Lawrence J Henderson. “The fitness of the environment, an inquiry into the biological significance of the properties of matter”. In: *The American Naturalist* 47.554 (1913), pp. 105–115.
- [14] Pier Luigi Luisi. “About various definitions of life”. In: *Origins of Life and Evolution of the Biosphere* 28 (1998), pp. 613–622.
- [15] Irwin Schrödinger. *What is Life?, reprinted in What is Life? and Mind and Matter*. 1944.
- [16] Laurent Boiteau and Robert Pascal. “Energy sources, self-organization, and the origin of life”. In: *Origins of Life and Evolution of Biospheres* 41.1 (2011), pp. 23–33.
- [17] Serhiy A Tsokolov. “Why is the definition of life so elusive? Epistemological considerations”. In: *Astrobiology* 9.4 (2009), pp. 401–412.
- [18] Edward N Trifonov. “Vocabulary of definitions of life suggests a definition”. In: *Journal of Biomolecular Structure and Dynamics* 29.2 (2011), pp. 259–266.
- [19] William F Martin and Martina Preiner. “Origin of life, theories of”. In: *Reference Module in Life Sciences* (2017).
- [20] Peter Schönheit, Wolfgang Buckel, and William F Martin. “On the origin of heterotrophy”. In: *Trends in microbiology* 24.1 (2016), pp. 12–25.
- [21] Georg Fuchs. “Alternative pathways of carbon dioxide fixation: insights into the early evolution of life?” In: *Annual review of microbiology* 65 (2011), pp. 631–658.
- [22] Rafael F Say and Georg Fuchs. “Fructose 1, 6-bisphosphate aldolase/phosphatase may be an ancestral gluconeogenic enzyme”. In: *Nature* 464.7291 (2010), pp. 1077–1081.
- [23] Richard V Eck and Margaret O Dayhoff. “Evolution of the structure of ferredoxin based on living relics of primitive amino acid sequences”. In: *Science* 152.3720 (1966), pp. 363–366.
- [24] Günter Wächtershäuser. “Groundworks for an evolutionary biochemistry: the iron-sulphur world”. In: *Progress in biophysics and molecular biology* 58.2 (1992), pp. 85–201.
- [25] Antonio Lazcano and Jeffrey L Bada. “Stanley L. Miller (1930–2007): reflections and remembrances”. In: *Origins of Life and Evolution of Biospheres* 38 (2008), pp. 373–381.

- [26] Stanley L Miller and Leslie E Orgel. “The origins of life on the earth”. In: (*No Title*) (1974).
- [27] Leslie E Orgel. “The origin of life—a review of facts and speculations”. In: *Trends in biochemical sciences* 23.12 (1998), pp. 491–495.
- [28] Matthew Levy, Stanley L Miller, and John Oró. “Production of guanine from NH₄ CN polymerizations”. In: *Journal of molecular evolution* 49 (1999), pp. 165–168.
- [29] Raffaele Saladino et al. “Formamide and the origin of life”. In: *Physics of life reviews* 9.1 (2012), pp. 84–104.
- [30] Thomas M McCollom. “Miller-Urey and beyond: what have we learned about prebiotic organic synthesis reactions in the past 60 years?” In: *Annual Review of Earth and Planetary Sciences* 41 (2013), pp. 207–229.
- [31] Daniel P Glavin et al. “Amino acids in the Martian meteorite Nakhla”. In: *Proceedings of the National Academy of Sciences* 96.16 (1999), pp. 8835–8838.
- [32] Pascale Ehrenfreund and Steven B Charnley. “Organic molecules in the interstellar medium, comets, and meteorites: a voyage from dark clouds to the early Earth”. In: *Annual Review of Astronomy and Astrophysics* 38.1 (2000), pp. 427–483.
- [33] Uwe J Meierhenrich et al. “Identification of diamino acids in the Murchison meteorite”. In: *Proceedings of the National Academy of Sciences* 101.25 (2004), pp. 9182–9186.
- [34] Keith Kvenvolden et al. “Evidence for extraterrestrial amino-acids and hydrocarbons in the Murchison meteorite”. In: *Nature* 228.5275 (1970), pp. 923–926.
- [35] Günter Wächtershäuser. “Before enzymes and templates: theory of surface metabolism”. In: *Microbiological reviews* 52.4 (1988), pp. 452–484.
- [36] Boris Ershov. “Natural Radioactivity and Chemical Evolution on the Early Earth: Prebiotic Chemistry and Oxygenation”. In: *Molecules* 27.23 (2022), p. 8584.
- [37] Christopher Chyba and Carl Sagan. “Electrical energy sources for organic synthesis on the early Earth”. In: *Origins of Life and Evolution of the Biosphere* 21 (1991), pp. 3–17.
- [38] Baruch S Blumberg. “The NASA Astrobiology Institute: early history and organization”. In: *Astrobiology* 3.3 (2003), pp. 463–470.

- [39] Leslie E Orgel. “The origins of life: molecules and natural selection”. In: (*No Title*) (1973).
- [40] Dirk Schulze-Makuch and Louis N Irwin. *Life in the Universe*. Springer, 2004.
- [41] Horst Rauchfuss. *Chemical evolution and the origin of life*. Springer Science & Business Media, 2008.
- [42] George H Shaw. “Earth’s atmosphere—Hadean to early Proterozoic”. In: *Geochemistry* 68.3 (2008), pp. 235–264.
- [43] James F Kasting. “Earth’s early atmosphere”. In: *Science* 259.5097 (1993), pp. 920–926.
- [44] John Tyler Bonner. “The origins of multicellularity”. In: *Integrative Biology: Issues, News, and Reviews: Published in Association with The Society for Integrative and Comparative Biology* 1.1 (1998), pp. 27–36.
- [45] David E Fastovsky and David B Weishampel. *Dinosaurs: a concise natural history*. Cambridge University Press, 2021.
- [46] Ian McDougall, Francis H Brown, and John G Fleagle. “Stratigraphic placement and age of modern humans from Kibish, Ethiopia”. In: *nature* 433.7027 (2005), pp. 733–736.
- [47] L Paul Knauth and Donald R Lowe. “High Archean climatic temperature inferred from oxygen isotope geochemistry of cherts in the 3.5 Ga Swaziland Supergroup, South Africa”. In: *Geological Society of America Bulletin* 115.5 (2003), pp. 566–580.
- [48] FW Aston. “The rarity of the inert gases on the Earth”. In: *Nature* 114.2874 (1924), pp. 786–786.
- [49] Stanley L Miller. “A production of amino acids under possible primitive earth conditions”. In: *Science* 117.3046 (1953), pp. 528–529.
- [50] David W Deamer. “The first living systems: a bioenergetic perspective”. In: *Microbiology and Molecular Biology Reviews* 61.2 (1997), pp. 239–261.
- [51] Harold J Morowitz. *Beginnings of cellular life: metabolism recapitulates biogenesis*. Yale University Press, 1993.

- [52] Pierre-Alain Monnard and David W Deamer. “Membrane self-assembly processes: Steps toward the first cellular life”. In: *The Anatomical Record: An Official Publication of the American Association of Anatomists* 268.3 (2002), pp. 196–207.
- [53] David W Deamer. “Polycyclic aromatic hydrocarbons: primitive pigment systems in the prebiotic environment”. In: *Advances in Space Research* 12.4 (1992), pp. 183–189.
- [54] John R Cronin, Sandra Pizzarello, and Dale P Cruikshank. “Organic matter in carbonaceous chondrites, planetary satellites, asteroids and comets.” In: *Meteorites and the early solar system* (1988), pp. 819–857.
- [55] Joan Oró et al. “Amino acid synthesis from formaldehyde and hydroxylamine”. In: *Archives of Biochemistry and Biophysics* 85.1 (1959), pp. 115–130.
- [56] Kensei Kobayashi et al. “Amino acid formation in gas mixtures by high energy particle irradiation”. In: *Origins of Life and Evolution of the Biosphere* 28 (1998), pp. 155–165.
- [57] Leonida Santamaria and L Fleischmann. “Photochemical synthesis of amino acids from paraformaldehyde catalysed by inorganic agents”. In: *Experientia* 22.7 (1966), pp. 430–431.
- [58] Wilhelm Groth and Hanns von Weyssenhoff. “Photochemische Bildung von Aminosäuren aus Mischungen einfacher Gase”. In: *Naturwissenschaften* 44 (1957), pp. 510–511.
- [59] Akiva Bar-Nun and A Shaviv. “Dynamics of the chemical evolution of Earth’s primitive atmosphere”. In: *Icarus* 24.2 (1975), pp. 197–210.
- [60] CU Lowe, MW Rees, and RFRS Markham. “Synthesis of complex organic compounds from simple precursors: formation of amino-acids, amino-acid polymers, fatty acids and purines from ammonium cyanide”. In: *Nature* 199.4890 (1963), pp. 219–222.
- [61] Sidney W Fox. “Thermal synthesis of amino acids and the origin of life”. In: *Geochimica et Cosmochimica Acta* 59.6 (1995), pp. 1213–1214.
- [62] Garrett A Soukup. “Nucleic acids: General properties”. In: *e LS* (2001).
- [63] John Oró. “Synthesis of adenine from ammonium cyanide”. In: *Biochemical and Biophysical Research Communications* 2.6 (1960), pp. 407–412.

- [64] R Sanchez, J Ferris, and LE Orgel. “Conditions for purine synthesis: did prebiotic synthesis occur at low temperatures?” In: *Science* 153.3731 (1966), pp. 72–73.
- [65] James P Ferris, Robert A Sanchez, and Leslie E Orgel. “Studies in prebiotic synthesis: III. Synthesis of pyrimidines from cyanoacetylene and cyanate”. In: *Journal of molecular biology* 33.3 (1968), pp. 693–704.
- [66] RA Sanchez, JP Ferris, and LE Orgel. “Cyanoacetylene in prebiotic synthesis”. In: *Science* 154.3750 (1966), pp. 784–785.
- [67] Francis A Carey and Robert M Giuliano. *Organic chemistry*. McGraw-Hill, 2017.
- [68] A Butlerow. “Bildung einer zuckerartigen Substanz durch Synthese”. In: *Justus Liebigs Annalen der Chemie* 120.3 (1861), pp. 295–298.
- [69] Alan W Schwartz and RM De Graaf. “The prebiotic synthesis of carbohydrates: A reassessment”. In: *Journal of molecular evolution* 36 (1993), pp. 101–106.
- [70] Thomas Zweckmair et al. “Accurate analysis of formose reaction products by LC–UV: an analytical challenge”. In: *Journal of chromatographic science* 52.2 (2014), pp. 169–175.
- [71] Irina V Delidovich et al. “Catalytic formation of monosaccharides: From the formose reaction towards selective synthesis”. In: *ChemSusChem* 7.7 (2014), pp. 1833–1846.
- [72] Cristofor I Simionescu, Marian I Totolin, and Ferencz Denes. “Abiotic synthesis of some polysaccharide-like and polypeptide-like structures in cold plasma.” In: *Bio Systems* 8.3 (1976), pp. 153–158.
- [73] A Ricardo et al. “Borate minerals stabilize ribose”. In: *Science* 303.5655 (2004), pp. 196–196.
- [74] James P Ferris and William J Hagan Jr. “HCN and chemical evolution: the possible role of cyano compounds in prebiotic synthesis”. In: *Tetrahedron* 40.7 (1984), pp. 1093–1120.
- [75] Feng Tian, JF Kasting, and K Zahnle. “Revisiting HCN formation in Earth’s early atmosphere”. In: *Earth and Planetary Science Letters* 308.3-4 (2011), pp. 417–423.
- [76] Stanley L Miller. “Production of some organic compounds under possible primitive earth conditions¹”. In: *Journal of the American Chemical Society* 77.9 (1955), pp. 2351–2361.

- [77] Debjani Roy, Katayoun Najafian, and Paul von Ragué Schleyer. “Chemical evolution: the mechanism of the formation of adenine under prebiotic conditions”. In: *Proceedings of the National Academy of Sciences* 104.44 (2007), pp. 17272–17277.
- [78] Stanley L Miller. “The mechanism of synthesis of amino acids by electric discharges”. In: *Biochimica et Biophysica Acta* 23 (1957), pp. 480–489.
- [79] J-Y Bonnet et al. “HCN Polymers: Composition And Structure Revisited by High Resolution Mass Spectrometry”. In: *41st Annual Lunar and Planetary Science Conference*. 1533. 2010, p. 1334.
- [80] Clifford N Matthews. “The origin of proteins: Heteropolypeptides from hydrogen cyanide and water”. In: *Origins of Life* 6.1-2 (1975), pp. 155–162.
- [81] Clifford N Matthews and Robert D Minard. “Hydrogen cyanide polymers, comets and the origin of life”. In: *Faraday discussions* 133 (2006), pp. 393–401.
- [82] Alan W Schwartz and M Goverde. “Acceleration of HCN oligomerization by formaldehyde and related compounds: implications for prebiotic syntheses”. In: *Journal of molecular evolution* 18 (1982), pp. 351–353.
- [83] Marta Ruiz-Bermejo et al. “New insights into the characterization of ‘insoluble black HCN polymers’”. In: *Chemistry & Biodiversity* 9.1 (2012), pp. 25–40.
- [84] John Desmond Bernal. “The origin of life”. In: (*No Title*) (1967).
- [85] TE Pavlovskaya. “Abiogenic synthesis of biologically important compounds”. In: *Problems of Origin and Essence of Life* (1973), pp. 38–72.
- [86] Thomas Oberholzer, Maria Albrizio, and Pier Luigi Luisi. “Polymerase chain reaction in liposomes”. In: *Chemistry & biology* 2.10 (1995), pp. 677–682.
- [87] Pierre-Alain Monnard and David W Deamer. “Nutrient uptake by protocells: a liposome model system”. In: *Origins of Life and Evolution of the Biosphere* 31 (2001), pp. 147–155.
- [88] Pere Alberch. “Kauffman, SA The origins of order. Self-organization and selection in evolution. Oxford University Press (1993). Price:£ 17.95 (pb),£ 51.00 (hb). ISBN: 0-19-505811-9 (hb) and 0-19-507951-5 (pb).” In: *Journal of Evolutionary Biology* 7.4 (1994), pp. 518–519.
- [89] Aleksandr I Oparin. *Die Entstehung des Lebens auf der Erde*. Literaturvertrieb d. P [artei] d. A [rbeit], 1945.

- [90] Florence Raulin-Cerceau. “The Concept of Chemical Evolution Before Oparin”. In: *Genesis-In The Beginning: Precursors of Life, Chemical Models and Early Biological Evolution*. Springer, 2012, pp. 891–906.
- [91] CH Bailey. *The origin of life (oparin, ai)*. 1938.
- [92] Harmke Kamminga. “Historical perspective: the problem of the origin of life in the context of developments in biology”. In: *Origins of Life and Evolution of the Biosphere* 18.1 (1988), pp. 1–11.
- [93] Stephanie Marie Colón Santos. “Exploring the untargeted synthesis of prebiotically-plausible molecules”. PhD thesis. University of Glasgow, 2019.
- [94] Stanley L Miller, J William Schopf, and Antonio Lazcano. “Oparin’s “Origin of Life”: Sixty Years Later”. In: *Journal of molecular evolution* 44 (1997), pp. 351–353.
- [95] Pierre-Alain Monnard and David W Deamer. “Membrane self-assembly processes: steps toward the first cellular life”. In: *The Minimal Cell: The Biophysics of Cell Compartment and the Origin of Cell Functionality*. Springer, 2010, pp. 123–151.
- [96] Christopher Wills and Jeffrey Bada. *The spark of life: Darwin and the primeval soup*. Oxford University Press, USA, 2001.
- [97] Carl R Woese. “On the evolution of cells”. In: *Proceedings of the National Academy of Sciences* 99.13 (2002), pp. 8742–8747.
- [98] Kenji Ikehara. “Evolutionary steps in the emergence of life deduced from the bottom-up approach and GADV hypothesis (top-down approach)”. In: *Life* 6.1 (2016), p. 6.
- [99] Mario Vaneechoutte and Renato Fani. “From the primordial soup to the latest universal common ancestor”. In: *Research in Microbiology* 160.7 (2009), pp. 437–440.
- [100] Juli Peretó, Jeffrey L Bada, and Antonio Lazcano. “Charles Darwin and the origin of life”. In: *Origins of life and evolution of biospheres* 39 (2009), pp. 395–406.
- [101] Adolph Strecker. “Ueber die künstliche Bildung der Milchsäure und einen neuen, dem Glycocoll homologen Körper”. In: *Justus Liebigs Annalen der Chemie* 75.1 (1850), pp. 27–45.

- [102] Victor E Ostrovskii and Elena A Kadyshevich. “Life Origination Hydrate Theory (LOH-Theory) and the explanation of the biological diversification”. In: *Journal of molecular evolution* 79 (2014), pp. 155–178.
- [103] David R Lide. *CRC handbook of chemistry and physics*. Vol. 85. CRC press, 2004.
- [104] CB Ould-Moulaye, CG Dussap, and JB Gros. “A consistent set of formation properties of nucleic acid compounds: Purines and pyrimidines in the solid state and in aqueous solution”. In: *Thermochimica acta* 375.1-2 (2001), pp. 93–107.
- [105] CB Ould-Moulaye, CG Dussap, and JB Gros. “A consistent set of formation properties of nucleic acid compounds: Nucleosides, nucleotides and nucleotide-phosphates in aqueous solution”. In: *Thermochimica acta* 387.1 (2002), pp. 1–15.
- [106] VE Ostrovskii and EA Kadyshevich. “Thermodynamics of formation of nitrogen bases and D-ribose from mineral substances in light of the problem of origination of simplest elements of living matter”. In: *Thermochimica acta* 441.1 (2006), pp. 69–78.
- [107] Victor Ostrovskii and Elena Kadyshevich. “Life origination hydrate hypothesis (LOH-hypothesis)”. In: *Life* 2.1 (2012), pp. 135–164.
- [108] Laura Toppozini et al. “Adenosine monophosphate forms ordered arrays in multilamellar lipid matrices: Insights into assembly of nucleic acid for primitive life”. In: *PloS one* 8.5 (2013), e62810.
- [109] David S Ross and David Deamer. “Dry/wet cycling and the thermodynamics and kinetics of prebiotic polymer synthesis”. In: *Life* 6.3 (2016), p. 28.
- [110] Marc Rodriguez-Garcia et al. “Formation of oligopeptides in high yield under simple programmable conditions”. In: *Nature communications* 6.1 (2015), p. 8385.
- [111] Paul G Higgs. “The effect of limited diffusion and wet–dry cycling on reversible polymerization reactions: implications for prebiotic synthesis of nucleic acids”. In: *Life* 6.2 (2016), p. 24.
- [112] Bruce Damer. “A field trip to the Archaean in search of Darwin’s warm little pond”. In: *Life* 6.2 (2016), p. 21.
- [113] Simon A Levin. “Ecosystems and the biosphere as complex adaptive systems”. In: *Ecosystems* 1 (1998), pp. 431–436.

- [114] Elizabeth A Felnagle et al. “Engineering synthetic recursive pathways to generate non-natural small molecules”. In: *Nature chemical biology* 8.6 (2012), pp. 518–526.
- [115] Hannes Mutschler, Aniela Wochner, and Philipp Holliger. “Freeze–thaw cycles as drivers of complex ribozyme assembly”. In: *Nature Chemistry* 7.6 (2015), pp. 502–508.
- [116] Laura Da Silva, Marie-Christine Maurel, and David Deamer. “Salt-promoted synthesis of RNA-like molecules in simulated hydrothermal conditions”. In: *Journal of molecular evolution* 80 (2015), pp. 86–97.
- [117] Jack W Szostak. “The eightfold path to non-enzymatic RNA replication”. In: *Journal of Systems Chemistry* 3 (2012), pp. 1–14.
- [118] Giovanni B Strambini and Edi Gabellieri. “Proteins in frozen solutions: evidence of ice-induced partial unfolding”. In: *Biophysical journal* 70.2 (1996), pp. 971–976.
- [119] Edi Gabellieri and Giovanni B Strambini. “Perturbation of protein tertiary structure in frozen solutions revealed by 1-anilino-8-naphthalene sulfonate fluorescence”. In: *Biophysical journal* 85.5 (2003), pp. 3214–3220.
- [120] Matteo Colombo and Patricia Palacios. “Non-equilibrium thermodynamics and the free energy principle in biology”. In: *Biology & Philosophy* 36.5 (2021), p. 41.
- [121] Albert Goldbeter. “Dissipative structures in biological systems: bistability, oscillations, spatial patterns and waves”. In: *Philosophical Transactions of the Royal Society A: Mathematical, Physical and Engineering Sciences* 376.2124 (2018), p. 20170376.
- [122] Aaron D Goldberg, C David Allis, and Emily Bernstein. “Epigenetics: a landscape takes shape”. In: *Cell* 128.4 (2007), pp. 635–638.
- [123] Barak Shenhav, Daniel Segrè, and Doron Lancet. “Mesobiotic emergence: Molecular and ensemble complexity in early evolution”. In: *Advances in Complex Systems* 6.01 (2003), pp. 15–35.
- [124] Raphael Plasson et al. “Autocatalyses”. In: *The Journal of Physical Chemistry A* 115.28 (2011), pp. 8073–8085.
- [125] David A Baum and Kalin Vetsigian. “An experimental framework for generating evolvable chemical systems in the laboratory”. In: *Origins of Life and Evolution of Biospheres* 47 (2017), pp. 481–497.

- [126] Alexander Graham Cairns-Smith. “Genetic takeover and the mineral origins of life”. In: *(No Title)* (1982).
- [127] Robert Shapiro. “Origins: A skeptic’s guide to the creation of life on earth”. In: *(No Title)* (1986).
- [128] Steven A Benner. *Life, the universe and the scientific method*. FfAME Press, 2009.
- [129] Noemí Nogal et al. “The protometabolic nature of prebiotic chemistry”. In: *Chemical Society Reviews* (2023).
- [130] Stephanie Colón-Santos, Geoffrey JT Cooper, and Leroy Cronin. “Taming the combinatorial explosion of the formose reaction via recursion within mineral environments”. In: *ChemSystemsChem* 1.3 (2019), e1900014.
- [131] Jun Korenaga. “Was there land on the early Earth?” In: *Life* 11.11 (2021), p. 1142.
- [132] Stanley L Miller and Harold C Urey. “Organic compound synthesis on the primitive Earth: Several questions about the origin of life have been answered, but much remains to be studied”. In: *Science* 130.3370 (1959), pp. 245–251.
- [133] Stephen G Brush. “Theories of the origin of the solar system 1956-1985”. In: *Reviews of Modern Physics* 62.1 (1990), p. 43.
- [134] Michael Jacobson et al. *Earth System Science: from biogeochemical cycles to global changes*. Academic Press, 2000.
- [135] Michael G Howlett et al. “An autonomously oscillating supramolecular self-replicator”. In: *Nature Chemistry* 14.7 (2022), pp. 805–810.
- [136] María Colín-García et al. “Hydrothermal vents and prebiotic chemistry: a review”. In: *Boletín de la Sociedad Geológica Mexicana* 68.3 (2016), pp. 599–620.
- [137] Verena Tunnicliffe. “The biology of hydrothermal vents: ecology and evolution”. In: *Oceanogr Mar Biol Annu Rev* 29 (1991), pp. 319–407.
- [138] Timothy West et al. “The origin of heredity in protocells”. In: *Philosophical Transactions of the Royal Society B: Biological Sciences* 372.1735 (2017), p. 20160419.
- [139] Egon T Degens and David A Ross. *Hot brines and recent heavy metal deposits in the Red Sea: a geochemical and geophysical account*. Springer-Verlag, 2013.

- [140] William Martin and Michael J Russell. “On the origin of biochemistry at an alkaline hydrothermal vent”. In: *Philosophical Transactions of the Royal Society B: Biological Sciences* 362.1486 (2007), pp. 1887–1926.
- [141] Michael J Russell and AJ Hall. “The emergence of life from iron monosulphide bubbles at a submarine hydrothermal redox and pH front”. In: *Journal of the Geological Society* 154.3 (1997), pp. 377–402.
- [142] Michael J Russell, Roy M Daniel, and Allan J Hall. “On the emergence of life via catalytic iron-sulphide membranes”. In: *Terra Nova* 5.4 (1993), pp. 343–347.
- [143] Michael J Russell, Allan J Hall, and Dugald Turner. “In vitro growth of iron sulphide chimneys: possible culture chambers for origin-of-life experiments”. In: *Terra Nova* 1.3 (1989), pp. 238–241.
- [144] HJ Cleaves, AD Aubrey, and JL Bada. “An evaluation of the critical parameters for abiotic peptide synthesis in submarine hydrothermal systems”. In: *Origins of life and evolution of biospheres* 39 (2009), pp. 109–126.
- [145] Barry Herschy et al. “An origin-of-life reactor to simulate alkaline hydrothermal vents”. In: *Journal of molecular evolution* 79 (2014), pp. 213–227.
- [146] Sidney W Fox and Kaoru Harada. “Thermal copolymerization of amino acids to a product resembling protein”. In: *Science* 128.3333 (1958), pp. 1214–1214.
- [147] AB Meggy. “293. Glycine peptides. Part II. The heat and entropy of formation of the peptide bond in polyglycine”. In: *Journal of the Chemical Society (Resumed)* (1956), pp. 1444–1454.
- [148] R Bruce Martin. “Free energies and equilibria of peptide bond hydrolysis and formation”. In: *Biopolymers: Original Research on Biomolecules* 45.5 (1998), pp. 351–353.
- [149] AW Flegmann and R Tattersall. “Energetics of peptide bond formation at elevated temperatures”. In: *Journal of Molecular Evolution* 12 (1979), pp. 349–355.
- [150] Ei-ichi Imai et al. “Autocatalytic synthesis of oligoglycine in a simulated submarine hydrothermal system”. In: *Origins of Life and Evolution of the Biosphere* 29 (1999), pp. 249–259.
- [151] Ei-ichi Imai et al. “Elongation of oligopeptides in a simulated submarine hydrothermal system”. In: *Science* 283.5403 (1999), pp. 831–833.

- [152] Hideaki Tsukahara et al. “Prebiotic oligomerization on or inside lipid vesicles in hydrothermal environments”. In: *Origins of Life and Evolution of the Biosphere* 32 (2002), pp. 13–21.
- [153] Md Nazrul Islam, Takeo Kaneko, and Kensei Kobayashi. “Reaction of amino acids in a supercritical water-flow reactor simulating submarine hydrothermal systems”. In: *Bulletin of the Chemical Society of Japan* 76.6 (2003), pp. 1171–1178.
- [154] Rihe Liu and Leslie E Orgel. “Polymerization on the rocks: β -amino acids and arginine”. In: *Origins of Life and Evolution of the Biosphere* 28 (1998), pp. 245–257.
- [155] Rihe Liu and Leslie E Orgel. “Polymerization of β -amino acids in aqueous solution”. In: *Origins of Life and Evolution of the Biosphere* 28 (1998), pp. 47–60.
- [156] Jose J Flores and JAMES O LECKIE. “Peptide formation mediated by cyanate”. In: *Nature* 244.5416 (1973), pp. 435–437.
- [157] Luke Leman, Leslie Orgel, and M Reza Ghadiri. “Carbonyl sulfide-mediated prebiotic formation of peptides”. In: *Science* 306.5694 (2004), pp. 283–286.
- [158] Hans-Dietrich Lüdemann et al. “Biomolecules are unstable under” black smoker” conditions”. In: *Naturwissenschaften* 71.11 (1984), pp. 583–586.
- [159] Stanley L Miller and Jeffrey L Bada. “Submarine hot springs and the origin of life”. In: *Nature* 334.6183 (1988), pp. 609–611.
- [160] Maria Koufaki, Theano Fotopoulou, and Georgios A Heropoulos. “Synergistic effect of dual-frequency ultrasound irradiation in the one-pot synthesis of 3, 5-disubstituted isoxazoles”. In: *Ultrasonics sonochemistry* 21.1 (2014), pp. 35–39.
- [161] J Bujdák and BM Rode. “Activated alumina as an energy source for peptide bond formation: Consequences for mineral-mediated prebiotic processes”. In: *Amino acids* 21 (2001), pp. 281–291.
- [162] Sara Murillo-Sánchez et al. “Fatty acids’ double role in the prebiotic formation of a hydrophobic dipeptide”. In: *Chemical Science* 7.5 (2016), pp. 3406–3413.
- [163] Alexander Graham Cairns-Smith and Hyman Hartman. *Clay minerals and the origin of life*. CUP Archive, 1986.

- [164] AG Cairns-Smith, P Ingram, and GL Walker. “Formose production by minerals: possible relevance to the origin of life”. In: *Journal of Theoretical Biology* 35.3 (1972), pp. 601–604.
- [165] Albert Rimola, Mariona Sodupe, and Piero Ugliengo. “Affinity scale for the interaction of amino acids with silica surfaces”. In: *The Journal of Physical Chemistry C* 113.14 (2009), pp. 5741–5750.
- [166] Raffaele Saladino, Veronica Neri, and Claudia Crestini. “Role of clays in the prebiotic synthesis of sugar derivatives from formamide”. In: *Philosophical Magazine* 90.17-18 (2010), pp. 2329–2337.
- [167] Joseph B Lambert, Senthil A Gurusamy-Thangavelu, and Kuangbiao Ma. “The silicate-mediated formose reaction: bottom-up synthesis of sugar silicates”. In: *Science* 327.5968 (2010), pp. 984–986.
- [168] Robert M Hazen et al. “Mineral evolution”. In: *American Mineralogist* 93.11-12 (2008), pp. 1693–1720.
- [169] Andrew J Surman et al. “Environmental control programs the emergence of distinct functional ensembles from unconstrained chemical reactions”. In: *Proceedings of the National Academy of Sciences* 116.12 (2019), pp. 5387–5392.
- [170] Jean-François Lambert. “Adsorption and polymerization of amino acids on mineral surfaces: a review”. In: *Origins of Life and Evolution of Biospheres* 38 (2008), pp. 211–242.
- [171] James P Ferris et al. “Synthesis of long prebiotic oligomers on mineral surfaces”. In: *Nature* 381.6577 (1996), pp. 59–61.
- [172] Cristina Cossetti et al. “Borate minerals and RNA stability”. In: *Polymers* 2.3 (2010), pp. 211–228.
- [173] Helen G Hansma. “Possible origin of life between mica sheets”. In: *Biophysical Journal* 98.3 (2010), 758a–759a.
- [174] Anand Kumar and Kamaluddin. “Possible role of metal (II) octacyanomolybdate (IV) in chemical evolution: interaction with ribose nucleotides”. In: *Origins of Life and Evolution of Biospheres* 43 (2013), pp. 1–17.
- [175] Hyo-Joong Kim et al. “Synthesis of carbohydrates in mineral-guided prebiotic cycles”. In: *Journal of the American Chemical Society* 133.24 (2011), pp. 9457–9468.

- [176] Yechezkel Wolman, William J Haverland, and Stanley L Miller. “Nonprotein amino acids from spark discharges and their comparison with the Murchison meteorite amino acids”. In: *Proceedings of the National Academy of Sciences* 69.4 (1972), pp. 809–811.
- [177] John F Kerridge and Mildred Shapley Matthews. “Meteorites and the early solar system”. In: *Meteorites and the early solar system* (1988).
- [178] Aaron S Burton et al. “Understanding prebiotic chemistry through the analysis of extraterrestrial amino acids and nucleobases in meteorites”. In: *Chemical Society Reviews* 41.16 (2012), pp. 5459–5472.
- [179] Christopher Chyba and Carl Sagan. “Endogenous production, exogenous delivery and impact-shock synthesis of organic molecules: an inventory for the origins of life”. In: *Nature* 355.6356 (1992), pp. 125–132.
- [180] Edward Anders. “Pre-biotic organic matter from comets and asteroids”. In: *Nature* 342.6247 (1989), pp. 255–257.
- [181] R PI Turco et al. “An analysis of the physical, chemical, optical, and historical impacts of the 1908 Tunguska meteor fall”. In: *Icarus* 50.1 (1982), pp. 1–52.
- [182] B Yu Levin and VA Bronshten. “The Tunguska event and the meteors with terminal flares”. In: *Meteoritics* 21.2 (1986), pp. 199–215.
- [183] Meixun Zhao and Jeffrey L Bada. “Extraterrestrial amino acids in Cretaceous/Tertiary boundary sediments at Stevns Klint, Denmark”. In: *Nature* 339.6224 (1989), pp. 463–465.
- [184] Christopher F Chyba et al. “Cometary delivery of organic molecules to the early Earth”. In: *Science* 249.4967 (1990), pp. 366–373.
- [185] Kevin Zahnle and David Grinspoon. “Comet dust as a source of amino acids at the Cretaceous/Tertiary boundary”. In: *Nature* 348.6297 (1990), pp. 157–160.
- [186] Martin JS Rudwick. *Earth’s Deep History: How it was Discovered and why it Matters*. University of Chicago Press, 2014.
- [187] Michael Ruse. “Charles Darwin’s theory of evolution: an analysis”. In: *Journal of the History of Biology* (1975), pp. 219–241.
- [188] Patrick N Wyse Jackson. “John Joly (1857–1933) and his determinations of the age of the Earth”. In: *Geological Society, London, Special Publications* 190.1 (2001), pp. 107–119.

- [189] Elso S Barghoorn and Stanley A Tyler. “Microorganisms from the Gunflint Chert: These structurally preserved Precambrian fossils from Ontario are the most ancient organisms known.” In: *Science* 147.3658 (1965), pp. 563–575.
- [190] HL Allsopp et al. “Rb-Sr age measurements on various Swaziland granites”. In: *Journal of Geophysical Research* 67.13 (1962), pp. 5307–5313.
- [191] Minik T Rosing. “¹³C-depleted carbon microparticles in 3700-Ma sea-floor sedimentary rocks from West Greenland”. In: *Science* 283.5402 (1999), pp. 674–676.
- [192] Allen P Nutman et al. “Rapid emergence of life shown by discovery of 3,700-million-year-old microbial structures”. In: *Nature* 537.7621 (2016), pp. 535–538.
- [193] Elizabeth A Bell et al. “Potentially biogenic carbon preserved in a 4.1 billion-year-old zircon”. In: *Proceedings of the National Academy of Sciences* 112.47 (2015), pp. 14518–14521.
- [194] Heinrich D Holland. “The oxygenation of the atmosphere and oceans”. In: *Philosophical Transactions of the Royal Society B: Biological Sciences* 361.1470 (2006), pp. 903–915.
- [195] Andrew H Knoll and Martin A Nowak. “The timetable of evolution”. In: *Science advances* 3.5 (2017), e1603076.
- [196] Howard H Pattee. “The measurement problem in artificial world models”. In: *BioSystems* 23.2-3 (1989), pp. 281–289.
- [197] Claus Emmeche. “Life as an abstract phenomenon: Is artificial life possible”. In: *Varela and Bourgine (1992)* (1992), pp. 466–474.
- [198] Claus Emmeche. “The computational notion of life”. In: *Theoria: An International Journal for Theory, History and Foundations of Science* (1994), pp. 1–30.
- [199] Shuhao Zhang et al. “Exploring the frontiers of chemistry with a general reactive machine learning potential”. In: (2023).
- [200] Lee-Ping Wang et al. “Discovering chemistry with an ab initio nanoreactor”. In: *Nature chemistry* 6.12 (2014), pp. 1044–1048.
- [201] Antonino Marco Saitta and Franz Saija. “Miller experiments in atomistic computer simulations”. In: *Proceedings of the National Academy of Sciences* 111.38 (2014), pp. 13768–13773.

- [202] David Ring et al. “Prebiotic synthesis of hydrophobic and protein amino acids”. In: *Proceedings of the National Academy of Sciences* 69.3 (1972), pp. 765–768.
- [203] Eric T Parker et al. “Primordial synthesis of amines and amino acids in a 1958 Miller H₂S-rich spark discharge experiment”. In: *Proceedings of the National Academy of Sciences* 108.14 (2011), pp. 5526–5531.
- [204] Carl Sagan and Stanley L Miller. “Molecular Synthesis in Simulated Reducing Planetary Atmospheres.” In: *Astronomical Journal, Vol. 65, p. 499* 65 (1960), p. 499.
- [205] Adam P Johnson et al. “The Miller volcanic spark discharge experiment”. In: *Science* 322.5900 (2008), pp. 404–404.
- [206] Jeffrey L Bada and Antonio Lazcano. “Prebiotic soup—revisiting the miller experiment”. In: *Science* 300.5620 (2003), pp. 745–746.
- [207] Théo Magrino, Fabio Pietrucci, and A Marco Saitta. “Step by step strecker amino acid synthesis from ab initio prebiotic chemistry”. In: *The Journal of Physical Chemistry Letters* 12.10 (2021), pp. 2630–2637.
- [208] Christopher Ramos. “The photochemistry and photophysics of diacetylene and cyanoacetylene: Applications to the atmosphere of Titan”. PhD thesis. Purdue University, 2002.
- [209] A Butlerow. “Formation synthétique d’une substance sucrée”. In: *CR Acad. Sci* 53 (1861), pp. 145–147.
- [210] H James Cleaves et al. “A reassessment of prebiotic organic synthesis in neutral planetary atmospheres”. In: *Origins of Life and Evolution of Biospheres* 38 (2008), pp. 105–115.
- [211] Joan Oro. “Synthesis of organic compounds by electric discharges”. In: *Nature (London)* 197.4870 (1963).
- [212] Gordon Schlesinger and Stanley L Miller. “Prebiotic synthesis in atmospheres containing CH₄, CO, and CO₂: II. Hydrogen cyanide, formaldehyde and ammonia”. In: *Journal of molecular evolution* 19 (1983), pp. 383–390.
- [213] Shin Miyakawa et al. “Prebiotic synthesis from CO atmospheres: implications for the origins of life”. In: *Proceedings of the National Academy of Sciences* 99.23 (2002), pp. 14628–14631.
- [214] Joaquín Criado-Reyes et al. “The role of borosilicate glass in Miller–Urey experiment”. In: *Scientific reports* 11.1 (2021), p. 21009.

- [215] Martin AA Schoonen and Yong Xu. “Nitrogen reduction under hydrothermal vent conditions: Implications for the prebiotic synthesis of CHON compounds”. In: *Astrobiology* 1.2 (2001), pp. 133–142.
- [216] Alexander Smirnov et al. “Abiotic ammonium formation in the presence of Ni-Fe metals and alloys and its implications for the Hadean nitrogen cycle”. In: *Geochemical Transactions* 9 (2008), pp. 1–20.
- [217] Eva Wollrab et al. “Chemical analysis of a “Miller-type” complex prebiotic broth: Part I: Chemical diversity, oxygen and nitrogen based polymers”. In: *Origins of Life and Evolution of Biospheres* 46 (2016), pp. 149–169.
- [218] Gary Steinman and Marian N Cole. “Synthesis of biologically pertinent peptides under possible primordial conditions.” In: *Proceedings of the National Academy of Sciences* 58.2 (1967), pp. 735–742.
- [219] Carl Sagan and Bishun N Khare. “Long-wavelength ultraviolet photoproduction of amino acids on the primitive Earth”. In: *Science* 173.3995 (1971), pp. 417–420.
- [220] Yuichi Utsumi and Jun-ichi Takahashi. “Synthesis of amino acids from N₂, H₂O vapor and CO₂ gas mixture by synchrotron radiation induced photochemical reactions at atmospheric pressure”. In: *Japanese journal of applied physics* 37.10B (1998), p. L1268.
- [221] Jun-ichi Takahashi et al. “Abiotic synthesis of amino acids by x-ray irradiation of simple inorganic gases”. In: *Applied physics letters* 74.6 (1999), pp. 877–879.
- [222] Deborah D Davis, George R Smith, and William A Guillory. “Infrared laser photolysis: A new tool for the study of prebiotic chemistry”. In: *Origins of life* 10 (1980), pp. 237–245.
- [223] Kensei Kobayashi, Takeo Kaneko, and Takeshi Saito. “Characterization of complex organic compounds formed in simulated planetary atmospheres by the action of high energy particles”. In: *Advances in Space Research* 24.4 (1999), pp. 461–464.
- [224] Elmira Mohammadi et al. “Formic acid, a ubiquitous but overlooked component of the early earth atmosphere”. In: *Chemistry–A European Journal* 26.52 (2020), pp. 12075–12080.
- [225] Hans Schulz. “Short history and present trends of Fischer–Tropsch synthesis”. In: *Applied Catalysis A: General* 186.1-2 (1999), pp. 3–12.

- [226] Sabrina Scherer et al. “Chemical analysis of a “Miller-type” complex prebiotic broth: part II: gas, oil, water and the oil/water-interface”. In: *Origins of Life and Evolution of Biospheres* 47 (2017), pp. 381–403.
- [227] James D Watson and Francis HC Crick. “The structure of DNA”. In: *Cold Spring Harbor symposia on quantitative biology*. Vol. 18. Cold Spring Harbor Laboratory Press. 1953, pp. 123–131.
- [228] Martin Ferus et al. “Formation of nucleobases in a Miller–Urey reducing atmosphere”. In: *Proceedings of the National Academy of Sciences* 114.17 (2017), pp. 4306–4311.
- [229] Thomas Geisberger et al. “Evolutionary steps in the analytics of primordial metabolic evolution”. In: *Life* 9.2 (2019), p. 50.
- [230] Albert-Laszlo Barabasi and Zoltan N Oltvai. “Network biology: understanding the cell’s functional organization”. In: *Nature reviews genetics* 5.2 (2004), pp. 101–113.
- [231] Kepa Ruiz-Mirazo, Carlos Briones, and Andres de la Escosura. “Prebiotic systems chemistry: new perspectives for the origins of life”. In: *Chemical reviews* 114.1 (2014), pp. 285–366.
- [232] Carlos F Barbas III. “Organocatalysis lost: modern chemistry, ancient chemistry, and an unseen biosynthetic apparatus”. In: *Angewandte Chemie International Edition* 47.1 (2008), pp. 42–47.
- [233] Martin Egli et al. “Crystal structure of homo-DNA and nature’s choice of pentose over hexose in the genetic system”. In: *Journal of the American Chemical Society* 128.33 (2006), pp. 10847–10856.
- [234] Jonathan R Nitschke. “Molecular networks come of age”. In: *Nature* 462.7274 (2009), pp. 736–738.
- [235] Viviana Serreli et al. “A molecular information ratchet”. In: *Nature* 445.7127 (2007), pp. 523–527.
- [236] Stuart A Kauffman. *The origins of order: Self-organization and selection in evolution*. Oxford University Press, USA, 1993.
- [237] Annick Vidonne and Douglas Philp. “Making molecules make themselves—the chemistry of artificial replicators”. In: *European Journal of Organic Chemistry* 2009.5 (2009), pp. 593–610.

- [238] R Frederick Ludlow and Sijbren Otto. “Systems chemistry”. In: *Chemical Society Reviews* 37.1 (2008), pp. 101–108.
- [239] David Gaddes et al. “Improved micromachined column design and fluidic interconnects for programmed high-temperature gas chromatography separations”. In: *Journal of Chromatography A* 1349 (2014), pp. 96–104.
- [240] Daniel C Harris. *Quantitative chemical analysis*. Macmillan, 2010.
- [241] Catherine L Arthur and Janusz Pawliszyn. “Solid phase microextraction with thermal desorption using fused silica optical fibers”. In: *Analytical chemistry* 62.19 (1990), pp. 2145–2148.
- [242] JS Aulakh et al. “A Review on solid phase micro extraction—high performance liquid chromatography (SPME-HPLC) analysis of pesticides”. In: *Critical reviews in analytical chemistry* 35.1 (2005), pp. 71–85.
- [243] Heather Lord and Janusz Pawliszyn. “Evolution of solid-phase microextraction technology”. In: *Journal of Chromatography A* 885.1-2 (2000), pp. 153–193.
- [244] J Ayrton et al. “Use of generic fast gradient liquid chromatography–tandem mass spectroscopy in quantitative bioanalysis”. In: *Journal of Chromatography B: Biomedical Sciences and Applications* 709.2 (1998), pp. 243–254.
- [245] R Barry Holtz. “Qualitative and Quantitative Analyses of Free Neutral Carbohydrates in Mushroom Tissues by Gas-Liquid Chromatography and Mass Spectroscopy”. In: *Journal of Agricultural and Food Chemistry* 19.6 (1971), pp. 1272–1273.
- [246] Chung Shun Ho et al. “Electrospray ionisation mass spectrometry: principles and clinical applications”. In: *The Clinical Biochemist Reviews* 24.1 (2003), p. 3.
- [247] Jürgen H Gross. *Massenspektrometrie*. Springer, 2019.
- [248] Shibdas Banerjee and Shyamalava Mazumdar. “Electrospray ionization mass spectrometry: a technique to access the information beyond the molecular weight of the analyte”. In: *International journal of analytical chemistry* 2012 (2012).
- [249] Erich Heftmann. *Chromatography: Fundamentals and applications of chromatography and related differential migration methods-Part B: Applications*. Elsevier, 2004.
- [250] JE Campana. “Elementary theory of the quadrupole mass filter”. In: *International Journal of Mass Spectrometry and Ion Physics* 33.2 (1980), pp. 101–117.

- [251] Tania Portolés et al. “Use of soft and hard ionization techniques for elucidation of unknown compounds by gas chromatography/time-of-flight mass spectrometry”. In: *Rapid Communications in Mass Spectrometry* 25.11 (2011), pp. 1589–1599.
- [252] Leila Hejazi et al. “Gas chromatography with parallel hard and soft ionization mass spectrometry”. In: *Rapid Communications in Mass Spectrometry* 29.1 (2015), pp. 91–99.
- [253] Kevin Downard. *Mass spectrometry: a foundation course*. Royal Society of Chemistry, 2007.
- [254] Ruedi Aebersold and Matthias Mann. “Mass spectrometry-based proteomics”. In: *Nature* 422.6928 (2003), pp. 198–207.
- [255] Michael E Wieser and Johannes B Schwieters. “The development of multiple collector mass spectrometry for isotope ratio measurements”. In: *International Journal of Mass Spectrometry* 242.2-3 (2005), pp. 97–115.
- [256] Eva Wollrab. “Emergente Strukturierung durch getriebene, chemische Reaktionen in komplexen, selbstorganisierten Gemischen”. In: (2013).
- [257] Jean-Pierre Schermann. *Spectroscopy and modeling of biomolecular building blocks*. Elsevier, 2007.
- [258] Eugene N Nikolaev, Yury I Kostyukevich, and Gleb Vladimirov. “Fundamentals and simulations in FT-ICR-MS”. In: *Fundamentals and applications of Fourier transform mass spectrometry*. Elsevier, 2019, pp. 89–111.
- [259] FA Mellon. “Mass spectrometry— Principles and instrumentation”. In: (2003).
- [260] Ron MA Heeren. “MALDI Techniques in Mass Spectrometry Imaging”. In: (2017).
- [261] G Arentz et al. “Applications of mass spectrometry imaging to cancer”. In: *Advances in cancer research* 134 (2017), pp. 27–66.
- [262] Mark D Kellogg. “Measurement of biological materials”. In: *Clinical and Translational Science*. Elsevier, 2017, pp. 137–155.
- [263] Marc Finkler. “In vitro Untersuchungen zu Proteinbiosynthese-assoziierten Prozessen: methylierungsabhängige Genregulation und Konkurrenz zwischen kanonischen und nicht-kanonischen Aminosäuren beim Einbau in Proteine”. In: (2022).

- [264] BA Mamyrin. “Time-of-flight mass spectrometry (concepts, achievements, and prospects)”. In: *International Journal of Mass Spectrometry* 206.3 (2001), pp. 251–266.
- [265] Tetsuya Suzuki et al. “A new, highly sensitive time-of-flight mass spectrometer consisting of a flangeon-type conical ion lens system and a proto-type Daly detector for exhaust gas analysis based on the Jet-REMPI technique”. In: *Analytical sciences* 21.8 (2005), pp. 991–996.
- [266] B Brehm et al. “Absolute detection efficiencies of a microchannel plate detector for ions”. In: *Measurement science and Technology* 6.7 (1995), p. 953.
- [267] M Båga et al. “Transcriptional activation of a pap pilus virulence operon from uropathogenic *Escherichia coli*.” In: *The EMBO journal* 4.13B (1985), pp. 3887–3893.
- [268] John R De Laeter, Paul De Bièvre, and HS Peiser. “Isotope mass spectrometry in metrology”. In: *Mass Spectrometry Reviews* 11.3 (1992), pp. 193–245.
- [269] Cs G Horvath and SR Lipsky. “Use of liquid ion exchange chromatography for the separation of organic compounds”. In: *Nature* 211.5050 (1966), pp. 748–749.
- [270] Csaba Horváth, Wayne Melander, and Imre Molnar. “Liquid chromatography of ionogenic substances with nonpolar stationary phases”. In: *Analytical Chemistry* 49.1 (1977), pp. 142–154.
- [271] Toshihiko Hanai. *HPLC: a practical guide*. Vol. 6. Royal Society of Chemistry, 1999.
- [272] Michael Swartz. “HPLC detectors: a brief review”. In: *Journal of Liquid Chromatography & Related Technologies* 33.9-12 (2010), pp. 1130–1150.
- [273] Abdu Hussen Ali. “High-performance liquid chromatography (HPLC): a review”. In: *Ann. Adv. Chem* 6 (2022), pp. 010–020.
- [274] Ian D Wilson et al. “HPLC-MS-based methods for the study of metabonomics”. In: *Journal of Chromatography B* 817.1 (2005), pp. 67–76.
- [275] Donald L Pavia et al. “Introduction to spectroscopy”. In: (2015).
- [276] Bernard Valeur and Mario N Berberan-Santos. “A brief history of fluorescence and phosphorescence before the emergence of quantum theory”. In: *Journal of Chemical Education* 88.6 (2011), pp. 731–738.

- [277] George Gabriel Stokes. “On the change of refrangibility of light”. In: *Philosophical transactions of the Royal Society of London* 142 (1852), pp. 463–562.
- [278] Aswathy Bose, I Thomas, and E Abraham. “Fluorescence spectroscopy and its applications: A Review”. In: *Int. J. Adv. Pharm. Res* 8.1 (2018), pp. 1–8.
- [279] Jan Perina, Zdeněk Hradil, and Branislav Jurco. *Quantum optics and fundamentals of physics*. Vol. 63. Springer Science & Business Media, 2012.
- [280] Vladimir K Zworykin. “The scanning electron microscope”. In: *Scientific American* 167.3 (1942), pp. 111–113.
- [281] Michael Dunlap and JE Adaskaveg. “Introduction to the scanning electron microscope”. In: *Theory, practice, & procedures. Facility for Advance Instrumentation. UC Davis* 52 (1997).
- [282] Deutscher Kalibrierdienst. “Guideline DKD-R 5-7, Calibration of Climatic Chambers. Guideline, Edition 07/2004”. In: *English translation* 2 (2009).
- [283] Tom Winkler et al. “Experimental Investigation of a New Ultra-Low Temperature Refrigerant in an Environmental Test Chamber”. In: (2022).
- [284] E Graham Bligh and W Justin Dyer. “A rapid method of total lipid extraction and purification”. In: *Canadian journal of biochemistry and physiology* 37.8 (1959), pp. 911–917.
- [285] Erica A Souza-Silva and Janusz Pawliszyn. “Direct immersion solid-phase microextraction with matrix-compatible fiber coating for multiresidue pesticide analysis of grapes by gas chromatography–time-of-flight mass spectrometry (DI-SPME-GC-ToFMS)”. In: *Journal of agricultural and food chemistry* 63.18 (2015), pp. 4464–4477.
- [286] Nengsheng Ye, Liqin Zhang, and Xuexin Gu. “Discrimination of green teas from different geographical origins by using HS-SPME/GC–MS and pattern recognition methods”. In: *Food Analytical Methods* 5 (2012), pp. 856–860.
- [287] Carol Turse et al. “Simulations of prebiotic chemistry under post-impact conditions on Titan”. In: *Life* 3.4 (2013), pp. 538–549.
- [288] Eric T Parker et al. “A plausible simultaneous synthesis of amino acids and simple peptides on the primordial Earth”. In: *Angewandte Chemie* 126.31 (2014), pp. 8270–8274.
- [289] Christian Reichardt. “Solvents and solvent effects: an introduction”. In: *Organic process research & development* 11.1 (2007), pp. 105–113.

- [290] Kira A Podolsky and Neal K Devaraj. “Synthesis of lipid membranes for artificial cells”. In: *Nature Reviews Chemistry* 5.10 (2021), pp. 676–694.
- [291] Robert A Friedel and Milton Orchin. *Ultraviolet spectra of aromatic compounds*. Vol. 40. Wiley New York, 1951.
- [292] Mariella Mella et al. “New synthetic methods via radical cation fragmentation”. In: *Chemical Society Reviews* 27.1 (1998), pp. 81–89.
- [293] Maurizio Fagnoni et al. “Photocatalysis for the Formation of the C- C Bond”. In: *Chemical Reviews* 107.6 (2007), pp. 2725–2756.
- [294] Robert M Silverstein and G Clayton Bassler. “Spectrometric identification of organic compounds”. In: *Journal of Chemical Education* 39.11 (1962), p. 546.
- [295] Norman Colthup. *Introduction to infrared and Raman spectroscopy*. Elsevier, 2012.
- [296] Ernő Pretsch et al. *Tables of spectral data for structure determination of organic compounds*. Springer Science & Business Media, 2013.
- [297] Rudolf Maly. “Spark ignition: its physics and effect on the internal combustion engine”. In: *Fuel economy: In road vehicles powered by spark ignition engines* (1984), pp. 91–148.
- [298] Thomas Kammermann et al. “Spark-induced breakdown spectroscopy of methane/air and hydrogen-enriched methane/air mixtures at engine relevant conditions”. In: *Spectrochimica Acta Part B: Atomic Spectroscopy* 148 (2018), pp. 152–164.
- [299] CG Parigger. *Laser-induced breakdown in gases: Experiments and simulation*. 2006.
- [300] R Mark Merer and James S Wallace. *Spark spectroscopy for spark ignition engine diagnostics*. Tech. rep. SAE Technical Paper, 1995.
- [301] N Kawahara et al. “Fuel concentration measurement of premixed mixture using spark-induced breakdown spectroscopy”. In: *Spectrochimica Acta Part B: Atomic Spectroscopy* 64.10 (2009), pp. 1085–1092.
- [302] Kazi Mostafijur Rahman et al. “Local fuel concentration measurement through spark-induced breakdown spectroscopy in a direct-injection hydrogen spark-ignition engine”. In: *International Journal of Hydrogen Energy* 41.32 (2016), pp. 14283–14292.

- [303] TD Fansler et al. “Local fuel concentration measurements in internal combustion engines using spark-emission spectroscopy”. In: *Applied Physics B* 75 (2002), pp. 577–590.
- [304] J Fischer et al. *Measurement of the equivalence ratio in the spark gap region of a gasoline direct injection engine with spark emission spectroscopy and tracer-LIF*. Tech. rep. SAE Technical Paper, 2004.
- [305] P Stavropoulos et al. “Laser-induced breakdown spectroscopy as an analytical tool for equivalence ratio measurement in methane–air premixed flames”. In: *Spectrochimica Acta Part B: Atomic Spectroscopy* 60.7-8 (2005), pp. 1092–1097.
- [306] Francesco Ferioli and Steven G Buckley. “Measurements of hydrocarbons using laser-induced breakdown spectroscopy”. In: *Combustion and Flame* 144.3 (2006), pp. 435–447.
- [307] Ahmad Farhadi et al. “Influence of electrode shape and size on electric arc channel and crater”. In: *Procedia Cirp* 68 (2018), pp. 215–220.
- [308] Ramona Pristavita et al. “Carbon blacks produced by thermal plasma: the influence of the reactor geometry on the product morphology”. In: *Plasma Chemistry and Plasma Processing* 30 (2010), pp. 267–279.
- [309] Mohammad Mahdi Moshrefi et al. “Methane conversion to hydrogen and carbon black by DC-spark discharge”. In: *Plasma Chemistry and Plasma Processing* 32 (2012), pp. 1157–1168.
- [310] Hui Chen et al. “Additive WO₂ promotes Ni-based catalyst for hydrogen production from auto-thermal reforming of acetic acid”. In: *Fuel* 339 (2023), p. 126914.
- [311] Zhigang Chen et al. “Metallic W/WO₂ solid-acid catalyst boosts hydrogen evolution reaction in alkaline electrolyte”. In: *Nature Communications* 14.1 (2023), p. 5363.
- [312] Marc J Ledoux et al. “Compared activities of platinum and high specific surface area Mo₂C and WC catalysts for reforming reactions: I. Catalyst activation and stabilization: Reaction of n-hexane”. In: *Journal of catalysis* 134.2 (1992), pp. 383–398.
- [313] Min Ku Jeon et al. “CO tolerant Pt/WC methanol electro-oxidation catalyst”. In: *Electrochemistry Communications* 9.11 (2007), pp. 2692–2695.

- [314] Min Ku Jeon et al. “Investigation of Pt/WC/C catalyst for methanol electro-oxidation and oxygen electro-reduction”. In: *Journal of Power Sources* 185.2 (2008), pp. 927–931.

Appendix

Description of the Table 15 elements:

No. : This column lists the entry number for each compound, serving as a sequential identifier for easy reference within the table. Each row corresponds to a unique compound detected in one or more of the samples.

NIST ID : NIST ID (NIST Mass Number) is the unique identifier number for each compound in the NIST (National Institute of Standards and Technology) mass spectral database.

S₁ ... S₈ : S₁ to S₈ (Sample 1 to Sample 8) are columns representing each of the eight analyzed samples. A "+" indicates that the compound was detected in that sample by GC-MS analysis, while a "-" indicates it was not detected.

Table 15: **Compound Detection Results in Samples S₁ to S₈ (Appendix table).**

No.	NIST ID	S ₁	S ₂	S ₃	S ₄	S ₅	S ₆	S ₇	S ₈
1	403456	-	-	-	-	+	-	-	-
2	137217	-	-	-	+	-	-	-	-
3	344067	-	-	-	-	+	-	-	-
4	155651	-	-	-	-	-	-	-	-
5	153605	-	-	-	-	-	+	-	+
6	141317	-	-	-	-	+	-	-	+
7	417798	-	-	-	-	+	-	-	-
8	135173	-	-	+	-	-	-	-	-
9	112646	-	-	-	-	+	-	-	-
10	401418	-	-	-	-	-	-	+	-
11	112654	-	-	-	-	+	-	-	-
12	403503	-	+	-	-	-	-	-	-
13	372753	-	-	-	-	-	-	+	-
14	309265	-	-	-	-	-	+	-	-
15	417810	-	-	-	-	+	-	-	-

Continued on next page

Table 15 Continued from previous page

No.	NIST ID	S ₁	S ₂	S ₃	S ₄	S ₅	S ₆	S ₇	S ₈
16	1120275	-	+	-	-	-	-	-	-
17	366615	+	+	-	+	+	-	-	-
18	61464	-	-	-	+	-	-	-	-
19	61465	-	-	+	+	-	-	-	-
20	333850	-	-	+	+	-	+	-	-
21	100379	-	-	-	-	-	-	+	-
22	61467	-	-	-	-	-	-	+	-
23	141339	-	-	-	-	-	-	-	+
24	10270	-	-	-	-	+	-	-	-
25	235551	-	-	-	-	-	-	+	+
26	151583	-	-	-	-	+	-	-	-
27	1226783	-	-	+	-	-	-	-	-
28	133154	-	-	+	-	-	-	-	-
29	61475	-	-	-	-	-	-	-	-
30	333854	-	-	+	-	-	-	-	-
31	141342	-	-	-	-	+	-	-	-
32	98344	-	-	-	-	+	-	-	-
33	333867	-	-	-	-	+	-	-	+
34	71724	+	-	-	-	-	-	-	-
35	161839	-	-	-	-	-	-	+	-
36	403503	-	+	-	+	-	-	+	+
37	292912	+	-	-	+	-	-	-	-
38	114738	-	-	+	-	-	-	-	-
39	129076	-	+	-	-	+	-	-	-
40	364597	-	-	-	-	+	-	-	-
41	364598	-	-	+	+	+	+	-	-
42	413748	+	-	-	-	-	-	-	-
43	360505	-	-	+	-	-	-	-	-
44	24634	-	-	-	-	+	-	-	-
45	108605	-	-	-	-	+	-	-	-
46	30784	-	-	-	+	-	-	-	-
47	366657	-	+	-	-	-	-	-	-

Continued on next page

Table 15 Continued from previous page

No.	NIST ID	S ₁	S ₂	S ₃	S ₄	S ₅	S ₆	S ₇	S ₈
48	364611	-	-	-	-	+	-	-	-
49	239688	-	-	-	+	-	-	-	-
50	30793	-	-	-	-	-	-	-	+
51	151626	-	-	-	-	+	-	-	-
52	196682	-	-	-	-	+	-	-	-
53	30796	-	-	+	-	-	-	-	-
54	20559	-	-	-	-	-	-	+	-
55	71759	-	-	-	-	-	-	+	-
56	141397	-	-	-	-	-	+	-	-
57	41048	-	-	-	-	+	-	-	-
58	22620	+	-	-	+	-	-	-	+
59	309341	-	+	-	-	-	-	-	-
60	10334	-	-	-	-	-	-	-	-
61	243807	-	-	-	-	+	-	-	-
62	73825	+	-	-	-	-	-	-	-
63	362594	-	-	-	-	-	-	+	-
64	286818	-	-	-	-	+	-	+	+
65	309346	+	-	-	-	-	-	-	-
66	30824	-	-	-	-	+	-	-	+
67	36971	-	-	-	-	-	-	+	-
68	192621	-	-	+	-	-	-	-	-
69	8305	-	-	-	-	-	-	+	-
70	120947	-	-	-	-	-	-	+	-
71	129141	-	-	-	-	-	+	-	-
72	307317	-	-	-	-	-	-	-	+
73	333943	-	+	+	+	+	+	+	+
74	30839	-	-	-	-	-	-	-	-
75	22650	-	-	-	-	-	-	-	-
76	397436	-	-	-	-	-	-	+	-
77	379004	-	-	-	-	-	-	+	-
78	333951	-	-	-	-	+	-	-	-
79	217216	-	-	-	-	-	-	+	-

Continued on next page

Table 15 Continued from previous page

No.	NIST ID	S ₁	S ₂	S ₃	S ₄	S ₅	S ₆	S ₇	S ₈
80	280703	-	+	-	-	-	-	-	-
81	229506	-	+	+	-	+	-	-	+
82	379010	-	-	-	+	-	-	-	-
83	77959	-	-	-	-	+	-	-	-
84	63624	-	-	-	+	-	-	-	-
85	39048	-	-	-	-	-	-	-	+
86	309388	-	-	+	-	-	-	-	-
87	139405	-	-	-	+	-	-	-	-
88	192654	-	-	-	-	+	-	-	-
89	24718	-	-	-	-	+	-	-	-
90	1194128	-	-	+	-	-	-	-	-
91	352400	-	-	-	-	-	-	-	-
92	61584	-	-	-	-	-	-	-	+
93	221332	-	-	+	-	-	-	-	-
94	28821	-	-	-	-	-	+	-	-
95	155799	+	+	+	-	-	-	-	-
96	151704	-	-	-	+	-	-	-	-
97	155801	-	-	-	-	-	-	-	-
98	1116319	-	-	-	-	-	-	+	-
99	403615	+	-	-	-	-	-	-	-
100	1052831	+	-	-	-	-	-	-	-
101	290979	-	-	+	-	+	-	-	-
102	276644	-	-	-	-	+	-	-	-
103	215205	+	-	+	-	-	-	-	-
104	157861	-	-	-	-	-	-	-	+
105	30890	+	-	-	-	-	-	-	-
106	71852	-	-	+	-	-	-	-	-
107	141484	-	+	+	-	-	-	-	-
108	141487	-	-	-	-	+	-	-	-
109	30899	-	-	-	-	+	-	-	-
110	10422	-	-	-	-	+	-	-	-
111	14518	+	-	-	-	-	-	-	-

Continued on next page

Table 15 Continued from previous page

No.	NIST ID	S ₁	S ₂	S ₃	S ₄	S ₅	S ₆	S ₇	S ₈
112	229560	-	-	+	-	-	-	-	-
113	352441	-	+	-	+	-	-	-	-
114	30904	+	-	-	-	-	-	-	-
115	63675	-	-	-	-	-	-	+	-
116	366781	-	-	+	-	-	-	-	-
117	8382	-	-	-	+	-	-	-	-
118	352446	-	-	-	-	-	-	-	-
119	30913	-	-	-	-	+	-	-	-
120	30915	-	+	-	+	+	-	+	+
121	24771	-	-	-	+	-	-	-	-
122	188614	-	-	-	-	+	-	-	-
123	352455	-	-	-	-	-	-	+	-
124	399562	-	-	-	+	-	+	+	+
125	149707	-	-	-	-	+	-	+	-
126	61644	+	+	-	-	-	-	-	-
127	37071	-	-	-	-	-	-	+	-
128	47312	-	-	-	+	+	-	+	-
129	71888	-	-	-	+	-	-	-	-
130	63701	-	-	-	-	-	-	+	-
131	147669	-	-	-	-	+	-	+	+
132	366808	-	-	-	-	-	-	+	-
133	133337	-	-	-	+	-	+	+	+
134	75995	-	-	-	-	-	-	+	-
135	352476	-	-	-	+	+	+	-	-
136	153821	+	-	-	+	+	-	-	-
137	129246	-	-	-	-	+	-	-	-
138	133340	-	-	+	-	-	-	-	-
139	12512	-	-	-	-	-	-	+	-
140	309471	-	-	-	+	-	-	-	-
141	4317	-	-	+	-	-	-	-	-
142	63711	+	+	-	-	-	-	-	-
143	153822	+	-	-	-	-	-	-	-

Continued on next page

Table 15 Continued from previous page

No.	NIST ID	S ₁	S ₂	S ₃	S ₄	S ₅	S ₆	S ₇	S ₈
144	1034462	+	-	-	-	-	-	-	-
145	149734	-	-	-	-	-	-	+	-
146	10470	-	-	-	-	-	-	+	-
147	71909	-	-	+	-	-	-	-	-
148	403689	-	-	-	-	-	-	+	-
149	332007	-	-	-	-	+	-	-	-
150	366824	-	-	-	-	+	-	-	-
151	76008	-	-	-	-	-	-	-	-
152	151788	-	-	-	-	-	+	-	-
153	375021	-	-	+	-	-	-	-	-
154	280814	-	-	-	-	+	-	-	-
155	12528	-	-	-	-	-	-	+	-
156	352501	-	-	-	-	+	-	-	-
157	352502	-	-	-	-	-	-	-	-
158	352503	-	+	+	+	+	+	+	-
159	229623	-	-	-	-	-	-	+	-
160	227575	-	-	-	-	-	-	-	-
161	227578	-	+	-	-	-	-	+	-
162	147708	-	-	-	-	-	-	+	-
163	2302	-	-	+	-	-	-	-	-
164	1071359	-	-	+	-	-	-	-	-
165	1071360	-	-	+	-	-	-	-	-
166	1071358	-	-	+	-	-	-	-	-
167	80130	-	-	-	-	-	-	+	-
168	153858	-	-	-	-	-	-	+	-
169	352519	+	-	-	-	-	-	-	-
170	237832	-	-	+	-	-	-	-	-
171	157961	+	-	+	+	+	+	+	-
172	22794	-	-	-	-	-	+	-	-
173	315659	-	-	-	-	+	-	-	-
174	6413	+	-	+	-	-	-	-	-
175	334099	-	-	+	-	-	-	-	-

Continued on next page

Table 15 Continued from previous page

No.	NIST ID	S ₁	S ₂	S ₃	S ₄	S ₅	S ₆	S ₇	S ₈
176	47380	+	-	-	-	-	-	-	-
177	45335	+	-	+	+	+	-	+	-
178	332057	-	-	-	-	+	-	-	-
179	352538	-	-	-	-	+	-	-	-
180	373020	-	-	-	-	-	-	-	-
181	114974	-	-	-	+	+	-	+	-
182	194847	-	-	-	-	+	-	-	+
183	366880	+	-	+	+	-	-	-	-
184	43297	-	-	+	-	-	-	-	-
185	303394	-	-	-	-	+	-	-	-
186	8483	-	-	-	+	-	-	-	-
187	186659	-	-	-	+	-	-	-	-
188	149796	-	-	-	-	-	-	-	+
189	16678	-	+	-	-	-	-	-	-
190	114983	-	-	-	-	-	-	+	-
191	352555	-	+	+	+	-	-	-	-
192	377133	-	-	-	-	-	+	-	-
193	22830	-	-	-	-	+	+	+	+
194	74029	-	-	-	-	-	-	-	-
195	12593	-	-	-	+	-	-	-	-
196	8501	-	-	-	-	-	-	+	-
197	194870	-	-	-	-	-	-	+	-
198	373047	-	-	-	+	-	-	-	-
199	293176	-	-	+	-	-	-	-	-
200	47419	-	-	-	+	-	-	-	-
201	395581	-	+	-	-	-	+	-	-
202	373054	-	-	-	-	-	-	+	-
203	153917	-	-	-	+	-	-	-	-
204	403774	-	-	-	-	+	-	-	-
205	352574	-	-	-	-	+	-	-	-
206	53566	+	+	-	-	-	-	-	-
207	24898	-	-	-	-	+	-	-	-

Continued on next page

Table 15 Continued from previous page

No.	NIST ID	S ₁	S ₂	S ₃	S ₄	S ₅	S ₆	S ₇	S ₈
208	278852	-	-	-	-	-	-	+	-
209	321855	-	-	+	-	-	-	-	-
210	117060	-	-	-	-	+	-	-	-
211	47428	-	+	-	-	-	-	-	-
212	321863	-	-	-	-	+	-	-	-
213	291148	-	-	-	-	-	-	+	-
214	414028	+	-	-	-	-	-	-	-
215	215379	-	-	-	+	-	-	-	-
216	76115	-	-	-	+	-	-	-	-
217	22871	+	+	-	+	-	+	+	-
218	395611	-	-	-	-	+	-	+	-
219	352603	-	-	-	-	+	-	-	-
220	72028	+	-	+	-	-	-	-	-
221	229726	-	-	+	+	-	+	+	-
222	252253	-	+	-	-	-	-	-	-
223	26977	-	-	-	-	+	-	-	-
224	403810	+	-	+	-	-	-	-	-
225	293219	-	-	-	-	-	-	-	-
226	149863	-	-	-	-	-	-	-	-
227	215400	-	-	-	-	-	-	+	-
228	47465	-	-	-	-	-	-	+	-
229	233832	+	+	+	+	+	-	-	-
230	149864	-	-	-	-	+	-	-	-
231	149865	-	-	+	-	-	-	-	-
232	246120	+	-	-	-	-	-	-	-
233	229740	-	-	-	-	+	-	-	-
234	12650	-	+	-	-	-	-	-	-
235	80240	-	-	-	+	-	-	-	-
236	67953	-	-	-	-	-	-	+	-
237	246129	-	-	-	-	+	-	-	-
238	215408	-	-	+	+	-	-	-	-
239	12658	-	-	-	+	-	-	-	-

Continued on next page

Table 15 Continued from previous page

No.	NIST ID	S ₁	S ₂	S ₃	S ₄	S ₅	S ₆	S ₇	S ₈
240	373109	-	-	-	-	-	-	-	+
241	153975	-	-	-	-	-	-	+	-
242	356727	-	-	-	-	-	-	+	-
243	153976	-	-	-	-	-	-	-	+
244	332154	-	-	-	-	+	-	-	-
245	31099	-	-	-	-	+	-	-	-
246	24956	-	-	-	-	-	+	+	+
247	61827	-	-	+	-	-	-	-	-
248	215434	+	-	+	-	-	-	-	-
249	98699	-	-	-	-	-	-	+	-
250	332171	-	-	+	-	-	-	-	-
251	401806	-	-	-	-	-	-	-	-
252	162199	-	-	-	-	-	-	-	-
253	174489	-	-	+	-	-	-	-	-
254	37275	-	+	+	-	-	-	-	-
255	324010	-	-	+	-	-	-	-	-
256	356783	-	-	-	+	-	+	+	-
257	47536	-	-	-	-	-	-	+	-
258	367024	-	-	-	+	-	-	-	-
259	373169	-	-	-	+	-	-	-	-
260	352690	-	-	-	-	+	-	-	-
261	401840	+	+	-	-	-	-	-	+
262	356789	-	-	-	-	-	+	-	-
263	1216949	-	-	-	+	-	-	-	-
264	215479	-	-	-	-	+	-	-	-
265	352695	-	-	-	+	-	-	-	-
266	356790	-	-	-	-	-	-	-	-
267	229823	-	-	-	+	-	-	-	-
268	151999	-	-	-	-	-	-	-	-
269	281026	-	-	-	-	-	-	-	-
270	121283	-	-	-	-	+	-	-	-
271	281029	-	-	-	-	-	-	+	-

Continued on next page

Table 15 Continued from previous page

No.	NIST ID	S ₁	S ₂	S ₃	S ₄	S ₅	S ₆	S ₇	S ₈
272	22981	-	-	-	-	+	-	-	-
273	1006021	+	-	-	-	-	-	-	-
274	352714	-	-	-	+	-	-	-	-
275	1196490	-	+	-	-	-	-	-	-
276	238029	+	-	-	-	-	-	-	-
277	326095	-	-	-	-	-	-	+	-
278	238031	-	-	+	+	-	-	-	+
279	240080	-	-	-	-	+	-	-	-
280	162255	-	-	-	+	-	-	-	-
281	244180	-	-	-	-	-	-	+	-
282	367061	-	-	-	-	+	-	-	-
283	12758	-	-	-	+	-	-	-	-
284	283095	-	-	-	-	+	-	-	-
285	332246	-	-	-	-	-	-	-	-
286	33245	-	-	-	-	-	-	-	+
287	334302	-	+	+	+	-	-	-	-
288	299487	-	-	-	-	+	-	-	-
289	229858	+	+	+	+	-	+	+	-
290	10725	-	-	+	-	+	+	-	-
291	305637	-	-	-	-	+	-	-	-
292	135655	-	-	-	-	-	-	+	-
293	10727	-	+	-	-	-	-	-	-
294	332264	-	-	-	-	+	-	-	-
295	283112	-	-	-	-	-	-	-	-
296	166378	-	-	-	-	+	-	-	-
297	78313	-	-	+	-	-	-	-	-
298	309736	-	-	-	-	-	-	-	-
299	10733	-	-	+	+	-	-	-	-
300	332270	-	-	-	-	+	-	-	-
301	158195	+	-	-	-	-	-	-	-
302	121335	-	-	+	-	-	-	-	-
303	135672	-	-	+	-	-	-	-	-

Continued on next page

Table 15 Continued from previous page

No.	NIST ID	S ₁	S ₂	S ₃	S ₄	S ₅	S ₆	S ₇	S ₈
304	2552	-	-	-	-	-	-	-	+
305	43513	-	-	-	-	-	-	-	+
306	162109	+	-	-	-	-	-	-	-
307	283133	-	-	-	-	-	-	-	-
308	164354	-	-	-	+	-	-	-	-
309	1120771	-	+	-	-	-	-	-	-
310	408069	-	-	-	-	-	-	+	-
311	231942	-	-	+	-	-	-	-	-
312	408071	-	-	-	-	+	-	-	-
313	147978	-	-	-	-	+	-	+	-
314	55819	-	-	-	-	-	-	+	-
315	72203	-	-	-	+	-	-	-	-
316	373261	-	-	-	-	-	-	+	-
317	160270	-	-	-	+	-	-	-	-
318	373264	-	-	-	-	-	-	+	-
319	186897	-	-	-	-	+	-	-	-
320	414229	-	-	-	-	-	+	-	-
321	197144	-	-	-	-	+	-	-	-
322	408089	-	-	+	+	-	+	+	-
323	61976	-	-	-	+	-	-	-	-
324	348699	-	-	+	-	-	-	-	-
325	332318	-	-	-	-	-	-	-	-
326	336416	+	-	-	-	-	-	-	-
327	373283	-	-	-	-	+	-	+	-
328	31267	-	-	-	-	-	-	-	-
329	404005	-	-	+	-	-	-	-	-
330	148006	-	-	-	-	+	-	-	-
331	1223204	+	-	-	-	-	-	-	-
332	1157673	-	-	+	-	-	-	-	-
333	414252	+	-	+	-	-	+	-	-
334	12848	-	-	-	-	-	-	+	-
335	373296	-	-	-	-	-	-	-	-

Continued on next page

Table 15 Continued from previous page

No.	NIST ID	S ₁	S ₂	S ₃	S ₄	S ₅	S ₆	S ₇	S ₈
336	74292	-	-	-	-	+	-	-	-
337	113206	-	-	-	-	-	+	-	-
338	74294	-	-	-	-	+	-	-	+
339	414263	-	-	-	+	-	-	-	-
340	1071674	-	-	+	-	-	-	-	-
341	197184	-	-	-	-	-	-	+	-
342	328258	-	-	-	-	-	-	+	-
343	408132	-	+	-	-	-	-	-	-
344	6725	-	-	-	+	-	-	-	-
345	1120837	-	-	-	+	-	-	-	-
346	1034833	-	+	+	-	-	-	-	-
347	115281	-	-	-	-	-	-	-	-
348	150102	-	-	-	+	+	-	-	-
349	356951	-	-	-	+	+	-	-	-
350	78423	-	-	-	-	-	-	-	+
351	236125	-	-	+	-	-	-	-	-
352	103011	-	-	-	-	-	-	+	-
353	103012	-	-	-	-	-	+	-	-
354	279141	-	-	+	-	-	-	-	-
355	408165	-	-	-	-	-	-	-	+
356	25191	-	-	-	+	-	-	-	-
357	43623	-	-	+	-	-	-	-	-
358	14952	-	+	-	-	-	-	-	-
359	141930	-	-	-	-	-	-	+	-
360	367216	-	-	-	-	-	-	+	-
361	307825	-	-	-	-	-	-	+	-
362	385648	+	-	-	-	-	-	-	-
363	141942	-	-	-	-	-	-	+	-
364	285303	+	+	+	+	+	+	+	+
365	78456	-	-	-	+	-	-	-	-
366	154233	-	-	-	-	-	+	-	-
367	47736	+	-	-	-	-	-	-	-

Continued on next page

Table 15 Continued from previous page

No.	NIST ID	S ₁	S ₂	S ₃	S ₄	S ₅	S ₆	S ₇	S ₈
368	43642	-	-	-	-	-	-	-	-
369	164483	-	-	-	-	+	-	-	-
370	107140	-	-	+	+	+	-	+	+
371	160387	-	-	+	-	-	-	-	-
372	25219	-	-	-	-	-	-	-	-
373	227975	-	-	-	-	-	-	+	-
374	154246	-	-	-	-	-	-	-	+
375	373385	-	-	-	-	-	+	-	+
376	107147	-	+	+	-	+	+	+	+
377	262796	-	-	-	-	-	-	-	-
378	156301	-	-	-	-	+	-	-	-
379	1053328	-	-	+	-	-	-	-	-
380	234130	+	+	-	+	-	-	-	-
381	348819	-	-	-	-	-	-	-	-
382	414356	-	-	-	-	-	-	+	-
383	408212	-	-	-	-	+	-	-	-
384	227992	-	-	-	+	-	-	+	-
385	47771	-	-	-	-	-	-	-	-
386	236194	-	-	-	-	-	-	-	-
387	27298	-	-	-	-	-	-	-	-
388	414375	-	-	-	-	+	-	-	-
389	414376	-	-	+	-	+	-	-	+
390	379563	-	-	-	-	-	-	-	-
391	219821	-	-	-	-	-	-	-	+
392	379567	-	-	-	-	-	+	-	+
393	6834	-	-	-	-	+	-	-	-
394	62131	+	+	-	+	-	+	-	+
395	271027	-	-	-	-	-	-	-	+
396	379574	+	-	-	-	-	-	-	-
397	23223	-	-	+	-	-	-	-	-
398	25273	-	-	-	-	-	-	+	-
399	148154	-	-	-	-	-	-	-	-

Continued on next page

Table 15 Continued from previous page

No.	NIST ID	S ₁	S ₂	S ₃	S ₄	S ₅	S ₆	S ₇	S ₈
400	142011	-	-	-	-	-	-	-	+
401	408253	-	-	-	+	-	-	-	-
402	373442	-	-	-	-	-	+	-	+
403	105161	-	-	-	-	+	-	-	-
404	297674	-	-	-	-	-	+	-	-
405	56010	-	-	-	-	+	-	-	-
406	336588	+	-	+	-	+	-	+	-
407	150220	+	+	-	-	-	-	-	-
408	408268	+	-	-	-	-	-	-	-
409	408271	-	-	-	-	+	-	-	-
410	334544	-	-	-	-	+	-	-	-
411	25300	-	+	+	+	-	-	-	-
412	318165	-	-	-	-	-	-	+	-
413	414421	-	-	-	-	-	-	+	-
414	379604	-	-	+	-	-	-	-	-
415	297686	-	-	+	-	-	-	-	-
416	404183	-	-	-	-	-	-	-	+
417	191196	-	-	-	-	+	-	-	-
418	326373	-	-	-	-	+	-	-	-
419	146156	-	-	-	-	-	-	-	-
420	154349	-	-	-	-	-	-	-	+
421	215791	-	-	-	-	-	-	+	-
422	47859	-	-	-	-	-	-	+	-
423	232179	-	-	+	-	-	-	-	-
424	414451	+	-	+	-	-	-	-	-
425	240380	-	-	-	+	-	-	-	-
426	307966	-	-	+	+	+	+	+	-
427	307970	-	-	-	-	+	-	-	-
428	152322	-	-	-	-	-	-	-	-
429	17156	-	-	-	-	+	-	-	-
430	408324	-	+	-	-	+	-	-	-
431	162566	-	-	-	-	-	-	+	-

Continued on next page

Table 15 Continued from previous page

No.	NIST ID	S ₁	S ₂	S ₃	S ₄	S ₅	S ₆	S ₇	S ₈
432	340742	-	-	-	-	+	-	-	-
433	414466	+	-	-	-	-	-	-	-
434	1227527	-	-	-	+	-	-	-	-
435	62218	-	-	-	+	-	-	-	-
436	8975	-	-	-	-	+	-	-	-
437	373521	-	-	-	+	-	-	-	-
438	25367	-	-	-	-	-	-	+	-
439	152343	-	-	-	-	-	+	-	-
440	310041	-	-	-	-	-	-	+	-
441	103192	-	-	-	-	+	-	-	-
442	404256	-	-	-	-	-	-	-	+
443	6950	-	-	-	-	-	-	+	-
444	408359	-	-	-	-	-	-	+	-
445	385830	-	-	-	-	+	-	-	-
446	62249	-	-	-	+	+	-	+	-
447	267047	-	-	-	-	+	-	-	-
448	107308	+	+	+	-	-	-	-	-
449	33581	+	-	-	-	-	-	-	-
450	336686	+	+	+	-	-	-	-	-
451	340783	-	-	-	-	-	-	-	-
452	162611	-	-	+	-	-	-	-	-
453	379701	-	-	-	-	-	-	+	-
454	336693	-	-	-	-	-	-	+	-
455	1116985	-	+	-	-	-	-	-	-
456	240443	-	-	-	-	-	-	-	-
457	387901	-	-	-	-	-	-	+	-
458	406338	-	-	-	-	+	-	-	-
459	336707	-	-	-	-	-	-	-	+
460	191300	-	-	-	-	+	-	-	-
461	52038	-	-	-	-	+	-	-	-
462	105288	-	-	-	-	-	-	-	-
463	1004364	+	+	+	+	-	-	-	-

Continued on next page

Table 15 Continued from previous page

No.	NIST ID	S ₁	S ₂	S ₃	S ₄	S ₅	S ₆	S ₇	S ₈
464	1213260	+	-	-	-	-	-	-	-
465	379726	+	+	+	+	+	+	-	+
466	1227602	-	-	+	-	-	-	-	-
467	273236	-	-	-	-	-	-	+	-
468	234324	-	-	-	-	-	-	+	-
469	66389	-	-	-	-	+	-	-	-
470	353113	-	-	-	+	-	-	-	-
471	15194	-	-	-	+	+	-	+	-
472	402265	-	-	-	-	-	-	-	-
473	45916	-	-	-	+	-	-	-	-
474	228187	-	-	-	-	-	-	-	-
475	281441	-	-	-	+	-	-	-	-
476	283491	+	-	-	-	-	-	-	-
477	406376	-	-	+	-	-	-	-	-
478	406377	-	-	-	-	-	-	+	-
479	404331	-	-	-	-	-	-	+	-
480	1190763	+	-	-	-	-	-	-	-
481	150381	+	-	+	-	+	+	-	-
482	107373	-	+	+	-	-	-	-	-
483	21359	-	-	-	+	-	-	-	-
484	131949	-	-	-	-	-	-	-	+
485	406386	-	-	-	-	+	-	-	-
486	244594	-	-	-	-	-	-	-	+
487	383859	+	+	-	-	-	-	-	-
488	396150	-	-	-	-	+	-	-	-
489	287607	-	-	-	-	-	-	-	+
490	164728	-	-	-	-	-	+	-	-
491	406392	-	-	-	+	-	-	-	-
492	164729	-	+	+	+	-	-	-	-
493	406393	+	-	+	-	-	-	-	-
494	25469	-	+	-	-	-	-	-	-
495	193406	-	-	-	-	+	-	-	-

Continued on next page

Table 15 Continued from previous page

No.	NIST ID	S ₁	S ₂	S ₃	S ₄	S ₅	S ₆	S ₇	S ₈
496	387967	-	-	-	+	-	-	-	-
497	25472	-	+	-	-	-	-	-	-
498	101249	-	-	-	-	-	-	+	-
499	375680	-	-	-	-	-	-	-	-
500	62339	-	-	-	-	-	-	+	-
501	9092	-	-	-	-	-	-	+	-
502	242562	-	-	-	+	-	-	-	-
503	25474	-	-	-	-	-	-	-	-
504	25476	-	-	-	-	+	-	-	-
505	152453	+	-	-	-	-	-	-	-
506	134026	-	-	-	-	+	-	-	-
507	156555	-	-	-	-	-	-	-	-
508	215949	-	-	-	-	-	-	-	+
509	336782	-	-	+	-	-	-	-	-
510	332687	-	-	-	-	-	-	-	-
511	1153937	-	-	+	-	-	-	-	-
512	99219	-	-	-	-	+	-	-	-
513	5014	-	-	-	+	-	-	-	-
514	5015	-	-	-	-	-	-	+	-
515	228254	+	-	+	+	-	-	-	-
516	283553	+	+	+	-	+	-	-	-
517	68514	-	-	-	-	+	-	-	-
518	373667	-	-	+	-	-	-	+	-
519	408482	-	-	-	+	-	-	-	-
520	279458	+	-	-	-	-	-	-	-
521	228263	-	-	-	-	-	-	+	-
522	322471	-	-	-	-	+	-	-	-
523	351146	-	-	-	-	-	-	+	-
524	1176494	-	-	+	-	-	-	-	-
525	123823	-	-	+	-	-	-	-	-
526	230325	-	-	-	-	+	-	-	+
527	281527	-	-	-	-	-	-	+	-

Continued on next page

Table 15 Continued from previous page

No.	NIST ID	S ₁	S ₂	S ₃	S ₄	S ₅	S ₆	S ₇	S ₈
528	388026	-	-	-	-	-	-	+	-
529	52159	+	-	+	-	-	-	-	-
530	52160	-	-	+	+	+	+	-	-
531	109506	-	-	-	-	-	-	+	-
532	157722	-	-	-	-	-	-	-	+
533	52162	-	-	-	+	+	-	-	-
534	400322	-	-	-	-	+	-	-	-
535	259010	-	-	-	-	+	-	-	-
536	279492	-	-	-	-	+	-	-	-
537	158658	-	-	-	-	+	-	-	-
538	402372	-	-	-	-	+	-	-	-
539	373699	-	-	-	+	-	-	-	-
540	144324	-	-	+	-	-	-	-	-
541	144326	-	-	+	-	-	-	-	-
542	115661	+	-	-	-	-	-	+	-
543	287688	-	-	-	-	-	-	-	+
544	158670	-	-	-	-	+	-	-	-
545	396239	-	-	-	-	+	-	-	-
546	132051	-	-	-	+	-	-	-	-
547	25557	-	-	-	-	-	-	-	+
548	113621	-	-	-	-	-	-	-	+
549	414679	-	-	+	-	-	-	-	-
550	99288	-	-	-	-	+	-	-	-
551	353241	-	-	-	+	-	-	-	-
552	52186	-	-	+	+	+	+	-	-
553	240603	-	-	-	-	+	-	-	+
554	353242	-	+	-	-	-	-	-	-
555	353244	-	-	-	+	-	-	-	-
556	23514	-	-	-	-	-	-	-	+
557	404452	-	-	-	-	-	-	+	-
558	279524	-	-	-	-	-	-	+	-
559	142309	-	-	-	-	+	-	-	-

Continued on next page

Table 15 Continued from previous page

No.	NIST ID	S ₁	S ₂	S ₃	S ₄	S ₅	S ₆	S ₇	S ₈
560	7144	-	-	-	-	-	-	+	-
561	1029097	-	-	+	-	-	-	-	-
562	23537	-	-	-	-	-	-	+	-
563	74738	-	-	-	-	-	-	+	-
564	74739	-	-	-	+	-	-	+	-
565	207862	-	-	-	-	-	+	-	-
566	1051640	-	-	+	-	-	-	-	-
567	197624	-	-	-	-	-	-	-	-
568	158716	-	-	-	-	-	+	-	-
569	115709	-	-	-	-	+	-	-	-
570	25599	-	-	-	+	-	-	-	-
571	13311	-	-	-	-	-	-	-	-
572	78850	-	-	-	+	-	-	-	-
573	322566	+	+	+	+	+	-	-	+
574	297991	-	-	-	-	+	-	-	-
575	396294	-	-	-	-	+	-	-	-
576	58376	-	-	-	-	-	-	-	-
577	228362	-	-	-	-	-	-	+	-
578	78859	-	+	-	-	-	-	-	-
579	353294	-	-	-	-	-	+	-	-
580	78864	-	-	-	+	-	-	-	-
581	1207312	-	-	+	-	-	-	-	-
582	78866	-	-	-	-	-	-	+	-
583	150544	-	-	-	-	-	-	-	-
584	332820	-	-	-	-	+	-	-	-
585	400405	-	-	-	-	-	+	-	-
586	78870	-	-	-	-	+	+	+	+
587	25623	+	+	+	-	+	-	+	-
588	25621	-	-	-	-	+	-	-	-
589	25625	-	-	+	+	+	+	-	-
590	267286	-	-	+	-	-	-	-	-
591	39963	-	-	-	-	+	-	-	-

Continued on next page

Table 15 Continued from previous page

No.	NIST ID	S ₁	S ₂	S ₃	S ₄	S ₅	S ₆	S ₇	S ₈
592	414743	-	-	-	-	-	-	-	+
593	150555	-	-	+	-	-	-	-	-
594	78874	+	-	-	-	-	-	-	-
595	35872	-	+	-	-	-	-	-	-
596	214058	-	+	-	-	-	-	-	-
597	150572	+	+	+	+	+	+	+	+
598	287789	-	-	-	-	-	-	+	-
599	150574	+	+	+	+	+	+	+	+
600	15405	-	-	-	-	+	+	+	-
601	150576	+	+	+	+	+	+	+	+
602	107569	+	+	+	+	+	+	+	+
603	148526	-	-	-	-	-	-	-	-
604	23603	-	-	-	-	-	-	+	-
605	152624	-	-	-	+	-	-	-	-
606	107568	-	+	-	-	-	-	-	-
607	78898	-	-	-	-	-	-	-	-
608	412724	-	-	+	-	-	-	-	-
609	62521	-	-	-	-	-	-	+	-
610	1006652	-	-	+	-	-	-	-	-
611	289853	-	-	-	-	+	-	-	-
612	35902	+	-	+	+	+	+	+	-
613	148544	-	-	-	-	-	-	-	+
614	244801	-	-	-	-	+	-	-	-
615	37953	-	-	-	-	+	-	-	-
616	78916	+	-	-	-	-	-	-	-
617	78918	-	-	-	+	-	-	-	-
618	412744	+	+	+	+	-	-	+	-
619	195658	-	-	-	+	-	+	-	+
620	279629	-	-	-	-	+	-	-	-
621	377935	-	-	+	-	-	-	+	-
622	109647	-	-	-	+	-	-	-	-
623	146514	-	-	+	-	-	-	-	-

Continued on next page

Table 15 Continued from previous page

No.	NIST ID	S ₁	S ₂	S ₃	S ₄	S ₅	S ₆	S ₇	S ₈
624	279635	+	-	+	-	-	-	-	-
625	146517	-	-	+	+	+	-	-	-
626	156759	-	-	-	-	-	-	+	-
627	343128	-	-	-	-	+	-	-	-
628	160856	-	-	+	-	-	-	-	-
629	160858	-	-	-	+	-	-	-	-
630	78936	+	-	-	-	-	-	-	-
631	406619	-	-	-	-	-	-	-	-
632	234590	-	-	-	-	-	+	-	-
633	113759	+	-	+	-	-	-	+	-
634	326750	-	-	-	-	+	-	-	-
635	164963	-	-	-	-	+	-	-	-
636	279652	-	-	-	-	-	-	-	-
637	152679	-	-	-	-	+	-	-	-
638	109671	+	-	-	-	-	-	-	-
639	279659	-	-	-	-	+	-	-	-
640	40044	-	-	+	-	-	-	-	-
641	142445	-	-	-	-	-	-	-	-
642	31855	-	-	+	-	-	-	-	-
643	332912	-	-	-	-	-	-	+	+
644	136304	-	+	-	-	-	-	-	-
645	287857	-	-	-	-	+	-	-	-
646	238707	-	-	-	-	-	-	-	-
647	281716	-	-	-	-	-	-	-	-
648	78965	-	-	-	+	-	-	-	-
649	78974	-	-	-	+	+	+	-	+
650	58494	-	-	-	-	-	-	-	-
651	160896	-	-	-	+	-	-	-	-
652	404608	-	-	-	+	-	-	-	-
653	285830	-	-	-	-	+	-	-	-
654	160902	-	-	-	-	+	-	-	-
655	78985	+	-	+	+	-	-	+	-

Continued on next page

Table 15 Continued from previous page

No.	NIST ID	S ₁	S ₂	S ₃	S ₄	S ₅	S ₆	S ₇	S ₈
656	1105033	-	-	+	-	-	-	-	-
657	281739	-	-	+	-	-	-	-	-
658	234637	-	-	-	-	+	-	-	-
659	46224	-	-	-	-	-	-	+	-
660	384145	-	-	+	-	-	-	-	-
661	384149	-	-	-	-	-	+	-	-
662	13461	-	-	+	-	-	-	-	+
663	418969	-	-	-	-	+	-	-	-
664	160921	-	-	-	-	+	-	-	-
665	267418	-	-	+	-	-	-	-	-
666	54431	-	-	-	+	-	-	-	-
667	152737	-	-	-	-	-	-	-	+
668	134306	-	+	+	-	+	+	-	-
669	79010	-	-	-	+	-	-	-	-
670	9377	+	-	-	-	-	-	-	-
671	337062	-	-	-	-	-	-	-	-
672	107687	-	-	+	-	-	-	+	-
673	79015	-	-	-	-	-	-	-	-
674	17577	-	-	-	-	-	-	-	-
675	366587	-	-	-	-	-	-	-	-
676	382123	-	+	-	-	-	-	-	-
677	279726	-	+	-	+	-	-	-	-
678	228815	-	-	-	-	-	-	+	-
679	79024	-	-	-	-	-	-	+	-
680	79023	-	-	-	+	-	-	-	+
681	283826	-	-	-	+	-	-	-	-
682	1074356	-	-	+	-	-	-	-	-
683	23733	-	+	+	+	-	-	+	-
684	187574	-	-	+	-	-	-	-	-
685	283832	-	-	-	-	-	-	-	+
686	283835	-	-	-	-	+	-	-	-
687	13500	-	-	-	+	-	-	-	-

Continued on next page

Table 15 Continued from previous page

No.	NIST ID	S ₁	S ₂	S ₃	S ₄	S ₅	S ₆	S ₇	S ₈
688	195773	-	-	+	-	-	-	-	-
689	396479	-	-	-	-	+	-	-	-
690	306370	-	-	+	-	-	-	-	-
691	279748	-	-	-	-	+	-	-	-
692	156871	-	-	-	-	-	-	+	-
693	130249	-	-	-	-	-	-	+	-
694	333006	-	-	-	-	-	-	-	-
695	1231	-	-	-	-	-	-	-	+
696	333008	-	-	+	-	-	-	-	-
697	240851	-	-	-	-	-	+	-	+
698	292052	-	-	+	-	+	-	-	-
699	660693	+	-	-	-	-	-	-	-
700	384215	-	-	-	-	+	-	-	-
701	283864	-	-	-	-	-	-	-	-
702	15577	-	-	-	+	-	-	-	-
703	156890	-	-	-	-	-	+	-	-
704	107738	+	-	+	+	-	+	-	-
705	283865	-	-	+	+	-	-	-	-
706	79068	-	-	-	+	-	-	-	-
707	79069	-	-	-	+	-	-	-	-
708	398553	+	-	-	-	-	-	-	-
709	113884	-	-	+	-	-	-	-	-
710	23773	-	-	-	-	-	-	-	+
711	79071	-	-	-	-	-	-	-	+
712	50400	-	-	-	-	-	-	-	+
713	152807	-	-	+	-	-	-	-	-
714	79080	-	-	-	-	-	-	+	-
715	79081	-	-	-	-	-	-	+	-
716	216296	-	-	-	-	+	-	-	-
717	333033	-	-	-	-	+	-	-	-
718	15592	-	+	-	-	-	-	-	-
719	79088	-	-	-	+	-	-	-	+

Continued on next page

Table 15 Continued from previous page

No.	NIST ID	S ₁	S ₂	S ₃	S ₄	S ₅	S ₆	S ₇	S ₈
720	249073	-	-	+	-	-	-	-	-
721	1004786	+	-	-	-	-	-	-	-
722	1006838	+	+	-	-	-	-	-	-
723	79095	-	-	-	-	-	-	-	+
724	158968	+	-	-	-	-	-	-	-
725	9465	+	+	-	-	-	-	-	-
726	105724	-	-	-	-	-	-	+	-
727	107774	-	-	-	+	-	-	-	-
728	230657	-	-	+	-	-	+	-	-
729	60673	+	-	-	-	-	-	-	-
730	9475	-	-	-	-	-	+	-	-
731	13572	-	-	-	-	-	+	-	-
732	333059	-	-	-	-	+	-	-	-
733	113925	-	+	-	-	-	-	-	-
734	7430	-	-	+	-	-	-	-	-
735	333063	-	-	-	-	-	-	-	-
736	144650	+	-	-	-	-	-	-	-
737	113940	-	-	+	-	-	-	-	-
738	60693	+	+	+	+	+	-	+	-
739	234773	-	-	-	-	+	-	-	-
740	333078	+	-	+	+	-	-	-	-
741	333083	-	-	-	+	-	-	-	-
742	132381	-	-	+	-	-	-	-	-
743	68895	+	+	+	-	-	-	-	-
744	333087	-	-	-	-	-	-	-	+
745	68897	-	-	-	-	-	-	-	-
746	392482	-	-	+	-	-	-	-	-
747	408867	-	-	+	+	+	+	+	+
748	11556	-	-	+	-	-	-	-	+
749	408869	-	-	+	-	+	+	-	-
750	245029	+	-	-	+	-	-	-	-
751	232738	-	-	-	-	-	-	-	+

Continued on next page

Table 15 Continued from previous page

No.	NIST ID	S ₁	S ₂	S ₃	S ₄	S ₅	S ₆	S ₇	S ₈
752	68904	+	-	-	-	-	-	-	-
753	232745	-	-	+	-	-	-	+	-
754	68908	-	-	+	-	-	-	-	-
755	68910	-	-	-	-	-	-	-	-
756	60722	+	-	-	-	-	+	-	-
757	257331	-	-	-	-	+	-	-	-
758	60724	+	+	-	-	-	-	-	-
759	156982	-	-	-	-	+	-	-	-
760	60726	-	-	-	-	-	-	-	+
761	60727	-	-	+	-	-	-	-	-
762	128313	-	-	-	+	-	-	-	-
763	1339	-	-	-	+	-	-	-	-
764	79164	-	+	-	-	+	-	-	+
765	60733	-	-	-	-	-	-	+	-
766	60731	+	-	-	-	-	-	-	-
767	60734	+	+	-	+	-	-	-	-
768	68927	-	-	-	-	-	+	-	-
769	60737	-	-	+	-	-	-	+	-
770	101697	-	+	-	-	-	-	-	-
771	75074	-	-	-	-	-	-	-	-
772	79171	-	-	-	-	-	-	-	-
773	30021	-	-	-	-	+	-	-	-
774	1135941	-	-	-	-	+	-	-	-
775	159046	-	-	+	-	-	-	-	-
776	150854	-	-	-	-	-	-	-	-
777	60745	+	-	+	+	+	-	+	-
778	60746	-	-	-	-	-	+	-	-
779	417098	-	-	-	-	-	-	-	-
780	1051980	+	-	+	-	-	-	-	-
781	5453	-	-	-	+	-	-	-	-
782	60750	-	-	+	-	-	-	-	-
783	187732	-	-	-	+	-	-	-	-

Continued on next page

Table 15 Continued from previous page

No.	NIST ID	S ₁	S ₂	S ₃	S ₄	S ₅	S ₆	S ₇	S ₈
784	1224024	-	+	+	-	-	-	-	-
785	333146	+	-	-	-	-	-	-	-
786	114012	+	-	+	-	-	-	-	-
787	23903	-	-	+	+	-	-	-	-
788	378208	-	-	-	-	+	-	-	-
789	54623	-	-	+	-	-	-	-	+
790	60770	-	-	+	-	-	-	+	-
791	5475	-	-	+	-	-	-	-	-
792	232804	-	-	-	-	+	-	-	-
793	60773	-	-	-	-	-	-	+	-
794	60771	+	+	+	-	-	-	-	-
795	23905	+	-	-	-	-	-	-	-
796	402791	-	-	+	-	-	-	-	-
797	60777	-	-	-	+	-	-	-	-
798	306539	-	-	-	+	-	-	-	-
799	234860	-	-	+	+	+	-	-	-
800	23915	-	-	-	-	-	-	-	+
801	23916	-	-	+	-	-	-	-	-
802	15726	-	+	+	-	-	-	-	-
803	195952	-	-	-	-	+	-	-	-
804	1219952	-	-	-	+	-	-	-	-
805	232818	-	-	-	-	-	-	+	-
806	1101169	-	-	-	+	-	-	-	-
807	378222	+	-	-	-	-	-	-	-
808	374129	-	-	-	-	-	-	-	+
809	232821	+	-	+	-	-	+	-	-
810	245109	-	-	-	+	-	-	-	-
811	60792	-	-	-	-	-	-	+	-
812	79222	-	-	-	-	+	-	-	-
813	62838	-	+	+	-	-	-	-	-
814	306553	-	-	-	+	-	-	-	-
815	60794	-	-	+	-	-	-	-	-

Continued on next page

Table 15 Continued from previous page

No.	NIST ID	S ₁	S ₂	S ₃	S ₄	S ₅	S ₆	S ₇	S ₈
816	44411	-	+	-	-	-	-	-	-
817	281980	+	-	-	-	-	-	-	-
818	249213	-	-	-	-	+	-	-	+
819	75133	-	-	+	+	-	-	-	-
820	23937	+	-	-	-	-	-	-	-
821	159105	+	-	-	-	-	-	-	-
822	237594	-	-	+	-	+	-	-	+
823	79236	-	-	-	-	-	-	+	-
824	7557	-	-	-	-	+	-	-	-
825	374150	-	-	-	-	+	-	-	-
826	1197449	-	-	-	+	-	-	-	-
827	40330	-	-	-	-	+	-	-	-
828	60814	-	-	+	-	-	-	-	-
829	212367	-	-	-	-	+	-	-	-
830	163214	+	-	-	-	-	-	-	-
831	60815	-	-	-	-	-	-	-	-
832	114065	-	-	+	-	-	-	-	-
833	157076	-	-	-	-	-	-	-	+
834	56725	-	-	+	-	-	-	-	-
835	114071	-	-	+	-	-	-	-	-
836	36249	-	-	-	-	-	-	+	-
837	333210	+	-	+	-	+	-	+	-
838	114073	-	-	-	+	-	-	-	-
839	394660	-	-	-	-	+	-	+	+
840	150948	-	-	-	-	-	-	+	-
841	79268	-	+	-	-	-	-	-	-
842	228773	+	+	+	-	-	-	-	-
843	9640	-	-	-	-	-	-	+	-
844	333222	-	-	+	-	-	-	-	-
845	333221	+	-	-	-	-	-	-	-
846	13737	-	-	-	-	-	-	-	-
847	333226	-	-	-	-	+	-	-	-

Continued on next page

Table 15 Continued from previous page

No.	NIST ID	S ₁	S ₂	S ₃	S ₄	S ₅	S ₆	S ₇	S ₈
848	253355	-	-	-	-	+	+	-	-
849	329133	-	-	-	-	-	-	-	-
850	243120	-	-	-	-	+	-	-	-
851	114098	-	-	+	+	-	-	+	+
852	159154	-	-	-	-	+	-	-	-
853	163250	-	-	-	-	+	-	-	-
854	17846	-	-	-	-	-	+	-	-
855	40374	-	-	-	+	-	-	-	-
856	341441	-	-	-	+	+	+	-	+
857	71106	-	-	-	-	-	-	+	-
858	60871	-	-	+	-	-	-	-	-
859	347593	-	-	-	-	-	-	+	-
860	232906	+	+	+	+	-	+	+	+
861	159177	-	-	-	-	+	-	-	-
862	216523	-	-	-	-	+	-	-	-
863	110028	-	-	+	-	-	-	-	-
864	239054	-	-	-	+	-	-	-	-
865	13775	-	-	-	-	-	-	-	-
866	196053	-	-	+	-	-	-	-	-
867	161246	-	-	-	-	+	-	-	+
868	333296	-	-	+	+	-	-	+	-
869	333298	+	-	+	+	+	-	-	-
870	22004	-	-	-	-	-	-	-	-
871	161274	+	-	+	+	+	-	+	-
872	333306	-	-	-	-	-	-	-	-
873	60927	+	+	-	-	-	-	-	-
874	366080	-	-	-	+	-	-	-	-
875	298499	+	-	-	-	-	-	-	-
876	255493	-	-	-	-	-	-	+	-
877	366087	-	-	-	-	-	+	-	-
878	333319	-	-	-	-	+	-	-	-
879	210441	-	-	-	-	+	-	-	-

Continued on next page

Table 15 Continued from previous page

No.	NIST ID	S ₁	S ₂	S ₃	S ₄	S ₅	S ₆	S ₇	S ₈
880	112137	+	-	+	-	-	-	-	-
881	232971	-	+	-	-	-	+	-	-
882	192013	-	-	-	-	-	-	-	+
883	114191	-	+	-	-	-	-	+	-
884	1000981	-	-	-	+	-	-	-	-
885	417301	+	+	+	-	-	-	-	+
886	54807	-	-	+	-	-	-	-	-
887	343579	-	-	-	-	-	-	-	+
888	351774	-	-	+	-	-	-	+	-
889	343583	-	-	-	-	-	-	+	-
890	230947	+	-	+	+	-	-	-	-
891	351780	-	+	+	-	+	-	-	-
892	153124	-	-	+	-	-	-	-	-
893	417318	-	+	+	+	+	-	+	-
894	417320	-	-	-	+	+	-	-	+
895	194089	-	-	-	-	+	-	-	-
896	296489	-	-	-	-	+	-	-	-
897	304683	-	-	-	-	-	-	-	-
898	185901	-	-	-	+	-	-	-	-
899	79407	-	-	-	-	+	-	+	-
900	114223	-	+	+	-	-	-	-	-
901	374323	-	-	-	+	-	-	-	-
902	245301	-	-	-	-	+	-	-	-
903	9783	+	-	-	-	-	-	-	-
904	50744	-	-	-	-	-	-	-	+
905	11834	-	-	-	-	-	-	+	-
906	79424	-	-	-	-	+	+	-	+
907	222788	-	-	+	-	-	-	-	-
908	7751	-	-	-	-	-	-	+	-
909	63048	-	-	-	-	-	-	+	-
910	306759	+	-	-	-	-	-	-	-
911	108104	-	-	-	+	-	-	-	-

Continued on next page

Table 15 Continued from previous page

No.	NIST ID	S ₁	S ₂	S ₃	S ₄	S ₅	S ₆	S ₇	S ₈
912	118347	-	-	-	-	-	-	+	-
913	79437	-	-	-	+	-	-	-	-
914	382543	+	+	+	-	-	-	+	-
915	114255	+	+	+	+	-	+	-	+
916	382544	-	-	+	-	-	-	-	-
917	386642	-	-	-	-	-	-	+	+
918	99921	-	-	-	-	-	-	-	-
919	99919	-	-	-	-	-	-	-	+
920	284244	-	-	-	-	+	-	-	-
921	280150	-	-	-	-	-	+	-	-
922	364117	+	-	-	-	-	-	-	-
923	317019	-	-	-	-	-	-	-	-
924	151136	-	-	-	-	-	-	+	-
925	104032	-	-	-	-	+	-	-	-
926	79456	-	-	-	+	-	-	-	-
927	157283	-	-	-	-	-	-	+	-
928	282210	+	-	-	-	-	-	-	-
929	79460	-	-	-	-	+	-	-	+
930	333413	-	-	-	-	+	-	-	-
931	159333	-	-	+	-	+	-	-	-
932	120421	-	-	-	-	+	-	-	-
933	233062	-	-	-	-	+	-	-	-
934	296559	-	-	-	-	+	-	-	-
935	61041	+	+	-	-	+	-	-	-
936	75381	+	-	-	-	-	-	-	-
937	24185	-	-	-	-	+	-	-	+
938	249466	-	-	+	-	-	-	-	-
939	24187	-	-	-	-	+	-	-	-
940	73341	-	-	-	+	-	-	+	-
941	63104	-	-	-	-	-	-	-	-
942	351875	-	-	-	+	-	-	-	-
943	22149	-	-	-	-	-	-	+	-

Continued on next page

Table 15 Continued from previous page

No.	NIST ID	S ₁	S ₂	S ₃	S ₄	S ₅	S ₆	S ₇	S ₈
944	351882	-	-	-	-	+	+	+	-
945	229003	+	+	+	-	+	+	-	-
946	280203	-	-	+	-	-	+	-	-
947	280202	-	-	-	+	-	-	-	-
948	405132	+	-	+	+	-	-	-	-
949	24205	-	-	-	-	-	-	-	-
950	308880	-	-	-	-	-	-	-	+
951	163473	-	-	-	-	+	-	-	-
952	104087	-	-	+	-	-	-	-	-
953	196252	-	-	-	-	-	-	-	-
954	157341	-	-	-	-	-	-	+	-
955	24220	+	-	-	-	-	-	-	-
956	1175198	-	-	+	-	-	-	-	-
957	79520	+	-	+	+	+	+	+	+
958	79519	-	-	-	-	-	-	-	+
959	241313	-	-	-	-	+	-	-	-
960	267937	-	-	+	-	-	-	-	-
961	79524	-	-	-	-	-	-	-	+
962	298662	-	-	-	-	-	-	+	-
963	24230	-	-	-	-	-	-	-	-
964	210603	-	-	-	-	-	-	+	-
965	190124	-	-	-	+	-	-	-	-
966	24237	-	-	-	-	-	-	+	-
967	401071	+	-	-	-	-	-	-	-
968	157360	+	+	-	-	-	-	-	-
969	63153	-	-	-	+	-	-	-	-
970	151218	+	-	-	+	+	-	+	-
971	73393	-	-	-	+	-	-	-	-
972	313012	-	-	-	-	+	-	+	-
973	1156789	-	-	+	-	-	-	-	-
974	157364	+	-	-	-	-	-	-	-
975	79542	-	-	-	-	-	-	-	-

Continued on next page

Table 15 Continued from previous page

No.	NIST ID	S ₁	S ₂	S ₃	S ₄	S ₅	S ₆	S ₇	S ₈
976	7864	-	-	-	-	+	-	-	+
977	71353	-	-	-	-	-	-	+	-
978	192187	-	+	-	-	-	-	-	-
979	280257	-	-	-	-	-	-	+	-
980	419521	-	-	-	-	+	-	-	-
981	419523	-	-	-	-	+	-	-	-
982	151237	-	-	-	+	-	-	-	-
983	417479	-	-	-	-	-	-	-	+
984	1033933	-	-	+	-	-	-	-	-
985	79572	-	-	-	+	-	-	-	-
986	1627862	-	-	-	-	-	+	-	-
987	79575	-	-	-	-	-	+	+	-
988	149207	-	-	+	-	-	+	-	-
989	1119958	+	-	-	-	-	-	-	-
990	196313	-	-	-	-	+	-	-	-
991	190173	-	-	-	-	-	-	+	-
992	417501	-	-	-	-	+	-	-	-
993	370401	-	-	-	-	+	-	-	-
994	79585	+	-	-	-	-	-	-	-
995	24296	+	-	-	-	-	-	-	-
996	79594	-	-	-	-	+	-	-	-
997	333547	-	-	-	+	-	-	-	+
998	1052395	-	-	+	-	-	-	-	-
999	302829	-	-	-	-	-	-	+	-
1000	106222	+	-	-	-	-	-	-	-
1001	14064	-	-	-	-	-	-	+	-
1002	3830	+	-	-	-	-	-	-	-
1003	157436	-	-	-	-	+	-	-	-
1004	147198	-	-	-	-	+	-	-	-
1005	102146	-	-	-	+	-	-	-	-
1006	161540	-	-	-	-	+	+	-	-
1007	79620	-	-	-	-	-	-	-	-

Continued on next page

Table 15 Continued from previous page

No.	NIST ID	S ₁	S ₂	S ₃	S ₄	S ₅	S ₆	S ₇	S ₈
1008	149254	-	-	+	-	-	-	-	-
1009	22280	-	-	-	-	-	-	+	-
1010	229129	+	+	+	-	-	-	-	-
1011	110349	-	-	-	-	+	-	-	-
1012	417556	+	-	-	-	-	-	-	-
1013	151317	-	-	+	-	-	-	-	-
1014	151318	+	+	-	-	-	-	-	+
1015	14103	-	-	+	-	-	-	-	+
1016	14105	-	-	-	-	-	-	+	-
1017	397087	-	-	-	-	-	-	+	-
1018	79647	+	-	+	-	-	-	-	-
1019	141088	+	-	-	-	-	-	-	-
1020	143139	-	-	-	-	-	-	-	-
1021	63269	-	-	-	-	-	-	+	-
1022	288550	-	-	-	-	-	-	-	-
1023	79657	-	-	-	-	-	-	-	+
1024	233260	+	+	+	-	-	-	-	-
1025	333613	-	+	-	+	-	-	-	-
1026	163630	-	-	-	+	-	-	-	-
1027	282412	+	-	-	-	-	-	-	-
1028	30512	-	-	-	-	-	-	+	-
1029	163629	+	-	-	-	-	-	-	-
1030	229166	+	-	-	-	-	-	-	-
1031	34612	-	-	-	-	-	+	-	-
1032	417588	-	-	-	-	-	-	-	+
1033	352053	-	-	+	-	-	-	-	-
1034	1005366	-	-	-	-	+	-	-	-
1035	65334	-	-	-	+	-	-	-	-
1036	1120055	-	-	+	-	-	-	-	-
1037	71482	-	-	-	-	+	-	-	-
1038	352056	-	-	-	-	-	-	-	+
1039	1120059	-	+	-	-	-	-	-	-

Continued on next page

Table 15 Continued from previous page

No.	NIST ID	S ₁	S ₂	S ₃	S ₄	S ₅	S ₆	S ₇	S ₈
1040	417597	-	-	-	-	-	-	+	-
1041	22332	-	-	-	-	-	-	-	-
1042	352063	-	-	-	-	-	-	+	-
1043	79679	-	-	-	-	+	-	-	-
1044	323397	-	-	-	-	-	+	-	-
1045	352070	+	-	-	-	-	-	-	-
1046	36680	-	-	-	-	-	-	+	-
1047	352073	-	-	+	-	-	-	-	-
1048	309066	-	-	-	+	-	-	-	-
1049	298829	+	-	-	-	-	-	-	-
1050	159568	-	-	-	-	-	-	-	-
1051	298838	-	-	-	-	-	-	+	-
1052	155479	-	-	-	+	-	-	-	-
1053	63319	-	-	-	+	-	-	-	-
1054	309079	+	-	-	+	-	-	-	-
1055	3935	-	-	+	-	-	-	-	-
1056	1152865	-	-	+	-	-	-	-	-
1057	360290	-	-	-	-	+	-	-	-
1058	79718	+	-	-	-	-	-	-	-
1059	352107	+	-	-	+	+	-	+	+
1060	352108	-	-	-	-	+	-	+	-
1061	229227	-	-	-	-	+	-	-	-
1062	368493	-	-	-	-	-	+	-	-
1063	10096	-	-	-	+	-	-	-	-
1064	368497	-	-	-	+	+	+	+	-
1065	282481	+	-	+	-	-	-	-	-
1066	376691	-	-	-	-	-	-	+	-
1067	368499	-	-	-	+	+	-	-	+
1068	376692	-	-	+	+	-	-	-	-
1069	368502	-	-	-	-	-	-	-	-
1070	368503	-	-	-	-	+	-	-	-
1071	137080	-	-	+	-	-	-	-	-

Continued on next page

Table 15 Continued from previous page

No.	NIST ID	S ₁	S ₂	S ₃	S ₄	S ₅	S ₆	S ₇	S ₈
1072	333689	-	+	-	-	+	-	-	+
1073	1212280	+	-	-	-	-	-	-	-
1074	417661	-	-	-	-	+	-	+	-
1075	147326	-	-	-	-	+	-	-	-
1076	266116	+	-	-	-	-	-	+	-
1077	333700	-	-	-	-	+	-	-	-
1078	24454	-	-	-	-	-	-	-	-
1079	403336	-	-	-	-	-	-	+	-
1080	333710	-	-	-	+	-	-	+	-
1081	333711	-	-	-	+	+	-	-	-
1082	46993	-	-	-	-	-	-	+	-
1083	155538	-	-	-	+	-	-	-	-
1084	374675	-	-	-	-	-	-	+	-
1085	216979	-	-	-	-	+	-	-	-
1086	333717	+	-	-	-	-	-	+	-
1087	403351	-	-	-	+	-	-	-	-
1088	374680	-	-	+	+	+	+	-	+
1089	333721	-	-	-	-	-	-	+	-
1090	417690	+	-	-	-	-	-	+	+
1091	368539	-	-	-	-	-	-	+	-
1092	374681	-	-	-	-	+	-	-	-
1093	376728	-	-	-	-	-	-	-	-
1094	417695	-	-	-	-	-	-	+	-
1095	333728	-	-	+	-	-	-	-	-
1096	333729	+	-	+	+	-	-	+	-
1097	368546	-	-	-	-	+	-	-	+
1098	47011	-	-	-	-	-	-	+	-
1099	368547	-	-	+	-	-	-	-	-
1100	333733	+	+	-	+	-	-	+	-
1101	34726	-	-	-	-	-	-	+	-
1102	333732	-	+	+	+	-	-	-	-
1103	354214	-	-	+	-	-	-	-	-

Continued on next page

Table 15 Continued from previous page

No.	NIST ID	S ₁	S ₂	S ₃	S ₄	S ₅	S ₆	S ₇	S ₈
1104	22438	-	-	-	-	-	-	-	-
1105	417706	-	-	-	-	-	-	+	-
1106	333738	+	-	-	-	-	-	-	-
1107	331692	-	-	-	+	-	-	-	-
1108	413614	-	-	-	-	-	-	-	-
1109	149423	-	-	-	-	+	-	+	+
1110	149425	-	-	-	-	-	-	+	-
1111	1212337	+	-	-	-	-	-	-	-
1112	47026	-	-	-	-	-	+	-	-
1113	292786	-	-	-	-	-	-	-	-
1114	229302	-	-	+	-	-	-	-	-
1115	57273	+	-	+	-	-	-	-	-
1116	227258	-	-	-	-	-	-	+	-
1117	333755	-	-	-	-	+	-	-	-
1118	368572	-	-	-	-	-	-	+	-
1119	794556	-	-	-	-	-	-	-	-
1120	16318	-	+	-	-	-	-	-	-
1121	16319	-	-	-	-	-	+	-	-
1122	63424	-	-	+	+	-	-	-	-
1123	239555	-	-	-	-	-	-	+	-
1124	333764	-	-	-	-	-	-	+	+
1125	298949	-	-	-	-	-	-	+	-
1126	372676	-	-	-	-	-	-	-	+
1127	337859	-	-	-	-	+	-	-	-
1128	36805	-	-	-	-	+	-	-	-
1129	282566	-	-	-	-	-	+	-	-
1130	16326	-	-	-	-	+	-	-	-
1131	331723	-	-	-	-	-	+	+	+
1132	32708	-	-	-	-	-	-	-	-
1133	1087430	-	-	+	-	-	-	-	-
1134	141253	-	-	-	-	-	-	-	+
1135	153546	-	-	-	-	+	-	-	-

Continued on next page

Table 15 Continued from previous page

No.	NIST ID	S ₁	S ₂	S ₃	S ₄	S ₅	S ₆	S ₇	S ₈
1136	241616	-	-	-	-	-	-	+	-
1137	272330	-	-	-	-	+	-	-	-
1138	313294	-	-	-	+	-	-	-	-
1139	131023	-	-	+	-	+	-	-	-
1140	14286	-	-	-	+	-	-	-	-
1141	352208	-	-	-	+	-	-	-	-
1142	235470	-	-	-	-	-	-	-	+
1143	147413	-	-	+	-	-	-	-	-
1144	368600	-	-	-	-	-	-	-	-
1145	360410	-	-	-	-	-	-	+	-
1146	245724	-	-	-	+	-	-	-	-
1147	71645	-	-	+	-	-	-	-	-
1148	61405	-	-	+	-	-	-	-	-
1149	71648	-	-	-	-	+	-	-	-
1150	34786	-	-	-	-	-	-	+	-
1151	296930	-	-	-	-	-	+	-	-
1152	245730	-	-	-	+	-	+	-	-
1153	141285	-	-	+	-	+	-	+	-
1154	215011	-	-	-	-	+	-	-	-
1155	120807	-	-	-	-	-	-	+	-
1156	71652	-	-	-	-	-	-	-	-
1157	1224677	-	-	+	-	-	-	-	-
1158	333797	+	-	-	-	-	-	-	+
1159	1179624	-	+	-	-	-	-	-	-
1160	331754	-	-	+	+	-	-	-	-
1161	61418	-	-	+	-	-	-	-	-
1162	153581	-	-	+	-	-	-	-	-
1163	366574	-	-	-	-	+	-	-	-
1164	360430	-	-	+	-	-	-	-	-
1165	26608	+	+	-	-	-	-	-	-
1166	366579	-	+	-	+	+	+	+	+
1167	366582	+	+	+	+	+	+	+	+

Continued on next page

Table 15 Continued from previous page

No.	NIST ID	S ₁	S ₂	S ₃	S ₄	S ₅	S ₆	S ₇	S ₈
1168	331769	-	-	-	-	+	-	+	+
1169	69626	-	-	-	-	-	-	+	-
1170	331771	-	-	+	-	-	-	-	-
1171	28669	-	-	-	-	-	+	-	-
1172	61438	+	-	+	-	-	-	-	-